University of Cyprus

DEPARTMENT OF PHYSICS

^{57}Fe MÖSSBAUER SPECTROSCOPIC STUDIES ON β-THALASSAEMIA USING A MOUSE MODEL FOR β-THALASSAEMIA AND RED BLOOD CELL SAMPLES FROM PATIENTS

CHARITOU GEORGIOS

A Dissertation Submitted to the University of Cyprus in Partial Fulfillment of the Requirements for the Degree of Doctor of Philosophy

MAY 2019

VALIDATION PAGE

Doctoral Candidate: Charitou Georgios

Doctoral Thesis Title: ^{57}Fe Mössbauer spectroscopic studies on β-thalassaemia using a mouse model for β-thalassaemia and red blood cell samples from patients

*The present Doctoral Dissertation was submitted in partial fulfilment of the requirements for the degree of Doctor of Philosophy at the **Department of Physics** and was approved on the 10/05/2019 by the members of the **Examination Committee**.*

Examination Committee:

Research Supervisor: Prof. Haralambos Tsertos,
Department of Physics, University of Cyprus_____

Committee Member: Prof. Andreas Othonos,
Department of Physics, University of Cyprus_____

Committee Member: Associate. Prof. Archontis Georgios,
Department of Physics, University of Cyprus_____

Committee Member: Prof. Leontios Kostrikis,
Department of Biological Sciences, University of Cyprus_____

Committee Member: Associate. Prof. Alexios Douvalis,
Department of Physics, University of Ioannina_____

DECLARATION OF DOCTORAL CANDIDATE

The present doctoral dissertation was submitted in partial fulfilment of the requirements for the degree of Doctor of Philosophy of the University of Cyprus. It is a product of original work of my own, unless otherwise mentioned through references, notes, or any other statements.

_____

Georgios Charitou (Γεώργιος Χαρίτου)

(This page intentionally left blank)

Περίληψη

Η β-θαλασσαιμία είναι μια κληρονομική αναιμία που προκαλείται από μεταλλάξεις του γονιδίου β-σφαιρίνης. Επηρεάζει πολλαπλά όργανα και συνδέεται με σημαντική νοσηρότητα και θνησιμότητα. Σε αυτή την εργασία χρησιμοποιήθηκε η φασματοσκοπία Mössbauer (MS) για τη μελέτη της θαλασσαιμίας, χρησιμοποιώντας για πρώτη φορά ένα μοντέλο θαλασσαιμικού ποντικού καθώς και δείγματα αίματος από ασθενείς με β-θαλασσαιμία.

Αρχικά μελετήθηκε η χρησιμότητα του θαλασσαιμικού μοντέλου και στη συνέχεια η συγκέντρωση του ^{57}Fe σε ποντίκια άγριου τύπου C57BL / 6 και ετερόζυγα β-θαλασσαιμικά αυξήθηκε μέσω μακροχρόνιας γαστρεντερικής απορρόφησης δίαιτας εμπλουτισμένης με ^{57}Fe. Δείγματα αίματος, καρδιάς, συκωτιού, νεφρών, σπλήνας και εγκεφάλου συλλέχθηκαν από ποντίκια ηλικίας 1, 3, 6 και 9 μηνών και φάσματα MS πάρθηκαν σε θερμοκρασίες 80K. Τα β-θαλασσαιμικά ποντίκια, σε αντίθεση με τα άγριου τύπου, έδειξαν μειωμένα επίπεδα αιμοσφαιρίνης στο αίμα τους ως αποτέλεσμα της αναιμίας, καθώς και σημαντική ποσότητα σιδήρου υπό μορφή φερριτίνης, η οποία μειωνόταν με την ηλικία των ποντικιών. Αυτό μπορεί να αντικατοπτρίζει την μείωση του αριθμού δικτυοερυθροκυττάρων που αναφέρεται στη βιβλιογραφία. Οι εναποθέσεις σιδήρου υπό μορφή φερριτίνης στην καρδιά και στον εγκέφαλο των θαλασσαιμικών ποντικών βρέθηκαν ελαφρώς αυξημένες ενώ σημαντικές ποσότητες σιδήρου υπό μορφή φερριτίνης βρέθηκαν στα νεφρά, το συκώτι και τον σπλήνα. Οι νεφρικοί ιστοί των θαλασσαιμικών ποντικών βρέθηκαν να έχουν ~ 16 φορές περισσότερο σίδηρο υπό μορφή φερριτίνης από τα ποντίκια άγριου τύπου και ~10 φορές στο συκώτι. Επιπλέον, στους σπλήνες βρέθηκε σίδηρος υπό μορφή αιμοσιδηρίνης και δισθενής σίδηρος υψηλού spin μη συνδεδεμένος με αίμη. Η διπλέτα της φερριτίνης που βρέθηκε στα όργανα, μπορούσε να χωριστεί περαιτέρω σε δύο υπο-διπλέτες που αντιπροσωπεύουν την εσωτερική και την επιφανειακή δομή του μεταλλικού πυρήνα της φερριτίνης. Ο σίδηρος επιφανείας βρέθηκε να επικρατεί στις καρδιές και τους εγκεφάλους όλων των ποντικιών και στα νεφρά των ποντικιών άγριου τύπου. Φερριτίνη πλούσια σε εσωτερικό σίδηρο βρέθηκε να επικρατεί στα νεφρά των θαλασσαιμικών ποντικών, στο συκώτι και στο σπλήνα. Η αναλογία εσωτερικού προς επιφανειακού σιδήρου ήταν αυξημένη σε όλα τα θαλασσαιμικά δείγματα.

Τα φάσματα MS από τα ερυθρά αιμοσφαίρια των ασθενών με θαλασσαιμία έδειξαν την ύπαρξη σημαντικών ποσοτήτων σιδήρου που υπό μορφή φερριτίνης, κυρίως στα δείγματα από ασθενείς με ενδιάμεση β-θαλασσαιμία, όπου το 82% από αυτούς εμφάνισε αυτό το σύμπλοκο. Ταυτόχρονα, όπως εκτιμήθηκε με εξετάσεις MRI, οι ασθενείς με ενδιάμεση β-θαλασσαιμία

βρέθηκαν να έχουν υψηλότερη συγκέντρωση σιδήρου στο συκώτι (LIC) σε σύγκριση με τους ασθενείς με μείζονα β-θαλασσαιμία, αν και είχαν κατά μέσο όρο περίπου το ήμισυ των επιπέδων φερριτίνης στον ορό αίματος.

Abstract

β-thalassemia is an inherited anaemia caused by mutations of the β-globin gene. It affects multiple organs and is associated with considerably morbidity and mortality. In this work, Mössbauer spectroscopy (MS) was used for the study of thalassaemia disease, utilising for the first time a thalassaemic mouse model, as well as blood samples from β-thalassaemia patients.

The usefulness of a thalassaemic mouse model was initially validated and subsequently the concentration of ^{57}Fe in *wild-type C57BL/6* and heterozygous β-thalassaemic mice was significantly increased through long-term gastrointestinal absorption of ^{57}Fe enriched diet. Samples of blood, hearts, livers, kidneys, spleen and brains were collected from mice at 1, 3, 6 and 9 months of age and MS spectra were acquired at 80K. The β-thalassaemic mice, in contrast to the *wild-type* ones, showed reduced haemoglobin levels in their blood as a result of anaemia, as well as significant amounts of ferritin-like iron, which decreased with mouse age. The later might reflect the pattern of reticulocyte count reduction reported in the literature. Ferritin-like iron depositions in the heart and the brain of the thalassaemic mice were found to be slightly increased while significant amounts of Ferritin-like iron were found in the kidneys, liver and spleen. The renal tissues of the thalassaemic mice were found to have ~16 times more Ferritin-like iron than the control equivalents and their livers ~10 times. Furthermore, haemosiderin and non-haem-high spin Fe(II) iron was found in their spleens. The Ferritin-like iron doublet, found in the organs, could be further separated into two sub-doublets representing the inner and surface structure of ferritin's mineral core. Surface iron sites were found to be predominant in the hearts and brains of all mice and in the kidneys of the *wild-type* ones. Ferritin rich in inner iron sites was predominant in the kidneys of the thalassaemic mice, in the livers and in the spleens. The inner-to-surface iron sites ratio was elevated in all thalassaemic samples.

The MS spectra from the red blood cells of the thalassaemia patients showed the existence of significant amounts of ferritin-like iron, mainly in the samples from the β-thalassaemia intermedia patients, where 82% of them showed evidence of this iron complex. At the same time, β-thalassaemia intermedia patients were found to have higher Liver Iron Concentration (LIC) when compared to the β-thalassaemia major patients, as assessed by MRI exams, although they had on an average about half the serum ferritin levels.

Acknowledgments

Firstly, I want to thank my supervisor Prof. Haralambos Tsertos for giving me the chance to organize and try my completely own work. I would also like to thank Dr. Yiannis Parpottas for his help establishing all the collaborations needed, for all the personal time he spent helping, for his advices and for his support.

I would also like to thank Dr. George Lapathitis and Christos Karaiskos from the Transgenic Mouse Facility of the Cyprus Institute of Neurology and Genetics, Prof. Marina Kleanthous and her team at the Molecular Genetics Thalassaemia Department, and foremost, I want to thank Dr. Marios Phylactides for the cooperation, the guidance and the time spent helping with the samples. Without his help this thesis would not have been completed.

Finally, I would like to thank my family and all the people who happened to cross paths with me all this time. Your support was important.

Table of Contents

List of Figures

List of Tables

Symbols & Abbreviations

(e)	Excited state
(g)	Ground state
+/+	Wild-type *C57BL/6* mouse
$2\pi\lambda^2$ s	Mössbauer Wavelength
abs_r	Relative absorption depth of the Mössbauer line
BMT	Bone Marrow Transplantation
c	Speed of light
CING	Cyprus Institute of Neurology and Genetics
CO-Hb	Carboxyhaemoglobin
Ctrl	Control
Deoxy-Hb	Deoxyhaemoglobin
DFO	Deferoxamine
DFP	Deferiprone / L1
DFX	Deferasirox / ExJade
d_{opt}	Optimal thickness
e	Electron/proton charge
EC	Electron Capture
EFG	Electric field gradient
EPO	Erythropoietin
E_R	Recoil Energy
f	Recoil-free fraction (Lamb-Mössbauer factor)
f_A	Debye-Waller factor of the absorber
f_S	Recoil free fraction of the source
Ft	Ferritin
g_N	Nuclear Landé factor
$\hbar$	Planck's constant
HbA	Adult haemoglobin ($\alpha_2\beta_2$)
HbF	Foetal haemoglobin ($\alpha_2\gamma_2$)
HMF	Hyperfine magnetic field
I	Spin quantum number
I/S	Inner-to-Surface iron sites

I_e	Spin of the excited state
I_g	Spin of the ground state
LHe	Liquid Helium
LIC	Liver Iron Concentrations
LN	Liquid Nitrogen
M	Nucleus Mass
MGTD	Molecular Genetics Thalassaemia Department of the Cyprus Institute of Neurology and Genetics
m_i	Spin quantum number
MRI	Magnetic Resonance Imaging
MS	Mössbauer Spectroscopy
NBIA	Neurodegeneration with Brain Iron Accumulation
NHHS	Non-Haem High-Spin
N_M	Number of Mössbauer nuclei per cm^2
Oxy-hb	oxyhaemoglobin
PBS	Phosphate-Buffered Saline
p_i	Mass fraction
PMMA	Poly (methyl methacrylate) - Plexiglass
p_n	Nucleus moment
PP	Polypropylene
p_γ	Photon's moment
RBC	Red Blood Cell
ROS	Reactive Oxygen Species
RT	Room Temperature – 298K
SFt	Serum Ferritin
SNR	Signal to Noise Ratio
SPF	Specific Pathogen Free
t	Effective thickness of the absorber
Tf	Transferrin
th3/+	β-thalassaemia heterozygous mouse
ThI	Thalassaemia Intermedia
ThM	Thalassaemia Major
TMF	Transgenic Mouse Facility
UCY	University of Cyprus

Z	Atomic number
α	Internal conversion coefficient
α_t	Total internal conversion coefficient
Γ	Peak Width, Full width at half maximum
Γ_{exp}	Experimental line-width
Γ_{nat}	Natural line-width
δ	Isomer Shift
ΔEq	Quadrupole Splitting
$\varepsilon(t)$	a zeroth-order Bessel function
η	Asymmetry parameter
HbA_2	A_2 haemoglobin ($\alpha_2\delta_2$)
μ_α	Mass absorption
μ_N	Nuclear magneton
$\rho(\tau)$	Charge density
σ_0	Resonance cross section
τ	Lifetime
χ^2	Reduced Chi-square Test

Introduction & Thesis outline

Thalassaemias are hereditary anaemias resulting from defects in haemoglobin production. The term thalassaemia is derived from the Greek, thalassa (sea) and haima (blood) because it was once thought to be limited around the Mediterranean Sea. β-thalassaemia, which is caused by any one of more than 200 mutations in the β-globin gene, is characterised by a decrease in the production of β-globin chains. It affects multiple organs and is associated with considerable morbidity and mortality. β-thalassaemia can cause various complications, including iron overload, bone deformities and cardiovascular illness. Iron deposition occurs in visceral organs causing tissue damage and ultimately organ dysfunction and failure. Cardiac events due to iron overload are still the primary cause of death. Patients are heavily dependent on frequent blood transfusions and medications. Even with the most modern treatments, patients face life threatening complications with reduced life expectancy.

Mössbauer Spectroscopy is a versatile technique used to study the environment of a nucleus, with the absorption and re-emission of gamma rays. This technique uses a combination of the Mössbauer effect and Doppler shifts to probe the hyperfine transitions as a consequence of the interactions between the nucleus and its surroundings. It has been used to study many problems in physics, chemistry, biology and materials science. Since there is a direct link between thalassaemia and iron, Mössbauer spectroscopy has been used in this field, mainly in the previous decades, by studying samples from human patients with various results. Major emphasis was given in β-thalassaemia major, leaving β-thalassaemia intermedia with little data. As the medical treatment of the patients has changed radically the recent years, modern studies are needed to evaluate the effectiveness not only in β-thalassaemia major patients, but also in patients with β-thalassaemia intermedia.

The aim of the present work is to utilize, for the first time, Mössbauer spectroscopy in a thalassemic mouse model, in order to investigate the iron complexes in all major visceral organs and provide data about how β-thalassaemia affects iron accumulation. Also, with this work we aim to study with Mössbauer spectroscopy blood samples from thalassaemia patients and look for iron complexes that up to now were not detected by mainstream biochemical tests.

Thesis outline

Chapter 1 covers the basic concepts around human iron homeostasis and thalassaemia disease. It describes how iron is absorbed from the body, the most important iron containing proteins, and how it is stored and transferred. Also, the pathogenesis of thalassaemia and how it is managed and treated are described.

Chapter 2 covers the fundamental theory of Mössbauer spectroscopy. The important Mössbauer spectral parameters, isomer shift, electric quadrupole splitting and hyperfine magnetic field splitting are explained and illustrated along with important various aspects and instrumentation.

Chapter 3 describes the Mössbauer experimental setup that was used for the purposes of this study and is installed at the nuclear physics laboratory of University of Cyprus. This chapter also provides details about the calibration method, the production of high transparency Mössbauer sample holders, the software used for the spectra analysis and various optimizations that were performed on the setup.

Chapter 4 is the first chapter of experimental results. Initially, the usefulness of the mouse model in relation to Mössbauer spectroscopy is evaluated. Subsequently, the iron in *wild-type* and thalassaemic mice was enriched with ^{57}Fe and samples from the blood and various organs were prepared and used for Mössbauer studies.

In chapter 5, blood samples from thalassaemia patients were acquired and studied by means of Mössbauer spectroscopy at 80K. The results are presented and discussed in relation to patients' medical data that were provided for the purposes of this study.

Finally, the last chapter summarises the results and the conclusions from this study and outlines future plans to extent this work.

Chapter 1

Human Iron homeostasis & β-thalassaemia

Iron is the fourth most abundant element of the earth's crust, and the second most abundant metal. It sits in the middle of the first transition series, it has incompletely filled d orbitals and therefore it has the possibility of various oxidation states, with the primary ones being Fe(II) and Fe(III). In biochemistry, Fe(II) and Fe(III) are frequently found with a coordination number of 6 giving octahedral stereochemistry. For octahedral complexes, iron can be observed in two spin states. Strong-field ligands (e.g. F^-, OH^-) give low-spin complexes while weak-field ligands (e.g. CO, CN^-) favour high spin complexes due to the maximum number of unpaired electrons. Four and five-coordinate complexes can also be found [1].

Iron is an essential bioelement found in almost all forms of life because of its ability to act as an electron donor, Fe(II), and as an electron acceptor, Fe(III). The special role of iron in health and disease was recognized from ancient times [2], but it was until 1932 that its importance was revealed, as convincing proof was provided that inorganic iron is needed for haemoglobin synthesis. In human metabolic process, iron serves as an oxygen carrier, as a transport medium for electrons within the cells, and as an integrated part of important enzyme systems in various tissues. In the human body, iron exists mainly in complex forms bound to proteins as haem (haemoglobin) or non-haem compounds (transferrin, ferritin) [2].

1.1 Human Iron homeostasis

The amount of iron in a healthy human adult is 4-5 g (40-50 mg/kg) of which 20-25 mg cycles daily for protein synthesis and cellular regeneration [3,4]. Haemoglobin, an oxygen-transport metalloprotein found in the Red Blood Cells (RBCs), contains about the two thirds of the total iron (2-3 g). Another 30-35% is stored in the liver and spleen primarily in the form of ferritin, an iron storage protein. Iron is also found in myoglobin, an oxygen-storage protein of the muscles and in smaller concentrations in the cells where it is essential for energy production, synthetic metabolism and other important functions. A small fraction of about 3mg is distributed to the tissues through the plasma bound to transferrin (Tf), which is an iron-transport glycoprotein [5,6].

Although iron is one of the most abundant elements of the earth's crust [1,5], iron scarcity is a condition that most organisms face due to the low solubility of natural iron oxides [5], hence iron deficiency is one of the most common nutritional disorders [7]. Iron is also biochemically toxic because of its ability to act as an electron donor and acceptor. Iron ions can easily form free radicals which can cause excessive tissue damage and DNA oxidation [1,4,8,9]. For these reasons, iron is efficiently economized and reused, with its absorption, transport and storage tightly regulated. Due to the efficient iron reutilization from the human body, iron excretion is not actively controlled. The body loses only 1-2 mg of iron per day, due to skin desquamation, exfoliation of mucosal cells of the gastrointestinal tract, urination and bleeding [1,4,10]. In the whole iron cycling process, there are four key cell types involved; the intestinal enterocytes, the erythroblasts, the splenic macrophages and the hepatocytes [6]. Figure 1.1 *shows the iron cycle in the human body.*

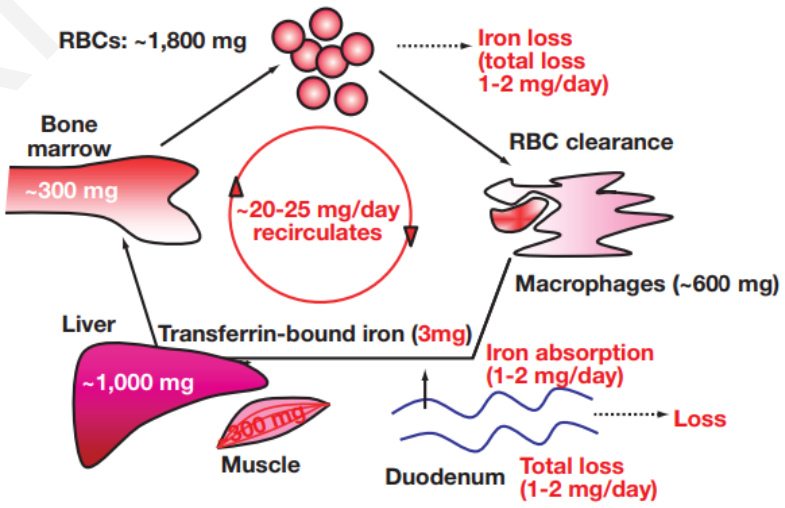

Figure 1.1: *Major iron flows and iron quantities found in human adults in normal conditions [6]*

1.1.1 Iron Absorption

Because of the minimum iron loses, the body's iron levels are mainly controlled through dietary iron absorption. To compensate the loses, the body absorbs through the duodenum[1] 1-2 mg of iron each day, which is only a small fraction of the daily cycling quantities. Iron in the diet exists in two major pools; non-haem iron found in plant-based foods and haem iron found in meat, fish and poultry. Non-haem iron is mainly composed from inorganic Fe(III) which has low solubility and therefore it must be firstly reduced to Fe(II) in order to be absorbed by the enterocytes[2]. Haem iron is absorbed by the enterocytes where it is degraded. In general, non-haem iron is not efficiently absorbed by the body while haem iron is absorbed well.

The iron from the enterocytes is released into the circulation via the metal transporter ferroportin where it binds to transferrin for further distribution [1,11]. Alternatively, the ferrous Fe(II) iron can be incorporated into ferritin. Gastrointestinal iron absorption is controlled mainly by the iron-regulatory hormone hepcidin which is secreted by the hepatocytes in the liver.

1.1.2 Erythropoiesis and erythrophagocytosis

The red blood cells (RBCs) are the most common cells in the human body and their primary function is to deliver oxygen to the tissues. They have a concave shape and are filled with 300 million molecules of haemoglobin. The average person produces about 2 million red blood cells per second thus from the 20-25 mg of iron that circulates daily, about 90% is used for the process of erythropoiesis, the production of RBCs. Erythropoiesis happens primarily in the bone marrow, or in the spleen and liver in periods of extreme erythropoietic stress [12]. RBC production is mainly controlled by erythropoietin (EPO), a protein growth factor secreted by the kidneys which stimulates the production of red blood cells in response to cellular hypoxia (e.g. from anaemia or hypoxaemia). Low levels of EPO are constantly secreted to stimulate normal erythropoiesis [1,13].

In the bone marrow, haemopoietic stem cells develop to erythroblasts in a multistep process seen in *Figure 1.2*. The most differentiated erythroblasts extrude their nucleus forming the reticulocytes, and get released into the blood stream. After one to two days, they shed specific membrane proteins like the transferrin receptors and internal organelles such as the

[1] Duodenum is the first part of the small intestine

[2] Enterocytes are absorption cells found in the small intestine

mitochondria [12] and differentiate further into mature RBCs, the erythrocytes, which under normal conditions continue to circulate for another 100-120 days [6,14].

The senescent RBCs are removed from circulation though the process of erythrophagocytosis which is carried out mainly by the macrophages of the spleen. There, the aged, inflexible RBCs get trapped within the spleen and get digested by the macrophages. The haem moieties get separated from the haemoglobin and the globin chains break down into amino acids. At the same time, the ferrous iron is removed from the haem compound. Just as in the enterocytes, the ferrous iron can be incorporated into ferritin or released into circulation by ferroprotein [6]. Phagocytosis can also happen in the liver and in the bone marrow. In each cycle, a small amount of iron is transferred to storage sites (mainly to the liver) where it is incorporated into ferritin [1].

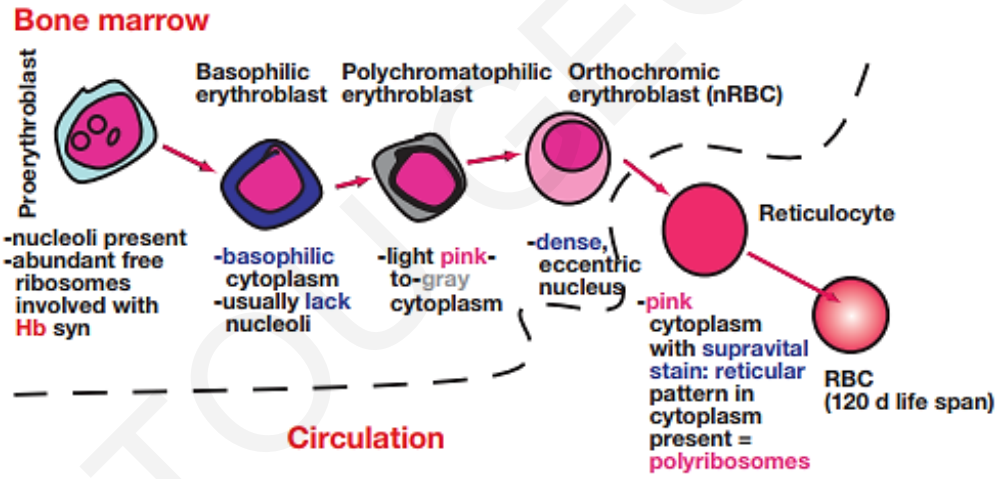

Figure 1.2: An outline of the multistep process where the erythroblasts transfrom into RBCs [6]

1.1.3 Major Iron Containing proteins

1.1.3.1 Haemoglobin (Hb)

Haemoglobin is an essential to life iron-containing metalloprotein found in the RBCs of almost all vertebrates. Its main function is to transport oxygen (O_2) from the lungs to the tissues It is also used to transport carbon dioxide (CO_2), carbon monoxide (CO) and nitric oxide (NO). The synthesis of haemoglobin takes place in the ribosomes and the mitochondria of the erythroid cells during the production cycle of erythrocytes; from the pro-erythroblast until the reticulocyte stage [12,15]. Mature RBCs do not produce haemoglobin as they lack the needed

ribosomes and mitochondria. Each haemoglobin molecule consists of two symmetric pairs of identical globin chains, (two alpha and two non-alpha chains), for a total of four chains per molecule that bind together to form a functioning tetrameric structure. The globin chains are synthesized in the erythroid cells and are encoded by genes located in two different clusters. The α-globin gene locus is located at chromosome 16 and consists of the embryonic ζ gene and the two adult α gens. The β-globin gene locus is located on chromosome 11 and consists of the embryonic ε gene, the two foetal genes $^{G}\gamma$ and $^{A}\gamma$, and the two adult genes β and δ. Since each cell has two copies of each autosomal chromosome, there are four alpha and gamma globin genes in the cell, and two beta genes.

Each globin chain contains a haem moiety which is produced in the mitochondrion from a protoporphyrin IX ring structure and an iron atom. This iron atom is coordinated to 4 pyrrole nitrogen atoms in one plane, to an imidazole nitrogen atom of the invariant histidine amino acid at position 8 of the "F"-helix, and to a gas atom on the opposite site [16] as seen in *Figure 1.3*.

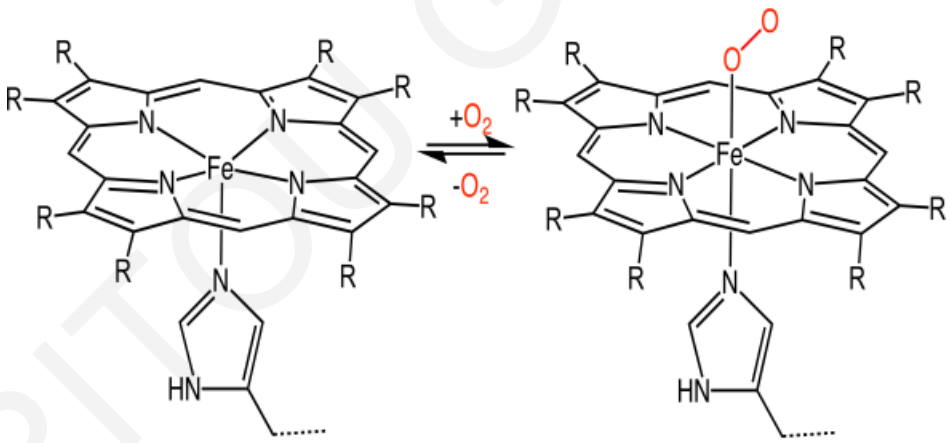

Figure 1.3: *The structure of the haem prosthetic group without* ***(left****) and with (****right****) an* O_2 *ligand*

With the exception of the very first weeks of embryogenesis, one pair of the globin chains is always alpha. The foetal haemoglobin (HbF), which is the main haemoglobin in human foetus and new-borns until the age of six months old, consists of two α- and two γ-chains ($\alpha_2\gamma_2$). At this age, HbF is replaced mainly by the adult haemoglobin HbA which consists of two α- and two β-chains ($\alpha_2\beta_2$). In normal conditions, human adults have 97% HbA ($\alpha_2\beta_2$), 2% HbA_2 ($\alpha_2\delta_2$) and 1% HbF ($\alpha_2\gamma_2$), but the ratio can change in various diseases like thalassaemia [16]. The structure of adult haemoglobin HbA is shown in *Figure 1.4* with the two α- and β-chains in red

and blue respectively and the haem structure in grey. Haemoglobin can also exist without an attached gas ligand. In this state it is called deoxy-haemoglobin (Deoxy-Hb) and the iron atom is in the ferrous Fe(II) state.

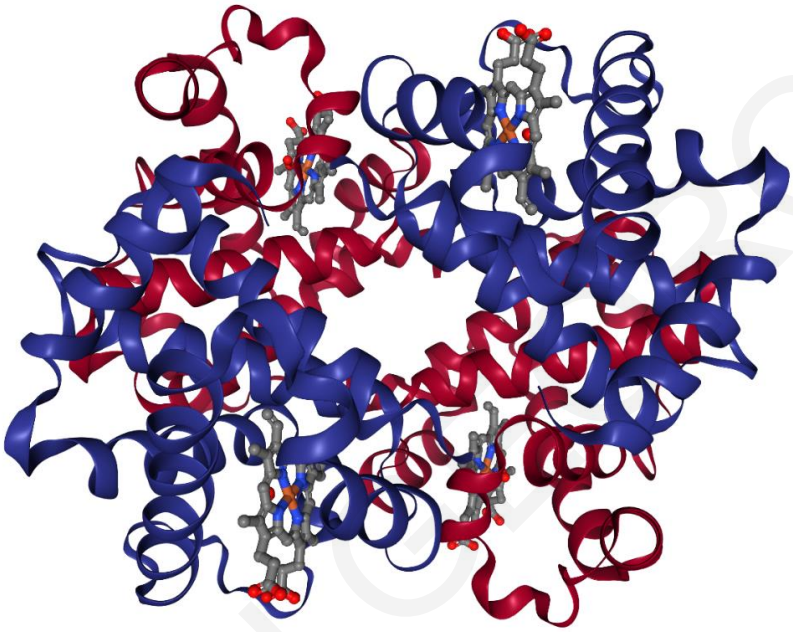

Figure 1.4: *HbA haemoglobin that consists of two α-chains (red) and two β-chains (blue). The iron containing haem group (grey structure) which is present in each globin chain is also shown [17]*

1.1.3.2 Ferritin and Haemosiderin

Ferritin (Ft) is an iron storage protein which exists in both intracellular and extracellular compartments and keeps iron in a soluble and non-toxic form. It provides a reserve for the element in times of increased needs, like in sudden blood loss, and it also safe-guards the cells from the potentially toxic free iron. Most ferritin is found in the liver, spleen and bone morrow, while a trace amount is found in the serum of the blood (serum ferritin - SFt) [11,17].

The ferritin molecule is composed of a hallow spherical protein shell with an outside diameter of 12-13 nm and a 7-8 nm central cavity in which a mineral iron core exists, as seen in *Figure 1.5*. The mineral core can hold 2000-4500 Fe(III) oxy-hydroxy-phosphate molecules. The protein shell (called apoferritin) in humans is composed of 24 polypeptide subunits of two different types, which are found in all the mammalians and are known as H- and L- polypeptide chains [17,18]. H-chains are important for Fe(II) oxidation (ferroxidase) while the L-chains assist in core formation (nucleation) [18]. The ratio of these subunits varies and depends on

the tissue type, and it can be modified in inflammatory and infectious conditions. H-chain rich ferritin is found mostly in the heart and kidneys, while L-chain rich ferritin is found in liver and spleen, and is characteristic of iron storing organs [17,18]. The centre cavity is connected to the surface by three-fold and four-fold channels which are formed at the intersection of the L and H subunits [19].

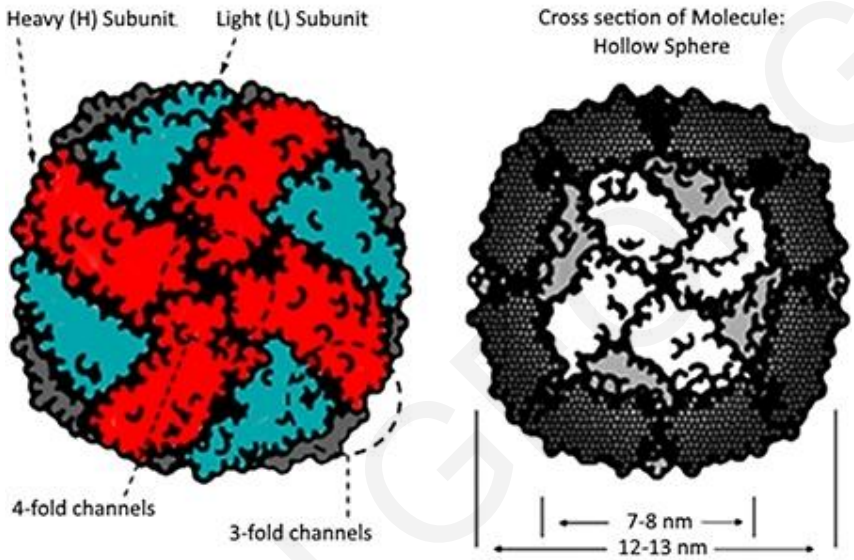

Figure 1.5: *Schematic representation of Ferritin. Ferritin has a hallow spherical shell that consists of 24 subunits of two types (H- and L- chains). The internal cavity has a diameter of 7-8 nm. At the intersection of the subunits, three-fold and four-fold channels are present that connect the internal cavity to the surface [19].*

Under condition of iron excess, iron can be stored in another form known as haemosiderin. Despite the name, it is a non-haem compound. It is an insoluble amorphous iron containing complex that is produced by the uptake of aggregated ferritin molecules into lysosomes[3] [6]. It accumulates in the macrophages and due to its size (1-2 μm), haemosiderin can be visible under light microscopy using tissue iron stains.

Serum ferritin (SFt)

Ferritin is also present extracellularly in the serum but in very small amounts. SFt was found to be correlated with total body iron stores thus it is used widely as a laboratory test for their

[3] The lysosomes are organelles found in the cells and contain hydrolytic enzymes in order to break down biomolecules. They also act as the waste disposal system of the cell.

estimation at a present time. However, the levels of SFt can be affected from various conditions like liver disease, acute and chronic inflammation and infection. Therefore, when using SFt as a biological marker to evaluate the iron stores, the data should be interpreted carefully [6,11].

1.2 Iron Overload

When for various reasons iron intake is increased, iron starts to accumulate in the body and iron overload occurs. When this happens, transferrin gets saturated and non-transferrin-bound iron (NTBI, also known as unbound or free iron) starts to circulate in the blood. Free iron, which is not safely shielded, is highly reactive and easily alternates between the Fe(II) and Fe(III) states, gaining and releasing electrons. Hence it has the capacity to generate highly reactive oxygen species (ROS) through the Fenton and Haber-Weiss reactions:

$$Fe^{2+} + H_2O_2 \rightarrow Fe^{3+} + OH^- + HO\cdot \quad (1.1)$$

$$Fe^{3+} + \cdot O_2^- \rightarrow O_2 + Fe^{2+} \quad (1.2)$$

$$\cdot O_2^- + H_2O_2 \rightarrow O_2 + OH^- + HO\cdot \quad (1.3)$$

ROS are known to cause an immersive amount of damage to cell membranes, organelles, DNA, and to various organs including the heart, liver, pancreas, endocrine glands and erythroid cells [20,21]. Therefore, iron overload can be toxic to many tissues causing heart failure, cirrhosis, liver cancer, growth retardation and endocrine abnormalities [20]

1.3 β-thalassaemia

Thalassaemias are a group of hereditary blood disorders that characterized by reduced or absent synthesis of normal globin chains due to single gene mutations. They are a major problem in the countries around the Mediterranean Sea, the Middle East, India, Central Asia and the Far East [20,22]. Unfortunately, due to population migration, thalassaemia has been introduced in almost every country of the world. The highest carrier frequency of β-thalassaemia is reported in Cyprus (14%), Sardinia (10.3%) and Southeast Asia. The high frequency in these regions is most likely resulting from selective pressure from Malaria [22].

Globally it is estimated that the 1.5% of the population are carriers of β-thalassaemia and about 60 000 symptomatic individuals are born annually [22].

Depending on the chain whose synthesis is impaired, the thalassaemia take the appropriate name. The most relevant types are α- and β-thalassaemia and result from the problematic synthesis of one of the two types of polypeptide chains that form the adult human haemoglobin HbA.

Responsible for β-thalassaemia are more than 200 mutations of the *HBB* gene which provides instructions for making the β-globin chains and the nature of the mutation determines the imbalance of the globin chains. β^0 refers to mutations which result in the complete absence of production of β-globin chains, β^+ refers to mutations with some residual production (~10%) while β^{++} refers to mutations with very mild effects on β-globin production.

As thalassaemia is a recessive disorder, defective genes from both parents must be inherited in order to develop severe clinical conditions. Individuals that inherit defective genes from both parents are described as homozygotes while individuals with only one defective gene are described as heterozygotes or carriers or having a β-thalassaemia trait. In Greece and Cyprus, individuals that have the β-thalassaemia trait are called "στίγμα (stigma)" carriers. Parents that are both β-thalassaemia trait carriers have 1 in 4 (25%) risk to affect their children with β-thalassaemia and 50% of being a carrier. Thus, thalassaemia screening programs have been implemented in various countries with significant results.

1.3.1 Pathophysiology of β-thalassaemia

As mentioned in the previous paragraphs, the blood of the foetus contains a different type of haemoglobin, called foetal haemoglobin (HbF), which is made up from one pair of α- and one pair of γ- globin chains. After birth, foetal haemoglobin continues to be produced at relatively high levels for the first six months of life but it is gradually replaced with the HbA adult haemoglobin which is made up of two α- and two β-chains. However, in β-thalassaemia the production of β-globin chains is reduced or absent and α-chains are in relative excess. This leads to a decrease in haemoglobin production and imbalance of the globin chains synthesis which only becomes apparent after adult haemoglobin replaced foetal haemoglobin. The chain imbalance and subsequently accumulation of α-globin chains leads to premature destruction of the red cell precursors in the bone marrow, a process referred to as "ineffective erythropoiesis" and is a hallmark of β-thalassaemia [20]. Because haemoglobin production is severely limited, the effective production of RBCs can be reduced by 95% [4]. Furthermore, as

the body produces normal amounts of α-chains that cannot be paired further on, they start to accumulate and deposited in the RBCs damaging their membranes and leading them to premature destruction, a process known as haemolysis. The ineffective erythropoiesis and the consequently reduced number of RBCs, along with their premature destruction and the observed haemolysis, leads to severe cases of anaemia with deadly complications if left untreated.

Thalassaemia patients with severe anaemia are pale, have slower rates of physical growth and suffer from tachycardia and abnormal heartbeat as the heart tries to compensate for the reduced oxygen capacity by beating faster which causes the heart to enlarge. The body, in response to anaemia starts to expand the bone marrow in order to produce more RBCs in an effort to increase their reduced numbers. This in turn forces the bones to expand resulting to deformities in the skull, the ribs and the vertebrae. The bones also become thinner and more fragile. The spleen, the organ responsible for breaking down the damaged RBCs, must also cope with the hyperactive bone marrow and the increased numbers of RBCs, therefore itself becomes overactive and enlarges. A condition known as hypersplenism. The overactive spleen, in addition to the damaged RBCs also destroys some white cells and young RBCs further worsening the symptoms. Due to the extreme haemopoietic stress, the spleen also starts to produce RBCs itself, further contributing to its enlargement. In response to anaemia, the body also starts to absorb more iron from the gastrointestinal tract which makes the situation worse as thalassaemia patients suffer from anaemia because of inefficient production of RBCs and not because of iron shortage. This error exposes the body to secondary iron overload with additional and severe complications. A diagram of β-thalassaemia's pathogenesis is shown in *Figure 1.6.*

The clinical severity of the disease (phenotype) corelates to the combination of the mutations. Thus, a broad spectrum of phenotypes can be observed. Based on this, three main β-thalassaemia forms have been described; β-thalassaemia major, β-thalassaemia intermedia and β-thalassaemia minor. **β-thalassaemia major** also known as "Mediterranean anaemia" and "Coolley's Anaemia", is the most serious form of β-thalassaemia and occurs when both defective genes carry a severe mutation. Anaemia, mild jaundice and hepatosplenomegaly occurs from the young age of 6-24 months. If left untreated, the patients suffer from growth retardation, jaundice, poor musculature, hepatosplenomegaly, ulcers and skeletal deformities due to the expansion of bone marrow and they usually die within the first few years of life. The necessary regular blood transfusion therapy leads to severe iron overload and its related complications like endocrine problems, growth retardation, failure of sexual maturation,

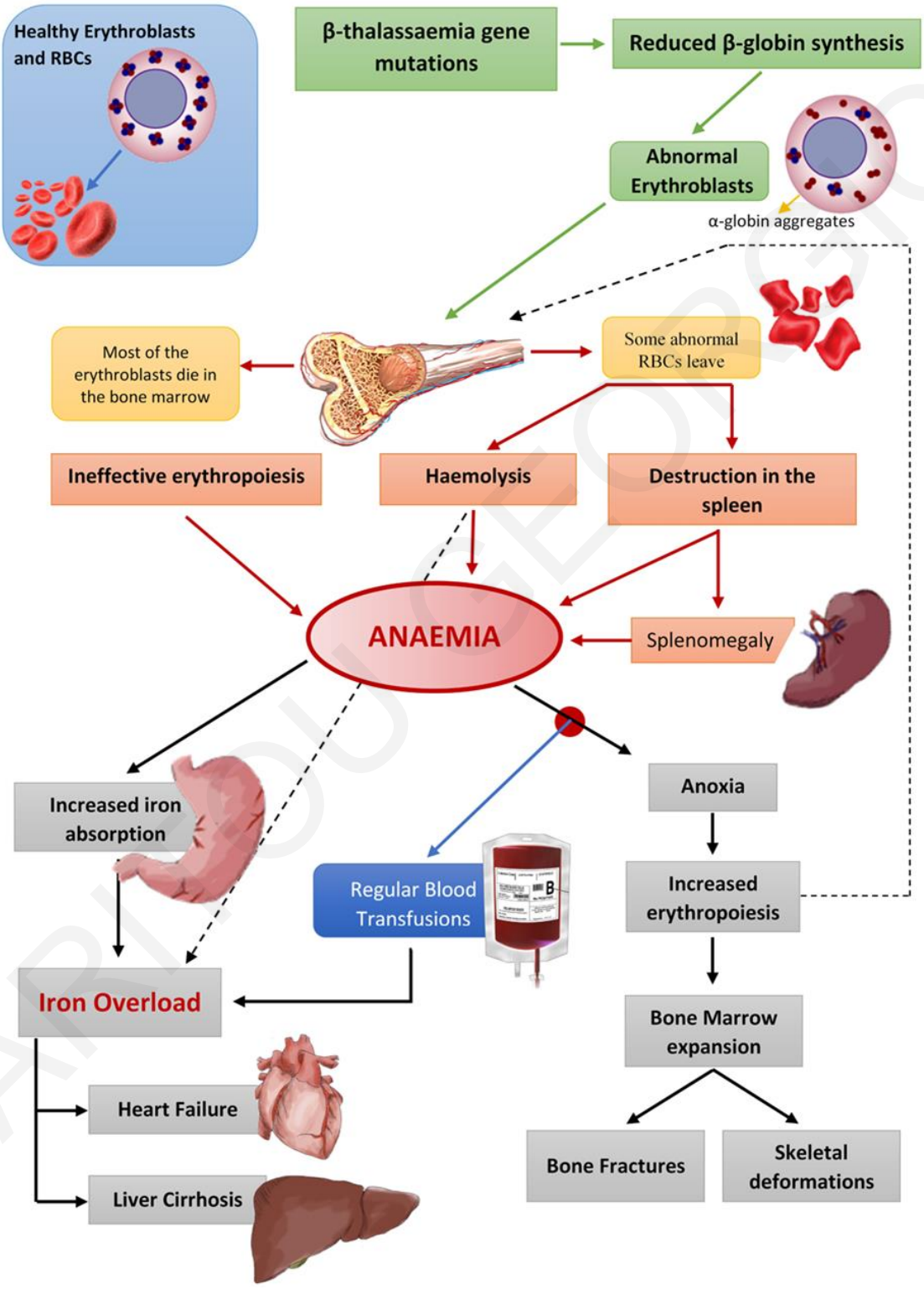

Figure 1.6: *Diagram of the pathogenesis of β-thalassaemia and the major complications*

diabetes mellitus, myocardiopathy, liver fibrosis and cirrhosis. **β-thalassaemia intermedia** which appears when at least one of the two defective genes carries a mild mutation, exhibit a broad range of phenotypes. Thalassaemia intermedia patients can show mild to moderate anaemia later in life, prominent splenomegaly and bone deformities. Depending on anaemia's severity, they are capable of surviving without regular blood transfusions. However, they are also at risk of iron overload due to increased gastrointestinal absorption. Individuals with **β-thalassaemia minor**, (heterozygous β-thalassaemia, trait of carriers) have only one defective gene and are usually clinically asymptomatic or they might experience mild to moderate anaemia.

1.3.2 β-thalassaemia management

The only known cure today for thalassaemia is bone marrow transplantation (BMT) from a healthy donor, which is by itself a serious medical procedure. Unfortunately finding a matching donor is difficult, and the transplantation procedure itself requires sophisticated medical infrastructure and knowledge. Therefore, only a minimum number of thalassaemia patients can try bone marrow transplantation. Besides BMT, other approaches for thalassaemia's cure are explored, with the most promising of them being the foetal haemoglobin inducers, where special drugs can increase the production of γ-chains in order to form HbF with the excess α-chains, and gene therapy where healthy genes can be transferred into the patient's bone marrow stem cells [4]. For the most patients, managing the symptoms is the only available approach.

Blood Transfusions

The goal of blood transfusions is to counter anaemia and supress the increased but ineffective erythropoiesis in order to reduce the resulting complications. Thus, for most thalassaemia patients, regular blood transfusions is a life-long treatment that starts from a very young age. Although blood transfusions are life savers for thalassaemia patients, they expose the patients to a variety of complications and risks thus, they are started with confirmed diagnosis of thalassaemia, when severe anaemia is present (Hb < 7 g/dl), or when physical characteristics are noted [4,22]. Transfusion regimes aim to keep the patient's haemoglobin levels between 9-10 g/dl before transfusion and 13-14 g/dl after [22]. This prevents most of the complications like growth impairment, organ damage and bone deformities allowing at the same time relatively normal activity and quality of life.

The volume of blood a patient requires, and the frequency of transfusion depend on the clinical status and the age of the patient. In moderate transfusion regimes, patents usually receive 10-

15 ml of concentrated RBCs per kg, transfused over 3-4 hours, every 2-5 weeks [4]. An average unit of blood contains about 250 ml of packed RBCs, with each ml of pure RBCs containing about 1.08mg of iron [20]. A 40 kg patient that receives 600 ml of blood every 4 weeks receives about 7.8 L of blood or 4.7 L of pure RBCs per year ($600\,ml \times 13\,transfusions \times 60\%\,average\,haematocrit = 4.7\,L\,of\,pure\,RBCs$). This is equal to an annual iron uptake of about 5 g or 13.5 mg (0.34 mg/kg) of Fe daily, much higher than the body's needs. Thus, iron overload is the most relevant complication associated with regular blood transfusion therapy as without further treatment it can be fatal even from the second decade of life.

Iron chelation therapy

Due to the nature of the disease, thalassaemia patients are subject to increase iron intake, either from the frequent blood transfusions or to a lesser extend from increase gastrointestinal absorption. Combined with the fact that the human body does not have an iron excretion mechanism this leads to significant iron accumulation in the organs with serious and deadly consequences as explained previously. Iron chelation therapy since its introduction in the 1970s, is responsible for a significant increase in the life expectancy of thalassaemia patients (*Figure 1.7)*.

The aim of iron chelation therapy is to counter the lack of iron excretion mechanism from the body and eventually manage the iron accumulation due to the increased iron intake. A key challenge of iron chelation therapy is to balance the benefits with the unwanted site effects, as iron is essential for other physiological purposes. Hence monitoring iron overload is crucial. Serum ferritin (SFt) generally correlates with body iron stores, and because its assessment is easy and inexpensive it is used widely in order to identify trends. SFt values below 2500 μg/L have been linked with significantly lower risk of cardiac disease and death, while SFt levels of 1000 μg/L may be associated with additional clinical advantages [20]. However, SFt levels can be influenced by other factors and diseases therefore as a single value it can be an unreliable marker to assess iron chelation response and the overall iron burden [20,22]. One other way to assess iron statues beside serum ferritin, is by measuring the liver iron concentration (LIC). This can be done directly with liver biopsy which is considered the gold standard for the evaluation of iron overload [22]. However, liver biopsy, is an invasive technique with possible complications. In recent years one other non-invasive technique is used for assessing iron overload in the liver and heart, the nuclear magnetic resonance imaging (MRI). Despite the fact that MRI is a non-invasive technique, it is expensive thus it cannot be repeated as frequently as SFt measurements.

Iron chelation therapy works by using special iron binders (chelators) that bind iron and remove it from the body through urine and/or stool. Three different drugs are available for iron overload treatment. Deferoxamine (DFO, Desferal), is the first iron chelation drug to be manufactured and was introduced in the 1970s. It is administrated by prolonged parenteral infusion, daily, for 8-12 hours, or by an implanted delivery system. However, because of the inconvenient method of administration and the side effects, a consistent proportion of patients cannot comply with this treatment, limiting its usefulness, even though DFO is an effective drug that decreases morbidity and mortality. The second drug, Deferiprone (DFP or L1), in contrast to DFO is administrated orally and is effective at reducing myocardial siderosis. It can be used in combination with DFO in order to increase iron excretion without increasing toxicity. The third drug, Deferasirox (DFX or ExJade), is the newer and was introduced in the 2000s. It is also an orally administrated iron chelator with promising effectiveness. Despite their effectiveness in reducing the iron burden, iron chelation therapy has side-effects like gastrointestinal problems or even renal and hepatic failure, therefore carefully monitoring is needed.

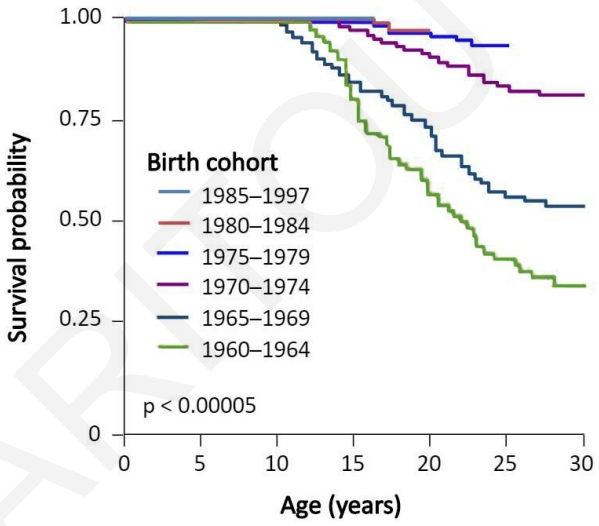

Figure 1.7: *Kaplan-Meier survival curves for Italian β-thalassaemia major patients relative to birth cohort that shows the increased survival rate as a result of the modern medical treatment and iron chelation therapy [23]*

Chapter 2

Mössbauer Spectroscopy

Since the 1930s and for almost 30 years, the observation of nuclear resonance absorption was a problem plaquing the experimental physicists. A nucleus in an excited state during his transition to the ground state, emits a γ-ray which subsequently should be absorbed by an unexcited nucleus of the same isotope ending in the same excited state. However, when a γ-photon is emitted during the transition, it imparts a recoil momentum to the nucleus due to the conservation of momentum meaning that the γ-photon will have less energy than the resonant line. This leads to a separation of the centres of the emission and absorption lines by twice the recoil energy. For nuclear transitions the recoil energy is much greater than the absorption and emission linewidths, therefore it is impossible for a free nucleus to excite a second one of the same species. For comparison, in optical resonance absorption the electronic transition energies are much smaller, in the order of a few eV, and the resultant recoil energy losses are negligible. Therefore, the emission and absorption lines overlap significantly.

To overcome this problem and reduce the "distance" between the emission and absorption lines in order to increase their overlapping area, some research groups tried to solve this issue by making use of the Doppler effect. Physicist Philip Moon(1951) [23] mounted the radioactive source on centrifuge and moved it towards the target in high velocities while Karl Malmfors (1953) heated both the source and the absorber with the aim that the broadened linewidths would overlap [24]. Both groups had little success.

In 1958, a German physicist named Rudolf Mössbauer discovered during his doctoral thesis the solution of the problem. For his discovery and the subsequent explanation of the effect, he was awarded the Nobel Prize in Physics in 1961. Mössbauer used a liquid nitrogen (LN) cooled ^{191}Os radioactive source which he placed on a rotating base, and an ^{191}Ir absorber in front of a detector (*Figure 2.1)*. In contrast to the previous groups, with this methodology Mössbauer tried to directly solve the problem rather than reducing its consequences. By cooling the source, Mössbauer manage to bound the nuclei onto a crystal eliminating the recoil energy losses. This approach gave him the ability to observe the nuclear resonance absorption. The first Mössbauer spectrum taken by Rudolf Mössbauer [25] is shown in *Figure 2.2*.

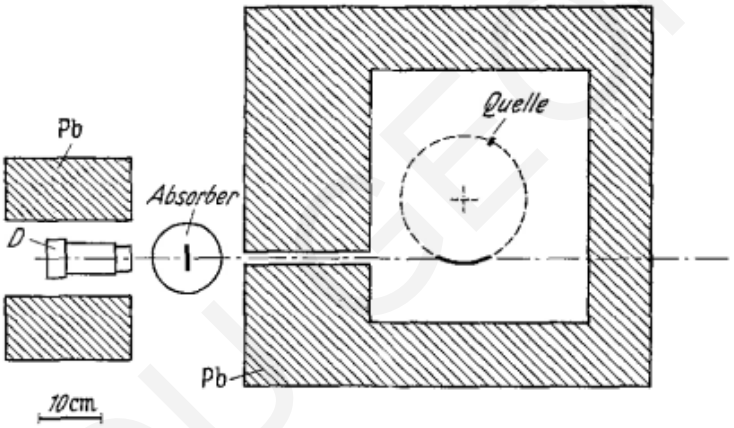

Figure 2.1: *The experimental setup used by Rudolf Mössbauer for the discovery of the effect [26]*

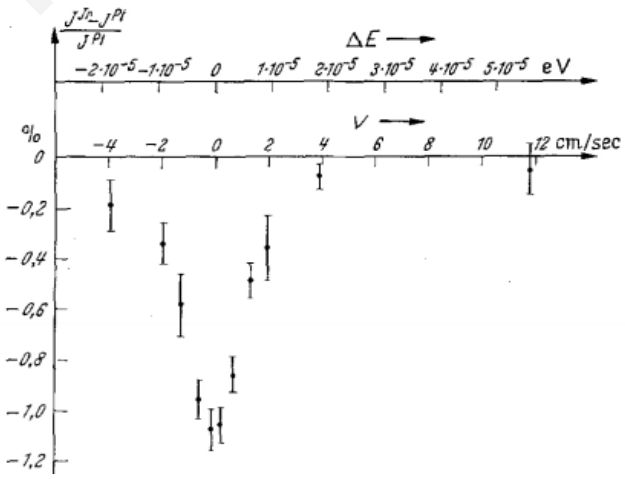

Figure 2.2: *The first Mössbauer spectrum taken by Rudolf Mössbauer using an ^{191}Os source and an ^{191}Ir absorber [25]*

The Mössbauer effect (bearing his name), is also known as recoilless nuclear resonance absorption. The resulting spectroscopic technique, Mössbauer spectroscopy, has been used in physics, chemistry, metallurgy, biology and material sciences, for problems directly related or arising from the electronic shell of the atoms and the charges around the nucleus, hence it serves as a fingerprint technique in the characterisation of materials. It is also utilized for the determination of the lifetimes of excited nuclear states, to study the electric and magnetic fields in atoms and crystals, for measurements of nuclear magnetic moments and for testing the special relativity among others.

2.1 The Mössbauer Effect

2.1.1 γ-photon emission

After a nuclear reaction (α-, β-decay and K-capture), an isotope is created in an excited state *(e)* with energy E_e. The excited nucleus has a limited lifetime τ and according to the exponential law of decay, will undergo a transition to its ground state *(g)* with energy E_g emitting a γ-photon. If the process occurs without energy losses, the γ-photon's energy will be $E_0 = E_e - E_g$ and a similar nucleus in the ground state will have the ability to absorb this γ-photon as shown in *Figure 2.3*.

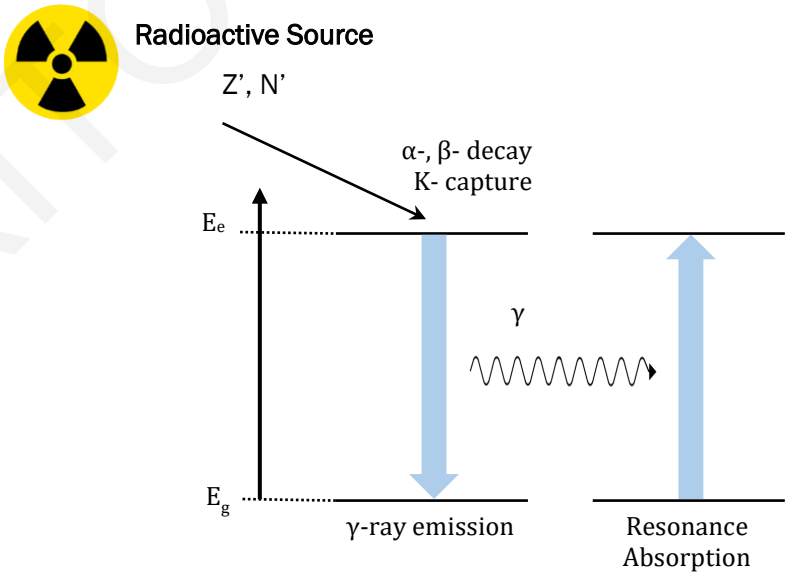

Figure 2.3: *Nuclear resonance absorption of γ-rays for a nucleus with Z protons and N neutrons*

2.1.2 Line width and shape

A nuclear (or electronic) excited state with a mean lifetime τ, does not have a specific energy, but exhibits a distribution ΔE around the mean value E_0. Responsible for this, is the Heisenberg's uncertainty relation:

$$\Delta E \Delta t \geq \hbar \tag{2.1}$$

where $h = 2\pi\hbar$ is the Planck's constant and $\Delta t \approx \tau$ the limited time interval available for the measurement.

As a result, the energy E of the photons emitted upon transition between the energy states scatters around the mean energy $E_0 = E_e - E_g$ (emission line) with an intensity that follows a Lorentzian curve (*Figure 2.4)* given by the Breit-Wigner equation [24]:

$$I(E) = \frac{\Gamma_{nat}/(2\pi)}{(E-E_0)^2+(\Gamma/2)^2} \tag{2.2}$$

where Γ_{nat} is the natural width (full width at the half maximum - FWHM). For $E = E_0 \pm \Gamma_{nat}/2$, $I(E) = \frac{1}{2} I(E_0)$.

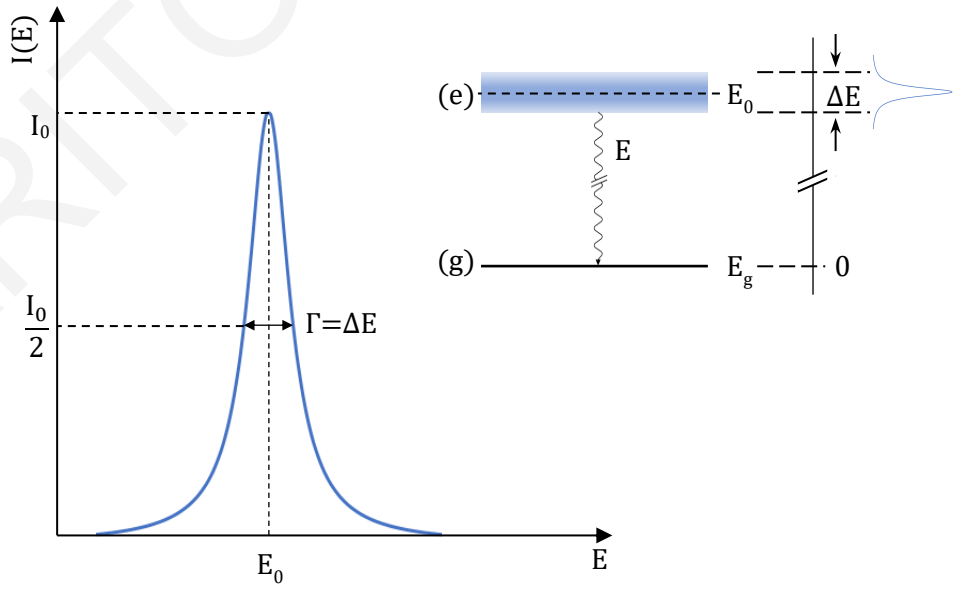

Figure 2.4: *Intensity distribution for the emission of γ-rays with a mean transition energy* E_0

Because of time-reversal invariance, the corresponding absorption line has the same shape as the emission line. The natural linewidth of the emission and absorption lines, as shown by the Weisskopf and Wigner, is determined by τ:

$$\Gamma_{nat}\tau = \hbar \tag{2.3}$$

Substituting in *Eq. 2.3*, $\tau = 1.43 \times 10^{-7}\ s$ (mean lifetime of the first excited state of ^{57}Fe), and $\hbar = 6.58 \times 10^{-16}\ eV \cdot s$, we find that the natural linewidth Γ_{nat} of the ^{57}Fe is equal to $4.60 \times 10^{-9}\ eV$. Compared to the isotope's γ-energy of 14.41 keV, this gives a relative resolution of 1 in 10^{12}.

$$\frac{\Delta E}{E_0} = \frac{4.6\times10^{-9}eV}{14.41\times10^{3}eV} \cong 10^{-12} \tag{2.4}$$

2.1.3 Nuclear Recoil

When a photon is emitted from a nucleus of mass M, recoil is impaired and consequently the nucleus moves with a velocity υ in the opposite direction of the photon's propagation vector. For a nucleus that was at rest, the recoil energy E_R is given by:

$$E_R = \frac{1}{2}M\upsilon^2 \tag{2.5}$$

and due to the requirements of momentum conservation:

$$p_n = -p_\gamma \tag{2.6}$$

with $p_n = M\upsilon$, $p_\gamma = -\frac{E_\gamma}{c}$, $E_\gamma = E_0 - E_R$ and c is the speed of light.

Because of the large mass of the nucleus and the low recoil velocity, Eq. 2.5 can be rewritten using the nonrelativistic approximation:

$$E_R = \frac{1}{2}M\upsilon^2 = \frac{(M\upsilon)^2}{2M} = \frac{p_n^2}{2M} = \frac{E_\gamma^2}{2Mc^2} \tag{2.7}$$

Assuming that $E_R \ll E_0$, $E_\gamma \approx E_0$ and therefore Eq. 2.6 can be written as:

$$E_R = \frac{E_0^2}{2Mc^2} \tag{2.8}$$

By substituting $M = m_{n/p}A$, where A is the mass number of the Mössbauer isotope and $m_{n/p} = 1u = 931.5\frac{MeV}{c^2}$ the mass of a nucleon, *Eq. 2.8* transforms to:

$$E_R = 5.37 \times 10^{-4} \frac{E_0^2}{A}\ eV \tag{2.9}$$

For the ^{57}Fe and the $E_0 = 14.4\ keV$ transition, $E_R = 1.95 \times 10^{-3}\ eV$, six orders of magnitude larger than the natural linewidth ($\Gamma_{nat} = 4.60 \times 10^{-9} eV$) of the transition.

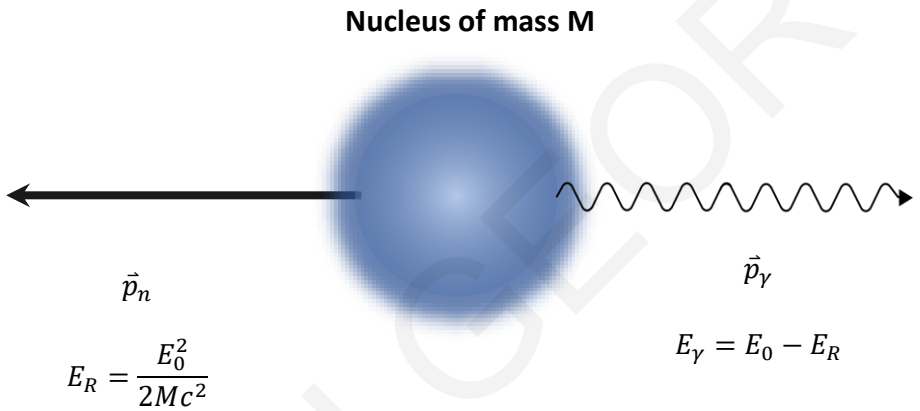

***Figure 2.5**: Recoil momentum imparted to a free nucleus upon γ-ray emission*

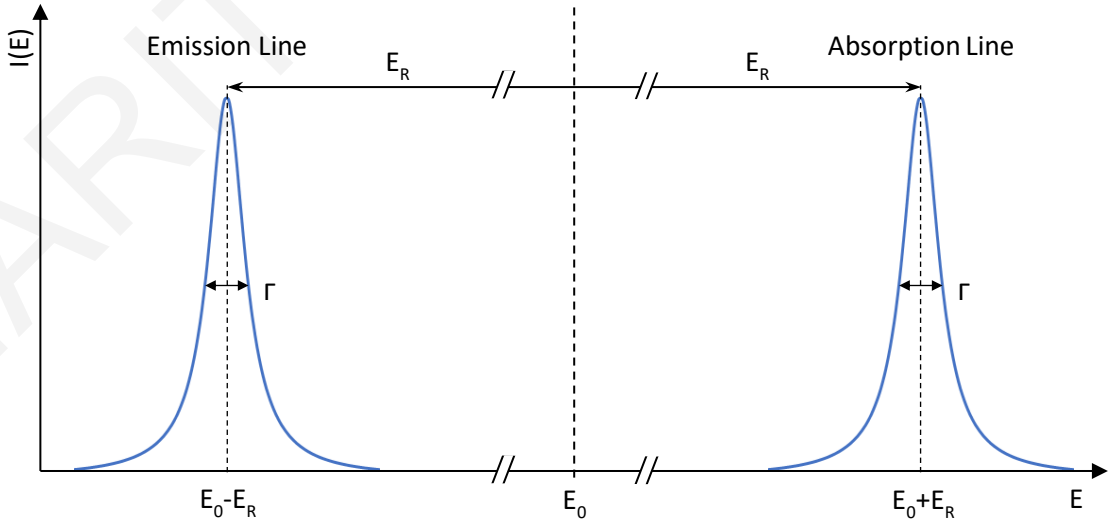

***Figure 2.6**: Energy separation between the γ-emission and absorption lines in a free nucleus caused by recoil*

The recoil effect and the corresponding energy shift occurs during the emission and during the absorption of the γ-photon. Therefore, the outcoming γ-photon carries energy $E_\gamma = E_0 - E_R$ while the nucleus requiring a γ-photon with energy $E_\gamma = E_0 + E_R$ in order to be excited. Therefore, an energy difference of $2E_R$ is observed. As the energy deficiency of the γ-photon is 10^6 times larger than the natural width, no overlap between the emission and absorption lines is observed, thus nuclear resonance absorption of γ-photons is not possible between free atoms. However, in contrast to the free nuclei, in the solid state a nucleus is tightly bound to its environment, therefore, a part of the recoil momentum is taken by the whole crystal: $p = M_{crystal}\upsilon$. Since the mass of the crystal ($M_{crystal}$) is significantly larger than the mass of a free nucleus, the velocity υ of the emitter is effectively zero, making the recoil energy, $E_R = \frac{1}{2}M_{crystal}\upsilon^2$, negligible.

However, even when the Mössbauer nucleus is in the solid state, a part of the energy E_0 of the transition can be transferred to the lattice vibrational system exciting a phonon leading to energy deficit which is again orders of magnitude larger than Γ_{nat}. Fortunately, the quantum mechanical nature of the vibrational excitations of the lattice of the solid includes a finite probability (f) for this not to happen (known as the Lamb-Mössbauer factor or recoil-free fraction) [24]:

$$f = exp\left[-\langle x^2\rangle E_\gamma^2/(\hbar c)^2\right] \tag{2.10}$$

where $\langle x^2\rangle$ is the expectation value of the squared vibration amplitude in the direction of γ-propagation. The factor f denotes the probability of a γ-emission (or absorption) to occur without recoil and it depends on the oxidation state, the spin state, the elastic bonds of the atom and the temperature (it increases with a decreasing temperature) [24].

2.2 The Basics of Mössbauer Spectroscopy

For a nuclear resonance absorption to occur, the emission and absorption lines should overlap significantly. The more the lines overlap, the bigger the resonance absorption becomes. Therefore, less transmission occurs resulting to a decrease in the numbers of photons the counter detects. The resonance absorption cross section, as a function of the energy E, $\sigma(E)$, is given by [27]:

$$\sigma(E) = \sigma_0 \frac{\Gamma_{nat}^2}{4(E-E_0)^2+\Gamma_{nat}^2} \quad (2.11)$$

$$\sigma_0 = 2\pi\lambda\!\!\!^{-2} \left[\frac{2I_e+1}{2I_g+1}\right] \cdot \left[\frac{1}{1+a_t}\right] \quad (2.12)$$

Where σ_0 is the maximum cross section, I_e and I_g the nuclear spin of the excited and ground spate respectively, $2\pi\lambda\!\!\!^{-2}$ the Mössbauer line wavelength and $a_t = \frac{number\ of\ de-excitations\ via\ electron\ emission}{number\ of\ de-exitations\ via\ gamma\ ray\ emission}$ the total internal conversion coefficient.

For ^{57}Fe, the maximum cross section of the resonance absorption is σ_0=2.56x10^{-18} cm^2 [24] and is observed when $E = E_0$ where the emission and absorption lines overlap completely.

As in the most spectroscopic techniques, the photons from the source are recorded with a detector after passing through an absorber (sample). In addition to this, in a Mössbauer transition experiment the radioactive source or the absorber are moved towards and against each other with a controlled velocity υ in order to scan an energy area for the absorption line (*Figure 2.7)*. This motion modulates the energy of the γ-photons because of the doppler effect [28]:

$$\Delta E_{doppler} = E_\gamma \frac{\upsilon}{c} \quad (2.13)$$

For ^{57}Fe where E_γ=14.41 keV, a velocity of 1mm/s provides an energy shift $\Delta E = 48.1 \times 10^{-9}\ eV$. For convenience, the energy axis of a Mössbauer spectrum is presented in units of mm/s. A velocity of 10 mm/s is usually more than enough to describe a ^{57}Fe Mössbauer spectrum.

The experimental lines continue to have a Lorentzian shape (for thin absorbers), with a linewidth Γ_{exp} twice the width of the natural linewidth, $\Gamma_{exp} = 2\Gamma_{nat}$. This is because an emission line scans for an absorption line of the same width [24].

2.3 Hyperfine interactions

Hyperfine interactions are small perturbations of 10^{-9} to 10^{-7} eV in the energies of the nuclear states. These perturbations arise from the interaction between the nucleus and its neighbouring electrons and more specific with the electron density at the nucleus, the gradient of the electric field and the unpaired electron spins. These hyperfine interactions named "isomer shift (δ)", "electric quadrupole splitting" (ΔEq) and "hyperfine magnetic field (HMF)

splitting" respectively, can reveal information about the atomic or electronic structure around the Mössbauer atom such as its valence, spin state or magnetic moment.

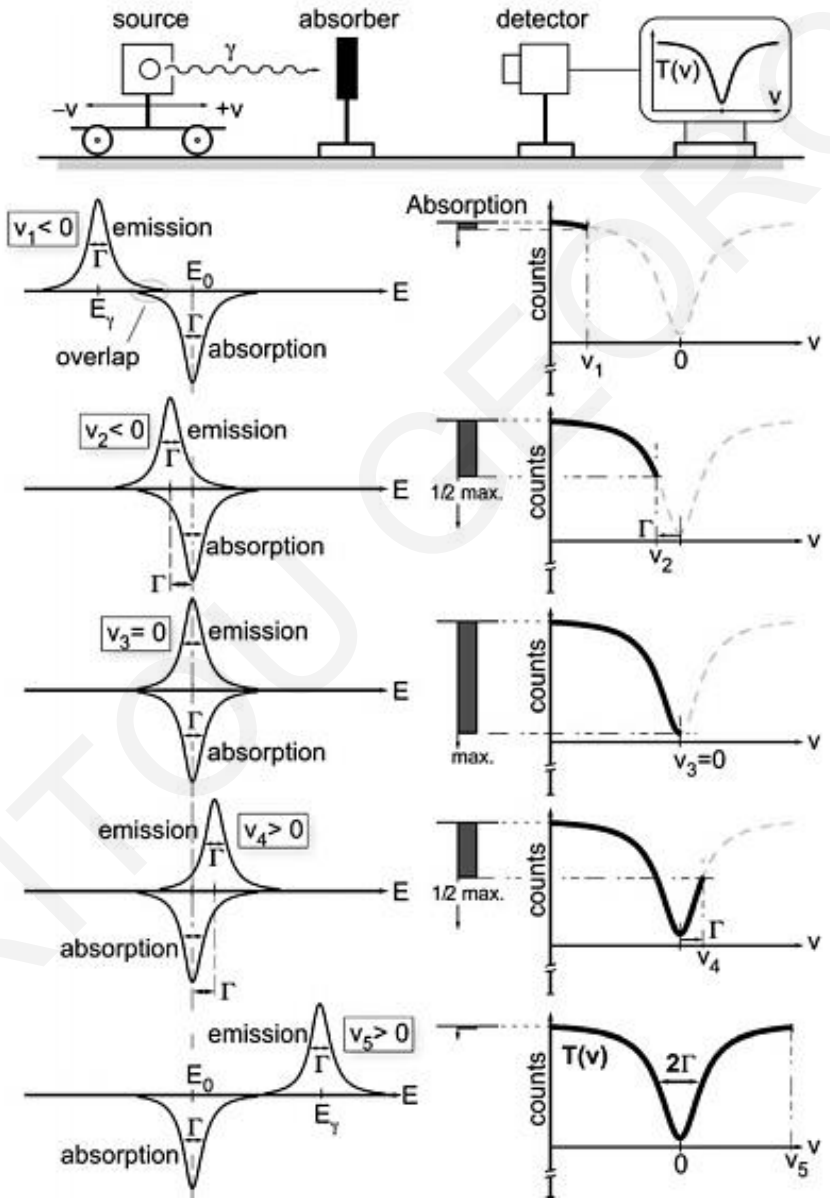

Figure 2.7: Schematic illustration of a Mössbauer transmission experiment in five steps. The "Absorption" bars indicate the strength of recoilless nuclear resonant absorption as determined by the "overlap" of emission and absorption lines when the emission line is shifted by Doppler modulation [24].

2.3.1 Isomer shift (δ)

The Isomer shift (also known as chemical shift) arises from the hyperfine interaction involving the nucleus and electrons from the atom. It is observed as a shift in the energy of the peaks of the Mössbauer spectrum (*Figure 2.8*) when the wavefunction of the s-electrons (and some relativistic p-electrons) overlaps with the finite nucleus and provides a Coulomb perturbation that lowers the nuclear energy levels. As the nuclear radius is different between the ground and the excited state, the two states experience a different energy modification because the total electrostatic attraction is stronger when the nucleus is smaller. This unequal reduction in the energy between the ground and the excited state causes a change in the transition energy. The shift (δ) in the position of the absorption's peak of the spectrum is given by [24]:

$$\delta = E_A - E_S = \frac{4\pi}{5} Z e^2 R^2 \left(\frac{\Delta R}{R}\right) \{|\psi(0)|^2_{abs} - |\psi(0)|^2_s\} \qquad (2.14)$$

where Z and e is the atomic number and proton charge, $\Delta R = R_e - R_g$ is the change in the radius of the nucleus between the excited and ground state, and $|\psi(0)|^2_{abs}$ and $|\psi(0)|^2_s$ the electron densities at the Mössbauer nuclei in the absorber and in the source, respectively.

For ^{57}Fe, the radius of the ground state is larger than the radius of the exited one therefore ΔR is a negative quantity and a decrease in the electron density at the nucleus of the absorber results in an increase of the isomer shift (the spectrum's peaks shift to a more positive velocity). The density of the s-electrons at the nucleus depends strongly in the chemical surrounding hence different compounds give a different energy shift.

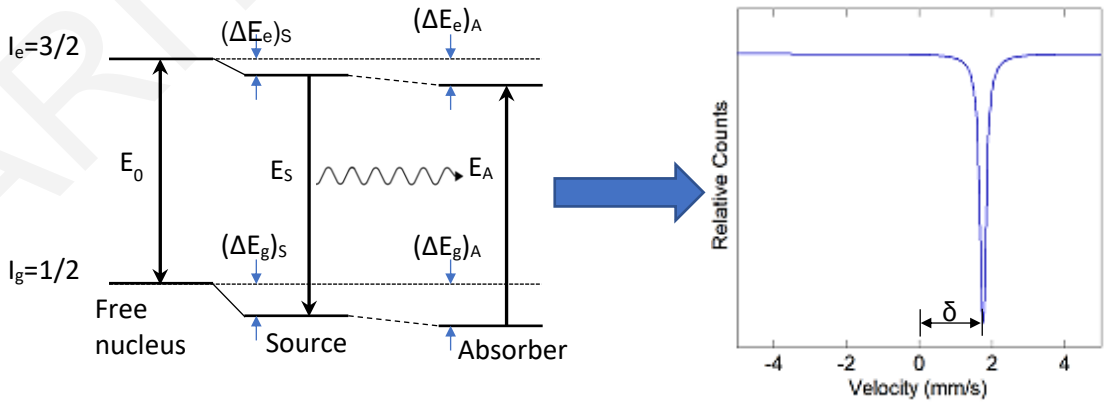

Figure 2.8: *Due to the Coulomb perturbation and the finite charge density in the nucleus, the energy nuclear levels shift without changing the degeneracy. The isomer shift (δ) is the difference in the transition energy between the source and the absorber* $\delta = E_A - E_S = (\Delta E_e - \Delta E_g)_A - (\Delta E_e - \Delta E_g)_S$

Besides the direct influence of the s-electrons, the electron density at the nucleus is also influenced by the partially filled valance states due to the screening effect. In the case of iron, the nuclear charge from the 4s electrons will be partially screened from the 3d electrons, therefore an increase in the 3d electron numbers will reduce the s-electrons density and cause a more positive isomer shit [29]. Therefore, Fe(II) compounds with $(3d)^6$ electronic configuration usually have a more positive δ than the Fe(III) compounds with $(3d)^5$ configuration. The influence of oxidation state and spin on the isomer shift of ^{57}Fe can be seen in *Figure 2.9*.

As Mössbauer spectroscopy is a "comparison" technique, and in a Mössbauer experiment the measured value is the difference in the shifts of the peaks between the absorber and the source, the isomer shifts must always be reported with respect to a reference material at a specific temperature. Nowadays, the isomer shifts are given relative to metallic iron at room temperature but in the previous decades components like sodium nitroprusside were used. For convenience, the isomer shift δ is expressed in mm/s.

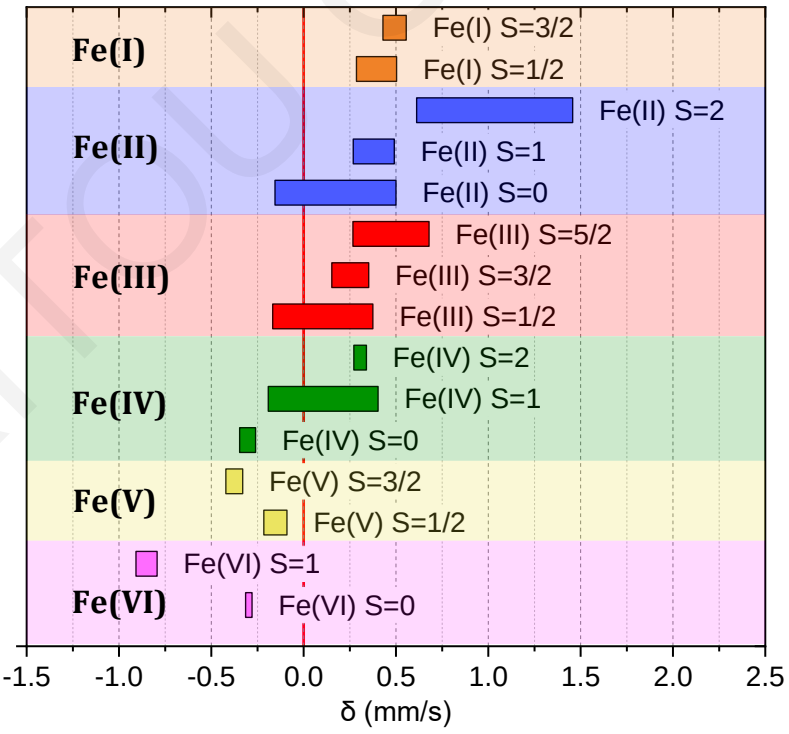

Figure 2.9: *Isomer Shifts for various iron complexes with oxidation states (I) to (VI) relative to metallic iron at room temperature (adapted from [24])*

2.3.2 Electric Quadrupole splitting (ΔE_q)

Nuclei with a spin quantum number higher than $I=1/2$ have an electric quadrupole moment (Q) which originates from its asymmetrical shape. This asymmetry depends on the spin therefore differs for the ground and the excited states. The electric quadrupole moment is given by [24]:

$$Q = \frac{1}{e}\int \rho(r) r^2 (3\cos^2\theta - 1) d\tau \tag{2.15}$$

where $\rho(r)$ is the charge density and θ is the angle to the nuclear spin quantization axis. The type of nuclear deformation determines the sign of Q; a positive Q indicates that the nucleus is elongate, whereas a negative sign indicates that the nucleus is oblate.

When an electric field gradient *(EFG)* is present due to non-cubic valance electron distribution or non-cubic lattice surrounding, electric quadrupole interactions occur with the electric quadrupole moment Q, and as a result the degenerate $I=3/2$ level splits in to two substates with nuclear magnetic spin quantum numbers $m_I=\pm 1/2$ and $m_I=\pm 3/2$ giving rise to a doublet in the Mössbauer spectrum (*Figure 2.10)*.

The interaction between the electric quadrupole moment of the nucleus and the *EFG* at the nucleus can be described by the Hamiltonian [24]:

$$\widehat{H}_Q = \frac{eQV_{zz}}{4I(2I-1)}\left[3\hat{I}_z^2 - I(I+1) + \frac{\eta}{2}\left(\hat{I}_+^2 + \hat{I}_-^2\right)\right] \tag{2.16}$$

where $\hat{I}_\pm = \hat{I}_x \pm i\hat{I}_y$ are shift operators and $\hat{I}_x, \hat{I}_y, \hat{I}_z$ are the operators of the nuclear spin projections into the principal axes. The product eQV_{zz} is also called the nuclear quadrupole coupling constant.

The *EFG* is a tensor quantity and is represented by three principal axes, V_{xx}, V_{yy} and V_{zz}, and can be specified by two parameters, the $V_{zz} \equiv eq$ and the asymmetry parameter $\eta = \left(\frac{V_{xx}-V_{yy}}{V_{zz}}\right)$. The electric quadrupole splitting (ΔE_q) of the energy levels (the difference in the energy between the two substates - lines) is given by [29]:

$$\Delta E_q = \frac{\pm 1}{4} eQV_{zz}\left(1 + \frac{\eta^2}{3}\right)^{1/2} \tag{2.17}$$

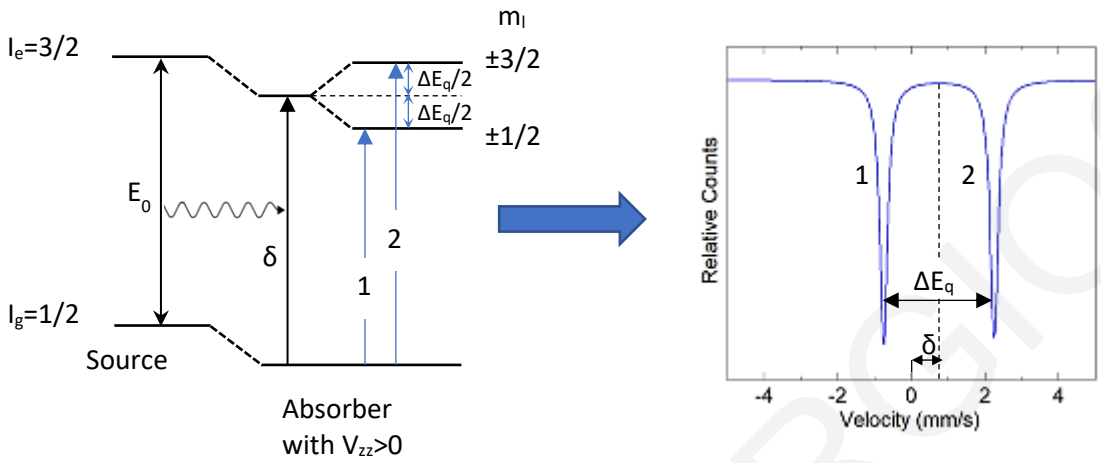

Figure 2.10: *The nuclear excited state with spin I_e=3/2 splits into two substates because of quadrupole interaction. This can be seen as two peaks in the Mössbauer spectrum. The middle in the distance of the two peaks corresponds to the Isomer shift δ*

High and low spin Fe complexes can be identified by differences in the ΔE_q. The electric quadrupole splitting is also sensitive to local atomic arrangements like the ligand charge and coordination. Hence ΔE_q can be used to determine the oxidation state, the spin state and the arrangement of the ligands.

2.3.3 Hyperfine Magnetic Field Splitting

When the nuclear states have spin $I>0$, and therefore magnetic dipole moments, they will interact with the magnetic field present at the nucleus, and subsequently modify the energies of their nuclear states. This interaction called magnetic dipole interaction or "nuclear Zeeman effect" (due to its analogy with the splitting of the energy levels of the atomic electrons when a hyperfine magnetic field (HMF) is present in the atom) is described by the Hamiltonian [24]:

$$\hat{H}_m = -\hat{\vec{\mu}} \cdot \hat{\vec{B}} = -g_N \mu_N \hat{\vec{I}} \cdot \hat{\vec{B}} \tag{2.18}$$

where the field $\vec{B}$ represents the magnetic induction, g_N is the nuclear Landé factor and $\mu_N = e\hbar/2M_p c$ is the nuclear magneton. The eigenvalues E_M from the diagonalization of the Hamiltonian matrix are:

$$E_M(m_I) = \frac{-\mu B m_I}{I} = -g_N \mu_N B m_I \tag{2.19}$$

The magnetic field experienced by the nucleus is a combination of fields that arise from the atom, from the lattice or from an external source. It lifts all degeneracies of the spin state of the nucleus resulting in separate and equally spaced substates (hyperfine magnetic field splitting), the transitions between which can be identified in a Mössbauer spectrum as different peaks (*Figure 2.11)*. The magnetic quantum numbers m_I range between $-I$ to $+I$ in increments of 1. For ^{57}Fe, the excited state $I_e=3/2$ splits to {-3/2, -1/2, +1/2, +3/2} and the ground state I_g to {-1/2, +1/2}. From this and the selection rule $\Delta m_I = 0, \pm 1$, six transitions are allowed for the 3/2→1/2 transition [29]; {(-1/2→-3/2), (-1/2→-1/2), (-1/2→+1/2), (+1/2→-1/2), (+1/2→+1/2), (+1/2→+3/2)}.

The intensities of the six lines depend on the field's orientation. For an isotropic distribution of the magnetic fields relative to the γ-ray propagation (like in powder samples), the intensity ratio of the lines is 3:2:1:1:2:3 (from left to right as seen in a Mössbauer spectrum). When the $\vec{B}$ is perpendicular to the γ-ray propagation the ratio is 3:4:1:1:4:3 and when the $\vec{B}$ is parallel to the γ-direction the ratio is 3:0:1:1:0:3 [24].

Without some exceptions, (like in the metallic iron), the magnetic dipole interaction is encountered together with an electric quadrupole interaction. Because both interactions depend on the magnetic quantum numbers m_I of the nuclear spin, their combined Hamiltonian can be difficult to evaluate. In the cases where the magnetic interaction is quite larger than the

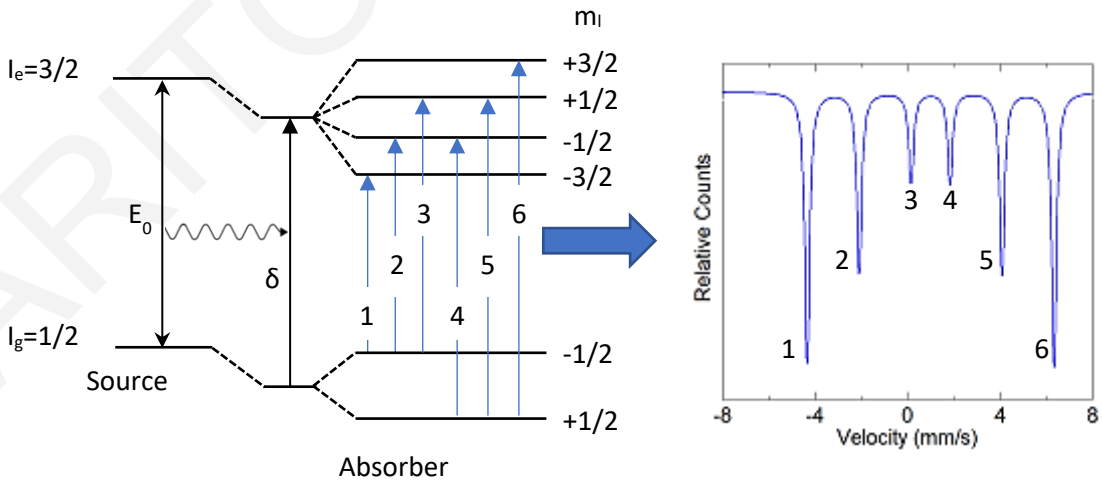

Figure 2.11: *The effect of the hyperfine magnetic field splitting on the energy levels for ^{57}Fe and the corresponding peaks on a Mössbauer "sextet" spectrum. The excited state with $I=3/2$ splits into four substates while the ground state with $I=1/2$ into two substates*

corresponding quadrupole interaction, the result of this is a shift in the relative positions of peaks 1 and 6 with respect to the peaks 2-5. For positive Vzz the four inner lines (2-5) are shifted to lower velocities whereas the outer 1 and 6 lines are shifted by equal amount towards higher velocities [24].

2.4 Practical aspects and Instrumentation

The main principle behind Mössbauer Spectroscopy is generally simple even though the effect was a problem that was troubling the physicist for decades. It is even possible to construct a Mössbauer spectrometer with simple laboratory equipment and a speaker as a velocity transducer. As mention previously, in Mössbauer spectroscopy the photons from a moving gamma source interact with the target (thin absorber) and with a detector (proportional counter) the intensity of the outcoming beam is measured as a function of the relative velocity between the source and the target.

More specifically, a radioactive Mössbauer source is attached to a Mössbauer Velocity Transducer (MVT) which moves the source following the signal from the Mössbauer Drive Unit (MDU) and changes the energy of the emitted photons via the doppler effect. The MDU strictly controls and evaluates the source's movement based on a signal produced by the Digital Function Generator (DFG) and the feedback received from the MVT. The velocity of the source is well known at any given time from the output of the DFG, which is separated into channels and fed to the Multichannel Analyzer (MCA) along with a start pulse for synchronization of the periodic movement of the source with the counting system. For validation purposes, a laser interferometer can be attached to the MVT, which detects the source's velocity and feeds the information to the MDU in order to verify the movement.

The pulses from the photons that arrive to the detector are fed initially to a preamplifier and subsequently to an Amplifier for further amplification and shaping. Finally, the amplified signal is fed to the MCA. There, for the duration of each velocity's channel, the pulses from the γ-photons (and noises) are counted, summed and stored into memory. Based on the frequency of the signal generated by the DFG, this is repeated numerous times per second until a significant number of events is recorded in order to obtain an acceptable signal to noise ratio (SNR). At the end of the measurement, the total counts for each channel (velocity) are known and can be accessed from a personal computer for further analysis with a specialised software. At the energies / velocities where the Mössbauer effect is detected, an increase in the

absorption (decrease in the transmission radiation (through the sample)) is observed as explained in the previous paragraphs.

The experimental setup can be further supplemented with various cryostats in order to cool the target typically to Liquid Nitrogen and, if required, down to Liquid Helium temperatures, with furnaces for measurements that require high temperatures and even with superconductive magnet systems for application of external magnetic fields. A typical scheme of a Mössbauer spectrometer, is shown in *Figure 2.12*.

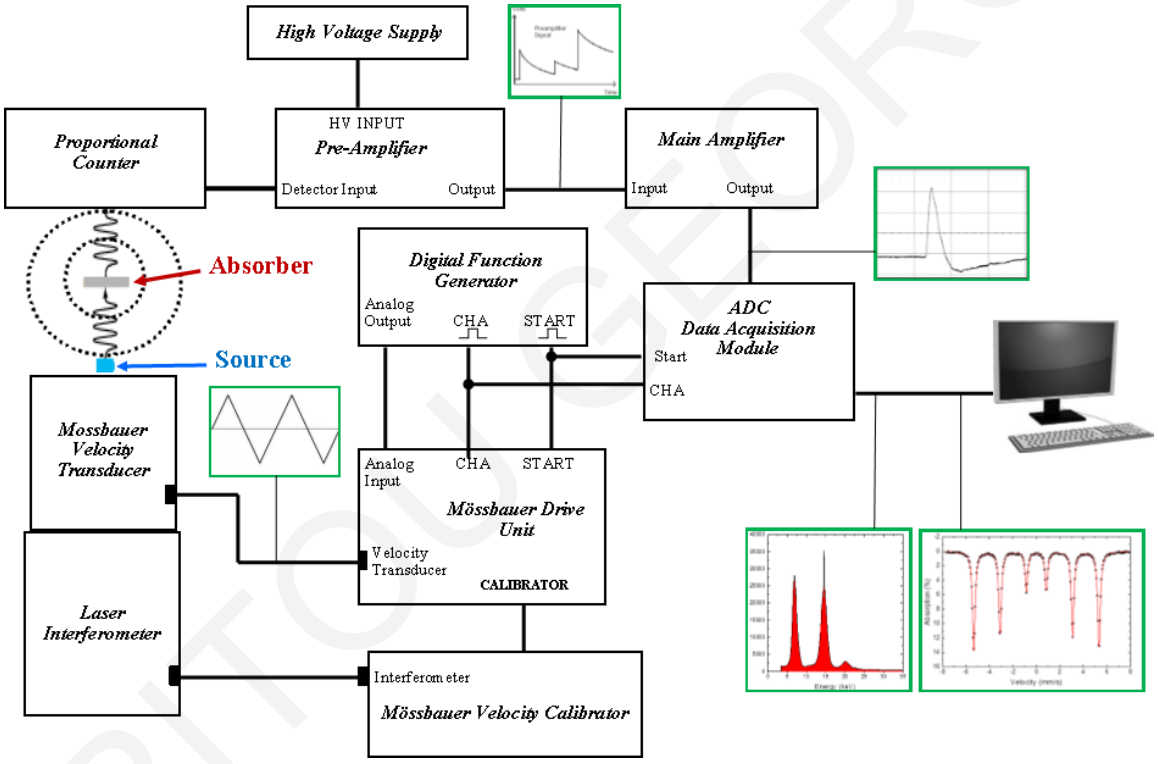

Figure 2.12: *Diagrammatic representation of a Mössbauer spectrometer for transmission measurements*

2.4.1 Mössbauer isotopes & sources

Unfortunately, not all gamma resonances can give a useful Mössbauer spectra as can be seen at *Figure 2.13* where the elements that display the Mössbauer effect are marked with red background. In order for an element to be usable for MS, it must have some specific properties which little more than 20 isotopes have and are in practical use [30]. The most popular ones are ^{57}Fe, ^{119}Sn and ^{151}Eu. ^{197}Au, ^{129}I, ^{121}Sb, ^{125}Te are also used among others.

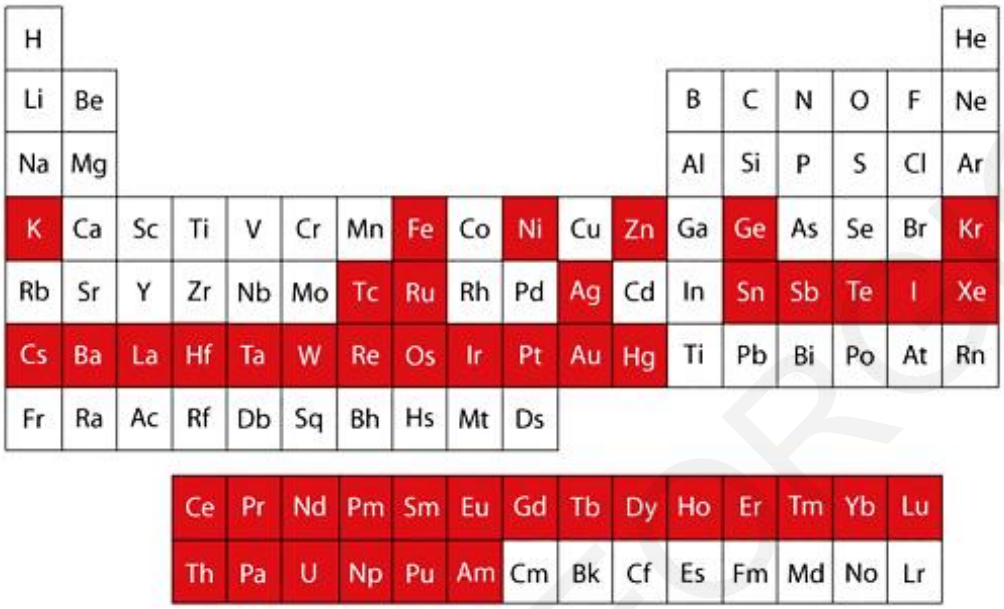

Figure 2.13: *Elements that display the Mössbauer effect*

The most important criteria that a Mössbauer isotope should satisfy in order to be usable are [30]:

- The photon's energy E_γ should be within 5-150keV and preferably <50keV as the recoilless fraction f and resonance cross section (σ_0) decrease as E_γ increases. When E_γ is <5keV, a significant percentage of the photons are self-absorbed from the source making the radiation very weak.
- The half-life $T_{1/2}$ of the excited state should lie within 1-100ns. Increased $T_{1/2}$ results into very narrow natural width Γ_{nat} of the excited state and the resonant can be destroyed even by the slightest vibration. If $T_{1/2}$ is very small and the Γ_{nat} wide, the resonance might not be possible to be resolved.
- The source should have small internal conversion coefficient ($\alpha<10$) in order to have large probability for γ-ray emission.
- The parent nucleus is preferred to have a long half-life
- The isotope should have low spin as higher spins can complicate the spectra and make the analysis difficult
- The natural abundance of the isotope should be high enough to avoid enrichments

In order to reduce the sources linewidth (achieving the highest monochromatization) and increase the recoil fraction, the parent nuclei are normally diffused into a metal matrix. For the ^{57}Fe 14.41 keV resonance, the parent ^{57}Co source atoms are usually diffused into metal Rhodium matrix or Palladium, giving an f-value of 0.784 at room temperature [30].^{57}Co has a half-life of ~272 days and decays mostly to ^{57}Fe (99.8%) through electron capture (EC). The resulted ^{57}Fe nucleus is at the second excited state with a nuclear spin of 5/2 and 136.47 keV of energy. This state decays directly to the ground state with a probability of 10.7%, emitting a γ-photon, while at the ~85.5% of the cases it decays to the first excited state with an energy of 14.41 keV and nuclear spin of 3/2. From the decay of this state to the ground state, the 14.41 keV gamma photons used for the Mössbauer measurements are emitted. At 78.6% of the time, the 14.41 keV level decays by internal conversion emitting a ~7keV electron while the decay with γ-emission has a probability of 9.2%. Therefore, from the ^{57}Co isotope, three gamma photons are emitted; at 136.46 keV, at 122.06 keV and at 14.41 keV along with two x-rays at 6.4 keV and 7.1 keV. Due to the rhodium matrix used, one x-ray at 20.6 keV is also observed (Rh-K_α). The decay scheme of ^{57}Co is shown in *Figure 2.14*. The previous values were taken from [31].

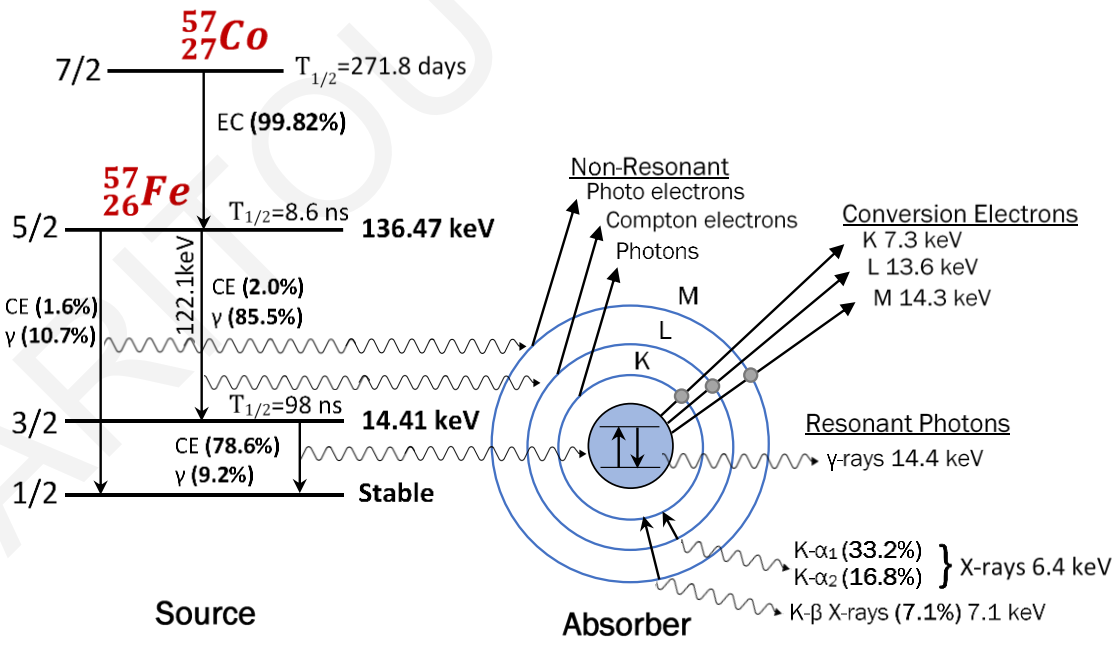

Figure 2.14 *The decay scheme of the ^{57}Co along with various backscattering processes that follows the resonant absorption of an incident γ-photon. The decay data were taken from [31]*

2.4.2 Detectors

For the Mössbauer Spectroscopy, the fundamental relative energy resolution of 10^{-12} cannot be experimentally observed directly, as no available detector comes even close to this level of energy resolution. This resolution is only achieved from the velocity modulation of the source's energy. Therefore, a detector is only used to record the numbers of transmitted photons hence a detector with modest energy resolution and high counting efficiency like gas proportional and NaI(Tl) scintillation counters can be used, and are usually preferable due to the lower cost and simplicity. Semiconductor detectors are rarely used due to their high price, but this might change in the near future as cheaper detectors with much bigger detection area have become commercially available.

Gas proportional counters are the detector of choice for ^{57}Fe MS as they are relatively cheap, robust, and have an excellent operational lifetime. Their ~12% resolution at 14 keV, is sufficient to separate the 14.41 keV γ-photons, from the 7 and 20 keV X-rays as seen in *Figure 2.15(a)*. A typical gas proportional counter for ^{57}Fe MS, is a 50mm diameter cylinder with a thin beryllium window filed with Krypton or Xenon gas at 1atm with 3% CO2 or 10% methane as a quench gas. Krypton and Xenon gases have enough stopping power for the 14.41 keV photons, but not enough for the 136.47 and the 122 keV ones. Therefore, background noise from higher energy photons is avoided.

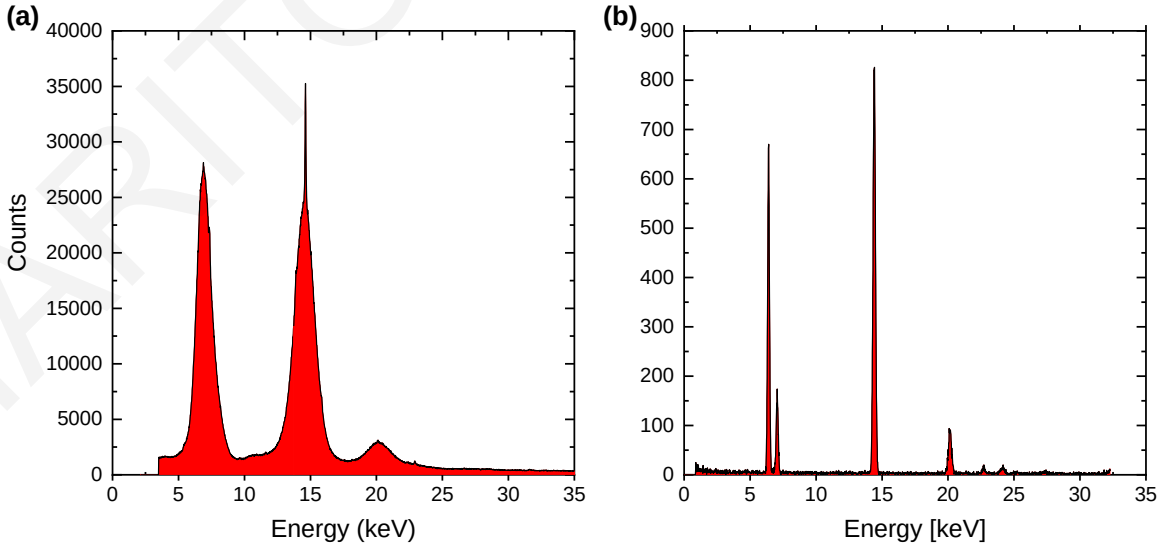

Figure 2.15: *Spectrum from a ^{57}Co/Rh source acquired with a Krypton Proportional counter **(a)** and a high-resolution Si-Pin X-ray detector **(b)**.*

Compact semiconductor detectors like Si-Pin and SDD (Silicon Drift Detector), without the need of complex cooling are nowadays available and can be used for MS. These detectors have very high energy resolution and high-count rates. Unfortunately, their active area is relatively small 4-50 mm^2 therefore a large proportion of the photons can be lost. However, detectors with up to 150 mm^2 active area have started to become available. SDD detectors were used in the MIMOS II MS systems that were placed on the mars exploration rovers Spirit and Opportunity. *Figure 2.15(a)* shows the spectrum from a ^{57}Co/Rh source measured with a Krypton filled proportional counter, while *Figure 2.15(b*) shows a spectrum measured with a high-resolution Si-Pin X-ray detector (Amptek XR-100CR) at the energies of <35 keV. The two X-rays at ~6.4 keV and 7.1 keV, the 14.41keV gamma-ray and the 20.6 keV X-ray from the Rhodium matrix are clearly seen in the case of the Si-Pin detector.

Scintillation counters can have a detection efficiency of ~100% and for ^{57}Fe MS, the NaI(Tl) crystal must be thin around 0.1-0.2mm in order to reduce the detection efficiency for the photons of higher energy. These detectors have an energy resolution of ~35% therefore they can barely resolve the 14.41 keV peak from the 7 keV X-rays. They are usually used for γ-rays with energy $E_\gamma$more than 15 keV, such as in ^{119}Sn.

2.4.3 Velocity Drive System

The velocity drive system is a unique feature of MS and the most important component. As mention previously, it is composed from a waveform generator (DFG) a drive and feedback circuit (MDU) and a velocity transducer (MVT).

The source is driven repetitively through a cycle of motion following a reference waveform from the DFG. The most common waveforms used are sinusoidal and triangular waves. The sinusoidal waveform is the most accurate as there are no abrupt changes in the acceleration, hence the systems inertia has minimum effect. This is suitable for measurements at high velocities or when the components of the transducer are heavy. Because the relationship between the velocity and the channel numbers is not linear when using the sinusoidal waveform, the visualisation of the spectrum is not straightforward. However, this can be easily fixed with a simple computer program. The biggest disadvantage of the sinusoidal waveform and the resulted non-uniform velocity coverage is that the wave spends most of its time at the extrema where only background contribution is expected and not the Mössbauer lines. This results to lower resolution in the most important areas of the spectra and increased counting time.

The triangular waveform, or "constant acceleration" mode, has linear mapping between channels and velocities therefore data visualisation is simplified. Also, the velocity resolution is constant. The drawback of this wave is the sudden acceleration changes at extrema that put significant strains on the transducer, thus some velocity error is inevitable. This error occurs at the extrema where again is a region of the spectrum where usually only background data are collected. In this waveform, the velocity starts from the $-\upsilon_{max}$ goes linearly through zero, increases to $+\upsilon_{max}$ and then it decreases linearly back to $-\upsilon_{max}$. In this mode, each velocity is passed twice; one in the forward movement and one in the backward hence the final data consists of two mirror images of the spectrum as seen in *Figure 2.16*. Using a suitable software, the data can be folded back to one spectrum. The triangular waveform is used for ^{57}Fe, ^{119}Sn and ^{151}Eu where the needed velocity ranges are modest.

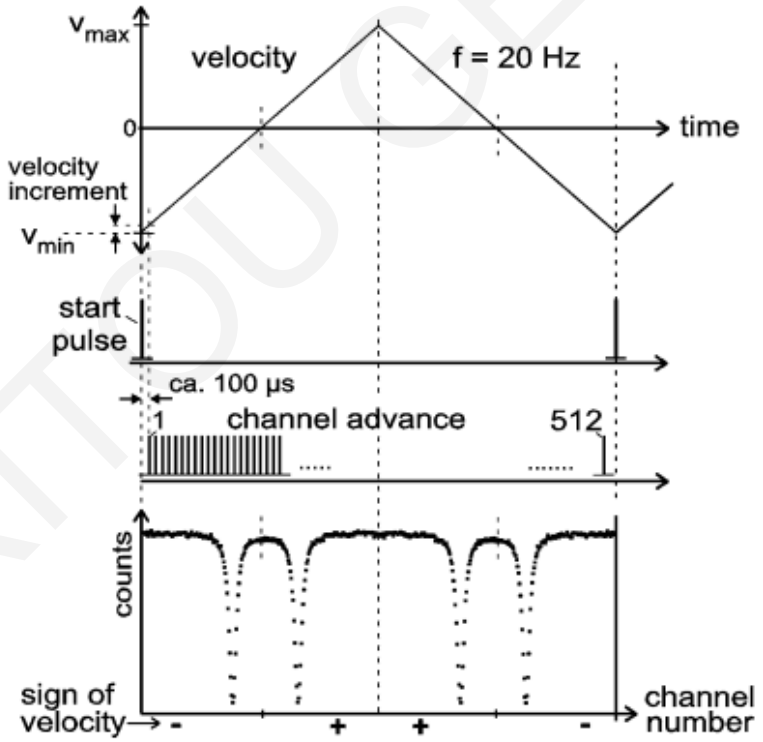

Figure 2.16: *Velocity control and synchronization of data recording by the multi-channel analyser (MCA) operated in multichannel scaling (MCS) mode with 512 channels. For the common triangular velocity profile shown here, the spectrum is recorded twice because each velocity increment is reached upon sweeping up and down. The sense of the velocity scales may also be opposite to that shown here [24].*

The DFG besides the reference signal provides a series of triggering pulses (start and channel advance pulses) to the MCA that are used for the timing and synchronization of data recording. The reference waveform from the DFG is fed to the MDU which amplifies it and transforms it as needed and then is passed to the MVT. The MVT is electro-mechanical and works like a loudspeaker; an electromagnet (drive coil) is attracted to and repelled from a permanent magnet, vibrating back and forth. The applied current from the MDU "converts" into velocity through a drive coil. A signal proportional to the actual velocity is produced through a sensitive pickup coil which is fed back to the MDU for movement evaluation and signal correction. The source is attached onto a shaft that passes through them and it is supported by springs that can move within a certain amplitude. A cross-section of a modern velocity transducer [30] is shown in *Figure 2.17*.

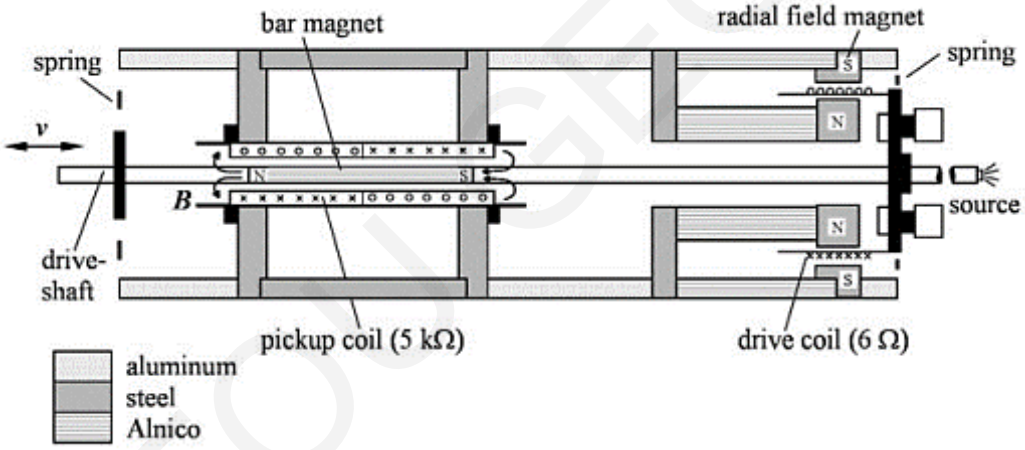

Figure 2.17: *Cross-section of a modern velocity transducer [30].*

2.4.4 Absorber thickness

A Mössbauer absorber (sample) can be a solid material, compact powder or frozen solution and must contain the Mössbauer isotope in sufficient concentrations. The bigger the Mössbauer isotope's concentration in the sample is, the higher the Mössbauer resonance's absorption will be, and therefore smaller uncertainties and acquisition times will be achieved. At the same time, thick samples can absorb a significant part of the Mössbauer radiation coming from the source, leading to significantly reduced count rates. Also, a thick absorber can lead to distorted Lorentzian lines. Therefore, for best results the absorber should have an optimal thickness d_{opt} (mg cm^{-2}):

$$\frac{1}{\mu_a} < d_{opt} < \frac{2}{\mu_a} \tag{2.20}$$

with $$\mu_a = \sum_i p_i \mu_a^i \tag{2.21}$$

where μ_a is the mass absorption of the sample and μ_a^i and p_i the mass absorption and mass fraction of each phase [30].

The Mössbauer resonance absorption is determined by the *effective thickness t*:

$$t = N_M f_A \sigma_0 \tag{2.22}$$

where N_M is the number of Mössbauer nuclei in the absorber per cm^2, f_A the recoil free fraction of the absorber and σ_0 the resonance cross section (for ^{57}Fe, $\sigma_0 = 2.56 \times 10^{-18}\ cm^2$) [24].

The experimental line-width Γ_{exp} depends on the effective thickness *t,* thus for a good thin absorber t should be limited to values of $t \approx 0.2 - 0.5$, as thick absorbers can lead to broadened lines which exhibit Gaussian line-shape. The experimental linewidth Γ_{exp} is given approximately by [24]:

$$\Gamma_{exp}/2 = (1 + 0.135t)\Gamma_{nat} \qquad \text{for } t \leq 4 \text{ and}$$

$$\Gamma_{exp}/2 = (1.01 + 0.145t - 0.0025t^2)\Gamma_{nat} \qquad \text{for } t \geq 4 \tag{2.23}$$

As a rule of thumb, an absorber with a recoil free fraction $f_A = 0.7$, exhibiting a symmetric quadrupole doublet of natural line-width, should contain 21 μg/cm^2 of ^{57}Fe or ~1mg/cm^2 of natural iron [24]. One such sample should give an experimental absorption depth (*abs*) no more than ~5% with a linewidth of 0.26-0.28 mm/s.

The *relative absorption depth* (abs_r) of the Mössbauer lines is given by:

$$abs_r = f_S \cdot \varepsilon(t) \tag{2.24}$$

where f_S is the recoil free fraction of the source and *ε(t)* a zeroth-order Bessel function. For *t* up to *t≈1, ε(t)≈ t/2*. Therefore the absorption depth of a Mössbauer line should not exceed 10-15% as this will lead to line broadening and distortions [24].

One can also calculate the needed acquisition time Δt, to reach a specific Signal-to-Noise Ratio (SNR), where $\mathrm{SNR} = \mathrm{N_S}/\Delta\mathrm{N_S}$ (the counts at the baseline over their standard deviation), if *C*

(the count rate per second per channel) and abs_r are known. As $\Delta N_S \approx \sqrt{N_S} = \sqrt{C \cdot \Delta t}$ the needed acquisition time Δt can by calculated by:

$$\Delta t = \frac{SNR^2}{abs_r^2 \cdot C} \tag{2.25}$$

As the acquisition time is inversely proportional to the square of the abs_r, and the noise improves with the square root of the time, ($\sigma \approx \sqrt{N} \equiv \sqrt{C \cdot \Delta t}$,) there is a minimal sample thickness in order to limit the experimental length to an acceptable timeframe (445h). For ^{57}Fe MS, the minimum effective thickness of a sample should be $t \approx 0.02$ which corresponds to 0.1 mg cm^{-2} of natural iron [24].

If the chemical composition of the sample is unknown, then the lower limit of the sample thickness, $\frac{1}{\mu_a}$, can be found experimentally as it is the point where the transmitted intensity is the $1/e$ of the incident intensity [24,30]. Therefore, a sample has the ideal thickness when it attenuates the incident intensity by 63-85%.

Chapter 3

The Experimental Setup

In the previous chapter, the basic theory behind Mössbauer spectroscopy was presented along with some practical and instrumentational aspects. In this chapter, the MS experimental setup which is installed at UCY and was used for this study will be discussed, along with various aspects of the experimental procedure like the calibration process, the production of high transparency sample holders and various problems that have been encountered and solved.

3.1 Experimental setup description

3.1.1 Mössbauer Source:

The source used was a ^{57}Co/Rh one (^{57}Co infused into rhodium matrix) and had an initial activity of ~50 mCi. The sources frame was made of light aluminium with a M4 thread on the back side in order to be firmly attached to the velocity transducer. The active diameter of the source was 5mm and the radioactive material was covered by a 20 μm Kapton window. The thin Kapton window seals and protect the radioactive material of the source and at the same time it provides high transmission to the 14.41 keV photons. According to the manufacturer's ("Cyclotron Co.") certificate, the isomer shift (δ) of the source relative to metallic α-Fe was 0.107 mm/s, the linewidth 0.112 mm/s and the recoilless fraction 0.78. A schematic view of the source is shown in *Figure 3.1*.

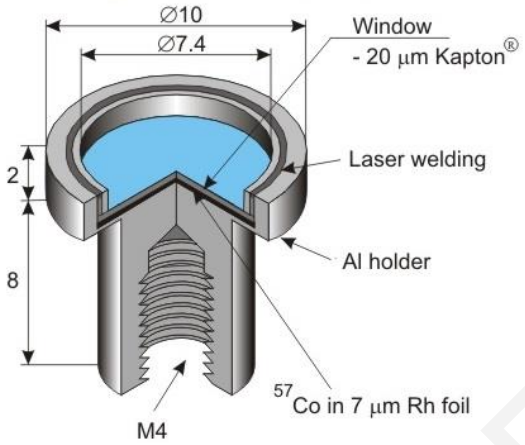

Figure 3.1: *Schematic view of a $^{57}Co/Rh$ source suitable for Mössbauer Spectroscopy (Cyclotron Co.)*

3.1.2 Mössbauer Electronics

Mössbauer spectroscopy, as all modern experimental setups found in nuclear physics, is in need of various electronics. In the following paragraphs, the electronic devices that were part of the experimental setup will be described. *Figure 3.2* shows a block diagram with the connections between the electronic devices.

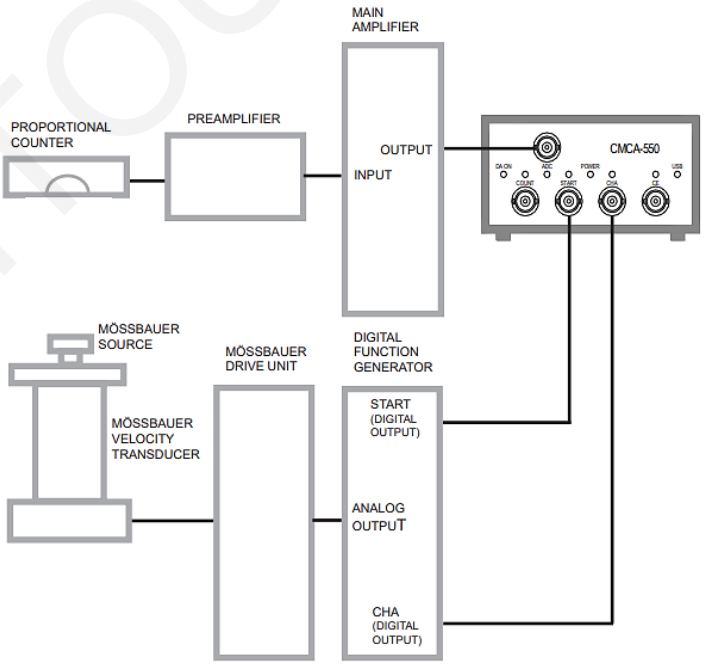

Figure 3.2: *Block diagram of the various electronics and the CMCA-550 data acquisition module*

3.1.2.1 Detector – Preamplifier – High Voltage power supply

A cylindrical gas proportional counter (LND-45431) was used. This counter model is filled with Krypton Gas at 800 Torr and its effective diameter and length is 47.8mm and 114.3mm respectively. The γ-ray window is placed on the side, it has a diameter of 25.4 mm and is made of beryllium with a thickness of 0.127 mm. The detector was placed inside a suitable cylindrical mounting element made of thick lead. An Ø20 mm hole on the site (in front of the detector's window) allows the γ-beam to pass by while unwanted background X- and γ-radiation is blocked.

The operating voltage of the counter was set at 1860V and was provided by a low noise High Voltage power supply (WissEl HVS-2). When a photon is detected by the proportional counter, a charge proportional to the photon's energy is produced. A charge sensitive preamplifier collects the charge with a capacitor over a period of time, effectively integrating the detectors pulses. The discharge of the capacitor results to exponentially decaying pulses with the amplitude being the carrier of the basic information. For this purpose, an Ordec 142PC charge sensitive preamplifier was used.

3.1.2.2 Main Amplifier

The main amplifier used was a WissEl AMP-1000. The radioactive decay is a random process, therefore the pulses from the preamplifier can overlap if the count rate is large, hence a pulse train with piled up pulses can occur. This amplifier integrates and shapes the exponential decayed pulses coming from the preamplifier into bipolar ones, as seen in *Figure 3.3*, amplifying the voltage at the same time from 0-10V. As pileup of the pulses is undesirable, the pulse shaping time of the amplifier must be set (using a rotary switch) for appropriate counting optimization. The amplitude of the amplifier's output pulses can be modified using the coarse and fine gain switches. This effectively changes the relative signals corresponding to the detected photons energy, that can be used from the rest acquisition system, therefore it must be set accordingly to the specific source that is in use.

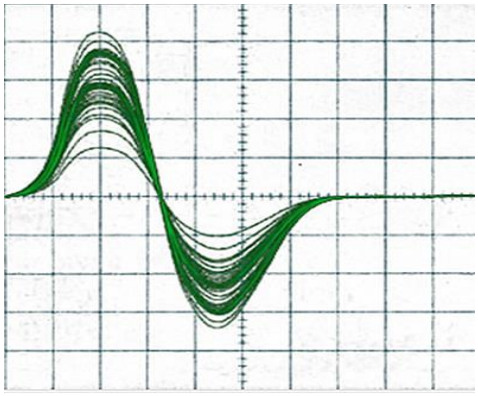

Figure 3.3: *The output bipolar pulses of the main amplifier as seen at the screen of an oscilloscope [31]*

3.1.2.3 Digital Function Generator (DFG)

The WissEl DFG-1200 Digital Function Generator was used. It can produce, besides the triangular and sinusoidal waves explained before, constant velocity and a region of interested waveforms (*Figure 3.4*). The later waveforms give the ability to the user to study specific velocities or regions. The velocity resolution of the spectrum is set by the DFG as it depends on the channels that the waveform is separated to. The DFG-1200 can provide spectra with velocity resolution up to 4096 channels. As the quality of the spectra is correlated with the collected counts of each channel, increasing the number of the channels leads to linearly increased acquisition times. ^{57}Fe MS is usually done at 512-1024 channels depending on the velocity range. For our measurements, 1024 channels were used even though the velocity range we worked with (~8mm/s) is relatively small. This gives a width for each channel about 0.016 mm/s (0.77×10^{-9} eV), ~7 times narrower than the natural linewidth of the 14.41 keV peak and more than 15 times narrower than an experimentally measured absorption peak.

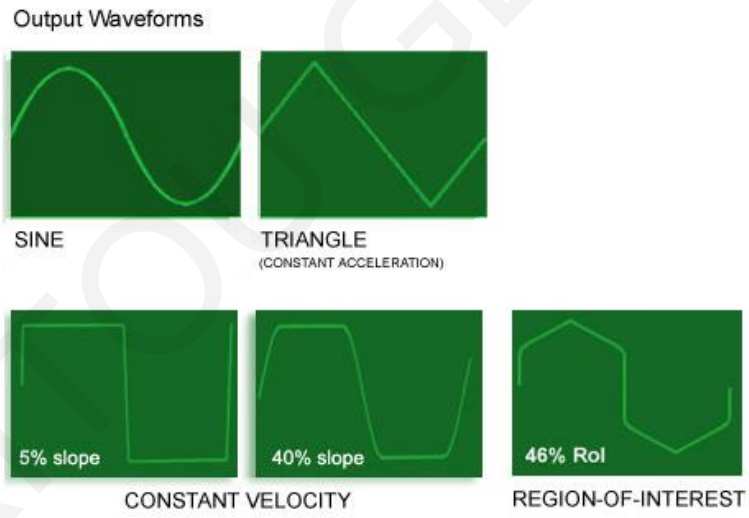

Figure 3.4: *Output waveforms from the WissEl DFG-1200 digital function generator*

The DFG, besides the waveform, has two more outputs responsible for the synchronization of the Data Acquisition Module and the Mössbauer Drive Unit. The first one is a START pulse that indicates, as seen in *Figure 3.5,* the positive maximum of the triangular waveform (maximum velocity), and a channel pulse (CHA) that controls the transition from one channel to the next.

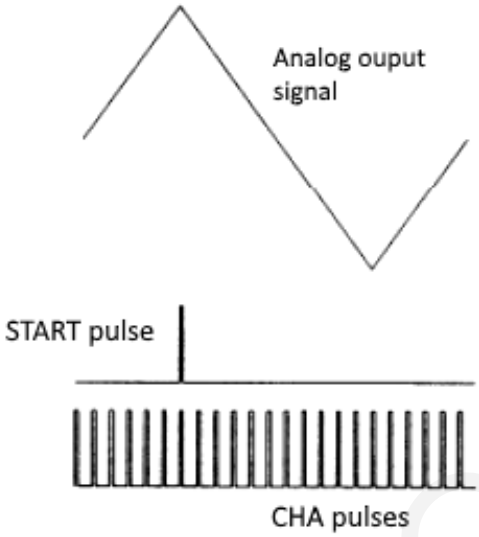

Figure 3.5: *The START and the CHA synchronization pulses that are produced from by the DFG are shown relative to the triangular waveform*

3.1.2.4 Mössbauer Velocity transducer (MVT) - Mössbauer Drive Unit (MDU) – Laser interferometer

The velocity transducer of our experimental setup was a WissEl MVT-1000. This velocity transducer is based on a solid steel housing, it is equipped with NdFeB and SmCO5 high field magnets and is capable of reaching velocities up to 300 mm/s. At the resonance frequency of ~25Hz, MVT-1000 has an accuracy of 0.5% in the sinusoidal mode and 1.5% in the triangular mode, with linearity better than 0.15%.

As a Mössbauer Drive Unit, the WissEl MDU-1200 was used. A potentiometer on the front gives to the user the ability to change easily the max velocity of the moving source. An important function of an MDU unit is the error minimisation between the waveform coming from the DFG (reference signal) and the true motion of the source. A LED line indicates the relative error in logarithmic scale. The error can be minimised by three potentiometers on the front; the gain potentiometer which adjust the amplification of the feedback loop, the P potentiometer which adjust the control circuit, whose signal is proportional to the reference signal, and the I potentiometer which adjust the control circuit, whose signal is proportional to the integral of the reference signal. Besides the LED error indicator, one can connect the MDU to an oscilloscope from the Error output in order to visualize the difference between the actual movement of the source and the reference signal. With the three previously mention

potentiometers, one must aim to reduce the amplitude of the Error signal, and at the same time to minimize the oscillation peaks at the extrema due to the triangular waveform and the sudden acceleration of the source.

The MDU-1200 was connected to a laser interferometer (WissEl MVC-450) that can be used for calibration purposes. A signal from the interferometer feeds the MDU and an internal microprocessor performs the channel to velocity conversion. On a two-line screen, one can see the velocity for each individual channel and subsequently to use it for velocity calibration purposes. This makes the calibration method easy and fast. Unfortunately, this method is suitable for velocities higher than 20 mm/s, therefore it is not suitable for precise velocity calibrations when used with ^{57}Fe MS, as the needed velocity is much less than 20 mm/s. The inability to calibrate velocities below the 20 mm/s is because between two CHA pulses the distance travelled by the source is equal or smaller than the wavelength of the Laser. However, as the measurements can last weeks, the laser interferometer can be used to observe the velocity at any given time, and make sure that it hasn't drifted from the initial settings.

The MVC-450 laser interferometer consists of a He-Ne 1 mW laser with a wavelength of 632.8nm, whose beam hits a beam-splitter prism. The beam passing through, hits a moving mirror attached to the rear end of the source's axle, while the beam exiting at 270-degrees hits a stationary one. The two beams after their reflection on the mirrors, travel back, superimpose at the splitter prism and exit at 90-degrees. A photodiode detects the intensity and produce an analog signal with variable frequency. The intensity is determined by the difference in the light paths, $\Delta S=2(L_1-L_2)$ where L_1 and L_2 the distance of the two mirrors from the splitter prism. The frequency of the signal is proportional to the source's velocity; $f = 2\upsilon/\lambda$ where λ is the wave-length of the laser. For a source's velocity of 1 mm/s, the frequency is $f = 3160Hz$ [24].

The signal from the photodiode feeds a Laser Control NIM module which transforms the analog signal to digital, which is subsequently passed to the MDU-1200 and the Data Acquisition Module. The user can record the interferometer's signal using the software of the data acquisition module (Wissoft2010) and use it to further validate the motion of the source. A graphical representation of the source's motion, as it was measured by the laser interferometer is shown in *Figure 3.6*, while a schematic of a laser interferometer can be seen in *Figure 3.7*.

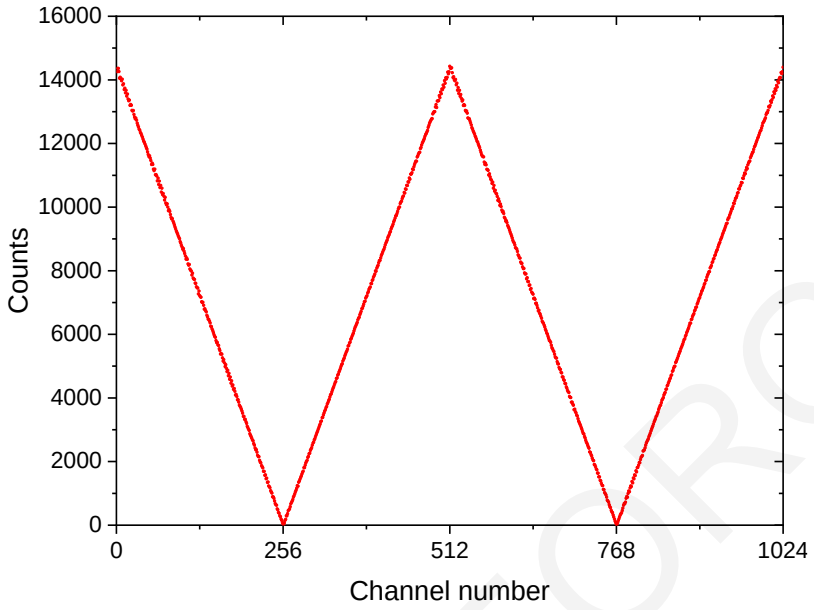

Figure 3.6: *A graphical representation of the source's motion, as it was measured by the laser interferometer*

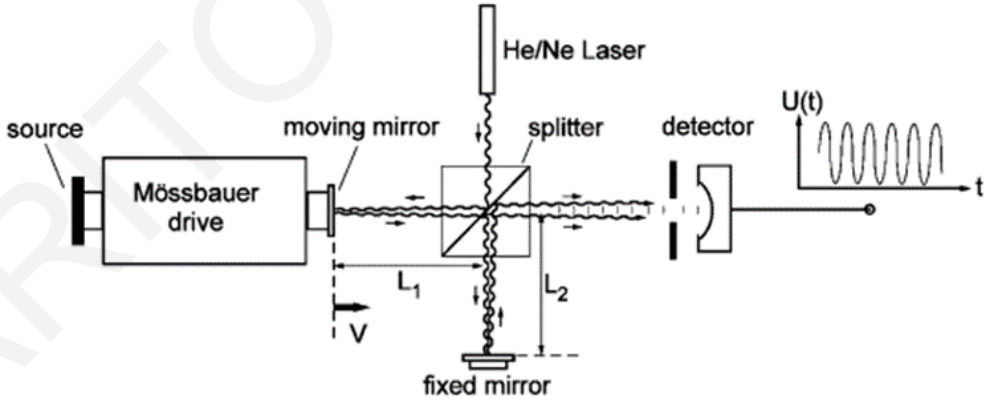

Figure 3.7*: "Principle of a laser interferometer for absolute calibration of the transducer velocity. L1 and L2 denote the lengths of the two light paths of the split laser beam, giving a path difference ΔS= 2(L1 -L2)" [24]*

3.1.2.5 Data Acquisition Module (DAM)

A WissEl CMCA-550 data acquisition unit was used. This unit can be connected to a PC with a USB cable and can be easily controlled from a suitable user-friendly software (Wissoft 2010) through Windows environment. This data acquisition module can work in a Pulse-Height Mode (PHA) to acquire the spectrum of the source directly from the detector; counts in relation to Channels / Energy, and in Multichannel Scaling (MCS) mode for Mössbauer measurements, where the counts are presented relative to the source's velocity.

3.1.3 Cryostat – Temperature Controller

The cryostat is an important tool for MS as the temperature is a significant parameter of the measurements. The cryostat used, ^{4}ICE^{BATH} by ICEoxford, is a top-loading, bath type cryostat. A top-loading system allows fast sample changing which is important for samples that cannot be thawed, like the frozen biological samples used in this study.

^{4}ICE^{BATH} cryostat has two concentric reservoirs that can be filled with liquid cryogens, like liquid Nitrogen for temperatures down to ~77K and Liquid Helium for even lower temperatures, down to ~1.4K. The cryogen from the internal reservoir passes from a capillary tube and cools a cooper heat exchanger that is connected to a central tube where the sample is located. The central tube is filled with a heat exchanging gas (helium or nitrogen) to ensure thermal coupling between the sample and the heat exchanger. The cryogen's flow from the capillary tube, therefore the cooling capacity is controlled with a needle valve. On the heat exchanger, a thermocouple and a heater are attached in order to monitor and control the temperature. The sample is placed on a holder on the edge of a ~80cm long stick (sample rod), on which another thermocouple is attached. The two thermocouples and the heater were connected to a temperature controller (Cryocon 32B), from where a desirable temperature can be set, and the controller feeds the heater as necessary in order to maintain it. A detailed schematic of the ^{4}ICE^{BATH} cryostat can be seen in *Figure 3.8*.

The reservoirs and the whole internal cryostat's assembly was thermally insulated from the environment through a 10^{-7} mbar vacuum. The vacuum was created and maintained by a turbomolecular pump system (Pfeiffer-Vacuum Turbopump) which was attached to the cryostat with flexible stainless-steel hoses.

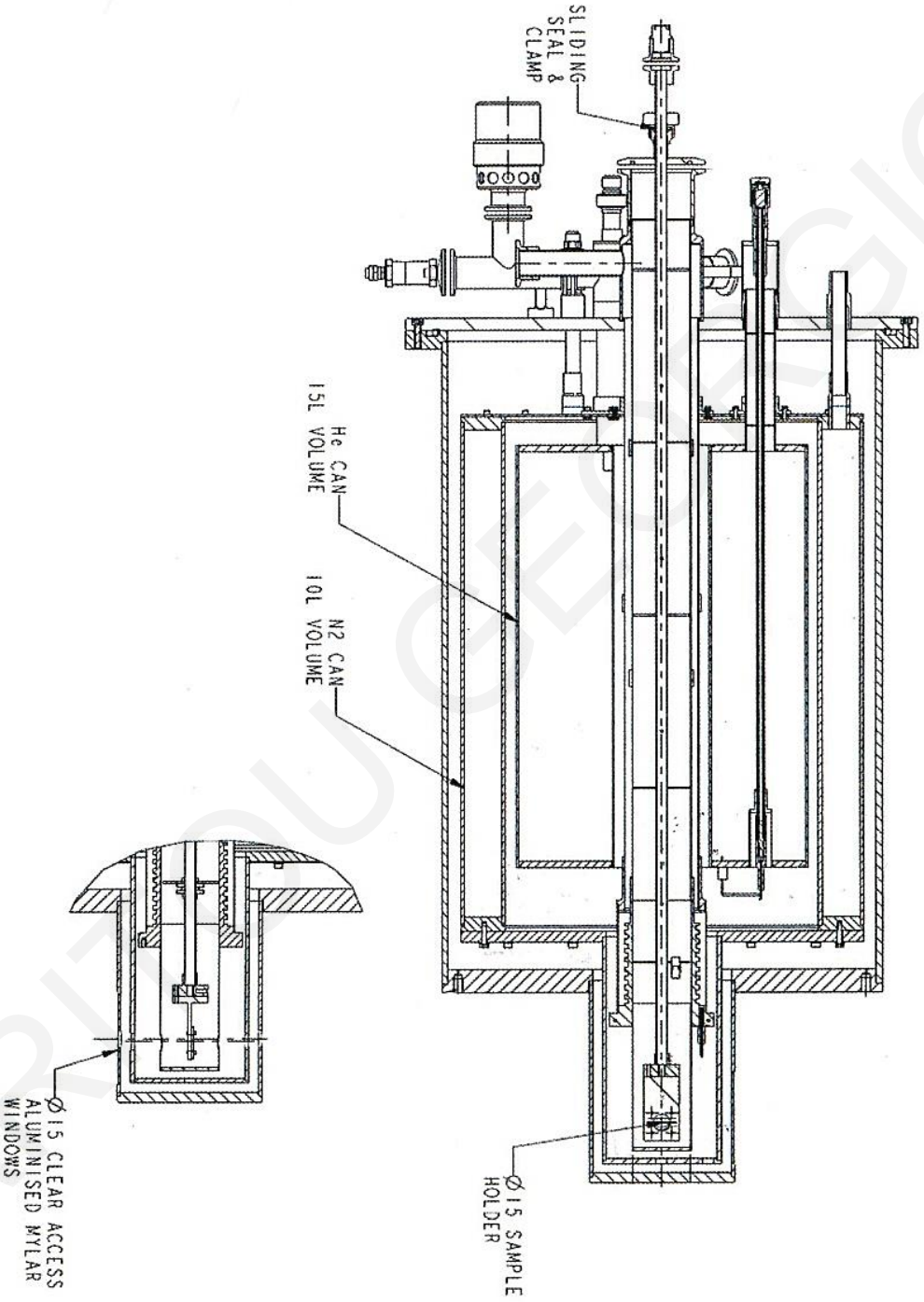

Figure 3.8: *Cross-section of the $^4ICE^{BATH}$ Cryostat [32].*

3.2 Geometry Optimization

MS is a slow method and sometimes days or even weeks are needed to measure a sample. Hence, one may be tempted to bring the source and the detector as near to the sample as possible in order to increase the count-rate. When the source is close to the detector, its motion causes high periodic variations in the solid angle θ and consequently to the incident count rate. As a result, the detector will record different counts for different positions of the source hence the baseline of the spectrum will be non-linear. This is shown in *Figure 3.9*. In the constant acceleration mode, this effect can be eliminated as long as θ remains small because the two mirror images of the spectrum are folded in the middle.

In addition to the non-linear baseline, when the distance of the source and the detector is small, the aperture α (the ratio of the detector's diameter[4] to the source-detector distance) is large, and a cosine smearing of the velocity is observed. Photons that arrive to the absorber (and subsequently to the detector) at an angle θ have a reduced Doppler energy due to the change of the velocity's vector as $v' = v\cos\theta$. Therefore, at a large aperture, the lines of a Mössbauer spectrum will be asymmetrically broadened because of the large angles. For optimum spectra quality, apertures higher than α≈0.2 should be avoided.

Besides the correct aperture and the source-detector distance, proper collimation is also important. Mössbauer samples emit substantial amount of scattered radiation originating from Compton scattering, and from X-ray fluorescence and γ-radiation that are emitted from the Mössbauer nuclei upon de-excitation. If the detector is positioned too close to the absorber, it will collect unwanted scattered radiation increasing the counting dead time. Also, the non-resonance background noise will increase, and the relative absorption of the peaks will decrease.

In our experimental setup the relatively large diameter of the cryostat (125mm) and the small windows (15mm), resulted to an aperture of less than 0.12. Thus the baseline's distortion and the cosine smearing of the velocity where minimum. In order to further decrease the non-resonance background noise, a lead collimator with a diameter of Ø12mm was placed in front

[4] If a collimator is in place in front of the detector, the collimator's diameter is used instead of the detector's one

of the detector in order to block any radiation resulting from scattering on the cryostat's window edges.

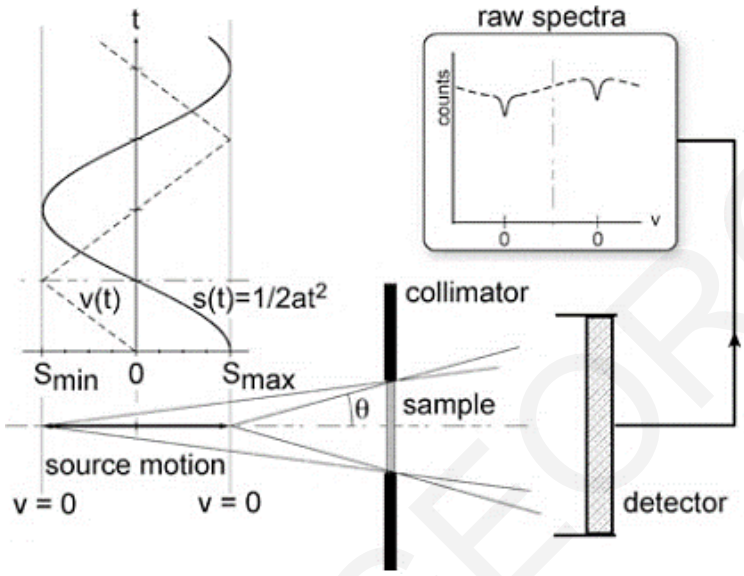

***Figure 3.9**: Variation of the spectrum's baseline as a function of the source's motion operated in constant acceleration mode [24].*

3.3 Mössbauer Spectrum Acquisition

The Mössbauer spectrum was acquired with the use of the Wissoft2010 software that accompany the Data Acquisition Module. As explained previously, a Mössbauer resonance energy is presented in the spectrum as a "dip"; a reduced count-rate relative to the count-rate of the background energies. When non-resonance photons (e.g. photons besides the 14.41keV peak) are counted, the dip decreases, therefore it is important to reject non-14.41 keV as much as possible. This can be done by excluding the non Mössbauer photons like the ~20 keV Rh X-rays and ~7 keV Fe X-rays from the counting window. In order to do that, a PHA spectrum is firstly taken (*Figure 3.10(a)*) and the minimum (lower level) and maximum (upper level) voltages of the Mössbauer 14.41 keV line are found. From optimization measurements, it was found that these two limits should be set at the ±2.5-3σ of the Mössbauer's peak for optimum count-rate and absorption. If the window is set narrower, useful counts will be rejected, while if it is set too wide more background radiation than Mössbauer photons will be measured. These two limits are set in the acquisition settings window of the software (*Figure 3.10(b)*). This makes the acquisition module to reject any pulses with voltage under the lower level and above the upper level, effectively ignoring any photons outside the emission line of choice.

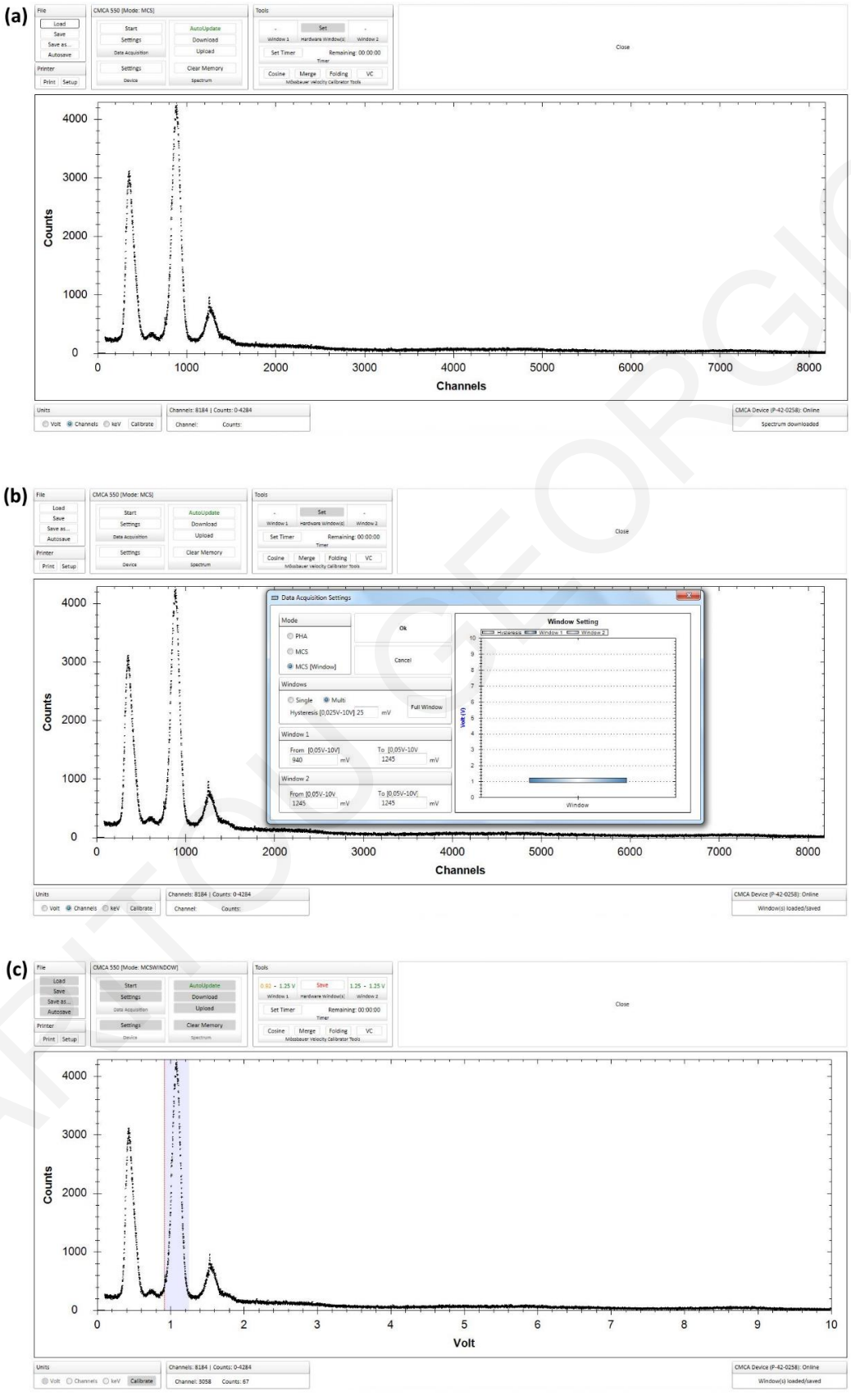

Figure 3.10: The Wissoft 2010 Data acquisition software

The selected window can be seen in *Figure 3.10(c)* as a shaded area around the second (14.41 keV) peak. With the counting window set, a Mössbauer spectrum can be taken from the MCS[window] mode. In this mode, the counts are presented relative to the source's velocity instead of the photon's energy. After the measurement (or along the measurement and upon a pre-set time window) the data are saved as a text file, which has 4 lines of general information (like the counting time and the total channels of the spectrum), followed by one column with the total counts of each channel (ascending from the zero channel).

3.4 Velocity Calibration

In order to calibrate the velocity scale, peaks with well-known positions are needed. Nowadays, the velocity calibration for the ^{57}Fe MS is performed by using pure metallic iron (5-25μm in thickness α-Fe foils) at room temperature which exhibit a sextet; six very narrow peaks well distributed between the velocities of ±10 mm/s. The distance between the inner, middle and outer peaks are D_1=1.677 mm/s, D_2=6.167 mm/s, and D_3=10.657 mm/s respectively [24] (*Figure 3.11)*. Calibration with an α-Fe foils is adequate for the most measurements, where the velocity range is less than ±10 mm/s.

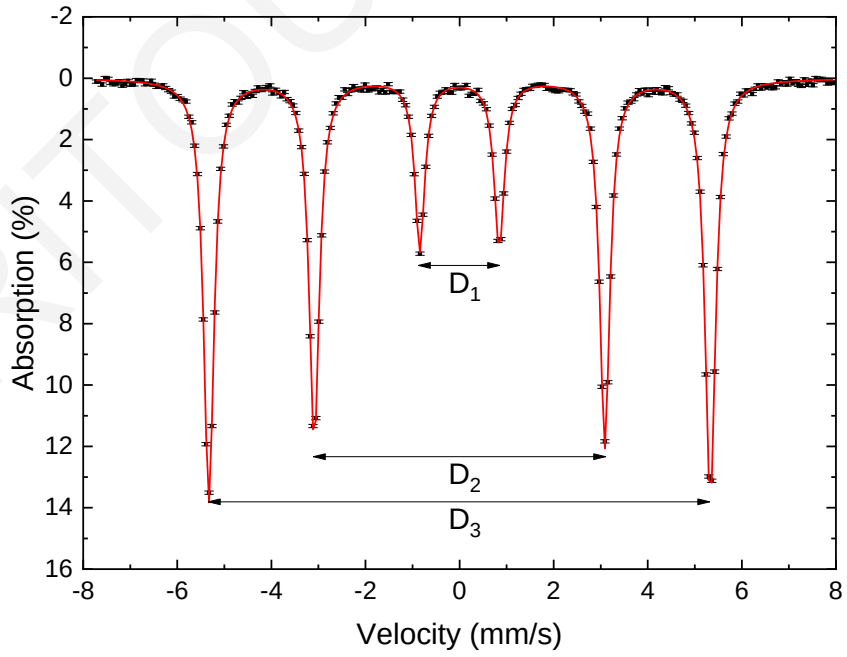

Figure 3.11*: Measured spectrum from an α-Fe foil at room temperature. The distance between the peaks is D_1=1.677 mm/s, D_2=6.167 mm/s, D_3=10.657 mm/s.*

Beside the channel to velocity matching, the point of zero velocity must also be defined. As zero velocity is set the point at the centre of the α-Fe calibration spectrum (the isomer shift (δ) of the calibration spectrum should be 0 mm/s). This makes the reported values of isomer shift irrespective of the type of the source used for the Mössbauer measurements. In the past, the velocity calibration was done with a variety of substances like sodium nitroprusside ($Na_2[Fe(CN)_5NO] \cdot 2H_2O$) therefore some caution should be given when comparing measured values with outdated bibliography.

In our experimental setup the velocity was calibrated at room temperature (RT, 298 K) using an α-Fe foil (Goodfellow Cambridge Limited) with 99.85% purity and a thickness of 8 μm. The isomer shift (δ) of the α-Fe foil relative to the ^{57}Co/Rh source at RT was found to be -0.108 mm/s, consistent with the source's manufacturing specifications and corresponding literature [24]. All following isomer shifts, and peak positions will be given relative to the α-Fe iron at RT. For the velocity of ~4 mm/s that was used for the purpose of this study, only the four inner peaks of the α-Fe foil were used for calibration purposes. Further details about the calibration process will be given in the next paragraph as each software has a different calibration procedure.

Besides the α-Fe foil, a 10 mg/cm^2 natural-abundance Fe powder absorber (≥99%, <10 μm, Sigma-Aldrich) was also used to verify the velocity and to ensure the good performance of the experimental setup, especially for the temperature of ~80K where the measurement is prone to vibrations. *Table 3.1* shows the peak positions of the α-Fe foil at RT and the natural iron absorber at RT and 78K. These values where used to ensure the good performance of the setup during the various calibrations and tests. Such measurements were performed every one to two weeks (after one to two samples)

Table 3.1 *The peak positions (X(i)) of an α-Fe foil (RT) and a Fe powder sample at 298K (RT) and 78K, where (i) is the line number, as well as the corresponding expected X(i) values [33]. The statistical errors for X(i) is ±0.002 mm/s. The instrumental error is <0.03mm/s*

Sample	Line number (i)	1	2	3	4	5	6
Reference Values (RT)	X(i) (mm/s)	-5.328	-3.083	-0.839	0.839	3.083	5.328
α-Fe foil (RT)	X(i) (mm/s)	-5.329	-3.087	-0.844	0.841	3.081	5.330
Fe powder (RT)	X(i) (mm/s)	-5.328	-3.084	-0.843	0.838	3.080	5.332
Fe Powder (78K)	X(i) (mm/s)	-5.338	-3.051	-0.753	0.967	3.265	5.558

3.5 Mössbauer spectra analysis software

Two Mössbauer spectra fitting programs were available for the analysis. The IMSG2014 (Ioannina Mössbauer Spectroscopy Group) which was given to our laboratory by the Mössbauer group of the University of Ioannina, and the WinNormos for Igor package which was purchased from WissEl with the rest of the experimental setup.

3.5.1 IMSG2014

IMSG2014 is a Mössbauer fitting software developed at the University of Ioannina and is written in Delphi. It uses full Hamiltonian matrices to generate theoretical Mössbauer spectral contributions for ^{57}Fe and ^{119}Sn which are then fitted to the experimental data based on a least-squares minimization procedure [34]. It has an interactive user interface which gives the ability to the user to easily built in real time a starting theoretical model for the experimental data. This is done just by clicking with the mouse on the spectra on the points where the user expects the peaks to be. Furthermore, the user can also modify easily the starting model and view the changes happen in real-time. This unique capability gives the ability to the user to fit with relative easiness even considerably complicated spectra. The user-interface of the IMSG2014 Mössbauer fitting software is shown in *Figure 3.12.*

Before analysing the spectrum from a sample, the user must first use a calibration spectrum (e.g from α-Fe) from which and through a user-friendly procedure, four values representing the folding point and the velocity calibration equation are extracted. These calibration values must be then written in the first line of the Mössbauer spectrum file that contains the data under study. With the addition of these data, the file can now be imported into the IMSG2014 software for further analysis.

3.5.2 WinNormos-for-Igor

WinNormos-for-Igor [35] is a user-friendly package designed for the Igor data analysis software and is specialised in fitting and analysing Mössbauer spectra. It has two panels, the WinSite (seen in *Figure 3.13*) and the WinDist. WinSite is used for treating a discrete set of sub-spectra while WinDist is intended to treat problems including a distribution of hyperfine parameters, e.g. in metallic glasses.

In the WinNormos package, one can calibrate the velocity with two ways. Either by using a WissEl laser file, or by setting manually the V_{max}. For a ^{57}Fe calibration spectrum showing all six

peaks, the software can automatically find the V_{max} by setting the hyperfine magnetic field (mention as BHF in the software) to 33.1 T. In our measurements, where the velocity was ±4 mm/s and the outer peaks of the α-Fe calibration spectra not visible, a manual procedure was followed in order to find the correct V_{max}. As the spectrum from the α-foil (or the metallic iron) exhibits four peaks in this velocity range, four singlets where placed with fixed isomer-shift to the values seen in *Table 3.1.* Then the V_{max} was manually changed (decreased or increased accordingly) and the spectra was fitted until the χ^2 was minimised. The V_{max}, which minimises the χ^2, indicates the best fit and thus it represents the correct maximum velocity in which the spectrum was taken. The laser calibration method was not used because, as explained previously, is not accurate enough in such small velocities. A screenshot of the WinNormos for Igor package is shown in *Figure 3.13*.

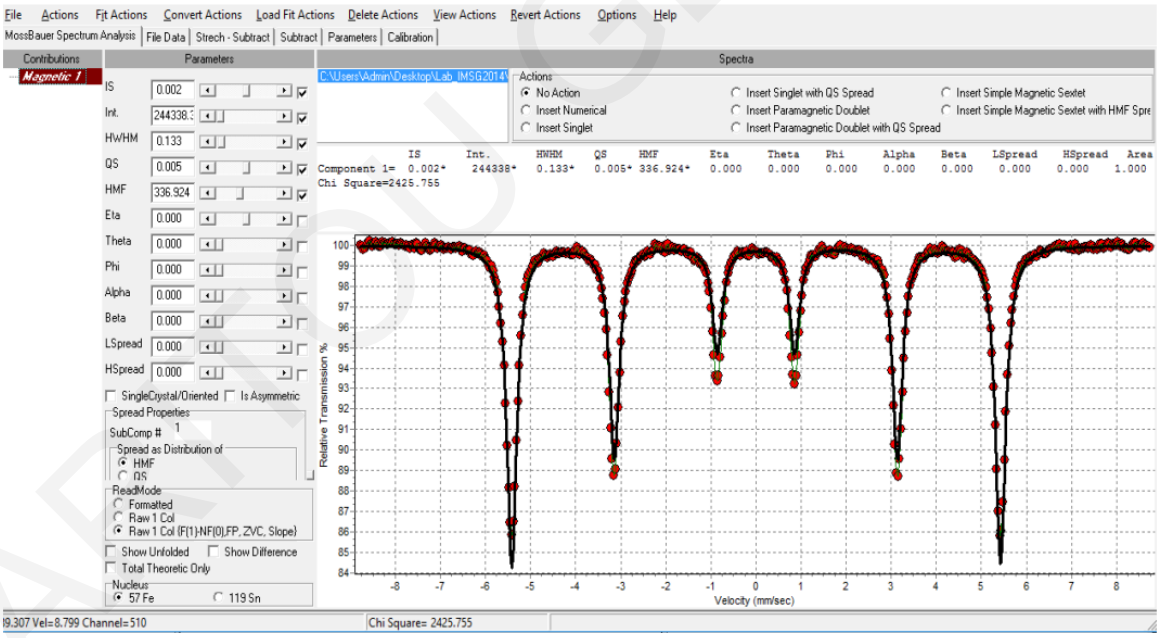

Figure 3.12 *Screenshot of the IMSG2014 program during an α-Fe analysis*

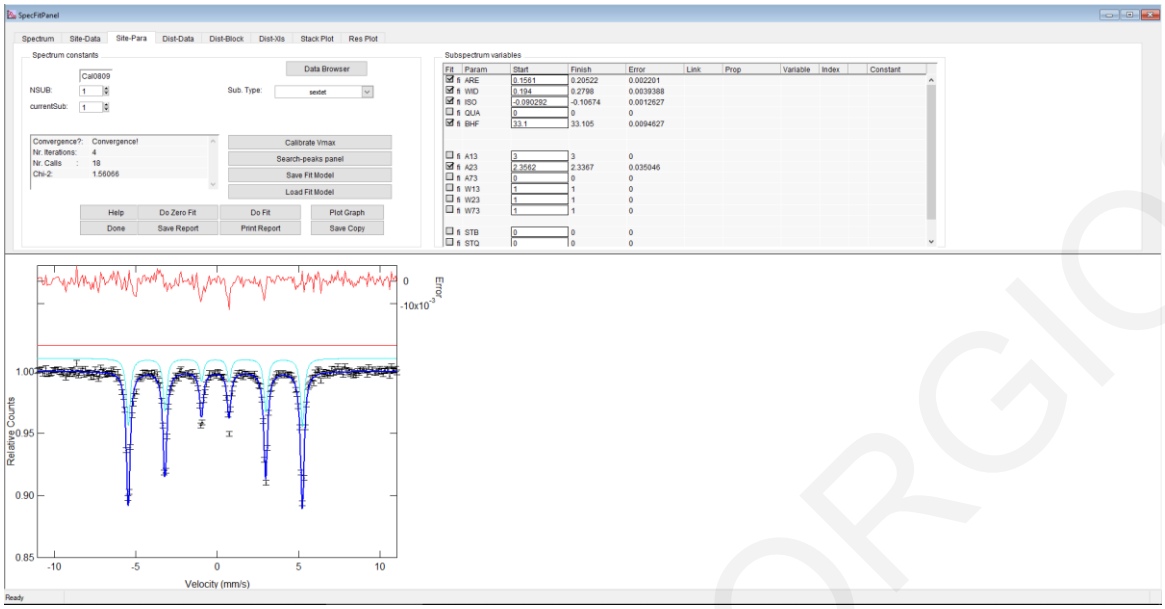

Figure 3.13: *Screenshot of the WinSite card, of the WinNormos for Igor software during an α-Fe foil fitting*

For the final analysis of our Mössbauer spectra, the WinNormos package was used due to its ability to provide to the user the Area of each sub-spectra, a value which is necessary for comparing the amount of iron complexes found in different samples.

3.6 Background Measurements

Before any measurements, it is important to evaluate the affect of the experimental setup to the measured spectra of the samples because iron can be found as impurity to the aluminized mylar windows of the cryostat, to the beryllium window of the detector and in the lead or copper material of the collimators. All this iron impurities within the beam's path can potentially add peaks to the spectrum, especially if the iron content in the sample is small, and eventually affect the results.

To evaluate this, an empty sample-holder was placed and measured to $3x10^6$ counts per channel (before folding), twice the counts of a typical measurement. As seen in *Figure 3.14,* the resulting spectrum can be described by a doublet with Γ=0.49 mm/s, δ=0.18 mm/s and ΔEq=0.56 mm/s. Its absorption is in the order of ~0.05 – 0.1% and it is too small to impact a typical measurement. Therefore, it won't be taken into consideration in the following fittings and analysis.

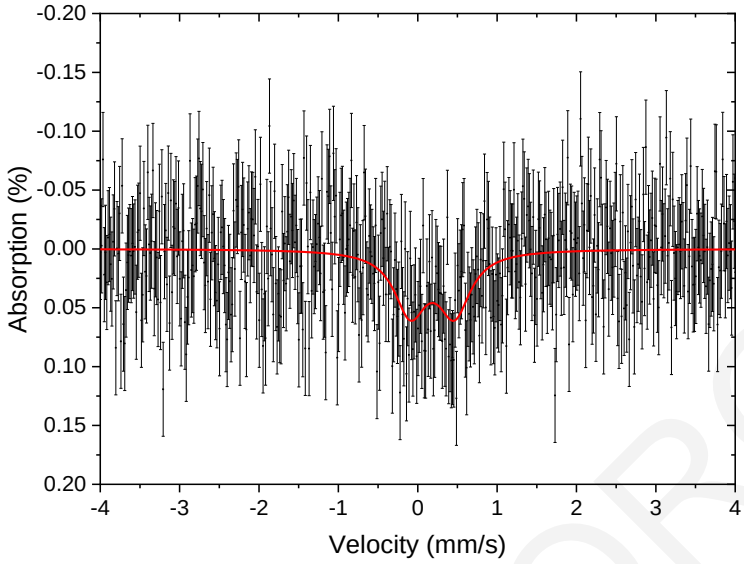

Figure 3.14: *MS spectrum with an empty sample-holder for background evaluation*

3.7 Sample holders

Most Mössbauer holders are thin empty cylinders with a suitable cap, around 15 mm in diameter (Ø15 mm), made of Plexiglass (PMMA) and are mostly suitable for powder samples or liquids with high iron content. They are usually hand made one by one on a lathe, which is a time-consuming and relative expensive method.

The biological samples that were used in this study had some unique features that made the standard PMMA, lathe fabricated holders unsuitable. Firstly, due to the nature of the bio-samples and the potential biological hazards that accompany them, the holders are preferable not to be washed and reused, thus they must be of one-use. Also due to the expected large number of the samples needed for the study, they should be able to be produced in large numbers. Therefore, the holders should be easily fabricated with a relatively low cost. Furthermore, the sample volume is limited because mice organs have various shapes and sizes. In general, mice organs are very small therefore Ø15 mm holders are inapplicable because if the sample does not cover the whole surface of the holder, a significant percentage of the beam will arrive to the detector without any interaction with the sample. As a result, lower absorption will be experienced, giving spectra with low signal-to-noise ratio.

To overcome these difficulties, custom-made holders for the bio-samples were fabricated with the vacuum thermo-forming method, using copper molds (to eliminate any iron contamination

to the holders), and polypropylene (PP) sheets. PP sheets of a thickness of ~0.75 mm where found to be both easy to work with, strong enough to hold their shape and durable at liquid nitrogen (LN) temperatures. Due to the ease with which items are made with the vacuum thermo-forming method, different holders of different dimensions can be easily crafted by just using different molds. The fabricated holder assembly consists of two parts: a cylindrical base (cup) where the sample is placed within, and a similar cap (plug). Both parts had a length around ~10 mm. The PP cap had slightly larger diameter (~0,5mm) but still slightly smaller than the external diameter of the base. This allow the cap to expand due to the small elasticity of the material, and fit tightly over the base. This way the whole holder assembly is both spillage resistant and hermitically sealed.

Because the new holders have different dimensions from the original ones, they do not fit in the existing place of the sample rod. To overcome this, aluminum rings were fabricated with the correct inner and outer diameter. These rings are placed and secured in the original Ø15 mm hole and decrease the diameter according to the external diameter of the holder in use. To make a measurement, the sample holder is just pushed tightly in the hole. Tightness of the whole assembly is essential in order to eliminate any vibrations due to sample's slack. Some PP holders and their rings are shown in *Figure 3.15*.

To prevent any radiation coming to the detector directly from the plastic sides of the holders or the aluminum ring without any interaction with the sample, 2mm thick copper plates that can effectively stop the 14.41 keV photons, with a hole in the center about 3mm smaller than the rings inner diameter, were attached to the very back of the assembly and used as collimators. A schematic diagram of the whole assembly is shown in *Figure 3.16*. The PP sample holder is shown with light blue, the aluminum ring with gray, the copper collimator at the very back of the assembly with red, and with gold-orange the final part of the sample rod.

Figure 3.15: *PP holders of various diameters and the rings used to be attached on the sample rod*

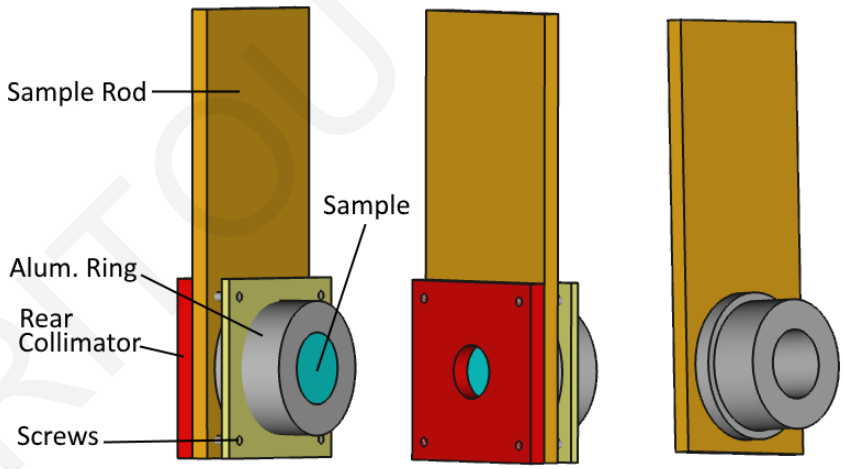

Figure 3.16: *Schematic diagram of the holder assembly. With light blue the PP sample holder, with grey the aluminium ring, with red the copper collimator at the back and with orange the final part of the sample stick.*

Besides the holder size and the collimation of the beam, one other important parameter is the material from which the sample holders are made of since the 14.41 keV photons are easily absorbed by various materials. The absence of atoms such as oxygen, nitrogen and chlorine in the polypropylene molecule $[(C_3H_6)_n]$ compared with other thermoplastics should result in high transparency to low-energy X- and γ- rays. A Si-Pin X-ray detector (Amptek XR-100CR) with high energy resolution was used to acquire the transmission spectra of a PP and an existing PMMA holder at ^{57}Co energies of 6.36 keV and 14.41 keV respectively. The measurements showed that at the energy of interest (14.41 keV), the transmission of our PP holder was 96%, significantly enhanced from the 56% transmission obtained from the standard PMMA holder. The new holder with its increased transmission should lead also to reduced acquisition times. The measured transmission spectra are shown in *Figure 3.17*. *Table 3.2* shows the measured FWHM, the net count rate (rate) and the percentage transmission without a holder, with the PMMA holder and with our custom-made PP holder.

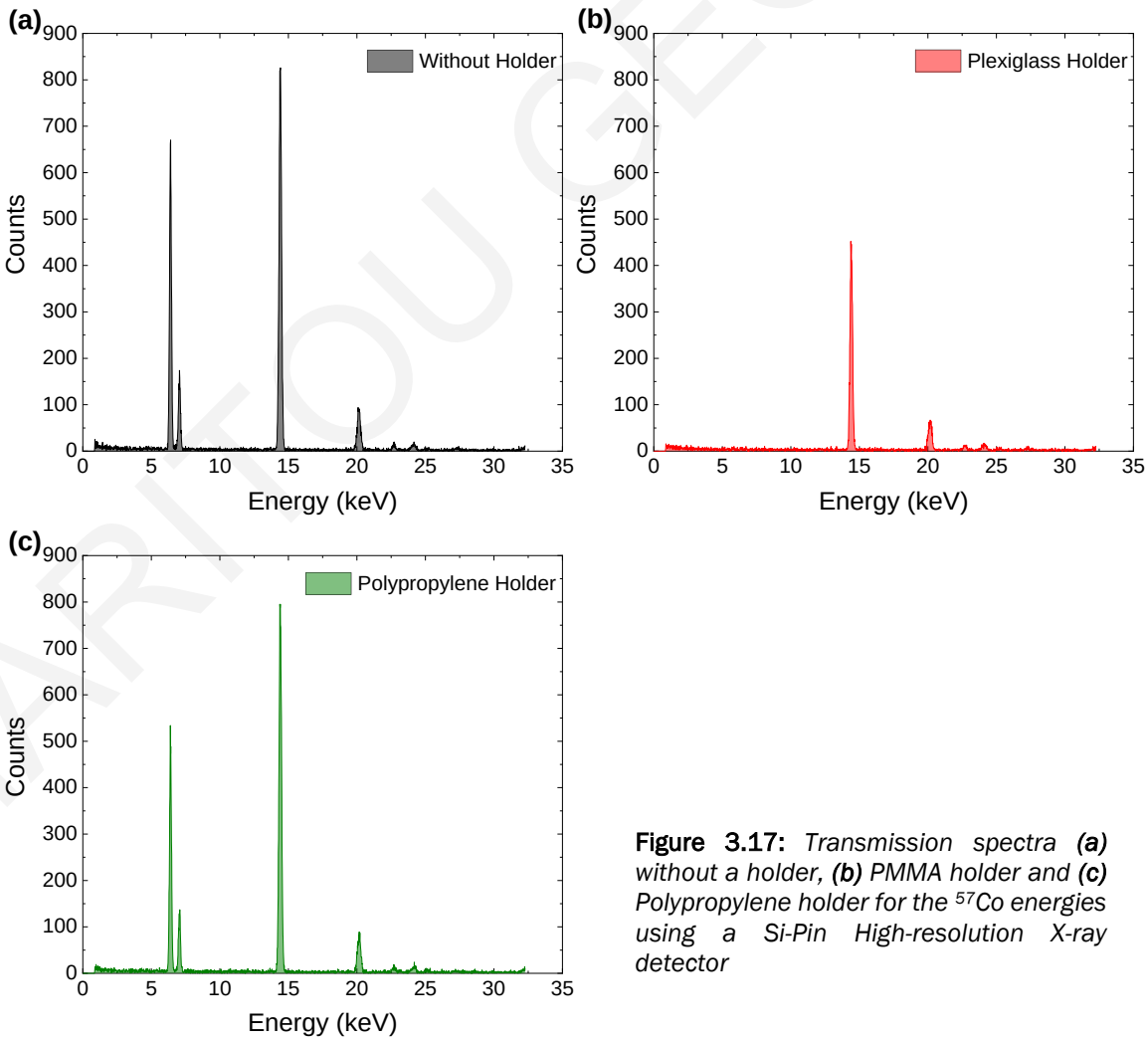

Figure 3.17: *Transmission spectra* ***(a)*** *without a holder,* ***(b)*** *PMMA holder and* ***(c)*** *Polypropylene holder for the ^{57}Co energies using a Si-Pin High-resolution X-ray detector*

Table 3.2: *The measured FWHM, net count rate (rate) and transmission (T) without a holder, and with a Plexiglass (PMMA) or a polypropylene (PP) holder at ^{57}Co energies*

Material	E_γ=6.36keV			E_γ=14.41keV		
	FWHM	Rate (cps)	T (%)	FWHM	Rate (cps)	T (%)
No holder	0.155	124	100	0.20	209	100
PMMA holder	-	-	-	0.22	117	56
PP holder	0.153	96	77	0.21	201	96

3.8 Levelling

Prior to collecting data, the experimental setup should be levelled, and the source-cryostat-sample-detector perfectly aligned as even the slightest misalignment can significantly reduce the beam's intensity and dramatically increase the acquisition times.

The main frame of the experimental setup is supported by four (4) legs, one in each corner. By adjusting their height, the frame and subsequently the cryostat can be levelled in all axes using a bubble level. The MVT (and hence the source) and the detector are placed on a bench using special mounts, therefore they are aligned one relative to the other. However, the mental line that connects the source and the detector must pass through the cryostat's windows (Ø15 mm) and the sample inside. The bench is held on the frame with four (4) screws and by adjusting them, the height and the angle of the bench relative to the frame can change.

To align the beam to the cryostat, the sample rod was removed and the MVT and detector were positioned on the edges of the bench (with the mental line that connects them passing through the cryostat's windows). PHA spectra were taken, keeping the acquisition time constant, and the four (4) screws were adjusted accordingly in order to find the position with the highest count-rate. After aligning the frame and the bench, a 6 mm sample ring was placed on the sample rod, which was then placed in the cryostat. PHA spectra were taken again and the length of the rod was changed until the position with the maximum count-rate was found. The effective diameter of the source is 5 mm, therefore a 6 mm ring ensures that the beam will pass from the very centre of the sample.

A schematic diagram of the experimental setup with the abovementioned parts and instruments is shown in Figure 3.18.

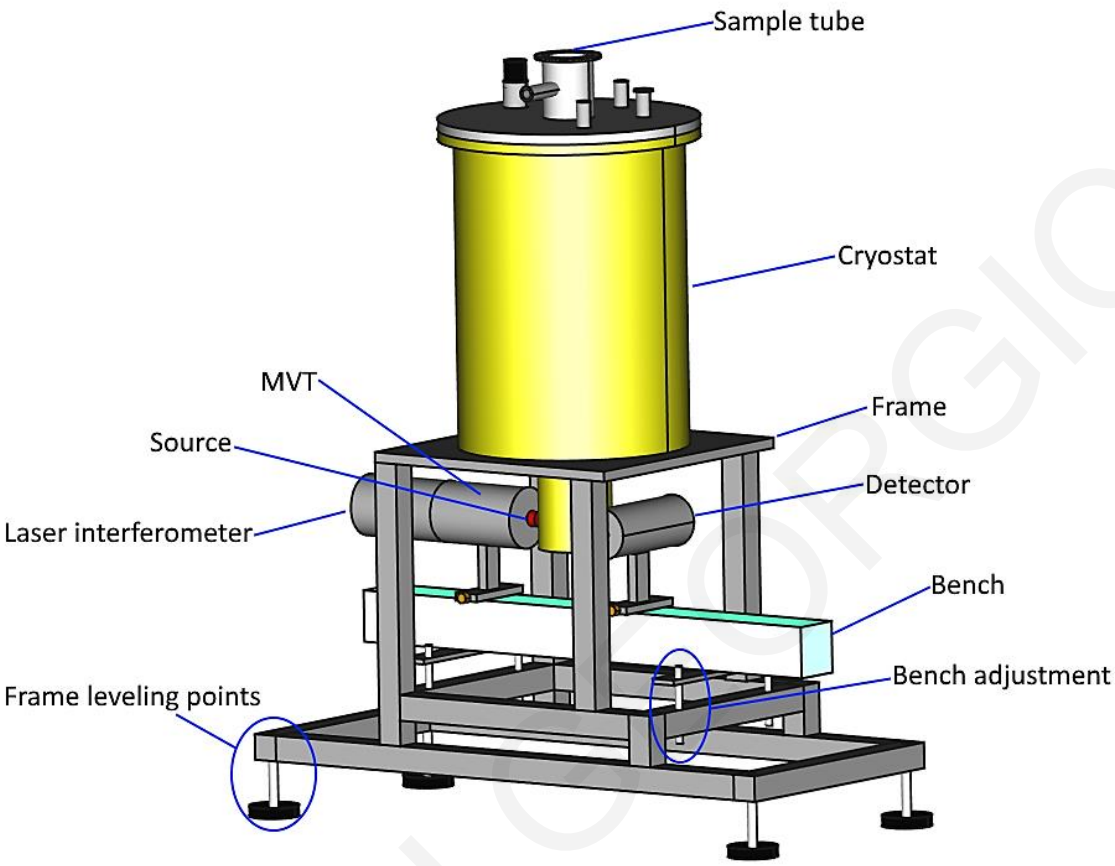

Figure 3.18: *Schematic view of the experimental setup which shows the position of each instrument.*

3.9 Vibrations

Vibrations is a serious problem in Mössbauer spectroscopy that must be avoided as it can lead to significant line broadenings. ^{57}Fe MS is very prone to vibrations that it is no exaggeration that the following rule of thumb is applied to a ^{57}Fe spectrometer: "If one touches the equipment lightly with the fingertips and notices any traces of vibration, the experiment will fail" [27]. Unfortunately, our experimental setup was not spared from this problem and significant line broadenings were experienced when the samples were placed inside the cryostat. The α-Fe foil's peaks were broadened to the unacceptable values of 0.6-0.8 mm/s, much higher than the normal 0.24-0.28 mm/s, resulting in unreliable measurements.

To overcome the problems arising from the vibrations, a lot of effort and time was spent. Initially their origin of the vibrations was investigated in order to take the appropriate measures, and

optimize the experimental setup. The first source of vibrations was found to be due to the evaporation of the LN. The cold LN vapours where exiting the cryostat from a pressure valve, which was found to vibrate considerably. To overcome this, the LN vapours were left to exit the cryostat unrestrictedly through a long 1 m hose, attached to a second opening. The long hose prevents the atmospheric air and moisture to come back inside the cryostat and create ice. The second problem was originating from the turbomolecular pump and more specifically from the vibrations traveling to the experimental setup through the stainless-steel vacuum hose. To eliminate these vibrations, the hose was initially fixed on the wall with clamps, an attempt to let the high mass of the wall to absorb them, but without much success. The opposite, that is, firmly fixing the hose on the wall seemed to make the problem even worst, probably due to oscillations. As a second approach, the hose was loosely secured on the wall by putting polyurethane foam insulation around the tube in the places where the clamps would attach, but with no significant broadening reduction. The biggest reduction in the line-width was achieved when the stainless-steel tube was left to hang from the cryostat and lie without any restrictions, freely on the floor.

To further reduce the vibrations, the mass of the whole setup was increased by putting lead bricks on the cryostat's stand and on top of the cryostat itself. Furthermore, a sheet of Sorbothane®, a visco-elastic polymer with a very high damping coefficient, was placed between the cryostat and its base in order to further absorb any vibrations travelling from the ground/building to the cryostat and the sample inside.

However, beside the previously mentioned vibration sources, the most important source of vibrations and the consecutively line broadening, was found to be the design of the sample rod and more specifically the radiation shields. These shields (stainless-steel disks along the main axis) had a diameter of ~1 mm smaller than the inner diameter of the sample tube. Thus, due to a very light bending of the rod along with minor misalignments during its placement, some disks were touching the walls of the sample tube transferring vibrations directly to the sample. As the cryostat was used only with LN (and not with LHe), the radiation disks on the sample rod were not necessary and a new "simpler" rod was fabricated eliminating this vibration source.

3.9.1 The new sample rod

The new rod is schematically shown in (*Figure 3.19*). It consists of three different segments; a nylon "plug" at the top, a long stainless-steel threated rod, and an aluminium fixing position at the bottom.

At the top, the nylon “plug” (beige part in *Figure 3.19*) was fabricated on the lathe and its role is to support and align the sample rod to the cryostat. Its lower section is positioned inside the sample tube and has diameter slightly smaller than the tube. In this way the sample is constantly placed in the centre. The middle sections seats on the upper external part of the sample tube and an O-ring provides sealing. In the middle along the main axis, a Ø12 mm thread was created in which a long Ø12mm solid stainless-steel threated rod is screwed. The overall length of the sample-rod assembly can be changed and fine-tuned by screwing the threated rod to the upper segment. The ability to fine-tune the overall length is important because the sample must be perfectly aligned to the radiation beam. At the bottom of the assembly, an aluminium fixing position is screwed where the sample holder (orange component in *Figure 3.19*) is placed and tightened.

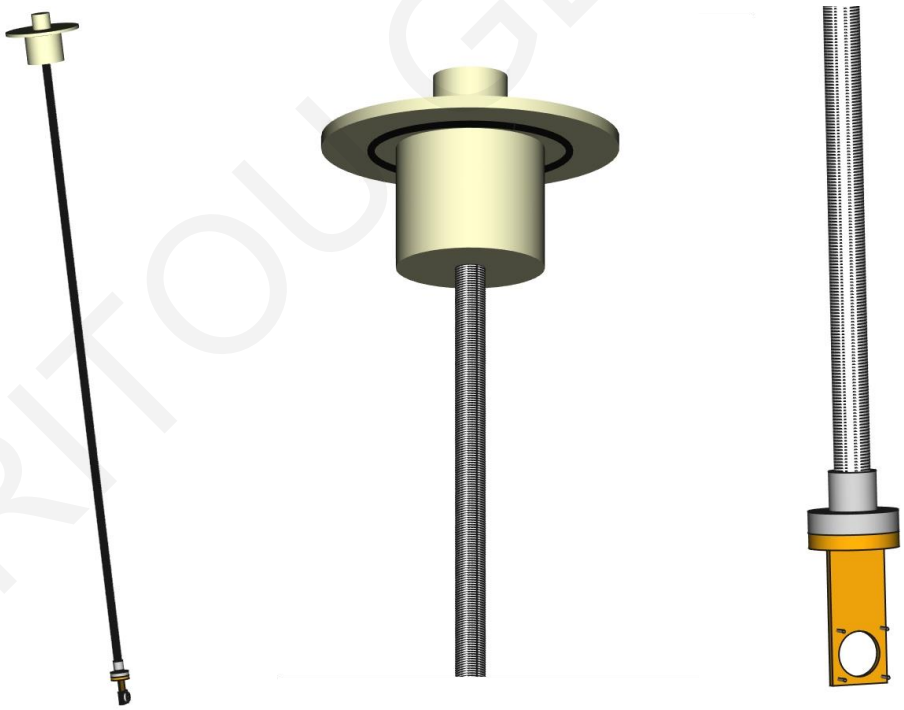

Figure 3.19: *A schematic diagram of the new sample rod is shown. The top (beige) part and the sample holder (orange) are connected with a solid stainless-steel threated rod.*

3.10 Performance evaluation

To probe the effectiveness of the abovementioned fixes and optimizations, test the reproducibility of the measurements and evaluate the good performance of the experimental setup, the spectrum from a ~10 mg/cm^2 metallic Fe absorber (described previously) was acquired five different times at 80K. For each measurement, the sample rod was completely removed from the cryostat and repositioned in order to take into account any possible variable that might affect a measurement. The average width of the five sextets was 0.272 mm/s, with the minimum and maximum values 0.270 mm/s and 0.275 mm/s, respectively. The small deviation among the measurements indicates that the vibration problem was resolved and the effect of the experimental setup to the width of the peaks is reproducible. Table 3.3 and Table 3.4 show the values of the width (Γ_i) and the position (X_i) of each individual peak from the five test spectra, along with their mean values.

Table 3.3: *The width (Γ_i) of the 6 peaks, fitted as singlets, from the five test spectra with a 10 mg/cm^2 metallic Fe absorber at 80K. The statistical error of the fit is 0.01 mm/s*

	Γ_i (mm/s)					
Peaks	**1**	**2**	**3**	**4**	**5**	**6**
Test 1	0.28	0.27	0.26	0.25	0.27	0.28
Test 2	0.27	0.27	0.26	0.26	0.27	0.28
Test 3	0.28	0.28	0.27	0.25	0.27	0.29
Test 4	0.28	0.26	0.26	0.26	0.27	0.27
Test 5	0.27	0.27	0.27	0.27	0.27	0.27
Mean Value	**0.28**	**0.27**	**0.26**	**0.26**	**0.27**	**0.28**

Table 3.4: *The position (X_i) of the 6 peaks, fitted as singlets, from the five test spectra with a 10 mg/cm^2 metallic Fe absorber at 80K. The statistical error of the fit is 0.010 mm/s*

	X_i (mm/s)					
Peaks	**1**	**2**	**3**	**4**	**5**	**6**
Test 1	-5.345	-3.056	-0.750	0.969	3.274	5.570
Test 2	-5.345	-3.054	-0.752	0.969	3.272	5.568
Test 3	-5.345	-3.056	-0.752	0.969	3.272	5.569
Test 4	-5.343	-3.055	-0.745	0.971	3.269	5.564
Test 5	-5.346	-3.053	-0.754	0.971	3.270	5.569
Mean Value	**-5.345**	**-3.055**	**-0.751**	**0.970**	**3.271**	**5.568**

Chapter 4

Thalassaemia studies via Mössbauer Spectroscopy and a mouse model

The mouse is a genetically and physiologically well characterized organism with close genetic and physiological similarities to humans. Mice develop various diseases common to humans naturally, but they can also be manipulated to develop diseases non-natural to them, like thalassaemia. They often respond to experimental interventions differently than humans, but they can be affected by diseases in a similar way. Additionally, the small size, quick reproduction and relative low maintenance cost makes it an ideal tool for in vivo studies. For these reasons, mice are used for over a century as a model organism for various diseases in a wide range of biomedical fields.

The thalassaemia mouse model [36] used in this study has both the *b1* and *b2* adult mouse globin genes deleted. Because homozygous mice die perinatally, mice heterozygous for this deletion which were bred on *C57BL/6* background were used. Heterozygous *(th3/+)* mice appear normal but they show haematologic indices characteristic of severe thalassaemia, exhibit tissue and organ damage typical of the disease, and develop spontaneous iron overload in the spleen, liver, and kidneys. Iron deposits appear very early and therefore they are suitable candidates to study iron accumulation in the organs. Adult *th3/+* mice have a degree of disease

severity similar to that of thalassaemia intermedia patients [37]. *C57BL/6 wild-type*[5] mice (*+/+*), a common strain of laboratory mice, were used as the control group.

In relation to Mössbauer spectroscopy, mice were rarely used in this field. In the literature only five (5) studies [38–42] were found where mice have been used in combination with MS, with the oldest one published in 2012. Therefore, even though thalassaemic mice have been utilized in various fields of research, this is the first time they are used with MS. More specifically, no thalassaemia animal model, of any kind, was ever used with Mössbauer spectroscopy.

Therefore, with this study[6], we aim firstly to show that various organs of mice can be used successfully with ^{57}Fe Mössbauer spectroscopy in order to study thalassaemia or any other iron related disease, and secondly to use MS in order to provide novel information about iron accumulation in the major organs when β-thalassaemia is present. Mice did not receive any chelation therapy like human patients, and therefore, the iron depositions and complexes due to thalassaemia are not altered.

[5] Wild-type (wt) refers to the phenotype of the typical form of a species as it occurs in nature

[6] The study was approved by the Cyprus Veterinary services. Project license: CY/EXP/PR.L2/2017

"All needed animals were provided and housed by the Transgenic Mouse Facility (TMF) at the Cyprus Institute of Neurology and Genetics (CING). The animals were kept in specific pathogen free (SPF) conditions, according to the regulations contained in the Cyprus Law (1994-2013) for the protection of animals used for scientific purposes, which is fully harmonized to the EU Directive 2010/63/EE. The facility is licensed by the Cyprus Veterinary Services (CY.EXP.101). The animals were maintained in cages with free access to water and food and were kept under a 12h light/dark cycle in a temperature-controlled environment (21oC, 45% humidity)".

4.1 Preliminary studies

As can be seen in *Table 4.1,* the organs of the average *C57BL/6* mouse are small, around 0.1-1 g, and therefore the available volume for sample preparation is insufficient for a standard ~Ø15mm MS absorber. Also, the fact that iron concentration in the biological tissues is very limited, makes the preparation of MS absorbers with sufficient amount of iron very difficult. Furthermore, the biological samples are very sensitive, especially to temperature, and freezing and thawing often destroys cells and proteins. Hence, special handling, preparation and storage is necessary otherwise they may be spoiled, resulting in unreliable results.

Therefore, since literature about MS and mice was very limited in the early stages of this work, thalassaemic mice were never used with MS, and raising mice is both cost and time consuming, it was important to firstly test and optimize the method and equipment, and subsequently evaluate and confirm the importance of the mouse model in general, and the thalassaemia model in particular.

Table 4.1: *Organ weight for 16week old female and male C57BL/6J mice. Data from "The Jackson Laboratory" [43].*

Organ	Female weight (g)	Male Weight (g)
Average body weight	22.15±2.09	29.97±1.87
Brain	0.415	0.420
Heart	0.145	0.200
Liver	1.038	1.444
Left Kidney	0.117	0.164
Right Kidney	0.134	0.174
Spleen	0.081	0.080

4.1.1 Sample Preparation

Similar amount of blood and wet tissue samples from the liver and spleen of one *wild-type C57BL/6* (+/+) and one thalassaemic (*th3*/+) mouse were investigated. The two mice were age and sex-matched and were raised in similar conditions with the same diet provided to them. Blood samples were collected in plain Eppendorf tubes by retro-orbital bleeding of anaesthetized (Tribromoethanol 10 μL/g) animals. Heparin was added to prevent coagulation.

Following euthanasia of the animals, the liver spleen and heart were isolated and washed several times with phosphate-buffered saline (PBS) to remove excess blood traces. All samples were then placed in the custom-made PP holders described previously (*paragraph 3.7)*, snap-frozen by dipping them into liquid nitrogen and stored at 78K in a LN Dewar suitable for bio-sample storage.

4.1.2 Results and Discussion

Blood Samples

Figure 4.1 (a) and (b) show the MS spectra at 78K of the blood samples for the *wild-type* and the *th3/+* mouse, respectively. The spectrum from the *wild-type* sample (*Figure 4.1(a)*) with a signal-to-noise ratio (S/N) of 23 was fitted with two quadrupole doublets, representing the α- and β-chains of oxy-haemoglobin. A significantly decreased absorption is observed in the spectrum (*Figure 4.1(b)*) of the thalassaemic sample, which is due to reduced haemoglobin levels. This indicates severe anaemia, which is also expected from a thalassaemia major patient without any treatment [4]. The parameters (δ, ΔEq and Γ) of the two doublets from the *wild-type* sample *(Table 4.2)* were used to fit the spectrum of the thalassaemic mouse (*Figure 4.1(b)*), allowing only the doublets area to vary. The fit was unsatisfactory, probably due to additional iron-containing complexes. Because of the low S/N ratio (~10) of this spectrum, a furthermore detailed analysis was not possible.

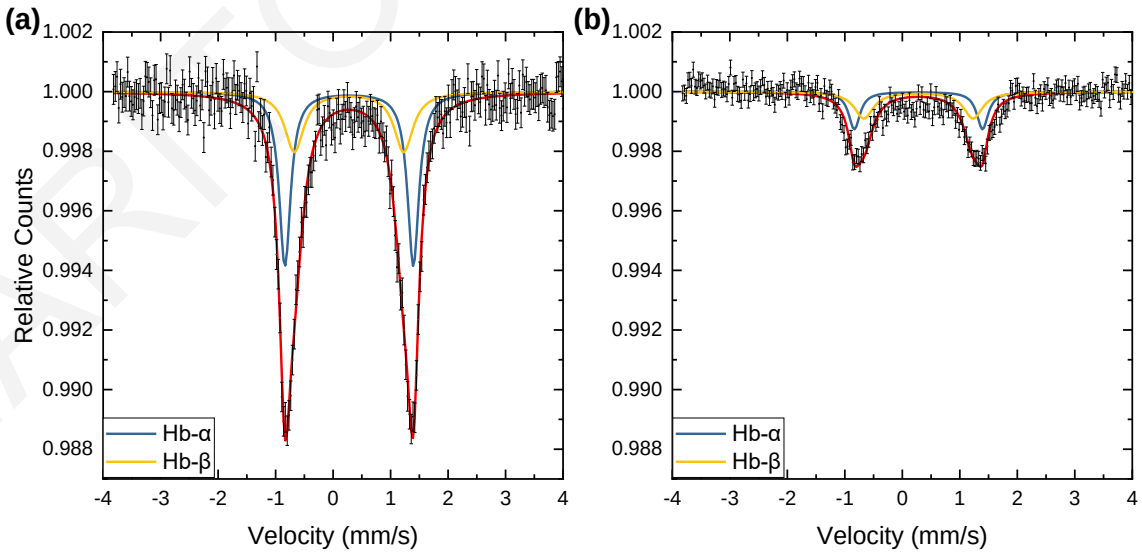

Figure 4.1: *Mössbauer spectra of blood samples from a wild-type (+/+)* ***(a)*** *and a th3/+ thalassaemic mouse* ***(b)*** *measured at 78K and ploted on the same scale. The two subspectra correspond to the α- and β- haemoglobin chains*

The values of the MS parameters for the two oxy-Hb subspectra, are similar to those reported in other studies which measured normal RBC samples of a human, a rabbit and a pig [44]. Also, the relative area of both the α- and β-subunits is comparable in amount, which is in agreement with the equal distribution of the iron nuclei in each type of subunits in haemoglobin tetramer [44].

Table 4.2: *The line width (Γ), isomer shift (δ), quadrupole splitting (ΔE_Q), and the relative area of the sub-doubles A and B, if any, from the Mössbauer fitting parameters of* Figure 4.1(a) & (b), Figure 4.2 (a),(b) (c) and (d). *The instrumental error is <0.03 mm/sec. The statistical error from the fit is shown next to the values*

Sample	Sub-spectra	Γ (mm/s)	δ (mm/s)	ΔE_Q (mm/s)	Area (%)
+/+ Blood	Hb-α	0.24±0.03	0.28±0.01	2.23±0.02	51
	Hb-β	0.40±0.03	0.28±0.01	1.90±0.07	49
th3/+ liver	Ferritin-like	0.63±0.02	0.46±0.01	0.71±0.01	100
+/+ spleen	Ferritin-like	0.58±0.01	0.47±0.01	0.69±0.01	100
th3/+ spleen	Ferritin-like	0.56±0.01	0.47±0.01	0.69±0.01	97
	Deoxy-Hb	0.24±0.06	0.86±0.02	2.27±0.03	3

Heart, Liver and Spleen

The spectra from the hearts were of no use as no significant absorption was observed. *Figure 4.2 (a) and (b)* show the MS spectra at 78K of the liver samples from the *wild-type* and the *th3*/+ mouse, respectively. The spectrum of the thalassaemic sample (*Figure 4.2 (b)*) with a S/N ratio of 16 was fitted with a single doublet while the spectrum of the normal sample (*Figure 4.2 (a)*) with a S/N ratio of ~5 could not be fitted. The MS spectrum of the normal sample presents lower absorption than the thalassaemic one due to lower iron concentration. The Mössbauer parameters of the doublet are shown in *Table 4.2* and agree with those for ferritin-like iron obtained at the same temperature from dietary iron overloaded and parenteral-loaded liver samples of rats [45].

Figure 4.2 (c) and (d) shows the MS spectra at 78K of the spleen samples from the *wild-type* and *th3*/+ mice, respectively. The spectrum from the normal sample *Figure 4.2(c)*, (S/N=27) was fitted with a single symmetrical doublet. Its Mössbauer parameters, given in *Table 4.2* are in agreement with those of a ferritin component observed in the corresponding MS spectra, at the same temperature, of human spleen samples [46]. The corresponding spectrum of the

spleen sample for the thalassaemic *th3/+* mouse, *Figure 4.2(d)*, (S/N=39) was fitted with two sub-doublets, a large component (97%) with a slightly asymmetric doublet of a ferritin-like component and another small component (3%) of deoxy-haemoglobin, which is probably due to remained blood residues within the spleen. The Mössbauer parameters for the fit are shown in *Table 4.2.* The extracted values are in agreement with those reported from dietary-iron-loaded and parenteral-loaded spleen samples of rats [45] and also from thalassaemia human spleen samples [46]. The sample was measured again at ±8 mm/s, but no evidence of a sextet (haemosiderin) was found.

Both thalassaemic spectra show increased ferritin-like iron amounts relatively to the normal ones, which reflect the increased iron deposition due to iron-overload.

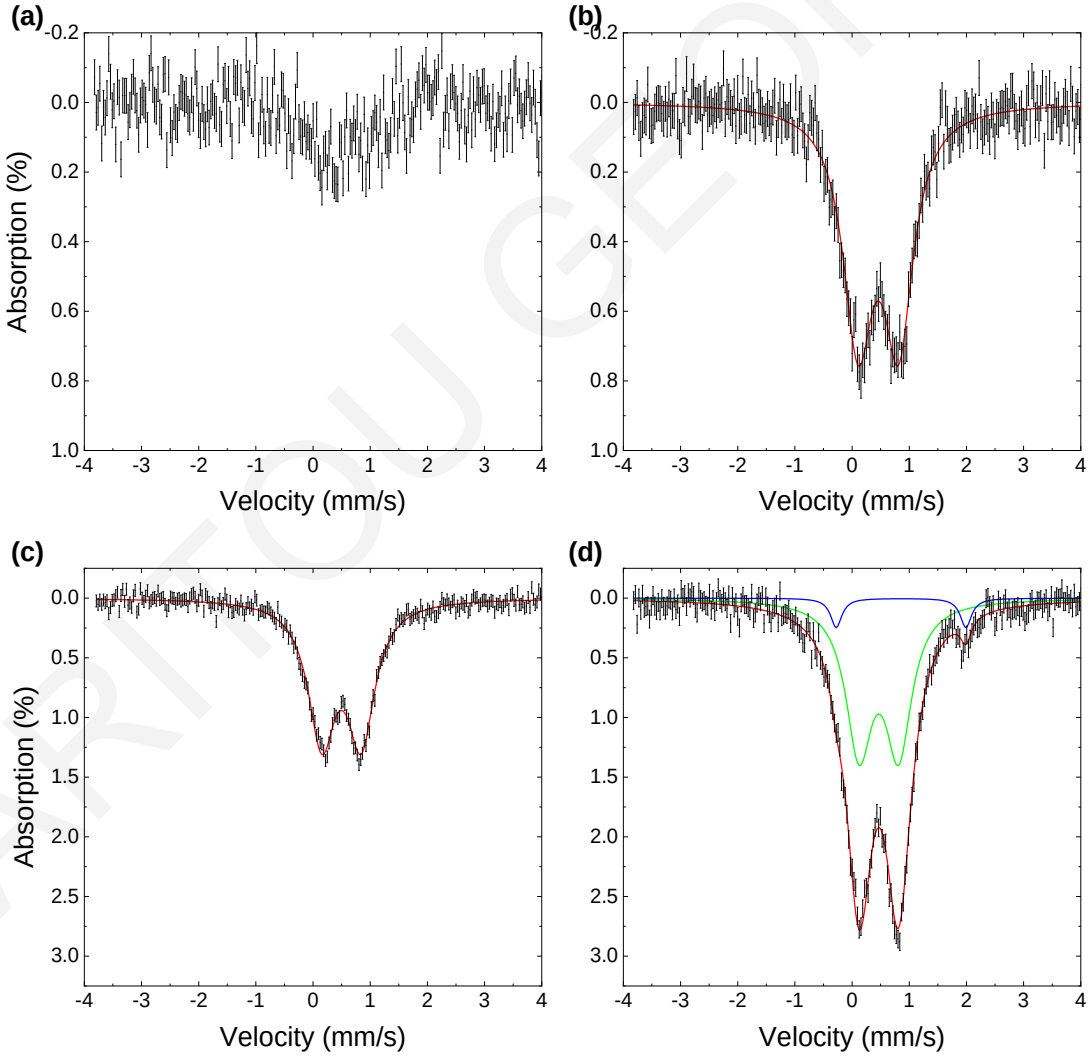

Figure 4.2: *The measured Mössbauer spectra, at 78K, of liver samples from one wild-type **(a)** and one th3/+ **(b)** mouse, and spleen samples from one wild-type **(c)** and one th3/+ **(d)** mouse, plotted at the same scale. The th3/+ spleen sample is fitted with two doublets, the green one indicating ferritin-like iron, and the small one (bleu) deoxy-haemoglobin residues*

4.1.3 Conclusions from the preliminary study

Mössbauer spectra of blood, heart liver and spleen samples from a *wild-type* and a heterozygous β-thalassaemic *th3/+* mouse were acquired at 78K. The MS spectrum of the *+/+* blood sample was well-fitted with two sub-doublets of the same area, representing the α- and β-subunits of oxy-haemoglobin. The blood sample of the thalassaemic mouse shows a decrease in absorption in its spectrum which makes any detailed fitting impossible. The decreased absorption in the spectrum reflects the decreased haemoglobin levels which is a result of the severe anaemia that the *th3/+* mice and the untreated thalassaemia patients suffer from. Unfortunately, because of the low SNR of the spectrum from the thalassaemic sample, besides the decreased absorption no more information, like the existence of NTBI or ferritin could be extracted. Ferritin-like iron was observed in the RBCs of (probably not receiving iron chelation therapy) thalassaemia intermedia patients some decades ago [47].

The spectra from the hearts of both mice were of no use as no significant absorption or distinguishable peaks were observed. The spectra from the liver and spleen samples shows, as expected, the existence of ferritin-like iron. Compared to the normal ones, the spectra from the two organs of the thalassaemic mouse show increased absorption, which reflects the increased iron depositions in them. Increased iron depositions in the organs, especially the liver, is expected to occur in thalassaemia due to the secondary iron overload that accompanies the disease. Similar to the non-transfused thalassaemia patients, the *th3/+* mouse presented iron overload because of increased gastrointestinal absorption.

The Mössbauer fitting parameters obtained from the samples of these two mice, are in a good agreement with those existing in the literature. As obtained from our results, *wild-type* and thalassaemic *th3/+* mice exhibit similar iron complexes to humans, both in their blood and organs. In this sense, the thalassaemic mouse model, besides the significant difficulties due to the small sized of the organs, represents a promising candidate to study thalassaemia with MS.

4.2 ^{57}Fe enriched mice

As seen in the previous paragraphs, samples from mice with naturally occurring iron give spectra that exhibit very low S/N ratio, and therefore, it is very difficult or impossible in some cases to study the iron complexes and their accumulation in the organs with high detail. As ^{57}Fe MS utilizes only the ^{57}Fe isotope, in order to improve the spectra quality, it is essential to increase its amount in the samples. At the same time, it is important to not artificially increase

the total iron levels of the mice as this will lead to iron overload due to un-healthy iron supply and not because of thalassaemia. Therefore, the only way to do this without interfering with the iron levels of the mice, is by exchanging the ^{56}Fe isotope with ^{57}Fe atoms and elevate its ratio from the natural 2.12%.

Normal, not thalassaemic mice were successfully enriched with ^{57}Fe and some organs like the brain, liver and heart were studied in the recent years [38–40] where they found iron components that were never noticed before. Therefore, ^{57}Fe enriched thalassaemic mice can help understand in a greater detail how and in what forms, the iron accumulates in the major organs of the body due to thalassaemia.

4.2.1 Enrichment method and ^{57}Fe enriched diet

Thalassaemia patients obtain their iron from gastrointestinal absorption and through the regular blood transfusions. The first one, gastrointestinal absorption, is the main way non-transfused thalassaemia intermedia patients get their iron, while thalassaemia major patients receive the majority of their iron mainly from the blood transfusions. For the purposes of this study, it was chosen to enrich the mice through continuous gastrointestinal absorption using ^{57}Fe enriched diet, because it is easier and safer than blood transfusions or intravenous injections with uncertified in purity substances that may lead to undesirable complications like toxicity and infections. Besides that, the results from this method might be useful in other iron overload conditions and disorders like haemochromatosis. To achieve the mouse enrichment, ^{57}Fe enriched food was prepared and given to the mice as described further on.

^{57}Fe enriched iron supplement

Not all iron complexes are safe for consumption nor all are absorbed efficiently. Therefore the iron atoms must first be converted into a suitable form. The main iron complexes used as iron supplements, therefore safe and with high absorption by the body, are among others: *Fe(II) fumarate*, *Fe(II) gluconate*, and *Fe(II) sulphate*. Fe(II) sulphate heptahydrate ($FeSO_4 \cdot 7H_2O$) was chosen because it is used as iron supplement in various mice diets, therefore, it is not toxic for the mice and can be absorbed efficiently. Also, it can be produced easily from metallic iron using “common” materials, without the risk of toxicity and contaminations.

Because ^{57}Fe has a relatively high price (~6 €/mg), regular iron powder (purity > 99%, Sigma Aldrich) was used preliminary in order to evaluate and perfect the $FeSO_4$ production method. The method of choice was the dissolution of metallic Fe into 1 M sulphuric acid (H_2SO_4) which, as seen in Eq. 5.1, gives the requested salt.

$$Fe + H_2SO_4 \rightarrow FeSO_4 + H_2 \quad (5.1)$$

Iron has a molecular weight of 55.845 (56.94 for ^{57}Fe) [48], thus 200 mg are equal to 0.00358 mols. As 1 mol of iron reacts with 1 mol of H_2SO_4 (Eq. 5.1), at least 0.00358 moles of sulphuric acid (3.58ml of 1M solution) are needed to completely dissolve that amount of iron. After various trials, we concluded that 200 mg of metallic iron are better dissolved into 6 ml of 1M sulphuric acid heated at the temperature of 38-40ºC.

After establishing the optimum procedure, metallic ^{57}Fe (>95, Isoflex USA) was used. Similarly to the previously described procedure, 200 mg of ^{57}Fe where dissolved into 6 ml of 1M H_2SO_4 at the temperature of 38-40ºC. When the iron has dissolved completely, 4ml of distilled water were added to the solution raising the iron density to 20 mg/ml. Subsequently it was stored in the refrigerator at the temperature of 4ºC until it was needed for the mice diet preparation. The resulted solution had a blue-green colour, indicating the existence of $FeSO_4 \cdot 7H_2O$ (iron sulphate heptahydrate).

To evaluate the products of the previously described method, a sample from the prepared $^{57}FeSO_4$ solution (further diluted with distilled water), and a sample from water diluted Fe(II) sulphate powder (Sigma-Aldrich), were measured with MS at 80K. In both samples, the spectrum was well fitted with a similar doublet having the MS parameters seen in *Table 4.3*. In *Figure 4.3* the spectrum of a sample from the prepared $^{57}FeSO_4$ solution at 80K is presented.

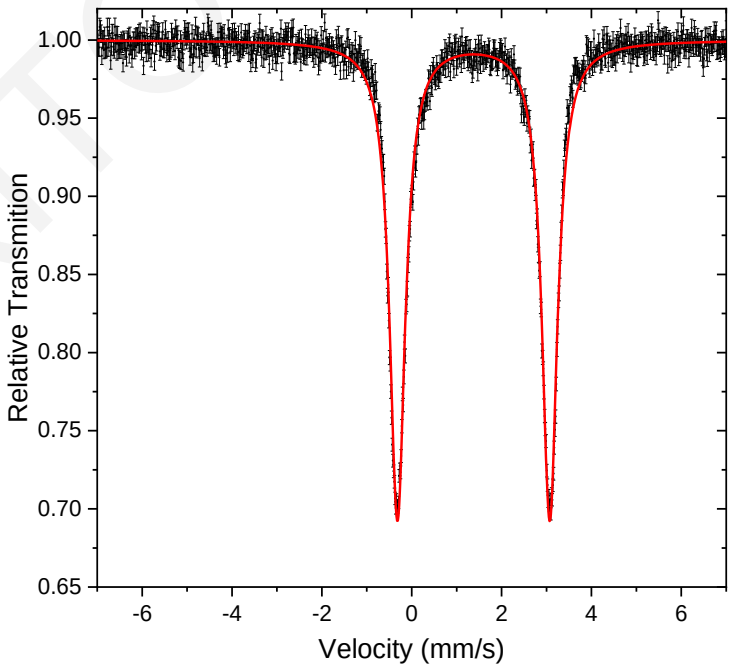

Figure 4.3: *Mössbauer spectrum of $^{57}FeSO_4$ prepared from metallic ^{57}Fe and 1M H_2SO_4, measured at 80K.*

Table 4.3: *Mössbauer parameters from water solution of pure FeSO4 powder and prepared $^{57}FeSO4$ from metallic ^{57}Fe and sulphuric acid. The measurements were performed at 80K. The instrumental error is <0.03mm/s. The statistical error of the fit is shown next to the value*

	δ (mm/s)	ΔEq (mm/s)	Γ (mm/s)
Water solution from $FeSO_4$ powder	1.38±0.01	3.36±0.01	0.40±0.01
Prepared $^{57}FeSO_4$ from iron powder	1.38±0.01	3.38±0.01	0.42±0.01

^{57}Fe enriched diet

According to the literature, the minimum requirements for iron in the mouse diet is 35 mg Fe/kg of diet, while the optimum quantities are about 120 mg Fe/kg [49]. Due to the high price of the ^{57}Fe isotope, we prepared mouse feed at 40-50 mg Fe/kg. To achieve this, 2 ml (containing 40 mg of ^{57}Fe) from the previously prepared solution were further diluted with 650 ml of sterilised water suitable for animal consumption, and slowly mixed with 1 kg iron deficient diet (<10mg Fe/kg, Ssniff E15510 in powder form). Subsequently, the mixture was cut into small portions, left to dry and stored at -18° C until needed. The resulted ^{57}Fe enriched diet was estimated to have around 40-50mg Fe/kg, of which ~40mg where ^{57}Fe. This corresponds to a ^{57}Fe/Fe ratio of over 80%, much higher than the naturally occurring 2.12%.

4.2.2 Sample Population - Mouse Breeding

Two groups of mice *C57BL/6* (+/+) and *th3/+* were raised and utilized for this study at 1, 3, 6 and 9 months of age (juvenile to mature adults). In addition to this, one 1-month old mouse was also raised with a typical diet for comparative purposes and to evaluate the enrichment method. Because as mention previously ^{57}Fe is relative expensive, the available amounts for this study was limited. In addition to this, the long acquisition times needed for a MS spectrum (~1 week but depends on the source activity) makes difficult the study of a large population of mice. Note that from each mouse five (5) to six (6) different measurements will be performed. Since the main objective of this study was for general observations and not statistical confirmation, only one mouse per group and age was studied. Some extra mice were also raised for backup or supplementary purposes.

Both *th3/+* and *+/+* mice can result from the same birth if one of the parents is heterozygous for thalassaemia *(th3/+)* and the other is a *wild-type* one (+/+). At first, six (6) female adult *C57BL/6 (+/+)* mice were partially enriched with ^{57}Fe. This was accomplished by feeding them

iron deficient diet (Ssniff, E15510, <10mg/kg Fe) for one month. The feed was subsequently changed to the ^{57}Fe enriched one, and after a week on the enriched diet, the females were separated into pairs and three males *th3/+* mice were introduced for mating. Upon pregnancy the males were removed from the cage. The females were receiving the ^{57}Fe enriched diet for the whole duration of mating, pregnancy and nurturing.

After weaning, the females (mothers) were removed and the offsprings were separated into the two groups based on their reticulocyte count levels (screening test). For this, 50 μL of blood was taken from the lateral tail vein and a haematology analyser (Sysmex XT2000 iVet, Sysmex Europe GmbH) was used for the analysis. Mice with >25% reticulocytes were considered thalassaemic *(th3/+)* while mice with <15% reticulocytes were considered *wild-type* (+/+). The pups had an unlimited access to fresh food and water and continued to receive the ^{57}Fe enriched diet throughout their lives

4.2.3 Sample acquisition and preparation

The mice were anaesthetized by intraperitoneal injection with tribromoethanol (10 μL/g) and blood was collected from the orbital sinuses into sodium heparin tubes (to inhibit clotting). The animals were then euthanized, and the heart, liver, kidneys, brain and spleen were carefully removed. The organs were then washed multiple times with Phosphate-Buffered Saline (PBS) and wiped thoroughly using clean sterile gauzes. Subsequently, the organs were weighted, placed in the appropriate holders and submerged into LN where they were stored until needed.

As mentioned in the previous chapters, it is essential that the sample should cover the whole area of the holder in order to eliminate any photons arriving to the detector without passing through the sample. The various organs have different shapes and sizes, therefore holders of different diameters were used as seen in *Table 4.4.* However, the size of the holder was kept constant for samples of the same organ in order to be comparable in terms of iron concentration (area of the fit). The livers were placed in Ø12 mm holders, the blood, the kidneys and brains in Ø10 mm holders and the hearts and spleens in Ø6 mm ones. Extra care was taken on order to place the samples as uniformly as possible in the holders. *Figure 4.4* shows the mice organs after their extraction (left) and after being placed in the holders (right).

Here it is necessary to emphasize that the blood was used as a whole, and was not separated into RBCs and plasma because the separation method (various centrifugations and washes) could result in the loss of a significant portion of the sample's volume. Also, some organs such as the heart and kidneys of the one-month old mice, and the spleen from the *wild-type* mice

were very small, hence the organs from two mice were used. The *th3/+* mice suffered from splenomegaly and therefore their spleen was significantly enlarged and only about half of it was used. Sample details are given in *Table 4.4*. For convenience, the samples where coded as follows: two letters MC (mouse control) for the control (*wild-type*) ones and MT (mouse thalassaemic) for the thalassaemic *th3/+* ones, followed by the age (in months), followed by a letter representing the organ (H: Heart, Bl: Blood, S: Spleen, L: Liver, Br: Brain, K: Kidneys).

Figure 4.4: *Organs from a wild-type mouse after their extraction (liver, heart, kidneys, spleen) (**top**). and in the appropriate PP holders (**bottom**)*

Table 4.4: *^{57}Fe enriched mice sample details. [1]: Organs from two mice were used*

a/a	Sample Code	Group	Age (months)	Organ	Holder Diameter (mm)	Weight (g)	Comments
1	MC1-H	Control	1	Heart	6	0.21	[1]
2	MC1-K	Control	1	Kidneys	10	0.60	[1]
3	MC1-L	Control	1	Liver	12	0.84	
4	MC1-S	Control	1	Spleen	6	0.11	[1]
5	MC1-Bl	Control	1	Blood	10		
6	MT1 -H	Thalas.	1	Heart	6	0.19	[1]
7	MT1-K	Thalas.	1	Kidneys	10	0.45	[1]
8	MT1-L	Thalas.	1	Liver	12	0.96	
9	MT1-S	Thalas.	1	Spleen	6	0.19	
10	MT1-BL	Thalas.	1	Blood	10		
11	MC3-H	Control	3	Heart	6	0.23	[1]
12	MC3-K	Control	3	Kidneys	10	0.50	
13	MC3-L	Control	3	Liver	12	1.04	
14	MC3-S	Control	3	Spleen	6	0.12	[1]
15	MC3-Bl	Control	3	Blood	10		
16	MT3-H	Thalas.	3	Heart	6	0.25	
17	MT3-K	Thalas.	3	Kidneys	10	0.38	
18	MT3-L	Thalas.	3	Liver	12	1.24	
19	MT3-S	Thalas.	3	Spleen	6	0.20	
20	MT3-BL	Thalas.	3	Blood	10		
21	MC6-H	Control	6	Heart	6	0.21	
22	MC6-K	Control	6	Kidneys	10	0.17	
23	MC6-L	Control	6	Liver	12	0.81	
24	MC6-S	Control	6	Spleen	6	0.17	[1]
25	MC6-Bl	Control	6	Blood	10		
26	MT6-H	Thalas.	6	Heart	6	0.27	
27	MT6-K	Thalas.	6	Kidneys	10	0.39	
28	MT6-L	Thalas.	6	Liver	12	0.93	
29	MT6-S	Thalas.	6	Spleen	6	0.27	
30	MT6-BL	Thalas.	6	Blood	10		
31	MC9-H	Control	9	Heart	6	0.21	
32	MC9-K	Control	9	Kidneys	10	0.55	
33	MC9-L	Control	9	Liver	12	1.35	
34	MC9-S	Control	9	Spleen	6	0.21	[1]
35	MC9-Bl	Control	9	Blood	10		

36	MC9-Br	Control	9	Brain	10	0.52
37	MT9-H	Thalas.	9	Heart	6	0.18
38	MT9-K	Thalas.	9	Kidneys	10	0.32
39	MT9-L	Thalas.	9	Liver	12	0.75
40	MT9-S	Thalas.	9	Spleen	6	0.20
41	MT9-Bl	Thalas.	9	Blood	10	
42	MT9-Br	Thalas.	9	Brain	10	0.42

4.2.4 MS spectra acquisition

Al spectra were acquired at 80±1 K. The max velocity was set at ~4.10 mm/s, and when necessary a second run was done at ~10 mm/s. At first, all spectra were fitted using free parameters, and the number of sub-spectra used for the fitting were in order to minimise the χ^2 value. From this first fit, strong similarities among the sub-spectra needed to fit the data where observed, and therefore a second fit was performed using the mean values for δ, ΔEq and Γ. Some of these values were let to change slightly (±0.03 mm/s) if needed, while their area was free to vary.

4.2.5 Results

4.2.5.1 Enrichment

Figure 4.5 shows the MS spectra from blood, liver and spleen samples of two *wild-type* mice at 1 month of age. The one (left) was raised in normal conditions and had access to ordinary mice diet while the second one (right) was raised with the previously described method in order to be enriched with ^{57}Fe. From the MS spectra it can be clearly seen that the absorption is significantly higher in the samples derived from animals on the ^{57}Fe enriched diet (right), resulting in spectra with distinctly improved signal-to-noise ratio, which is adequate for a detailed quantitative analysis. Note that the pups had been weaned for around 21-26 days after birth, therefore, most of the ^{57}Fe identified in their tissues originated from maternal milk. Hence this specific enrichment method can give mice that are suitable for MS studies even from very young age.

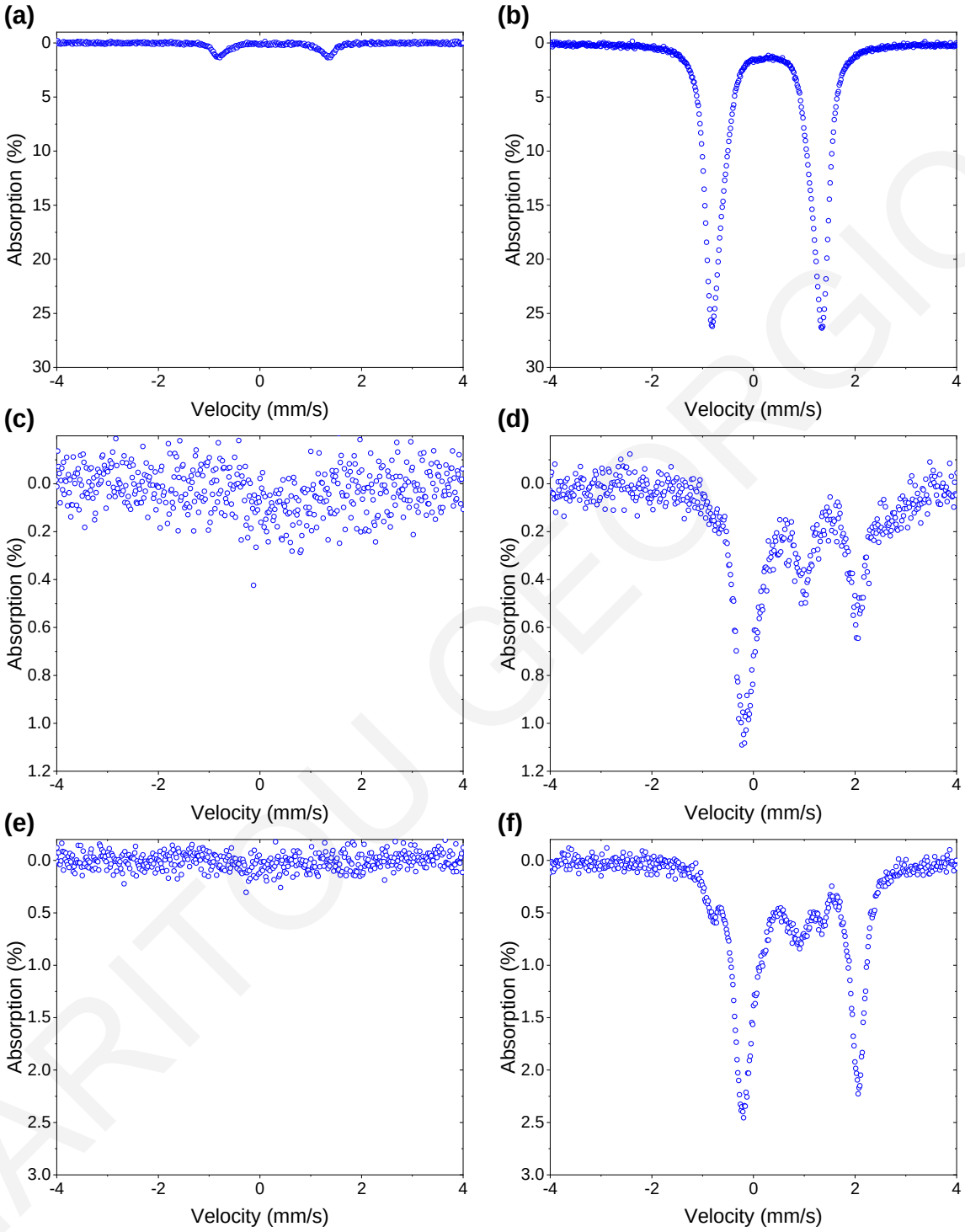

Figure 4.5: *Spectra from blood **(top)**, liver **(middle)** and spleen **(bottom)** of non-enriched **(left)** and ^{57}Fe enriched **(right)** mice at 1 month of age. The scale is kept the same to emphasize the absorption increase due to the ^{57}Fe enrichment*

4.2.5.2 Studies on blood samples

Blood samples from *wild-type* and *th3/+* ^{57}Fe enriched mice at 1, 3, 6 and 9 months of age (one mouse per age and group) were studied. In all spectra, a major doublet that exhibits the parameters of oxyhaemoglobin (oxy-Hb) is observed. This doublet, according to the fitting models of the latest published MS studies [50–52], can be fitted with two different sub-doublets indicating the α- and β-globin chains of haemoglobin's tetramer (denoted as Hb-α and Hb-β, respectively). Thus, the spectra from the *wild-type* mice were initially fitted with free Hb-α and Hb-β Lorentzian sub-doublets, but this resulted to a Hb-α/Hb-β ratio of 2.86, significantly increased from the expected 1:1. Therefore, a second fit was performed where the two doublets were forced to have equal areas (the width, isomer-shift and quadrupole splitting of the doublets were free to vary). Deviations from the expected 1:1 ratio have also been discussed in the literature, and similarly, they also used sub-doublets of equal area [52]. After the fitting of all wild-type spectra, the average values of the three parameters were calculated in order to be used in the fitting procedure of the blood spectra from the thalassaemic mice. As β-thalassaemia affects the production of β-globin chains, forcing the two sub-doublets to have equal areas (1:1 ratio) could be wrong hence the area of the two doublets was free to vary. The fitting parameters are shown in Table 4.5.

The spectra from the thalassaemic mice are more complex, consisting of up to four overlapping sub-doublets as can be seen in Figure 4.7(b, d). Therefore, the spectra from the *th3/+* mice were simultaneously fitted by the Hb-α and Hb-β sub-doublets fixed to the average values of mentioned previously and presented in Table 4.5, and by two additional sub-doublets with free varying parameters. From the results of this fit, the two additional sub-doublets were attributed to deoxy-haemoglobin and ferritin-like iron.

To eliminate any variations in the fit due to the strong overlapping, and to achieve maximum consistency between the spectra analysis, the thalassaemic spectra were refitted again having all doublets fixed with only their area free to vary. The two oxy-haemoglobin's doublets were fixed to the average values extracted from the spectra of the *wild-type* mice. The ferritin-like iron doublet was fixed to the values Γ=0.49 mm/s, δ=0.50 mm/s and ΔEq=0.72 mm/s, which resulted from the average fitting values extracted in the previous step and the deoxy-haemoglobin's doublet was fixed to the values Γ=0.29 mm/s, δ=0.92 mm/s and ΔEq=2.28 mm/s. Because the relative percentage of deoxy-haemoglobin's doublet in the spectra of the mice at 1 and 3 months of age were too small to obtain reliable values, only the results from the mouse at 9 months of age were used. It should be noted that the values used for deoxy-haemoglobin and ferritin-like iron are in line with the results available in current literature

[50,53–57]. The final results of the extracted MS parameters are summarised in Table 4.5. Spectra from the blood samples of *wild-type* and *th3/+* mice at 1 and 9 months of age are shown in *Figure 4.7*. The corresponding spectra from the mice of the remaining ages can be found in Appendix II.

The Hb-α/Hb-β ratio of the *th3/+* mice was found slightly elevated, with values between 1 and 1.16. The latter increased ratio might be due to the excess of α-globin chains associated with β-thalassaemia. The deoxy-haemoglobin, which is haemoglobin without any attached ligand normally present in the venous blood, and found in three thalassaemic samples, (*th3/+* mice at 1, 3 and 9 months of age) was probably due to some amount of deoxy-haemoglobin that did not get oxygenated during the sample collection and preparation process. On an average, for all studied ages, the *th3/+* mice had about 45% less total haemoglobin (fitting area of Hb_{total} = Hb-α + Hb-β + deoxy-Hb = 0.16) relative to the *wild-type* ones (fitting area of Hb_{total} = 0.29). This is in agreement with the values reported in the literature, as *wild-type C57BL/6* mice have Hb levels of ~16 g/dl [43] and *th3/+* mice 8-9 g/dl [37] (45-50% reduction). The reduced haemoglobin levels are an indication of severe anaemia. *Figure 4.6* shows the fitted area of Hb in the spectra from the *wild-type* and *th3/+* mouse samples, for all ages investigated. Haemoglobin levels were also found to be unaffected by mouse age. This was expected for the samples from the *wild-type* mice, but not for the *th3/+* ones, since in most human thalassaemia intermedia patients the anaemia worsens, later on, in life.

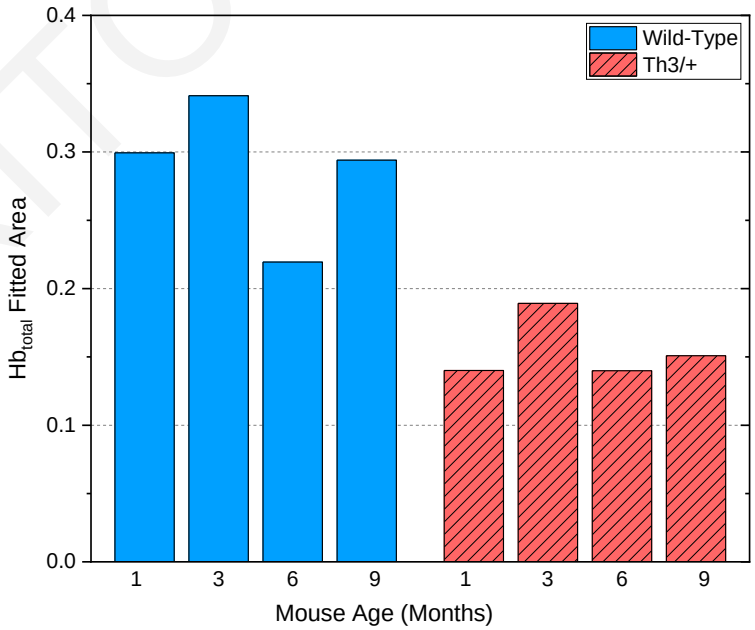

Figure 4.6: *Haemoglobin levels in the mice's blood samples. The thalassaemic th3/+ mice have about half the haemoglobin of the normal ones, an indication of anaemia.*

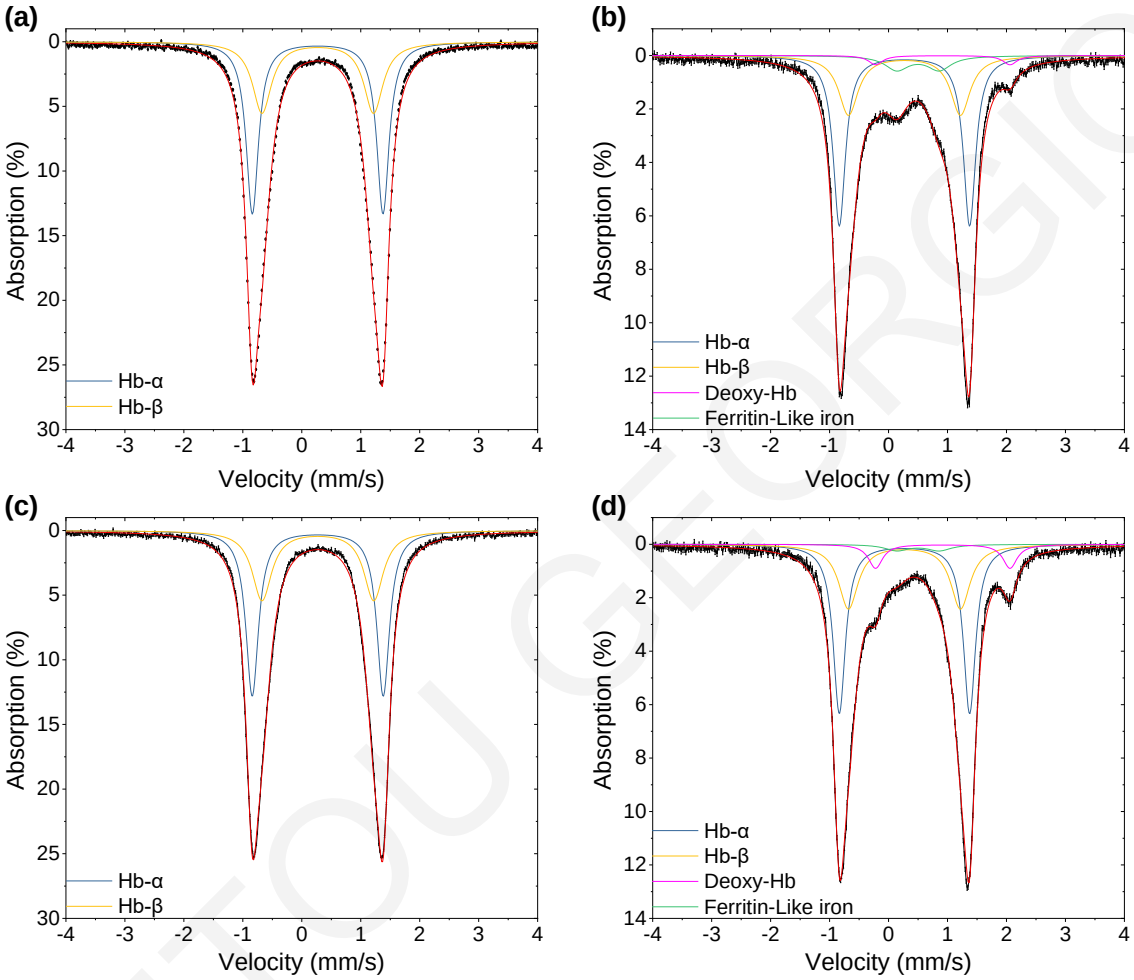

***Figure 4.7**: Mössbauer spectra obtained at 80K from the blood samples of ^{57}Fe enriched mice at 1 (a, b) and 9 (c, d) month of age[7]. Spectra (a) and (c) correspond to wild-type mice and spectra (b) and (d) to th3/+mice.*

[7] The spectra from the mice of the remaining ages are presented in Appendix I.

***Table 4.5**: The Mössbauer fitting parameters (relative percentage of the sub-doublet in the spectrum, Γ: FWHM, δ: isomer shift, ΔEq: quadrupole splitting, and the area of the sub-doublet) from the blood sample spectra of wild-type and thalassaemic mice at 1, 3, 6 and 9 months of age. The instrumental error is < 0.03 mm/s. The statistical errors are also shown. Note that no errors are reported for the parameters fixed in the fitting procedure. The corresponding MS spectra can be found in Appendix II.*

	Age (Months)	Sub-Doublet	Relative Percentage	Γ (mm/s)	δ (mm/s)	ΔEq (mm/s)	Area (x10^{-2})	Hb-α / Hb-β
Wild-type	1	Hb-α	50	0.25±0.01	0.27±0.01	2.22±0.01	14.97±0.02	1
		Hb-β	50	0.39±0.01	0.27±0.01	1.89±0.01	14.97±0.02	
	3	Hb-α	50	0.25±0.01	0.27±0.01	2.21±0.01	17.06±0.02	1
		Hb-β	50	0.40±0.01	0.27±0.01	1.89±0.01	17.06±0.02	
	6	Hb-α	50	0.25±0.01	0.27±0.01	2.21±0.01	10.97±0.02	1
		Hb-β	50	0.39±0.01	0.27±0.01	1.90±0.01	10.97±0.02	
	9	Hb-α	50	0.26±0.01	0.27±0.01	2.22±0.01	14.70±0.02	1
		Hb-β	50	0.40±0.01	0.27±0.01	1.90±0.01	14.70±0.02	
	Average	Hb-α		0.25	0.27	2.21		
		Hb-β		0.40	0.27	1.90		
Th3/+	1	Hb-α	43.8	0.25	0.27	2.21	7.13±0.02	1.12
		Hb-β	39.1	0.40	0.27	1.90	6.36±0.04	
		Deoxy-Hb	3.2	0.29	0.92	2.28	0.52±0.02	
		Ferritin-like iron	13.9	0.49	0.50	0.72	2.27±0.02	
	3	Hb-α	45.0	0.25	0.27	2.21	9.39±0.04	1.01
		Hb-β	44.5	0.40	0.27	1.90	9.30±0.05	
		Deoxy-Hb	1.1	0.29	0.92	2.28	0.23±0.03	
		Ferritin-like iron	9.4	0.49	0.50	0.72	1.97±0.04	
	6	Hb-α	49.6	0.25	0.27	2.21	7.50±0.03	1.16
		Hb-β	43.0	0.40	0.27	1.90	6.49±0.04	
		Deoxy-Hb	0	0.29	0.92	2.28	0	
		Ferritin-like iron	7.4	0.49	0.50	0.72	1.12±0.04	
	9	Hb-α	43.5	0.25	0.27	2.21	6.98±0.02	1.03
		Hb-β	42.2	0.40	0.27	1.90	6.78±0.03	
		Deoxy-Hb	8.3	0.29	0.92	2.28	1.33±0.03	
		Ferritin-like iron	6.0	0.49	0.50	0.72	0.96±0.02	

Ferritin-like iron was observed in the spectra from the blood samples of all *th3/+* mice, in contrast to the *wild-type* ones where no such component was found. Unfortunately, it is not possible to determine from our methodology whether the ferritin-like iron was found inside the RBCs or in the serum since no cellular separation was performed for the reasons stated previously. Gardenghi et al. [37] showed that the *th3/+* mice have serum iron levels of 20-30 mM which are slightly elevated compared to the serum iron levels in *wild-type* mice (~20 mM). Since ferritin-like iron in the spectra from blood samples of *wild-type* mice was untraceable in our spectra, we can assume that the ferritin-like iron observed in the blood of the *th3/+* mice should not be found in the serum, therefore it should exist mainly in the RBCs. Ferritin-like iron was observed in the RBCs of thalassaemia intermedia patients in the late 1970s [47].

Furthermore, the percentage of the ferritin-like iron in the spectra from the blood of thalassaemic mice was found to decrease with age. This observation was unexpected since iron overload is known to get worst with age (this is also shown in the next paragraphs with the iron depositions in the organs). The one-month old mouse exhibited ferritin-like iron of ~ 14% while the nine-month old ~ 6%. More interesting is that, the reduction of the ferritin-like iron with the age of the *th3/+* mice, seems to follow closely the corresponding reduction of the reticulocyte count, as presented by Gardenghi et al. [37]. This is demonstrated in *Figure 4.8* where the percentages of the ferritin-like iron extracted from the MS spectra (red bars) and the reticulocyte counts (green dots), measured by Gardenghi et al. [37] are plotted together.

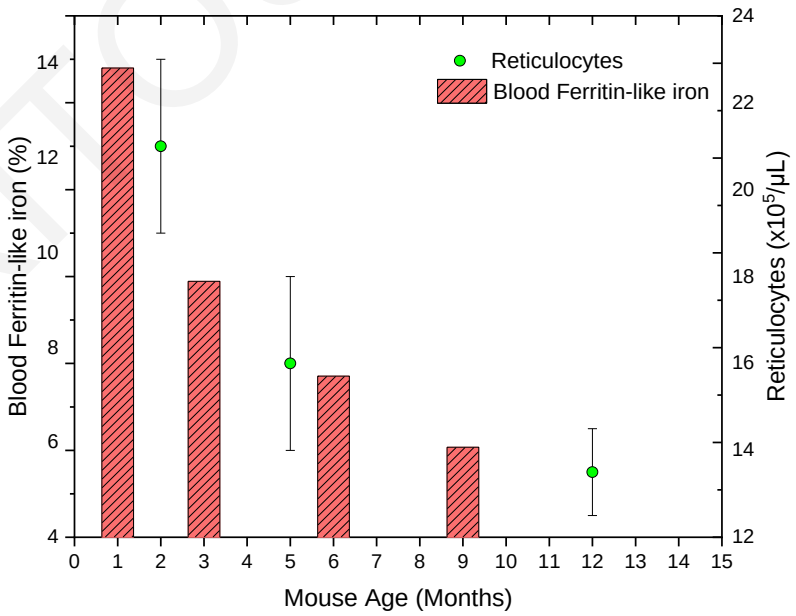

Figure 4.8: *Percentage of ferritin-like iron in the Mössbauer spectra from the blood samples of th3/+ mice at 1, 3, 6 and 9 months of age (red bars). The reticulocyte count of 2, 5, and 12 month old th3/+ mice, as measured by Gardenghi et al. [37] is also shown for comparative purposes (green dots).*

These observations indicate that most of the ferritin-like iron found in the blood samples of the thalassaemic mice may be present in the reticulocytes. Thus, RBCs and more specifically the reticulocytes of thalassaemia patients might be possible carriers of a significant amount of iron. Note that the role of ferritin in the erythroid cells is still unclear. Ferritin has been suggested to act as an intermediate for haem synthesis in erythroid cells, but this has not yet been proven [12]. On the contrary, strong evidence has been provided that ferritin is not involved in haemoglobinization [58].

4.2.5.3 ^{57}Fe enriched organs

The spectra from the organs were initially fitted with free Lorentzian peaks. From the initial results, it was observed that four similar doublets could be used to fit most of the samples, while in two of them a sextet could also be observed. Based on the results from the initial fits, the mean values for these components were calculated for each group of mice. As no major differences were observed between the MS parameters of the two groups, the overall mean values were calculated and subsequently all spectra were re-fitted with the values seen in *Table 4.6.* The quadrupole splitting *(ΔEq)* was kept fixed, while the width *(Γ)*, and isomer shift *(δ)*, was left to vary slightly. By using fixed values, the χ^2 of the fit was slightly increased when compared to the fitting with free parameters, because the sub-doublets were not placed in the best possible positions. However, we believe that with this method, the extracted area of the sub-doublets will be more comparable between different spectra. Note that the spectra consist of superimposed sub-doublets and not well-defined ones. All final MS parameters for all spectra analysed, are presented in Appendix III.

In all samples High Spin Fe(II) haem iron with fitting parameters δ=0.91 mm/s and ΔEq=2.28 mm/s was found. This iron has similar parameters with deoxy-haemoglobin and its presence is probably due to trapped blood residues that could not be remove during the exsanguination and rising with PBS. In another work [39], ^{57}Fe enriched livers of normal *C57BL/6* mice were studied, where they tried to reduce the haem iron by flushing the organs (puncturing the heart with a needle and passing Ringer's buffer throughout the mouse). The haem percentage in their liver samples, even with extensive flushing, was ~20%. In our liver samples, haem iron's percentage for the *C57BL/6* adult mice (three-month old and older) was 14-28%. Similar amounts (<20%) were found in the spleen and in the brain of these mice, therefore exsanguination from the orbital sinus can be as effective in removing the blood residues, as flushing the whole mouse with Ringer's buffer.

Table 4.6: *The mean values used for the final fit of the spectra from the organ samples. They were calculated based on initial fits with free parameters. N: the number of the different spectra used to calculate the mean value, +/+: wild-type mice, th3/+: thalassaemic mice*

		N	δ (mm/s)	Γ (mm/s)	ΔEq (mm/s)	HMF (T)
High spin Fe(II) haem (Deoxy-Hb)	Average for +/+	17	0.91	0.32	2.28	
	Average for *th3/+*	17	0.91	0.32	2.28	
	Average	34	0.91	0.32	2.28	
NHHS Fe(II) [38,39]	Average for +/+	6	1.35	0.45	2.83	
	Average for *th3/+*	9	1.36	0.41	2.94	
	Average	15	1.36	0.43	2.90	
Ferritin-like (I) [59]	Average for +/+	13	0.45	0.40	0.59	
	Average for *th3/+*	17	0.46	0.42	0.59	
	Average	30	0.46	0.42	0.59	
Ferritin-like (II) [59]	Average for +/+	17	0.46	0.41	1.06	
	Average for *th3/+*	17	0.45	0.45	1.05	
	Average	34	0.46	0.43	1.05	
Haemosiderin [60]	Average *th3/+*	2	0.48	1.04	-0.25	45.91

The second component found in some organs, showed broadened linewidth and was fitted with parameters of δ=1.36 mm/s and ΔEq=2.90 mm/s. This component present's small percentage and area in the samples that was observed with the peak of the lowest energy well hidden in more intense components. Hence, the exact values of the shown parameters *Table 4.6* must be taken with some scepticism. A similar component was found in mice livers [39] and brains [38] and was attributed to Mononuclear Non-haem high-spin Iron (NHHS Fe^{II}). NHHS Fe^{II} complexes can have labile ligands that undergo Fenton chemistry, which are responsible for the creation of reactive oxygen species (ROS) [38,39]. These are known to cause extensive cellular damage.

NHHS Fe^{II} was found in the kidneys, liver and brain of the control and *th3/+* mice. It was also found in the spleen of the adult *th3/+* mice only. In the liver, adult *th3/+* mice had an average

of 14% more NHHS Fe^{II} per sample mass than the control group, while in the kidneys 5 times the "normal" amount was found. In the spleens of the *th3/+* adult mice only, NHHS Fe^{II} iron was found in high concentration (doublet's area per sample's mass), while no samples from the control group showed any signs of NHHS Fe^{II} iron. *Figure 4.9* shows the average concentration of NHHS Fe^{II} in the brain, kidneys, liver and spleen of the *wild-type* and *th3/+* adult mice. Note that the concentration might not be directly comparable among samples in holders of different diameters due to the non-uniform distribution of the sources beam in the targets surface area. The source's active diameter was 5 mm.

Th3/+ mice suffer from splenomegaly, a condition that thalassaemia patients also suffer from. As described in chapter 1, the spleen enlarges greatly in size to cover the needs of increased erythrocyte production and destruction, hence the increase in the NHHS Fe^{II} concentration in the thalassaemic spleen tissue, might be related to phenomena associated with erythropoiesis and/or erythrophagocytosis.

Besides the abovementioned iron compounds, ferritin-like iron and haemosiderin was also observed and will be described in the following paragraphs in further detail.

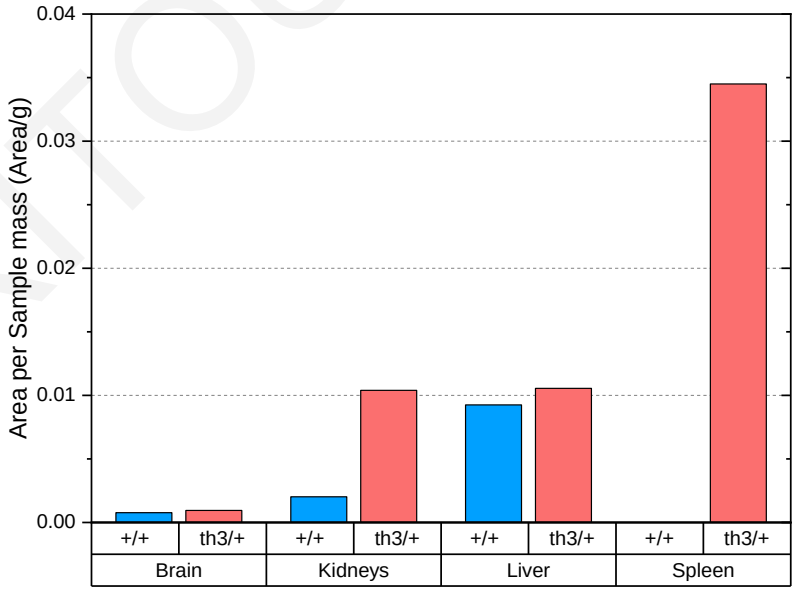

Figure 4.9: *NHHS Fe^{II} average concentration (doublet's area per sample's mass) for the brain, kidneys, liver and spleen samples of th3/+ and wild-type (+/+) adult mice. Note that the concentration might not be comparable between different organs due to differences in the diameter of the absorbers.*

4.2.5.4 Ferritin-Like Iron

A major feature in all spectra, especially the thalassaemic ones, was a wide doublet with δ≈0.46 mm/s and ΔEq≈0.74 mm/s. This doublet was observed in previous Mössbauer studies in samples of various organs from humans and animals and was contributed to ferritin-like iron [46,61–63]. The use of one doublet to fit the data (as in most previous studies) was inadequately therefore two sub-doublets were used which improved the fitting. These sub-doublets showed fitting parameters of δ=0.47 mm/s and ΔEq=0.59 mm/s the first one, and δ=0.46 mm/s and ΔEq= 1.05 mm/s the second one, as seen in *Table 4.6*.

Two doublets have already been used to describe this area of the spectrum for the liver and brain of mice but with different parameters [38,39]. The authors attributed their sub-doublets to ferritin and to mitochondrial respiratory complexes ($[Fe_4S_4]^{2+}$ clusters and low-spin Fe^{II} haem centres). In a different study, Bou-Abdallah et al. [59] after studying the cores of human H-chain ferritin with 500 Fe/shell, they described their spectra by the superposition of two magnetic substances in nearly equal amounts that arises from the ferritin's mineral core. At 120K, the two substances are presented by two doublets which give rise to magnetic ones at lower temperatures. The parameters of the doublets between 4.2-120K are δ=0.46 mm/s (for both substances), and ΔEq of 0.55-0.59 mm/s and 1.01-1.04mm/s for each one respectively. These parameters are similar to the ones found in this work. According to the authors, the doublet with the smaller ΔEq corresponds to the iron sites at the interior of the mineral core while the second one to the iron sites at the surface of the core.

As described in chapter 1, the ferroxidase centres are located in the H-subunits, thus H-rich ferritin catalyses the oxidation of Fe(II) while L-subunits appears to play a role in nucleation of the mineral core. Responsible for its development are three chemical pathways:

$$2Fe^{2+} + O_2 + 4H_2O \rightarrow 2Fe(O)OH_{(core)} + H_2O_2 + 4H^+ \quad (4.2)$$

$$2Fe^{2+} + H_2O_2 + 2H_2O \rightarrow 2Fe(O)OH_{(core)} + 4H^+ \quad (4.3)$$

$$4Fe^{2+} + O_2 + 6H_2O \rightarrow 4Fe(O)OH_{(core)} + 8H^+ \quad (4.4)$$

Once a sufficient core has been developed (≥800 Fe/Shell) from the *Eq.(4.2) and Eq.(4.3), Eq.(4.4)* becomes dominant and Fe^{2+} is oxidized on the surface of ferritin's mineral core. Iron cores resulted from *Eq.(4.2)* and *Eq.(4.3)* shows similar MS characteristics [59].

In contrast to the study by Bou-Abdallah et al [59], which they found the two sub-doublets in almost similar amounts, their ratio in our measurements was found to be depended on the organ and the mice group type. In the healthy *wild-type* mice, the hearts and kidneys showed higher concentration of surface iron sites while the spleen and liver showed higher concentration of inner iron sites. This pattern is similar with the one expected from the light and heavy chains of ferritin in the organs. L-subunits are predominant in tissues with high levels of stored iron, like spleen and liver, and H-subunits are predominant in tissues with no iron-storage function, like the heart [64]. Based on this, the inner iron sites might relate to the L-chains and long-term iron storage, while the surface iron sites to the H-chains and the ferroxidase activity.

Hearts

In the cardiac tissues, the surface iron sites were found to be the predominant one for both groups of samples and for mice of all ages. Their concentration (doublet's area per sample's mass) seems to increase slightly with age while the concentration of the inner iron sites increases clearly, as seen in *Figure 4.10(a)* and *(b)*. Because of this, the inner-to-surface iron sites (I/S) ratio increases in favour of the inner iron sites and with a similar rate for both groups (*Figure 4.11*). Based on the measurements, juvenile *th3/+* mice begin their lives with increased total ferritin-iron levels (sum of the area of both iron sites) in the cardiac tissue compared to the *wild-type* ones, but the latter seem to catch-up at the age of 9 months. Thalassaemia patients without iron chelation treatment present significantly higher iron amounts in the cardiac tissues than the healthy individuals. This is in contrast with the abovementioned results. A similar observation was done by Gardenghi et al. [37] with different type of measurements. MS spectra from the hearts of *wild-type* and *th3/+* mice at 9 months of age are shown in *Figure 4.12(a)* and *(b)* respectively. The spectra from the remaining mice are presented in Appendix II.

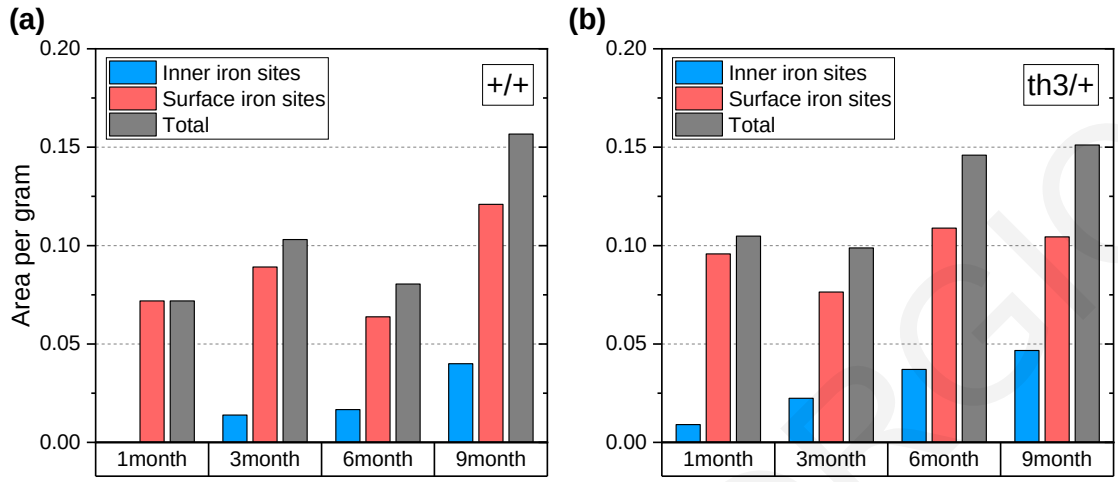

Figure 4.10: *Ferritin-like iron concentration in the cardiac tissue of heart samples for the wild-type* ***(a)*** *and the th3/+* ***(b)*** *mice*

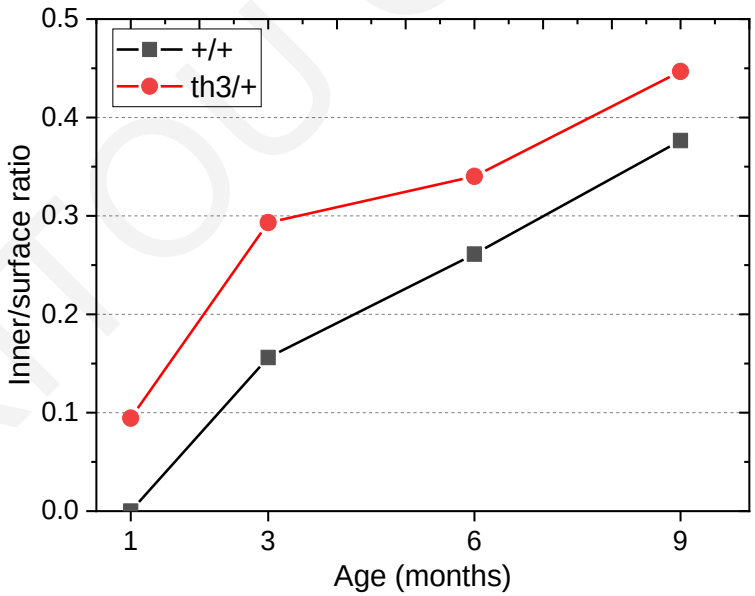

Figure 4.11*: The inner-to-surface iron sites ratio calculated from the heart samples of wild-type (++) and thalassaemic th3/+ mice*

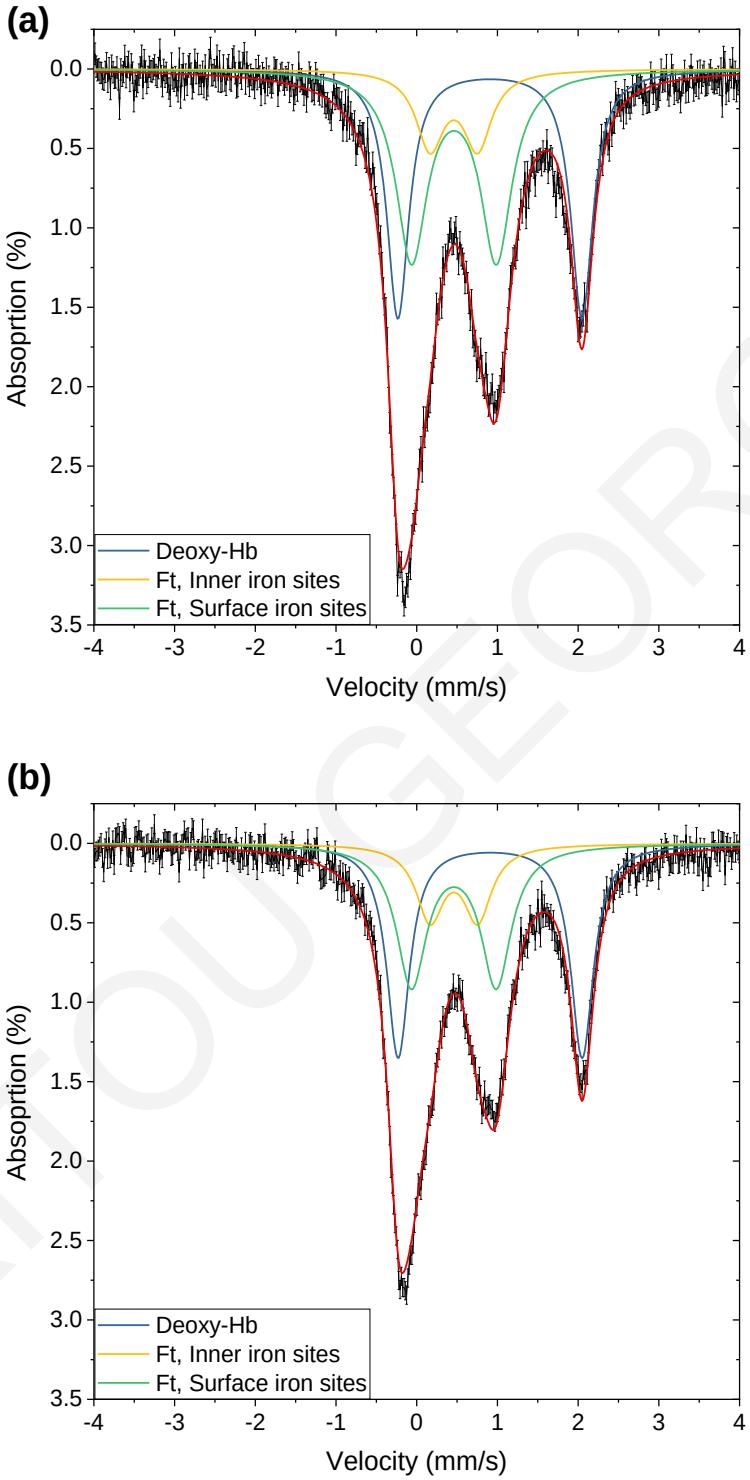

Figure 4.12: *MS spectra from the hearts of mice at 9 months of age[8]. The spectrum from the wild-type mouse is shown at* ***(a)*** *and from the th3/+ at* ***(b)***

[8] The spectra from the mice of the remaining ages are presented in Appendix I

Kidneys

In contrast to the cardiac tissues where *wild-type* and *th3/+* mice showed little difference, the effect of thalassaemia to the iron accumulation in the kidneys of the *th3/+* mice is more severe, especially for the adult mice. In the renal tissues of all *wild-type* mice, the predominant ferritin iron sites are the surface-type (*Figure 4.13*), with inner-to-surface ratio similar with the ones in the cardiac tissues. The *th3/+* mouse at 1 month of age showed increased I/S (inner to surface iron sites) ratio (I/S ratio = 0.55) compared to the *wild-type* mice (I/S ratio = 0.13-0.42) but still the predominant iron sites were the surface-type. On the other hand, at 3 months of age, *th3/+* mice show significantly increased renal iron depositions, especially in the form of ferritin's inner iron sites. Because of this, the I/S ratio increases dramatically (I/S ratio = 1.5) as the mice ages (*Figure 4.13*).

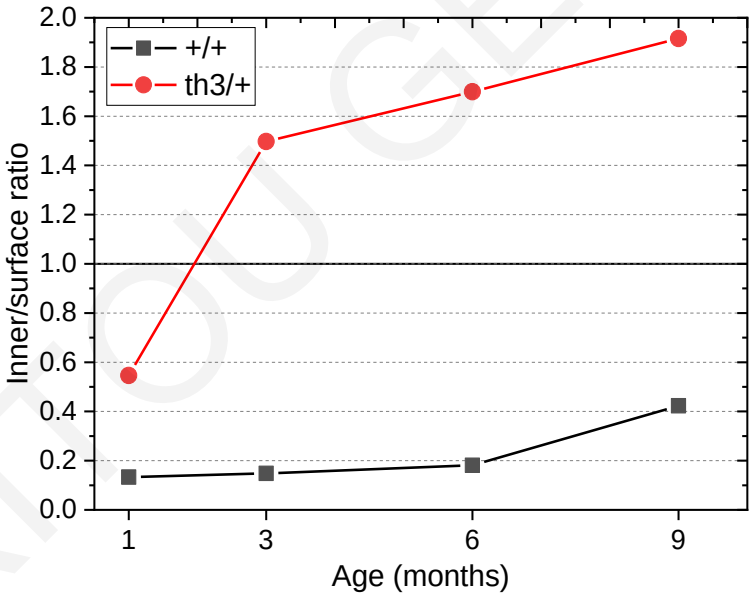

Figure 4.13: *The inner-to-surface ferritin's iron sites ratio calculated from the kidney samples of wild-type (++) and thalassaemic th3/+ mice*

Relative to the total iron concentration, the thalassaemic mouse at 1 month of age showed 2.4 times higher values than the *wild-type* equivalent. The *th3/+* adult mice showed tremendous renal iron accumulation, with the *th3/+* mouse at 6 months of age having 15.7 times higher iron concentration than the *wild-type* one. On an average, the adult *th3/+* mice showed ~11.6 times higher iron concentration than the control group. The iron concentration in the renal

tissues of *wild-type* and *th3/+* mice are presented in *Figure 4.14(a)* and *(b)*, and spectra from mice at 9 months of age in *Figure 4.15(a)* and *(b)*. The spectra from the mice of the remaining ages are presented in Appendix II.

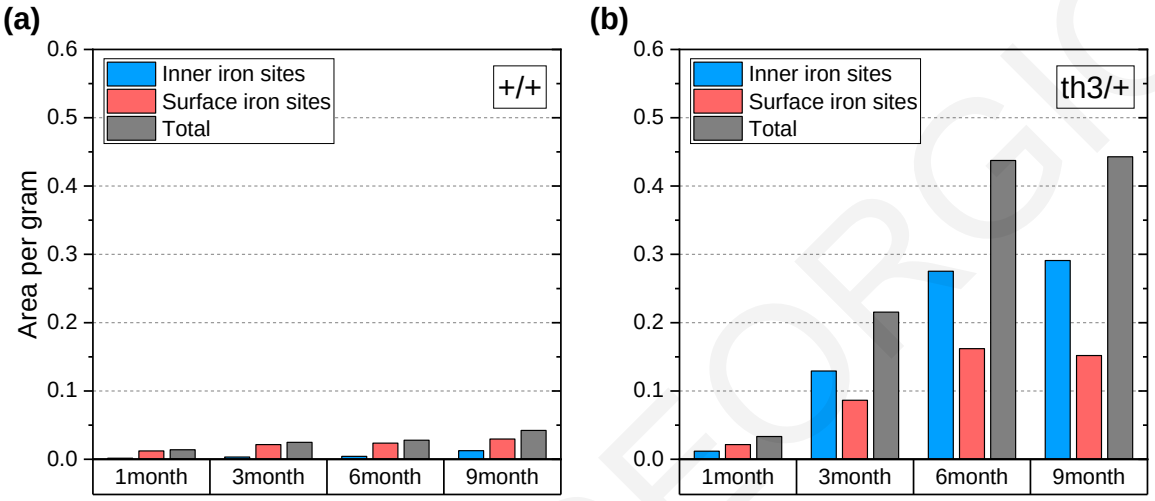

Figure 4.14: *Ferritin-like iron in the kidney samples of wild-type **(a)** and thalassaemic th3/+ **(b)** mice. A huge increase in both ferritin iron sites can be seen in the th3/+ samples*

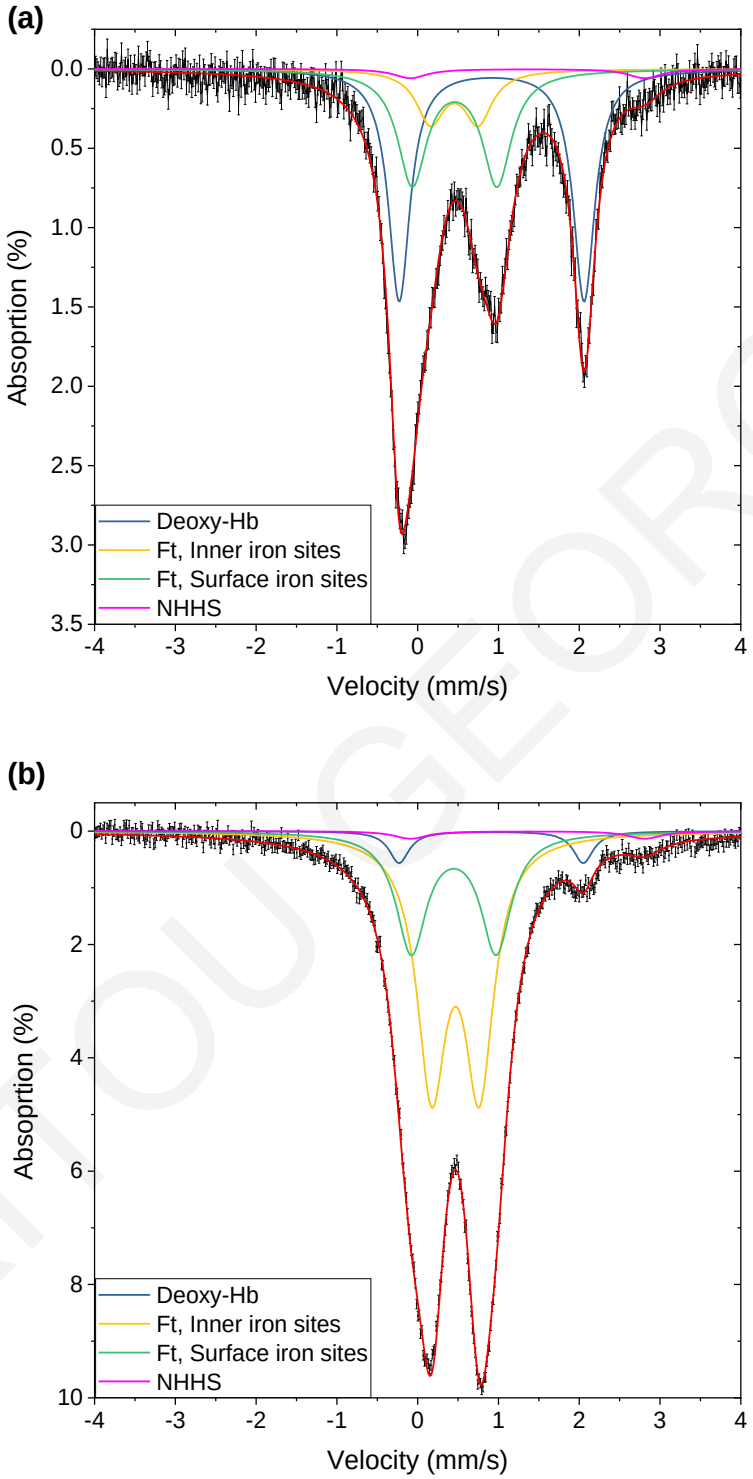

Figure 4.15: *Spectra from the kidneys of mice at 9 months of age*[9]*. The spectrum from the wild-type mouse is shown at* ***(a)*** *and from the th3/+ at* ***(b).*** *Notice the difference in the absorption's scale*

[9] The spectra from the mice of the remaining ages are presented in Appendix II

Brains

In order to investigate if there are indications of increased iron accumulation in the brain as a result of thalassaemia, brain tissues from mice at 9 months of age were studied. Some neurodegenerative diseases like Alzheimer and Parkinson might be correlated to increased iron in the brain [65,66]. Therefore, as thalassaemia patients suffer from increased iron deposition in various organs, it is essential to study the brains. Increased iron levels might indicate new medical problems that thalassaemia patients might face as they age.

The predominant ferritin's iron sites in both groups, as seen in *Figure 4.16,* are the surface-type one. As with cardiac and renal tissues, the *th3/+* mouse showed increased inner iron sites and thus, elevated inner-to-surface ratio (0.81) compared to the *wild-type* one (I/S = 0.61). Overall the thalassaemic brain showed ~10% more ferritin iron than the control one but due to the small sample population, no conclusive observations can be made about the iron concentrations in the brain tissues. The MS spectra from the two mice are shown in *Figure 4.17.*

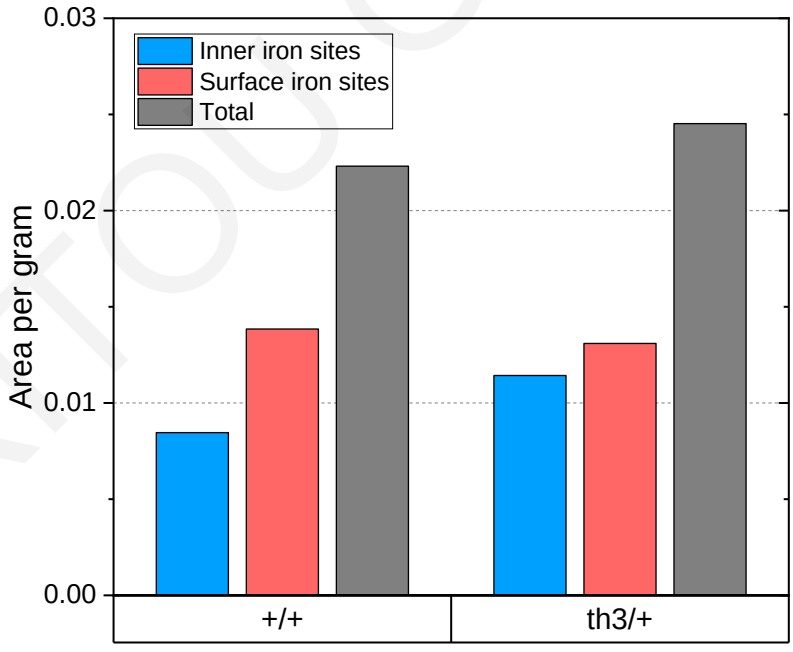

Figure 4.16: *Ferritin-like iron in the brain samples of one wild-type (+/+) and one th3/+ mouse at 9 months of age*

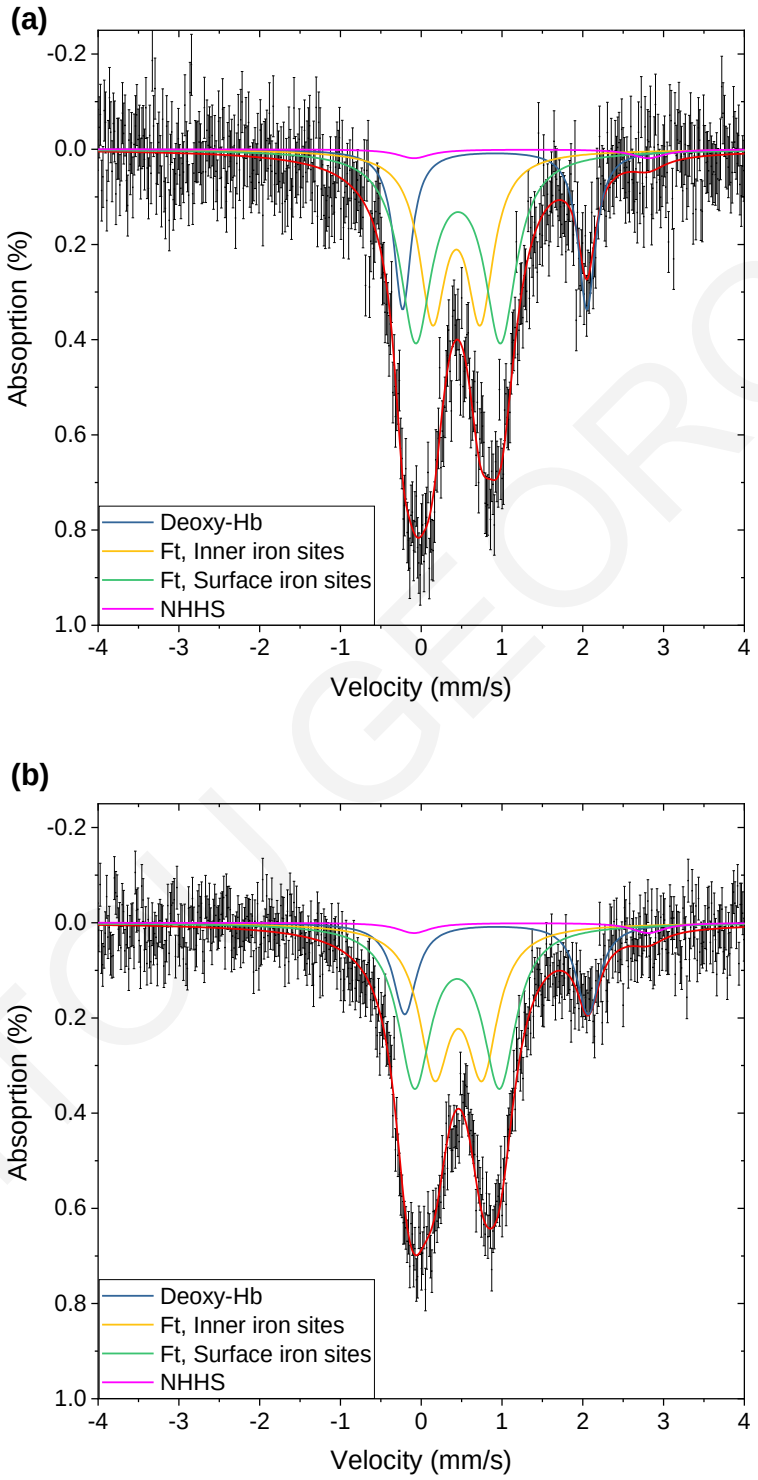

Figure 4.17: *Mössbauer spectra from the brains of a wild-type **(a)** and a th3/+ mice **(b)** at 9 months of age*

Livers:

In the juvenile *wild-type* mice, only surface iron sites were found, while in the adult mice the inner iron sites were the predominant one. This can be seen in *Figure 4.18(a) and (c)*. The overall ferritin levels of the adult mice do not seem to change significantly with age (*Figure 4.18(a)*) nor the inner-to-surface ratio. The *th3/+* mouse at 1 month of age was found with the same amount of both types of iron sites, but the total ferritin was increased by 2.4 times when compared to the control equivalent. In the adult *th3/+* mice, the predominant ferritin iron sites were again the inner-type, with slightly increased inner-to-surface ratio. In contrast to the control samples, the total ferritin's concentration was found to increase linearly over time (*Figure 4.18(d)*) with the samples from the adult *th3/+* mice having 4 - 9.5 times more ferritin iron than the same-age controls. MS spectra from the liver samples of mice at 9 months of age are shown in *Figure 4.19*. The spectra from the remaining mice are shown in Appendix II.

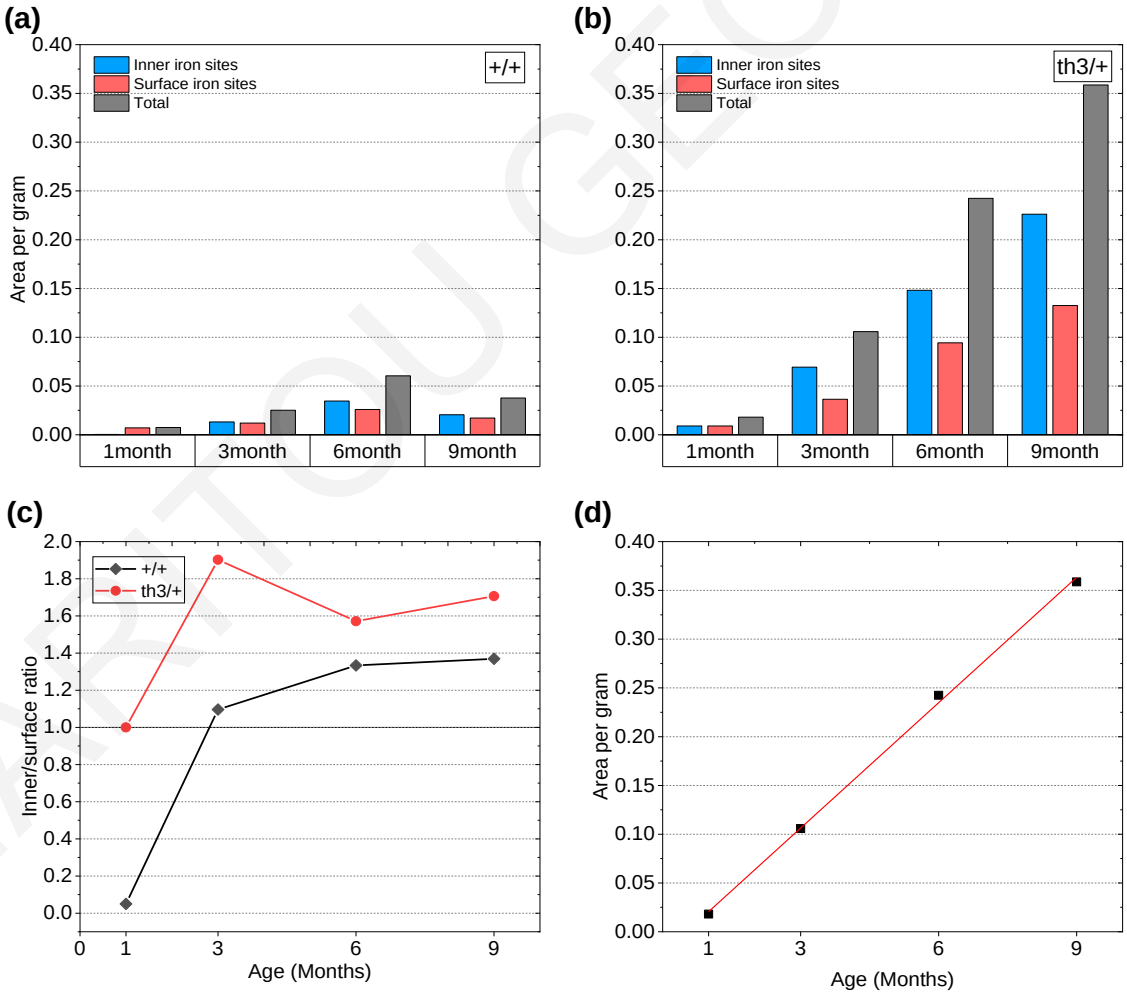

Figure 4.18: *Ferritin-like iron in the liver samples of wild-type **(a)** and th3/+ **(b)** mice. **(c)** shows the Inner-to-surface ferritin's iron sites ratio in the liver samples. Figure **(d)** shows the linear correlation of liver's total ferritin-like iron with the mouse age in the th3/+ mice*

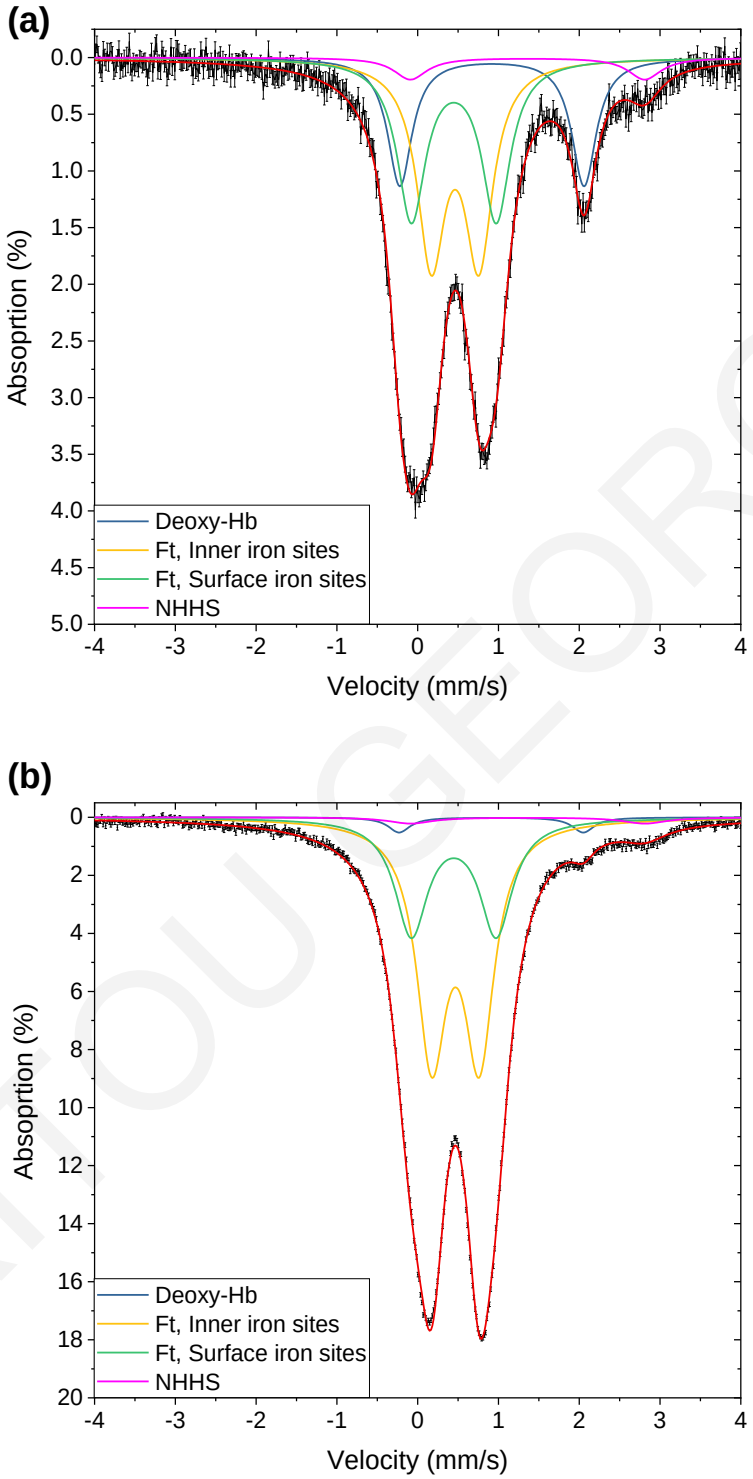

Figure 4.19: *MS spectra from the Livers of mice at 9 months of age[10]. The spectrum from the wild-type mouse is shown at **(a)** and from the th3/+ at **(b).** Notice the difference in the absorption's scale*

[10] The spectra from the mice of the remaining ages are presented in Appendix II

Spleens:

Similar to the liver tissues, the predominant type of ferritin's iron sites in the spleen samples was found to be the inner-type for both groups and all ages. All adult mice show similar inner-to-surface ratio (*Figure 4.20(c)*) with a mean value of 2.34:1 (~70% inner-core ferritin). The spectra from the spleen samples of the six and nine-month old *th3/+* mice show an extra component not observed in the previous samples. The samples were measured for the second time, and spectra were taken at higher velocity (V_{max} = ±10 mm/s). This component is presented as a wide sextet (*Figure 4.20(b)*), with fitting parameters of δ=0.48 mm/s, ΔEq=-0.25 mm/s, HMF=45.91 T. It can be attributed to haemosiderin with mineral goethite structure [60]. Haemosiderin is an iron storage complex found mainly in iron-overload conditions, and was observed in iron overloaded spleen tissues of thalassaemia patients [60,61] and iron overloaded rats [45]. From this observation, we can fairly assume that the 6 and 9 months old *th3/+* mice of this study exhibit advance iron-overload conditions.

As seen in *Figure 4.20(a) and (b)*, the total iron's (ferritin and haemosiderin) concentration increases with mice age for both groups. However, *th3/+* mice seem to depose iron in their spleen in a higher rate than the *wild-type* ones. Overall, the thalassaemia samples showed about 250-290% more ferritin and haemosiderin iron per sample's mass than the healthy controls. Spectra from the spleen samples of mice at 9 months of age are presented in *Figure 4.21*. The rest spectra can be found in Appendix II.

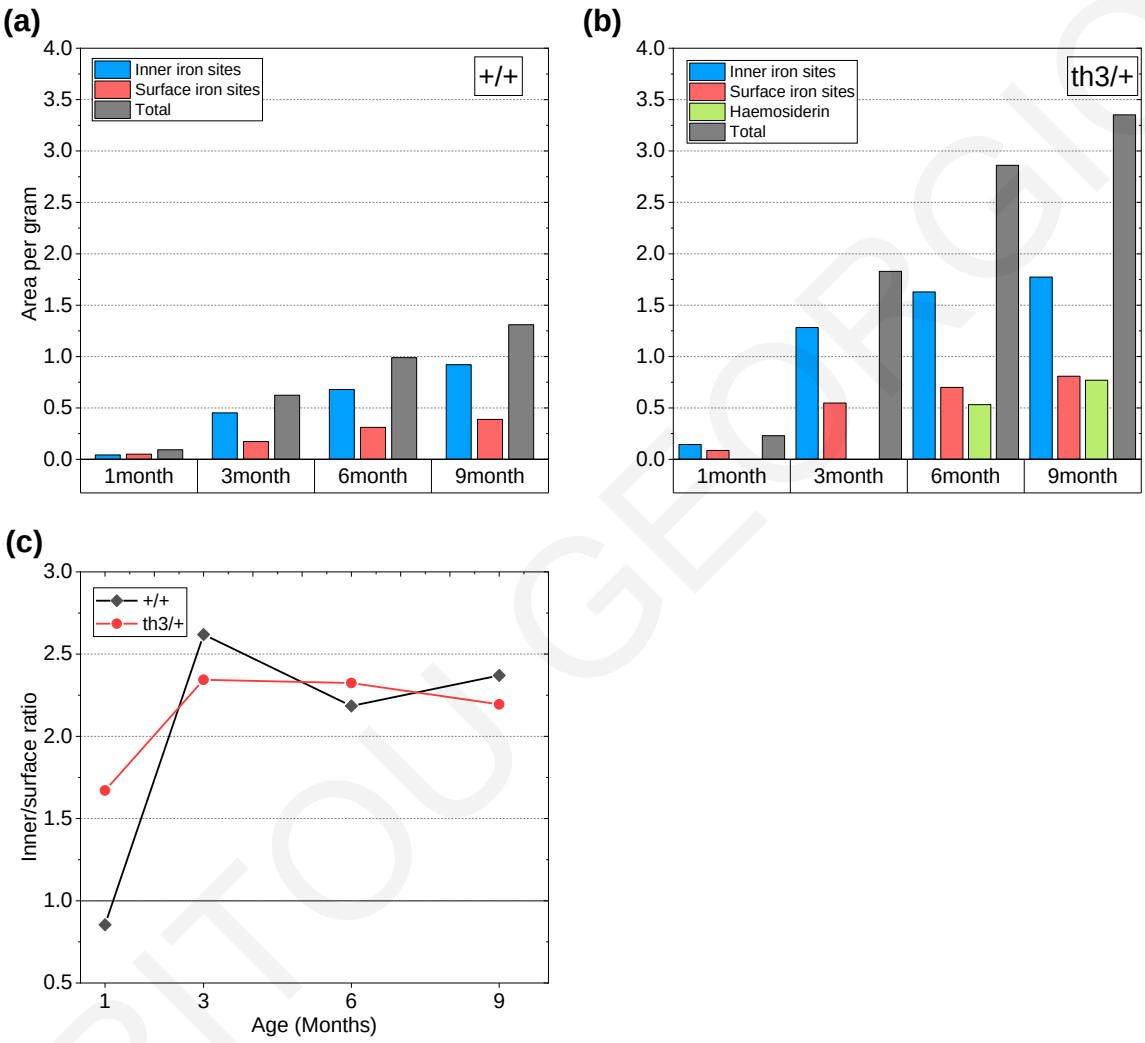

Figure 4.20: *Ferritin-like iron in the spleen samples of wild-type (+/+)* ***(a)*** *and thalassaemic th3/+* ***(b)*** *mice. In the th3/+ mice at 6 and 9 months of age, a new iron complex (green) can be seen which can be attributed to haemosiderin. Figure* ***(c)*** *shows the Inner-to-Surface ferritin's iron sites ratio in the spleen samples. The ratio for the adult mice seems to be independent of the sample group.*

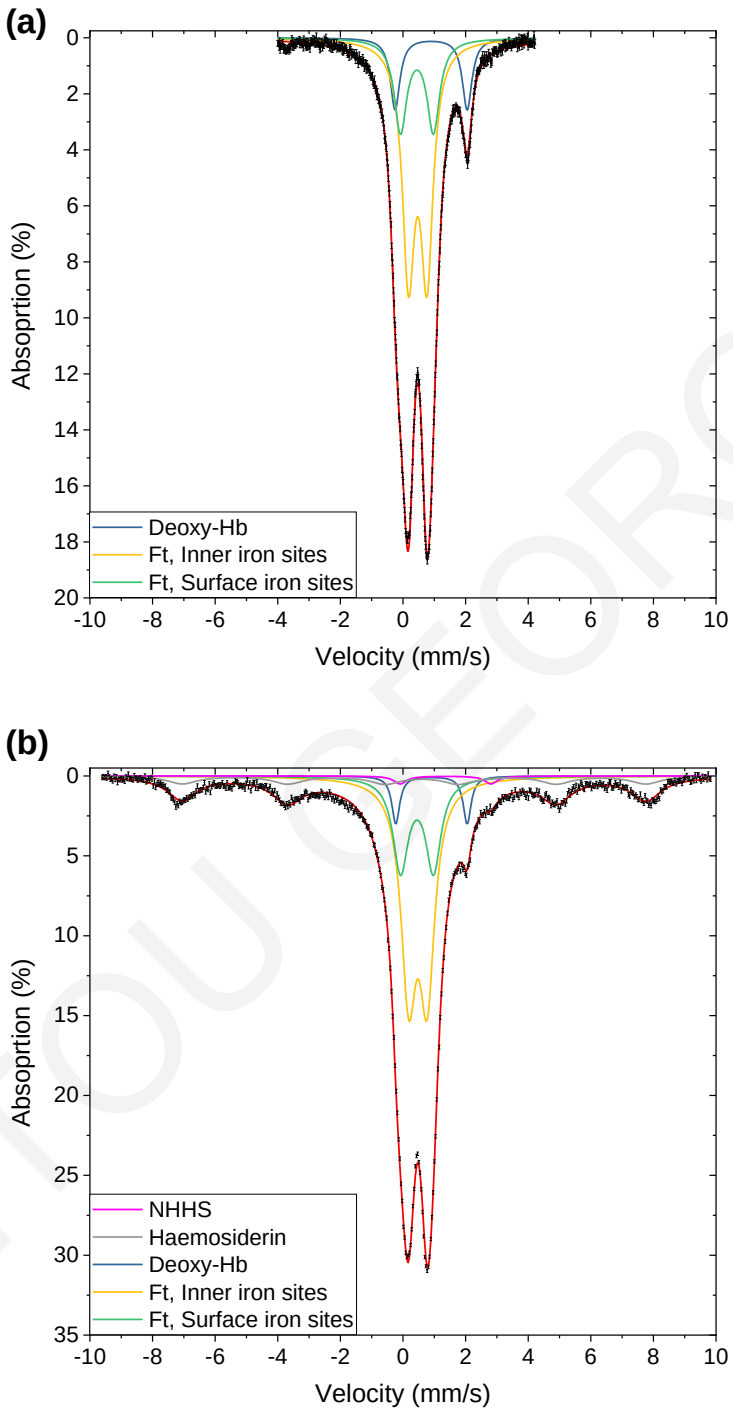

Figure 4.21: *Mössbauer spectra from the spleens of wild-type **(a)** and th3/+ mice **(b)** at 9 months of age[11]. The hemosiderin's sextet, a sign of iron overload is clearly seen in the th3/+ sample. The spectra from the thalassaemic spectra was acquired at higher velocity due to the sextet*

[11] The spectra from the mice of the remaining ages are presented in Appendix II

4.3 Summary – Discussion

Mössbauer spectra of blood, liver and spleen samples from a *wild-type* and a thalassaemic *th3/+* mouse were acquired at 78 K in order to evaluate if the *th3/+* thalassaemic mouse can be used with MS in order to study thalassaemia. Adult *th3/+* mice have a degree of disease severity similar to thalassaemia intermedia patients. They show haematologic indices characteristic of severe anaemia and develop spontaneous iron depositions in their organs.

Besides extreme anaemia, an increased amount of ferritin-like iron was observed in the thalassaemic liver and spleen samples compared with the normal ones, as expected since thalassaemic tissues exhibit increased iron deposition due to iron overload. The Mössbauer fitting parameters obtained were in good agreement with those reported in the literature. Therefore, based on this results, *wild-type* and thalassaemic mice exhibit iron complexes similar to humans, in both blood and organs. In this sense, the *th3/+* thalassaemic mouse model was found to be a promising candidate to study thalassaemia using MS.

Following the preliminary studies, ^{57}Fe enriched mice diet was prepared, and *wild-type C57BL/6* and thalassaemic *th3/+* mice were enriched through continuous gastrointestinal absorption in order to increase the spectra quality and characterize in more detail the iron complexes presented in the MS spectra. The enrichment method was validated by comparing, the MS spectra from the blood, liver and spleen of a non-enriched and a ^{57}Fe enriched *wild-type* mouse at 1 month of age. The enrichment method was found to be very successful as the MS spectra of the ^{57}Fe enriched mice showed significantly increased absorption. Based on this, ^{57}Fe enriched mice can be used in studying iron depositions in the organs using Mössbauer spectroscopy. This method can be further applied not only to thalassaemia disease but also to other iron related diseases as well.

Afterwards, MS spectra from blood, heart, liver, spleen, kidney and brain samples of *wild-type* and *th3/+* ^{57}Fe enriched mice at 1, 3, 6, and 9 months of age, were obtained at 80K. The spectra from the *wild-type* and *th3/+* mice were compared in order to identify any differences between the healthy and thalassaemic mice, as well as any age-related differences.

The spectra from the blood samples of the *wild-type* mice showed only the presence of oxy-haemoglobin, which were fitted by two Lorentzian sub-doublets of equal areas, representing the α- and β-globin chains of haemoglobin. The oxy-haemoglobin of the thalassaemic mice was fitted by the same sub-doublets but these spectra exhibited an increased α/β ratio due to the reduced β-chains in the thalassaemic (β-thalassaemia) mice.

The main difference between the blood sample spectra from the *wild-type* and *th3/+* mice is that, for all studied ages, a significant amount of ferritin-like iron (up to 14% of the blood's total iron), was observed in the thalassaemic samples but not in the normal ones. The observed ferritin-like iron in the blood of the *th3/+* mice cannot be explained by an increase in the serum iron levels due to thalassaemia, as Gardenghi et al. [37] showed that the serum iron levels in the *th3/+* mice are only slightly elevated compared to the iron levels of the *wild-type* ones. Thus, the ferritin-like iron identified in our study is likely to be located mainly in the RBCs of the mice. Furthermore, the percentage of the ferritin-like iron in the MS spectra from the thalassaemic mice were found to decrease with the age of the mice. A similar decrease was observed in the reticulocyte count of the thalassaemic mice by Gardenghi et al. [37]. The developing erythroid cells can continue to take up iron beyond the cell's apparent needs [12], therefore the reticulocytes could be released into circulation with already high levels of ferritin-like iron in them. Based on this, it might be possible that the ferritin-iron found in the reticulocytes can be a promising biomarker for assessing and managing iron overload. Moreover, these observations suggest that the RBCs might be a "hidden" storage of a significant amount of iron for thalassaemia patients, therefore, more investigations relative to this ferritin-like iron and its source are needed.

In the organs, iron complexes of four iron "categories" where found. A doublet from high-spin Fe(II) iron with deoxy-haemoglobin parameters was found in all samples and was attributed to blood residues inside the tissues. The method of exsanguination (removal of blood from the orbital sinus) that was used, was effective with results similar to the more complicated method of extensive flushing with Ringer's buffer by heart puncture which was used in a different study [39].

The second component was attributed to Mononuclear Non-haem high-spin Iron (NHHS Fe^{II}). These complexes can undergo Fenton chemistry due to labile ligands, therefore they can be responsible for the creation of reactive oxygen species, which is a major issue for the thalassaemia patients and responsible for cell and eventually organ damages. NHHS Fe^{II} iron was found in elevated values in the brain, kidneys and the liver of the *th3/+* mice compared to the *wild-type* ones. Also, high amounts of NHHS Fe^{II} iron were found in the spleen of adult *th3/+* mice only. *Th3/+* mice suffer from splenomegaly, a condition that thalassaemia patients also suffer from, where the spleen enlarges greatly in size in order to cover the increased erythrocyte production and destruction. Thus, it is possible that the increased NHHS Fe^{II} concentration in the thalassaemic spleen tissue might be related to phenomena associated with erythropoiesis and/or erythrophagocytosis.

Besides the NHHS Fe^{II} and deoxy-haemoglobin, ferritin-like iron was found in all organs, as expected. The wide ferritin-like doublet found in many previous studies could be further fitted with two sub-doublets which relate to the ferritin's mineral core structure, and more specifically to the iron sites on the surface and in the centre of the core. The ratio of these two sub-doublets was found to depend greatly on the organ and the mice group. In the *wild-type* mice, (a) hearts, kidneys and brains, organs with no long-term iron storage function, showed greater amounts of surface iron sites, while (b) in the liver and spleen the predominant ferritin's iron sites were the inner-core ones. A correlation with the L and H chains of ferritin might be possible, as cardiac tissues are rich in H-chain ferritin, and liver and spleen rich in L-chain ferritin. Thalassaemic *th3/+* mice favoured the formation of inner iron sites than the surface-type ones. Based on these two observations, we might assume that when large amounts of iron are present, they are stored in the center of the ferritin's mineral core and not on its surface. Also, the two chemical pathways responsible for the production of the inner-core, either produce or utilize hydrogen peroxide (H_2O_2), which is a major contributor to oxidative damage.

In the kidneys of the thalassaemic mice, major ferritin-like iron depositions were found when compared to the *wild-type* equivalents. The *th3/+* mice at 6 months of age showed ~16 times more ferritin-like iron in the renal tissues than the healthy controls. This finding indicates that kidneys might accumulate iron in great amounts and hence be vulnerable to iron overload. This might create new complications for the thalassaemia patients that can face further on, in life.

In the two examined brains, around 10% more ferritin-like iron was found in the *th3/+* one. This need further research as brain iron might be linked to various neurodegenerative diseases. In the cardiac tissues, small increases in iron concentration were found, especially for the juvenile mouse. However, the *wild-type* mouse at 6 to 9 months of age revealed similar iron concentration with the thalassaemic one. This observation is not consistent with the thalassaemic patients, as the iron concentration in their cardiac tissues increases significantly over time. Thalassaemic liver tissues showed huge increases in iron concentration, up to ~10 times the normal amount, which was expected to some degree, as iron accumulation in the liver is a well-known complication in thalassaemia patients. The rate at which iron accumulates in the *th3/+* livers seems to be corelated linearly with the mouse age.

Haemosiderin, an iron storage complex that is found in the spleen of thalassaemia and iron overloaded patients, was also observed in the spleens of *th3/+* mice at 6 and 9 months of age. This indicates that these mice suffered from advanced iron-overload conditions even though the iron content in their diet was in relative low levels. This can be useful for the planning of future studies.

Chapter 5

Iron studies in thalassaemia patients

Thalassaemias are hereditary anaemias resulting from defects in haemoglobin production. β-thalassaemia, which is caused by a decrease in the production of β-globin chains, affects multiple organs and is associated with considerable morbidity and mortality. Accordingly, lifelong care is required including frequent blood transfusions and iron chelation therapy. β-thalassaemia has a strong presence in Cyprus and among the local population of ~750000 people, one out of seven are thalassaemia carriers.

Previous Mössbauer studies characterized iron complexes in blood and organs of humans. In particular, comparing RBC samples from healthy humans and thalassaemia patients, a new component was identified in the patient's spectra which were considered to be ferritin-like iron [47,55,67,68]. These studies were carried out in the 80s-90s and since then a big progress has been achieved in the medical treatment of thalassaemia, especially after the introduction of iron chelators like deferoxamine (Desferal), deferiprone (L1) and deferasirox (ExJade) and the ability to assess myocardial and liver iron concentrations through MRI exams.

With this study, we aim to investigate using MS, blood samples from β-thalassaemia patients to evaluate the effectiveness of the current medical treatment in Cypriot thalassaemia patients. In contrast to other tests that detect and distinguish specific iron complexes, MS can detect all of them when found in sufficient amount.

5.1 Methodology

MS spectra form blood samples of β-thalassaemia patients were acquired at 80K and compared with equivalent spectra from healthy volunteers (control group). Even though blood and RBC samples were studied thoroughly with MS in the literature, new control spectra are needed in order to have a comparative base-line (e.g. for the absorption) for our experimental setup. At the same time, as supplementary to the main MS study, personal and medical data relative to iron's concentration and iron overload management were collected from the patient's medical records for basic statistical analysis and possible correlation/explanation purposes.

For the above purposes, venous blood from the volunteers was acquired through phlebotomy in sodium-heparin Eppendorf tubes (heparin is used as anticoagulant). The blood samples from the healthy volunteers were extracted from the clinical personnel at CING, while the samples from the thalassaemia patients were taken at the Nicosia Thalassaemia Centre of Archbishop Makarios III Hospital during their scheduled visits. The vials with the blood samples were transported the same day to the Molecular Genetics Thalassaemia Department (MGTD) of the Cyprus Institute of Neurology and Genetics for further processing.

At the MGTD, the Red Blood Cells (RBCs) were isolated from the plasma with the following procedure:

1. The whole blood was centrifuged at 500xg for 10 min at 4ºC.
2. The supernatant was aspirated and placed in a second tube and cell wash buffer was added to the erythrocytes.
3. The erythrocytes were centrifuged at 500xg for 10 min at 4ºC.
4. The supernatant was aspirated and discarded. Cell wash buffer was added to erythrocyte pellet.
5. Steps 3 and 4 were repeated two more times for a total of 3 washes of the erythrocytes.

After the isolation, the RBCs were placed on ice and transferred to the nuclear physics laboratory at UCY where MS absorbers where prepared by placing 750 μl of RBCs in Ø15 mm PP MS holders (described previously). Subsequently, the absorbers were snap-frozen by submerging them into liquid nitrogen and stored in an LN Dewar until used for measurements Excess blood and other biohazard waste were placed in special containers and subsequently stored and disposed according to the university's protocol.

All MS spectra were recorded at 1024 channels in transmission geometry, using a ^{57}Co/Rh source. The source was driven at constant acceleration from -4 mm/s to 4 mm/s and the samples were kept at 80±1 K. For consistency, the samples were measured until a background rate of ~1.5x10^{6} counts per channel was obtained.

The procedure of sample collection and storage, and the method of personal/medical data collection, protection and storage, has been approved by the Cyprus National Bioethics Committee, and the Office of the Commissioner for Personal Data Protection[12].

5.2 Sample population

As a baseline, 7 control (Ctrl) samples from healthy adult volunteers of both sexes were measured. The sample collection from the patients were random and it was based on their good-will to provide them for the study. Therefore 11 samples from 10 different β-thalassaemia intermedia (ThI) patients were studied, 7 samples from equal number of β-thalassaemia major (ThM) patients, and one sample from a patient with H-disease[13] (HbH).

The collected patients' medical and personal information (age, sex, thalassaemia genotype, ferritin levels, iron chelation therapy, frequency of blood transfusion, and myocardial and liver iron concentration as assessed from MRI scans) are given in *Table 5.1*. In this Table, the iron concentration from the MRI scans are coded and classified (by the diagnostic centre) as 0: normal levels (<1.5 mg Fe/g dry tissue), 1: Successful chelation (1.5-2.9 mg Fe/g dry tissue), 2: Mild haemosiderosis (3.0-6.9 mg Fe/g dry tissue), 3: Moderate haemosiderosis (7-15mg Fe/g dry tissue). Note that MRI scans could be up to 1-2 years old and Serum ferritin (SFt) was measured the same day or in some cases within 2 weeks from the date that our samples were collected. The average serum ferritin from their last 3 haematological tests was also calculated and given in *Table 5.1*.

[12] Approval by the Cyprus National Bioethics Committee: **ΕΕΒΚ/ΕΠ/2015/32**

Approval from the Office of the Commissioner for Personal Data Protection: **3.28.468**

[13] H-disease is a severe form of α-thalassaemia

Table 5.1: *Medical/personal information of the volunteer patients. Nomal levels for serum ferritin (SFt) are 15-300 ng/ml for males and 15-150 ng/ml for females. The iron consentrations in liver (LIC) and heart (MIC) were assesed by MRI exams and the levels are 0: Normal, 1: Successful chelation, 2: Mild haemosiderosis, 3: Moderate haemosiderosis. Samples ThI-003 and ThI-009 come from the same patient with 1 year appart.*

Sample	Genotype	Sex	Age	SFt (ng/m)	Average SFt (ng/ml)	Transfusion frequency	LIC	MIC	Chelation treatment
Th. Intermedia									
ThI-001	33/C39	F	39	819	1111	Every 2-6 Months	2	0	ExJade
ThI -002	IVS1/-92c>T	F	21	588	677	2-3 per year	2	0	L1
ThI -003	IVS1-110/-87	F	64	553	926	Every 2 Weeks	1	0	Desf+L1
ThI -004	IVS1-6/IVS1-1	F	60	852	804	Every 2 Months	2	0	Desf+L1
ThI -005	IVS1-110/IVS1-6	M	44	1469	996	Monthly	2	0	Desf+L1
ThI -006	IVS1-6/IVS1-1	M	64	541	579	Rarely	2	0	Desf
ThI -007	IVS1-110/IVS1-110	M	59	168	183	Weekly	1	0	Desf+L1
ThI -008	IVS1-6/IVS1-6	M	53	398	458	Rarely	2	0	ExJade
ThI -009	IVS1-110/-87	F	65	235	202	Rarely	1	0	Desf+L1
ThI -010	-87/C39	M	48	1667	1859	Every 1-2 Weeks	3	0	Desf+L1
ThI -011	IVS1-110/IVS1-6	M	55	1076	916	Every 2-3 Months	2	0	Desf+L1
Th. Major									
ThM-001	IVS1-110/IVS1-1	M	40	1247	1247	Every 2 Weeks	2	0	ExJade
ThM-002	IVS1-110/IVS1-110	F	51	1598	1665	Every 2-3 Weeks	2	0	Desf + L1
ThM-003	IVS1-110/IVS1-110	M	42	3006	3076	Weekly	2	0	ExJade
ThM-004	IVS1-110/IVS1-110	F	41	643	701	Every 2 Weeks	0	0	Desf+L1
ThM-005	IVS1-110/IVS2-745	F	39	1336	1433	Every 2 Weeks	1	0	Desf+L1
ThM-006	IVS1-110/IVS1-110	M	-	720	1061	Weekly	1	0	Desf+L1
ThM-007	IVS1-110/IVS1-110	M	46	2200	2490	Every 2-3 Weeks	2	0	Desf+L1
HbH		M	59	557	476	Monthly	0	0	Desferal

5.3 Patient statistics

Patients were separated to three groups based on their type of thalassaemia; β-thalassaemia intermedia (ThI), β-thalassaemia major (ThM) and H-Disease (HbH). The average age of the patients, as shown in *Figure 5.1*, was 52 years for the ThI ones, 43 years for the ThM patients, while the HbH patient was 59 years old.

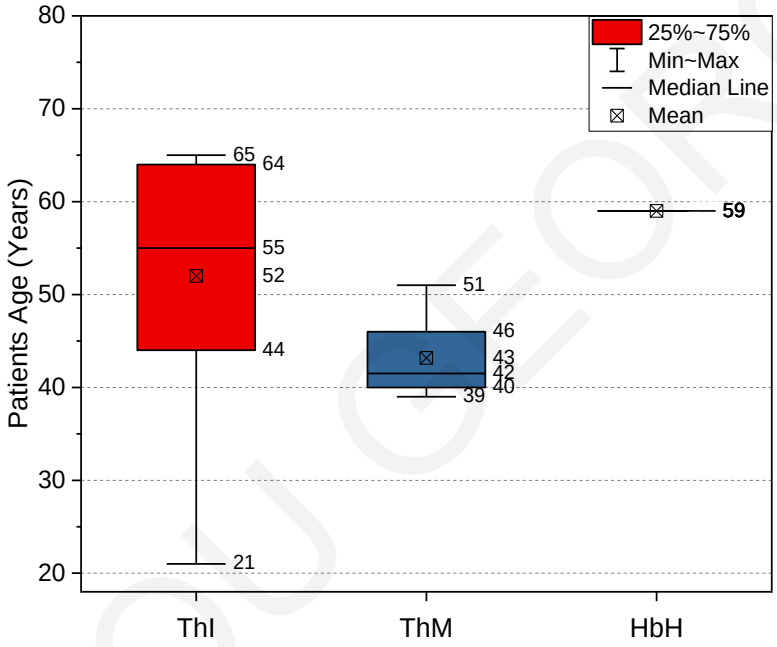

Figure 5.1: The *age distribution for each patient group is shown*

On an average, ThI patients had serum ferritin (SFt) levels around ~761 ng/ml, with half of them below the 588 ng/ml and 75% (3rd quartile) of them below 1079 ng/ml. On the other hand, ThM patients had almost twice the serum ferritin levels of the ThI patients, with an average of ~1536 ng/ml while 75% of them had SFt levels between 643 – 2200 ng/ml. The rest of them presented higher serum ferritin levels, up to ~3000 ng/ml. The normal limits for serum ferritin are 15-300 ng/ml for males and 15-150 ng/ml for females. For patients with transfusion depended thalassaemia, serum ferritin levels consistently less than 2500 ng/ml are linked to improved survival, with even better outcome when SFt levels are <1000 ng/ml [20]. The serum ferritin level distribution in the thalassaemia patients are shown in *Figure 5.2*.

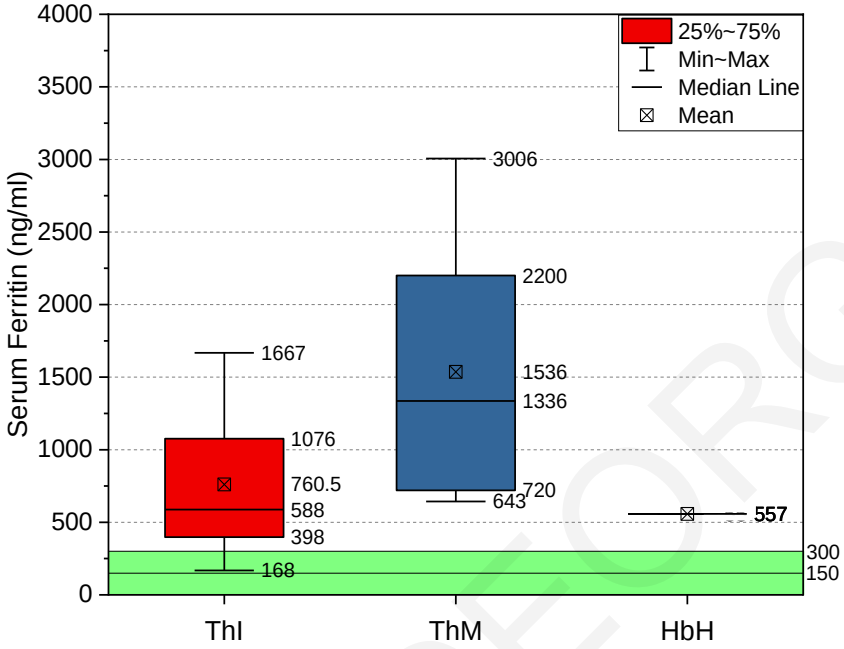

Figure 5.2: *The distribution of serum ferritin levels for the thalassaemia patients is shown. The thalassaemia intermedia patients (ThI) had ~50% less serum ferritin than the thalassaemia major (ThM) ones. With HbH is noted the patient with H-disease. With green the normal limits are shown (15-300 ng/ml for males and 15-150 ng/ml for females)*

The MRI scans showed that none of the patients have myocardial iron concentration (MIC) beyond the normal limits while almost all of them, with the exception of one ThM patient, had increased liver iron concentrations (LIC). However, in contrast to the patients serum ferritin levels, β-thalassaemia intermedia patients showed increased liver iron consentration when compared to the β-thalassaemia major patients. According to the acquired data, which are presented in *Figure 5.3*, 73% of the ThI patients showed mild or moderate haemosiderosis while the equivalent proportion for the ThM patients was 57%. This observation is in contrast to the previous one from the serum-ferritin levels, as ThI patients had almost half the SFt amount of the ThM ones. Based on this, it can be assumed that SFt is not a reliable bio-marker to assess iron-overload in ThI patients. However, it should be noted that the MRI data were not acquired at the same time-period (e.g. same month) with the SFt tests, therefore, this observation, although strong, is not conclusive and further studies are necessary.

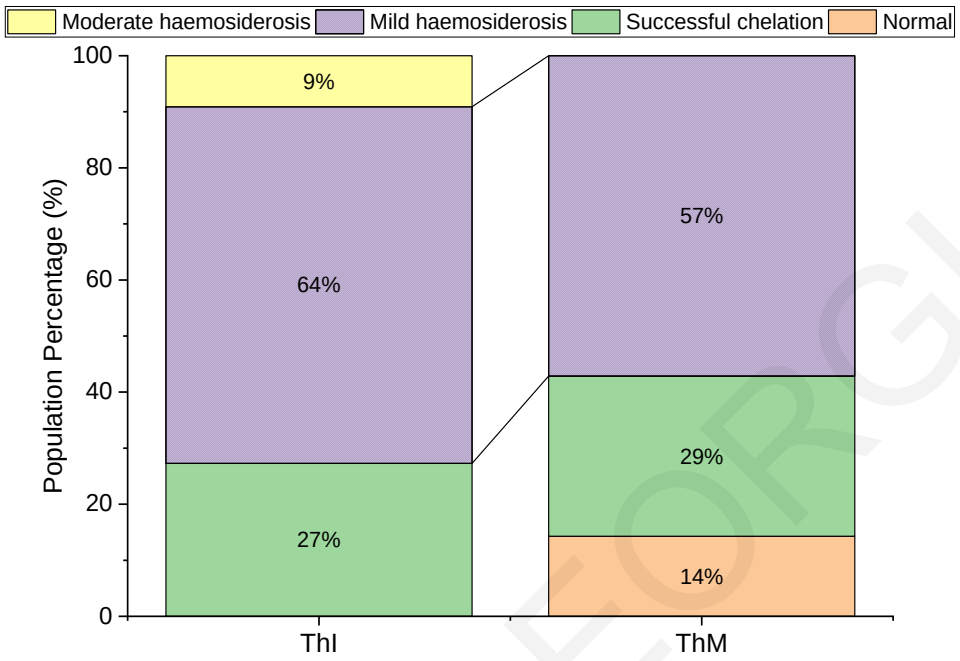

Figure 5.3: *Liver iron concentrations distribution among the sample population, as assed from MRI scans. They were classified in four groups according to the diagnostic centre: normal levels (<1.5mg Fe/g dry tissue), Successful chelation (1.5-2.9 mg Fe/g dry tissue), Mild haemosiderosis (3.0-6.9 mg Fe/g dry tissue), Moderate haemosiderosis (7-15mg Fe/g dry tissue)*

5.4 Mössbauer spectroscopy studies

5.4.1 Carboxy-haemoglobin (CO-Hb)

Haemoglobin in venous blood is found mainly in three forms. Oxy-haemoglobin (oxy-Hb) which is haemoglobin combined with oxygen, deoxy-haemoglobin (deoxy-Hb) which is haemoglobin not combined to anything, and carboxy-haemoglobin (CO-Hb) which is formed when haemoglobin is attached to carbon monoxide (CO). For non-smokers, CO saturation is <3% while smokers can have chronic saturations of 3-8% [69]. Therefore, CO-Hb could have a measurable portion in the MS spectra, and its Mössbauer parameters should be known. According to the literature [50], CO-Hb is expected as a doublet with δ=0.23 mm/s and ΔEq=0.39 mm/s.

To verify the above parameters and to also have the linewidth (Γ) of carboxy-haemoglobin, RBCs from a healthy volunteer were saturated in CO gas (to saturate the haemoglobin molecules with CO ligands) before being placed into the MS holder and frozen into LN. Subsequently, the sample was measured at 80K and the spectrum, which is shown in *Figure 5.4*, was analysed.

Co-Hb's MS parameters where found to be: δ=0.26 mm/s, ΔEq=0.37 mm/s and Γ= 0.26 mm/s, which are in agreement with literature [50].

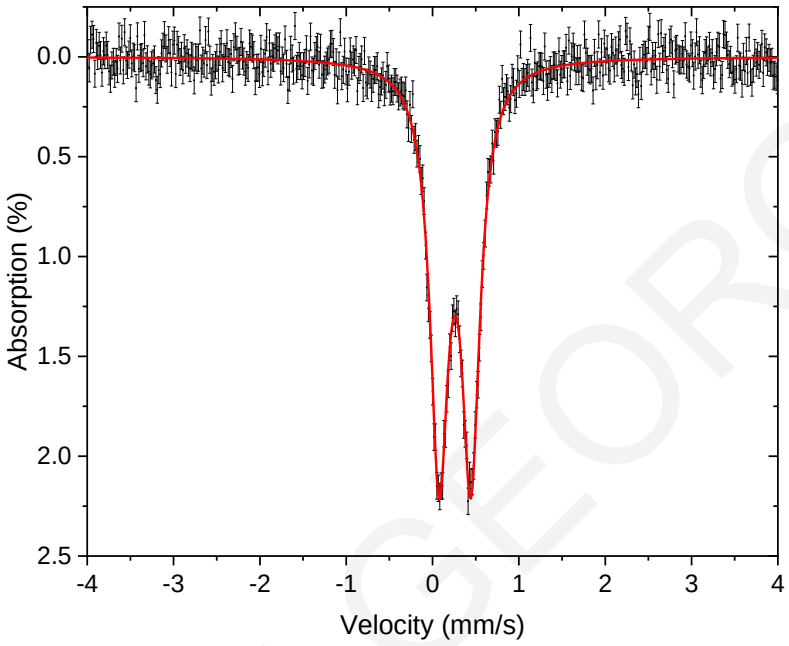

Figure 5.4: *MS spectrum from RBCs saturated in CO gas, acquired at 80K*

5.4.2 Fitting model

At first, all spectra were fitted with doublets with their number varying in order to achieve the smaller χ^2. A CO-Hb doublet was fitted to all spectra with δ, ΔEq and Γ fixed to the previous mention values, but with its area free to vary. Then two doublets corresponding to the α- and β-chains of oxy-haemoglobin were added to the fitting model. In some spectra deoxy-haemoglobin was presented, thus a fourth doublet was also added to the fit. Deoxy-haemoglobin is found in the venous blood resulting from the release of oxygen to the tissues. During transportation and preparation, the blood in the sample tubes can absorb atmospheric oxygen and transform to oxy-haemoglobin. For some thalassaemia major and in most of the thalassaemia intermedia samples, these four doublets could not fit the spectra satisfactorily. In some spectra, a new non-haem component with ferritin-like parameters could be clearly identified (*Figure 5.5*) while in some others, this component, even though it was not clearly distinguishable, it was necessary to be inserted so as to improve the fit.

Therefore, in order to keep the fitting method constant for all samples (control and thalassaemic), a fitting model with 5 Lorentzian doublets was used and all spectra were fitted again. The 5 doublets used, along with their initial parameters, are shown in *Table 5.2*. Values kept fixed are indicated with bold fonts (CO-Hb and ferritin-like iron).

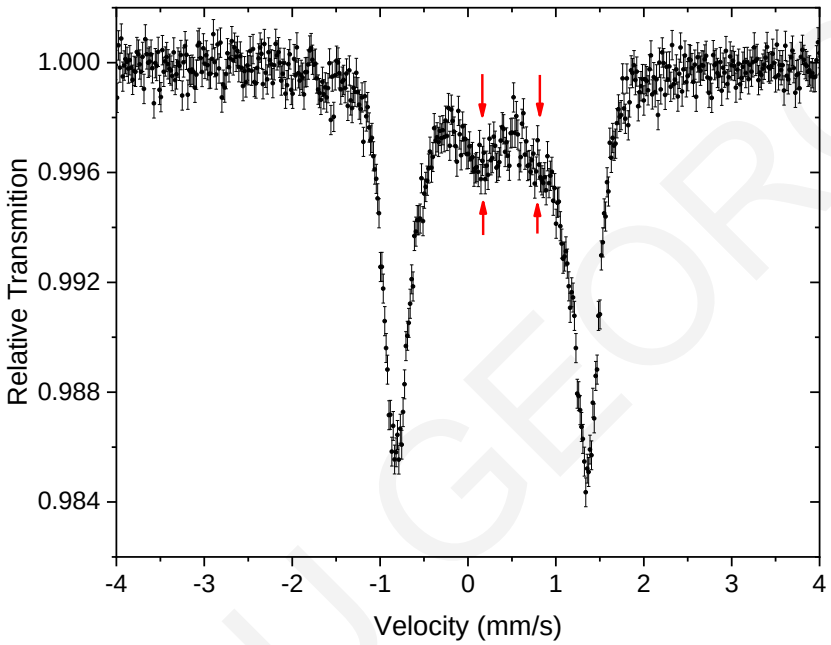

Figure 5.5: *Mossbauer spectrum at from the RBCs of a thalassaemia intermedia patient. The two peaks of a non-haem doublet are shown with the arrows.*

Table 5.2: *The starting values of the doublets used in the spectra fitting model. With bold fonts the fixed values are noted*

Component	Γ (mm/s)	δ (mm/s)	ΔEq (mm/s)
CO-Hb	**0.26**	**0.26**	**0.37**
Oxy-Hb-α	0.26	0.27	2.20
Oxy-Hb-β	0.37	0.27	1.86
Deoxy-Hb	0.26	0.92	2.29
Ferritin-like iron	**0.55**	**0.48**	**0.72**

5.4.3 Mössbauer Spectroscopy Results

Initially, 7 samples from healthy young adults (mid 20s to late 30s) of both sexes were measured with MS and analysed in order to verify that our results are in line with the published literature. The oxy-haemoglobin's doublet could be further divided into two sub-doublets, corresponding to the α- and β-chains of haemoglobin, denoted as Hb-α and Hb-β respectively. Also, carboxy-haemoglobin could be fitted as expected using the previous mentioned values as the area of the peaks was too small and the software could not fit it freely. CO-Hb was found to be 2-5% of the total haemoglobin, in agreement with the expected values for non or light smokers. Some amounts of deoxy-haemoglobin were found in two samples. The two oxy-haemoglobin's doublets present the MS parameters seen in *Table 5.3*; mean value for the α-chains: δ=0.26±0.01mm/s, ΔEq=2.19±0.01mm/s, Γ=0.25±0.01mm/s, and for the β-chains: δ=0.27±0.01mm/s, ΔEq=1.84±0.03mm/s, Γ=0.36±0.02mm/s. The errors shown are the statistical standard deviation (σ) while the instrumental error is <0.03mm/s. The values are in agreement with the corresponding literature [51,52]. The α- and β-chains were expected to have ~1:1 ratio, as normal adult haemoglobin consists of 50% α-chains, and 45-48% β-chains, with the rest being δ- and f-chains as described in Chapter 1. However, the observed α/β ratio was ~1.9:1. Difficulties of having 1:1 ratio were mentioned in the literature [51–53], where the doublets were forced to have equal areas, or they used doublets with fixed parameters in order to achieve it. Trial fits with fixed values or equal areas gave results with high diversion in the parameters among the samples. Therefore, the fitting parameters were left free to vary and were only fixed when the fitting parameters where abnormal (e.g. Γ < 0.24 mm/s). The "ferritin's" doublet area fitted by the software was zero in all control spectra.

The spectra from the ThM patients are similar to the control ones, with the two oxy-haemoglobin doublets having similar parameters. Even though all patients had serum ferritin levels well above the normal limits (average serum ferritin 1536ng/ml), the software managed to fit small amounts of ferritin in just two of the seven spectra, with relative percentages of 1±1% and 5±3% respectively. In the most recent (1994) publication found, K. Jiang et al. [55] did not observed any ferritin-like iron in the RBCs of their thalassaemia major patients that underwent iron chelation therapy with deferoxamine.

The oxy-haemoglobin in the blood samples of the thalassaemia intermedia patients also showed parameters similar to the control ones. The software was able to fit the "ferritin's" doublet in the ~80% of the samples (9 out of 11 samples), with 6 of them showing more than 5% ferritin. *Figure 5.6* shows the ferritin-like iron's percentage, relative to the total area of the spectra, for all samples. Even though it was not possible to verify the results with a different

method, the ferritin-like iron found in most of the RBC samples of the ThI samples should not be due to experimental errors. Most of these samples were taken, processed and measured in completely different times and in parallel with thalassaemia major samples. Therefore, there was not any difference in the methodology or handling that could be responsible for the additional ferritin-like doublet in the ThI spectra.

The final fitting parameters, linewidth (Γ), isomer-shift (δ), and quadrupole splitting ΔEq, for the two Hb-α and Hb-β sub-doublets of all spectra are shown in *Figure 5.7(a), (b) and (c)* respectively. All MS parameters from all spectra can be found in Appendix III, *Table 0.6*. The mean values for each group, and for all examined population are shown in *Table 5.3*. From these values, one can observe that the two sub-doublets used to fit the overall oxy-haemoglobin, are similar for all groups. The average values from all spectra are for Hb-α: δ=0.26±0.01 mm/s, ΔEq=2.19±0.01 mm/s, Γ=0.26±0.01 mm/s, and for Hb-β: δ=0.27±0.01 mm/s, ΔEq=1.85±0.03 mm/s, Γ=0.37±0.02 mm/s. The errors shown are the standard deviation (σ) of the measurements. The experimental error is <0.03 mm/s. The higher deviation in the measurements of the ThI samples for the Hb-β doublet seen in *Figure 5.7* are probably due to the presence of the ferritin's-like doublet as the two doublets overlap in some areas of the spectra. Spectra from RBC samples of a healthy volunteer and one thalassaemia intermedia patient is shown in *Figure 5.8(a) and Figure 5.8(b)*, respectively. The corresponding spectra from all the samples studied are presented in Appendix II.

Table 5.3: *The mean values for the MS parameters of the two fitted oxy-haemoglobins sub-doublets for each population group, along with the standard deviation (σ)*

Sub-doublet	Sample group	Γ (mm/s)	σ_Γ (mm/s)	δ (mm/s)	σ_δ (mm/s)	ΔE_Q (mm/s)	$\sigma_{\Delta EQ}$ (mm/s)
Hb-α	Control	0.25	0.01	0.26	0.01	2.19	0.01
	ThM	0.27	0.01	0.27	0.00	2.19	0.01
	ThI	0.26	0.01	0.27	0.01	2.20	0.01
	All	0.26	0.01	0.27	0.00	2.19	0.01
Hb-β	Control	0.36	0.02	0.27	0.00	1.84	0.01
	ThM	0.37	0.01	0.28	0.01	1.83	0.02
	ThI	0.37	0.02	0.27	0.01	1.86	0.03
	All	0.37	0.02	0.27	0.01	1.85	0.03

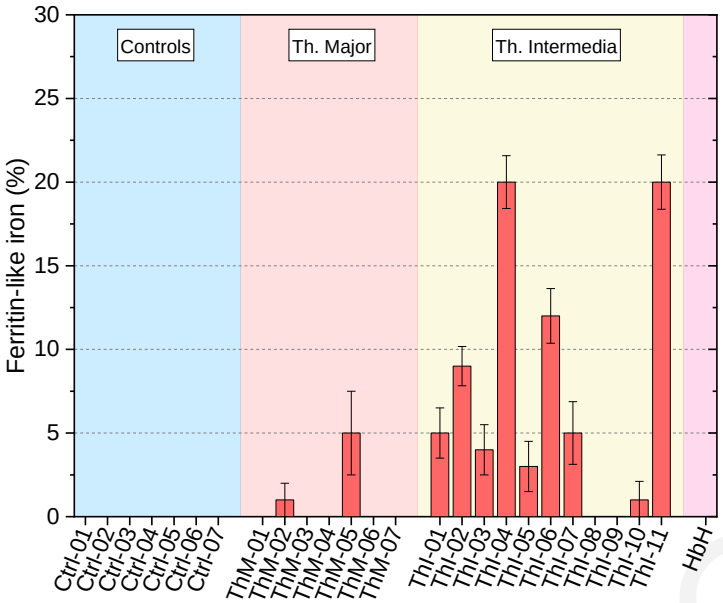

Figure 5.6: *The ferritin amount, as percentage relative to the total iron in the RBC samples of healthy volunteers (Ctrl), β-thalassaemia major (ThM), β-thalassaemia intermedia (ThI) and H-disease (HbH) patients. The errors shown are the statistical errors from the fit*

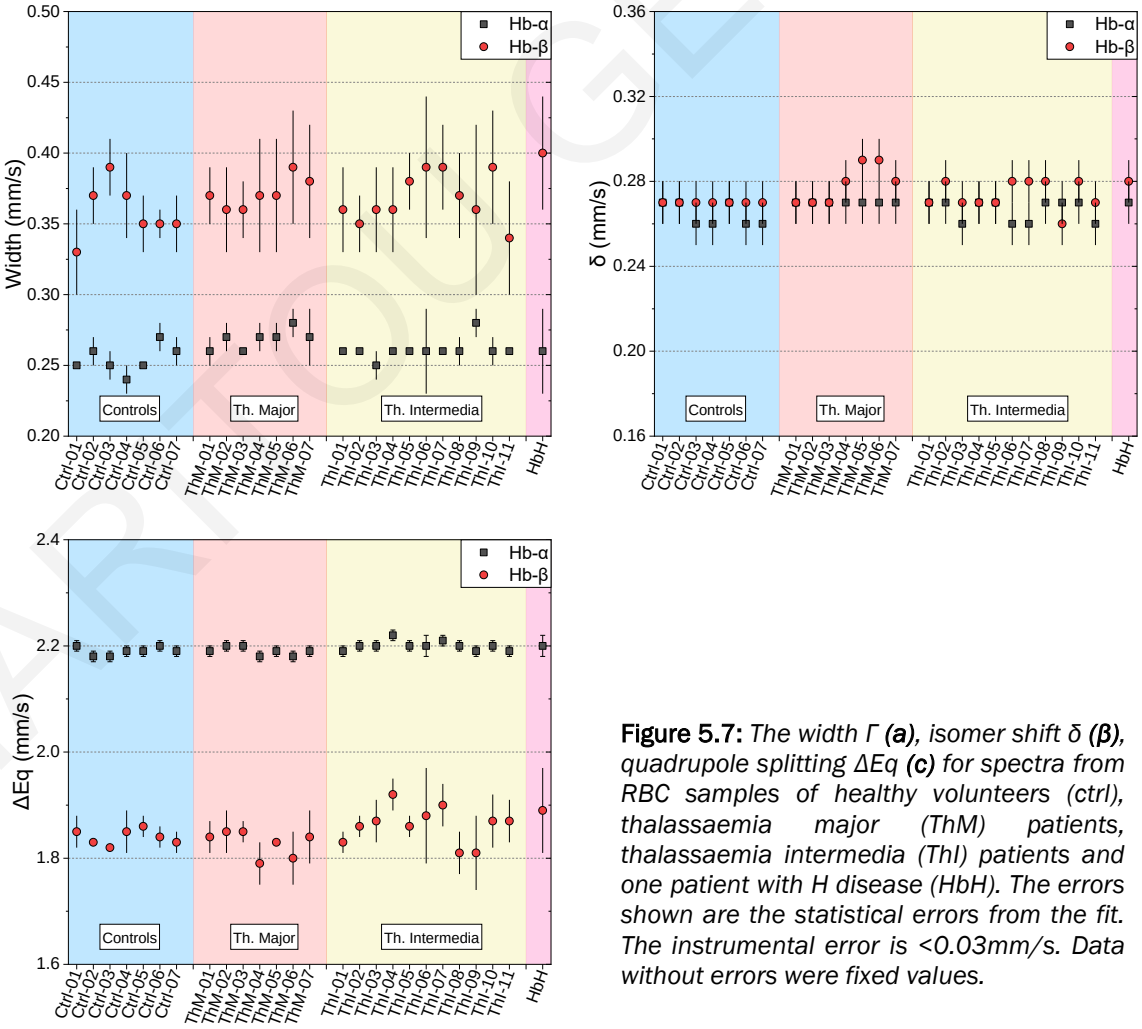

Figure 5.7: *The width Γ **(a)**, isomer shift δ **(β)**, quadrupole splitting ΔEq **(c)** for spectra from RBC samples of healthy volunteers (ctrl), thalassaemia major (ThM) patients, thalassaemia intermedia (ThI) patients and one patient with H disease (HbH). The errors shown are the statistical errors from the fit. The instrumental error is <0.03mm/s. Data without errors were fixed values.*

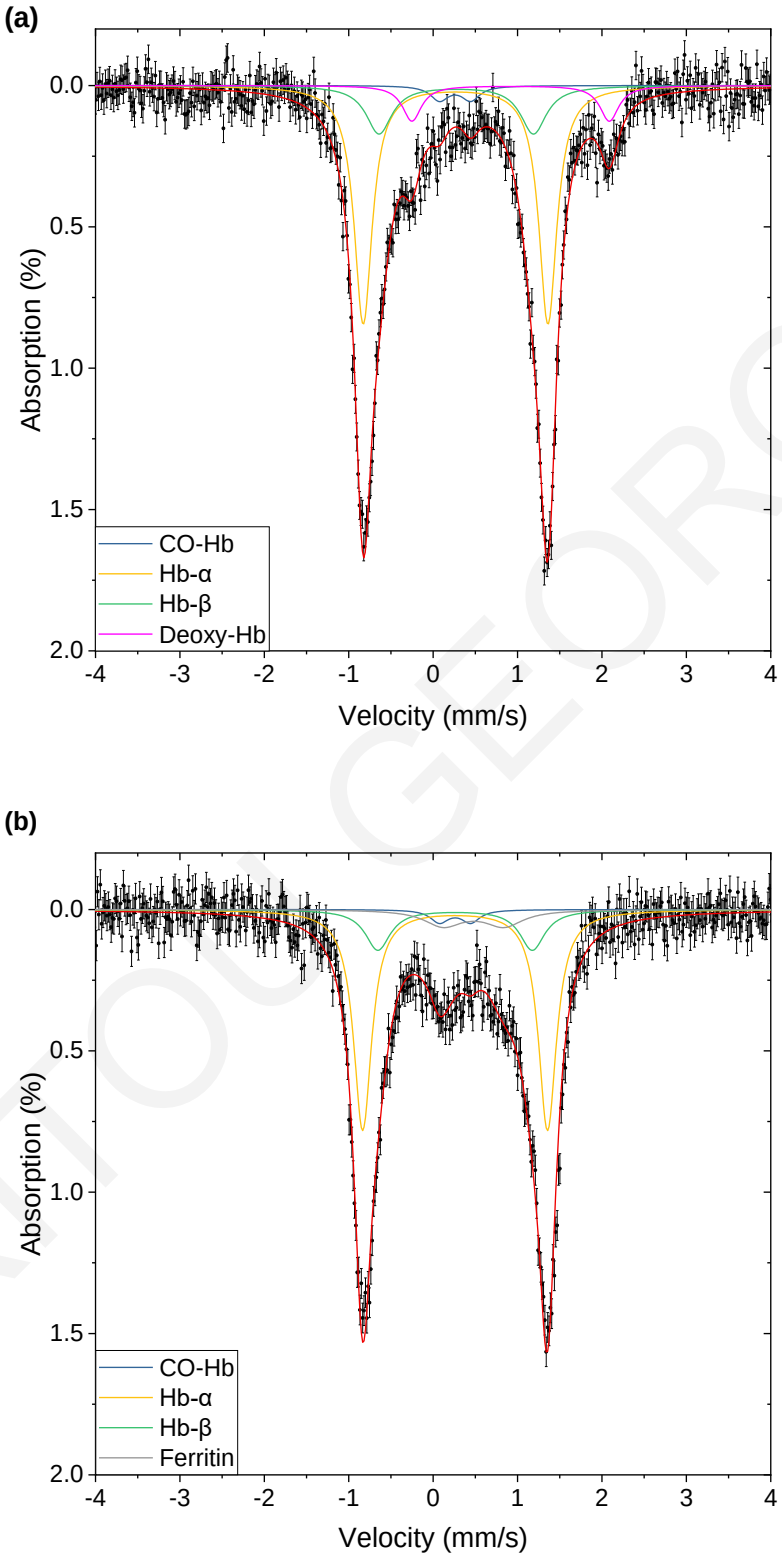

Figure 5.8: *MS spectra from the RBCs of a healthy volunteer **(a)** and a thalassaemia intermedia patient **(b)**, acquired at 80K*

5.5 Summary - Discussion

The oxy-haemoglobin's area of the spectra was fitted with two sub-doublets corresponding to the α- and β-globin chains of oxy-haemoglobin's tetramer, similar to the most recent literature [50–52]. These two doublets should have near or equal amounts (~1:1 ratio) as in healthy individuals 50% of the globin chains are always α- and 45-48% are β-. However, it was found that this ratio is difficult to be achieved in an MS fit with unrestricted doublets. These difficulties are probably due to statistical reasons and software limitations (like the minimization of χ^2), as the two doublets describing the α- and β-globin chains overlap significantly. Also, other minor components that could exist in the samples due to the method of collection and preparation, such as coagulates and methaemoglobin, could "widen" the sub- doublets and even add small ones that cannot be resolved. Fitting a MS spectrum using data taken from mass spectrometry analysis, might explain this problem. Similar difficulties to achieve ~1:1 ratio with unrestricted doublets have been found in the literature [51–53] but no explanation was given.

Besides the above measurements, 7 β-thalassaemia major (ThM), 11 β-thalassaemia intermedia (ThI) and one patient with H-disease (HbH) were also studied. Based on the data acquired from their medical records, it was observed that ThI patients had on an average half the serum-ferritin levels of the ThM ones. Furthermore, 73% (8/11) of ThI patients were below the limit of 1000 ng/ml, which is linked with increased survival, while in the group of ThM patients only two (29%) were under this limit. This can be explained by the fact that ThI patients have mild anaemia, therefore their needs in blood transfusion, and thus iron intake, is significantly less. This can be seen in *Table 5.1,* where ThM patients are transfused every 1-3 weeks, while ThI patients do so, normally after a period of few months or even yearly in some occasions. However, ThI patients had an increased liver iron concentration (LIC) compared to the ThM ones, as assessed by MRI exams. 73% of them showed signs of mild and moderate haemosiderosis while the equivalent ratio for the ThM ones was 57%. It is interesting that some β-thalassaemia intermedia patients with normal amounts of SFt (patients ThI-007, and ThI-009) or relatively low SFt (patient ThI-008) still had an abnormal LIC. It is worth mentioning that all patients are under medical supervision and undergo iron chelation therapy and blood transfusions, as needed. These increased liver iron depositions in the ThI patients have also been reported in different studies and the Liver Iron Concentration was evaluated by R2 MRI or biopsy [70,71] but no explanation was given. As seen in *Figure 5.9*, β-thalassaemia intermedia patients can develop high values of LIC despite the much lower serum ferritin values.

Based on these observations, we can assume that serum ferritin it might not reflect the level of iron overload in ThI patients in the same way as in the ThM patients, and it might be an unreliable marker to asses iron-overload in this group of patients. As a result of this, physicians might underestimate iron overload in β-thalassaemia intermedia patients with consequences in the effectiveness of iron-chelation therapy, resulting in an increased liver iron concentration.

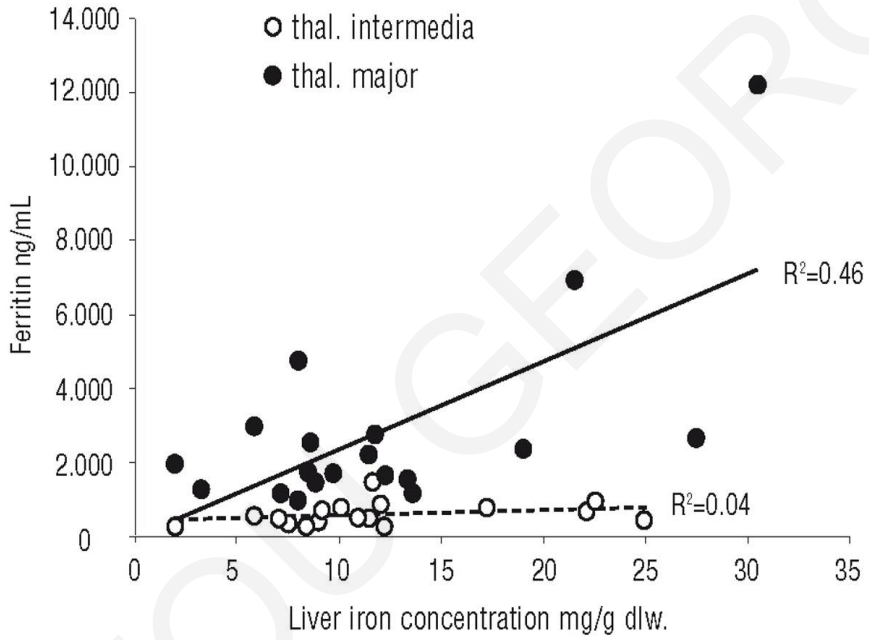

Figure 5.9: *Correlation between liver iron concentration and serum ferritin in patients with β-thalassemia. The solid line represents the linear regression for thalassemia major, and the dashed line that for thalassemia intermedia [70]*

Mössbauer spectroscopy has the ability to detect all iron complexes that are present in sufficient amounts in a sample, hence it is a very useful tool for sample analysis. RBC samples from the two groups were measured with MS at 80K and analysed. The results showed that ferritin-like iron was present in the samples of most β-thalassaemia intermedia patients (9 out of the 11) and to a lesser extend to some samples (2 out of 7) from β-thalassaemia major patients. This observation was unexpected as most of the thalassaemia intermedia patients did not have significantly increased serum ferritin. Ferritin iron was observed with MS in the RBCs of thalassaemia intermedia and major patients in the late 1970s [67], but it was at a time where iron chelation therapy was not common and iron in the patients was very high. It

was also observed with other methods in the 80s with some patients on iron chelation therapy [72].

In addition to the previous observations, although MS cannot give numeric concentrations (e.g. mg/ml), it is possible to estimate to some extent the amount of ferritin-like iron in the RBCs. At the temperature of 80K, where the spectra were taken, ferritin-iron and haemoglobin have comparable recoil free efficiencies (f-values), as seen in *Figure 5.10* [47]. Each ml of RBCs contains about ~1.16 mg of haemoglobin iron [4], and therefore, a sample with a MS spectrum from which 10% of the area is due to ferritin-like iron, should have around ~125 μg/ml ferritin-like iron. Some samples showed ferritin-like iron percentage of up to 20% which is roughly equal to ~290 μg/ml. This is a significant quantity, comparable with the amount of iron that is found in the RBCs, and much higher than the total iron found in the serum, which is about 0.7-1.4 μg/ml[14] in a healthy individual [73]. Therefore, one may assume that the RBCs in the thalassaemia intermedia patients can contain large amounts of ferritin-like iron and hence they can be a significant iron store.

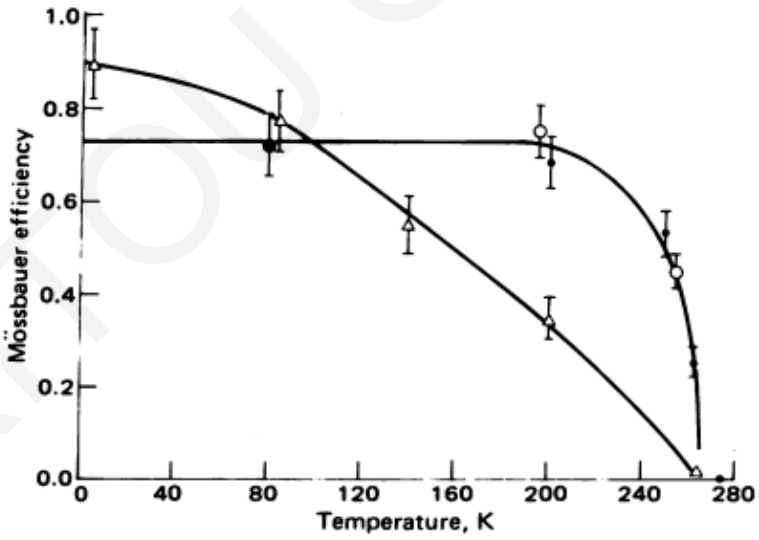

Figure 5.10: *Recoil-free efficiencies (f-values) of haemoglobin and ferritin as a function of temperature. △, Hb; ○, data obtained from a frozen aqueous solution of horse spleen ferritin; •, data obtained from ferritin in RBC. [47].*

[14] The serum iron of a healthy adult, non-pregnant woman, lies between 13 and 27 μmol/L [73]. Iron has a molar mass of 55.8 g/mol

Reticulocytes are immature red blood cells which are released mainly from the bone marrow into the circulation one to two days before maturation. The developing erythroid cells have ribosomes for continued haemoglobin synthesis, and they can take up transferrin bound iron through transferrin receptors and synthesize ferritin [74]. Additionally, the developing erythroid cells can continue to take up iron beyond the cell's apparent needs (like in sideroblastic anaemia) [12]. Therefore, the reticulocytes can be released into circulation with already high levels of iron in them. β-Thalassaemia major patients, as explained in chapter 1, have no or very limited ability to produce new functioning erythroid cells, therefore they need frequent blood transfusions from very young ages. Because of this, the RBCs found in their blood come from donors. On the other hand, β-thalassaemia intermedia patients have the ability to produce their own erythroid cells. Based on these observations and previous arguments, we can make two hypotheses that can partially explain the observations:

I. The ferritin-like iron found mostly in the RBCs of β-thalassaemia intermedia patients could be due to the release of iron-rich reticulocytes.
II. The unexplainable high liver iron concentrations (in relation with the serum ferritin levels) in the ThI patients might be the result, or even the cause, of the significant ferritin-like iron amounts that were found in their RBCs, and therefore it might be linked to the release of iron-rich reticulocytes. If this can be proven, then erythrocyte (or reticulocyte) ferritin might be a useful bio-marker to assess and manage iron overload in β-thalassaemia intermedia patients or even in other diseases like hereditary haemochromatosis.

The first hypothesis can be further supported by the results of the first study in chapter 4, where blood samples from a thalassaemic mouse model *(th3/+)* were studied with Mössbauer spectroscopy and similar concentrations of ferritin-like iron were observed in their blood (7-17%). Some indications were also found showing that this iron could be linked to their reticulocytes. Also, both *th3/+* mice and ThI patients have relatively low serum iron but exhibit major iron amounts in the organs. Unfortunately, the medical data of the patients that we had access to, were not adequate or detailed enough in order to perform strong observations and correlations. For example, even though we know that all patients are under iron-chelation therapy, details about the frequency or the dosage are unknown. The same can be assumed for the blood's amount used in the transfusions. Furthermore, thalassaemia intermedia, as explained in chapter 1, may occur with various phenotypes that make correlations much more complicated. A more throughout investigation with more data and larger sample population might be necessary in order to better study the clinical significance of the RBC ferritin in the β-

thalassaemia intermedia patients. *Table 5.4* shows the acquired medical/clinical data of the patients and the measured ferritin-like iron as a percentage of the total MS spectrum's area.

Beside the possible usage of erythrocyte ferritin as a bio-marker, it might also have further importance. Ferritin iron must be firstly released in order to be utilized by the cell for haem and iron-cluster biosynthesis in the mitochondria [75]. Iron enters the ferritin molecule in the ferrous Fe^{2+} state and then is oxidized by the ferroxidase activity of the H-chain, a process that consumes hydrogen peroxide H_2O_2 [76]. Hydrogen peroxide can also be produced during iron oxidization as seen in *Eq. 4.2*. The oxidized iron is then transported to the inner cavity of ferritin and is stored as a mineral core, aided by the nucleation process of the L-chain. Iron exit from ferritin involves the reduction of the mineralized Fe^{3+} iron with reducing molecules such as $O2^{\bullet-}$ and $NO^{\bullet}$ [76] which are damaging to cells. Therefore, RBC ferritin in high concentrations, as in the ThI patients, might be a significant source of ROS for the patients and might cause premature death to the RBCs or other cells.

Table 5.4: *Clinical and medical regarding the patients. acquired from their medical records. RBC Ferritn% was calculated from the spectra. The error shown was calculated from the ferritin doublet's area statistical error due to the fit.*

Sample	Genotype	Sex	Age	SFt (ng/m)	Average SFt (ng/ml)	Transfusion frequency	LIC	MIC	Chelation treatment	RBC Ferritin-like iron (%)
Th. Intermedia										
ThI-001	33/C39	F	39	819	1111	Every 2-6 Months	2	0	ExJade	**5±2**
ThI -002	IVS1/-92c>T	F	21	588	677	2-3 per year	2	0	L1	**9±1**
ThI -003	IVS1-110/-87	F	64	553	926	Every 2 Weeks	1	0	Desf+L1	**4±2**
ThI -004	IVS1-6/IVS1-1	F	60	852	804	Every 2 Months	2	0	Desf+L1	**20±2**
ThI -005	IVS1-110/IVS1-6	M	44	1469	996	Monthly	2	0	Desf+L1	**3±2**
ThI -006	IVS1-6/IVS1-1	M	64	541	579	Rarely	2	0	Desf	**12±2**
ThI -007	IVS1-110/IVS1-110	M	59	168	183	Weekly	1	0	Desf+L1	**5±2**
ThI -008	IVS1-6/IVS1-6	M	53	398	458	Rarely	2	0	ExJade	**0**
ThI -009	IVS1-110/-87	F	65	235	202	Rarely	1	0	Desf+L1	**0**
ThI -010	-87/C39	M	48	1667	1859	Every 1-2 Weeks	3	0	Desf+L1	**1±1**
ThI -011	IVS1-110/IVS1-6	M	55	1076	916	Every 2-3 Months	2	0	Desf+L1	**20±2**
Th. Major										
ThM-001	IVS1-110/IVS1-1	M	40	1247	1247	Every 2 Weeks	2	0	ExJade	**0**
ThM-002	IVS1-110/IVS1-110	F	51	1598	1665	Every 2-3 Weeks	2	0	Desf + L1	**1±1**
ThM-003	IVS1-110/IVS1-110	M	42	3006	3076	Weekly	2	0	ExJade	**0**
ThM-004	IVS1-110/IVS1-110	F	41	643	701	Every 2 Weeks	0	0	Desf+L1	**0**
ThM-005	IVS1-110/IVS2-745	F	39	1336	1433	Every 2 Weeks	1	0	Desf+L1	**5±3**
ThM-006	IVS1-110/IVS1-110	M	-	720	1061	Weekly	1	0	Desf+L1	**0**
ThM-007	IVS1-110/IVS1-110	M	46	2200	2490	Every 2-3 Weeks	2	0	Desf+L1	**0**
HbH		M	59	557	476	Monthly	0	0	Desferal	**0**

Conclusions & Future Work

β-thalassaemia is a form of inherited autosomal recessive blood disorder that can be caused by any one of more than 200 mutations in the β-globin gene and is characterized by reduced or absent of β-globin chain synthesis. This anomaly prevents the production of normal levels of adult haemoglobin (HbA) which in turn limits the effective production of Red Blood Cells (RBCs) leading to mild or severe anaemia. β-thalassaemia, affects multiple organs and is associated with considerable morbidity and mortality. Accordingly, lifelong care is necessary. In individuals with moderate to severe anaemia, regular blood transfusion therapy is required to maintain haemoglobin in healthy levels which allows for improved growth and development and also reduces hepatosplenomegaly and bone deformities. Iron chelation is also a vital component of the treatment regime of thalassemia patients. Currently, iron overload causes most of the mortality and morbidity associated with thalassaemia. Both transfusional iron overload and excess gastrointestinal absorption are contributory. Iron deposition occurs in visceral organs (mainly in the heart, liver, and endocrine glands), causing tissue damage and ultimately organ dysfunction and failure. Cardiac events due to iron overload are still the primary cause of death. Accurate, preferably noninvasive, measurement of iron stores is crucial for the evaluation and management of chelation therapy. Serum ferritin which is most commonly measured as an indicator of iron stores, is highly unreliable, particularly when liver disease is present.

Mössbauer Spectroscopy is a versatile technique used to study the environment of a nucleus, with the absorption and re-emission of gamma rays. The technique uses a combination of the Mössbauer effect and the Doppler shifts to probe the hyperfine transitions between the excited and the ground states of the nucleus. The sensitivity of Mössbauer spectroscopy to subtle

changes in the chemical environment of the iron nucleus, makes it capable to detect and fingerprint different states of iron.

In this work, iron studies where performed utilizing Mössbauer spectroscopy on samples from thalassaemic subjects and more specifically, from a thalassaemic mouse model and from β-thalassaemia patients.

The mouse is a genetically and physiologically well characterized organism which has close genetic and physiological similarities to humans. Due to the similarities, mice develop various diseases common to humans, but they can also be manipulated to develop diseases non-natural to them, like thalassaemia. Even though mice are widely used in biomedical research for over a century, they were rarely used with MS due to major difficulties having to do with their small size and available sample amounts. Thus, the existing literature is very limited. Moreover, no thalassaemic animal model was ever used with Mössbauer spectroscopy in order to study the disease and its resulting iron depositions. Therefore, this is for the first time that thalassaemia has been studied with MS using laboratory animals.

The β-thalassaemia mouse model used in this study has both the *b1* and *b2* adult mouse globin genes deleted. Because homozygous mice die perinatally, mice heterozygous for this deletion were bred on *C57BL/6* background and were used for the purposes of this study. Heterozygous *(th3/+)* mice appear normal but they show haematologic indices characteristic of severe thalassaemia, exhibit tissue and organ damage typical of the disease, and develop spontaneous iron overload in the spleen, liver, and kidneys. Iron deposits appear very early and therefore they are suitable candidates to study iron accumulation in the organs.

Initially, in order to evaluate the usefulness of the mice in relation to MS and to optimize the experimental setup for usage with samples with minimal iron concentration and volume, Mössbauer spectra of blood, liver and spleen samples from a *wild-type (C57BL/6)* and a thalassaemic *th3/+* mouse were acquired at 78K. The MS spectrum of the *wild-type* blood sample was well-fitted with two sub-doublets of the same area, representing the α- and β-subunits of oxy-haemoglobin. The blood sample of the thalassaemic mouse showed reduced absorption in its spectrum which made any detailed fitting impossible. The reduced absorption reflects the decreased haemoglobin levels which is a result of the severe anaemia that the *th3/+* mice and the untreated thalassaemia patients suffer from. The spectra from the liver and spleen samples showed, as expected, the existence of ferritin-like iron. Compared to the normal ones, the spectra from the two organs of the thalassaemic mouse showed increased absorption, which reflects the increased iron depositions in them. Similar to the non-transfused

thalassaemia patients, the *th3/+* mouse presented iron overload because of increased gastrointestinal absorption.

The Mössbauer fitting parameters obtained from the samples of these two mice, were in a good agreement with those existing in the literature for the specific iron complexes. As obtained from this preliminary results, *wild-type* and thalassaemia *th3/+* mice exhibit similar iron complexes to humans, both in their blood and organs. In this sense, the thalassaemic mouse model was found to be a promising candidate to study thalassaemia with MS despite all the initial difficulties.

Following the preliminary study, mice were enriched with ^{57}Fe through the continuous consumption of custom prepared ^{57}Fe enriched diet in order to increase the spectra quality. Two mice at 1 month of age, an enriched and a non-enriched one, where used to evaluate the enrichment method by studying blood, liver and spleen samples, with the results showing increased absorption and significantly enchased spectra quality. For the main study, *wild-type* (control) and thalassaemic *th3/+* mice were raised and enriched, and MS spectra from blood, liver, spleen, heart and kidney samples at 1, 3, 6 and 9 months of age were acquired at 80K. The brains of the 9-month old mice were also studied.

From the following analysis, it was found that thalassaemic mice, showed significant amounts (6-14%) of ferritin-like iron in their blood, in contrast to the *wild-type* ones where no such component was found. Using data from the literature, it was concluded that the observed ferritin-like iron should exist in the RBCs, and more specifically in the reticulocytes. From the analysis of the spectra acquired from the organs, increased amounts of non-haem-high-spin *(NHHS) Fe(II*) iron were found in the brain, kidneys and liver of the *th3/+* mice. Furthermore, significant amounts were found in the spleen of adult *th3/+* mice only and could be related to phenomena associated with erythropoiesis and erythrophagocytosis. *NHHS Fe(II)* complexes can have labile ligands that undergo Fenton chemistry and produce reactive oxygen species which are toxic and can cause extensive cellular damage.

Iron depositions in the heart and brain of the *th3/+* mice were found to be slightly increased (10%) while significant amounts of ferritin-like iron were found in the kidneys, liver and spleen. The renal tissues of the *th3/+* mice were found to have ~16 times more ferritin-like iron than the control equivalents and the *th3/+* livers ~10 times.

The ferritin-like iron's doublet found in the organs, could be further separated into two sub-doublets representing the inner and surface structure of ferritins mineral core. Surface iron sites were found to be predominant in the hearts and brains of all mice, and in the kidneys of

the *wild-type* ones. Inner iron sites were predominant in the livers and spleen, and in the kidneys of the thalassaemic mice. This pattern is similar with the expected one from the *H-* and *L*-chains of ferritin. Furthermore, thalassaemic tissues seem to promote the creation of ferritin rich in inner iron sites as the ratio of inner-to-surface type was found to increase in all thalassaemic samples. This is probably due to the body's effort to store excess amounts of iron in a long-term storage form. Haemosiderin, an iron storage complex that is found in the spleen of thalassaemia and iron overloaded patients, was also observed in the spleen of mice at 6 and 9 months of age. This indicates that these mice suffered from advanced iron-overload conditions.

In the second part of this doctoral thesis, RBC samples from seven (7) healthy volunteers, eleven (11) samples from β-thalassaemia intermedia patients (ThI), seven (7) samples from β-thalassaemia major (ThM) patients, and one (1) sample from a patient with H-disease, were studied with MS, and the results were compared with data extracted from their medical records. From the data taken from the patients' medical records, it was found that on an average, β-thalassaemia patients had almost half the serum ferritin levels (761 ng/ml) than the β-thalassaemia major patients (1536 ng/ml). However, despite their lower serum ferritin levels, ThI patients had higher liver iron concentration *(LIC)*. 73% of ThI patients had mild or moderate haemosiderosis in their liver while the equivalent portion for the ThM patients was 57%. This shows that iron chelation therapy might be not as effective in the ThI patients as in the ThM ones, probably because serum ferritin might be an unreliable marker in the ThI patients and therefore the physicians might underestimate iron overload. As a result of this, ThI patients eventually develop increased iron depositions in their hepatic tissues.

The MS spectra of the RBC samples showed the existence of significant amounts of ferritin-like iron, mainly in the samples from the ThI patients, where 82% of them showed this iron complex. In contrast to the ThM patients that are fully dependant on blood transfusions for RBCs, ThI patients can produce some numbers by their own. Therefore, it is possible, that the observed ferritin-like iron is found in their own RBCs or reticulocytes. This is supported by the results from the thalassaemic mice.

Furthermore, this ferritin-like iron might be the result, or even the cause of the un-explainable high liver iron concentrations (in relation to the serum ferritin levels) in the ThI patients. Hence, RBC (or reticulocyte) ferritin might be a useful bio-marker to assess and manage iron overload in β-thalassaemia intermedia patients. This can increase the iron chelation treatment effectiveness and subsequently decrease the morbidity associated with iron overload, improving their health and life quality.

5.6 Future Work

Mice:

From the results of this work we have showed that ^{57}Fe enriched mice can be used with great success and can be very useful in studying iron depositions in the organs using Mössbauer Spectroscopy. This enrichment method can be further applied not only to thalassaemia disease but also to other iron related diseases using different mouse models.

The enriched samples showed ferritin-like iron in the blood, *NHHS Fe(II)*, two types of ferritin-like iron and haemosiderin in various organs. In a future work, thalassaemic mice can be introduce to different iron-chelation agents in order to study their interaction with these iron complexes and evaluate their effectiveness in removing these types of iron from specific organs.

A similar but complementary work to the presented one can also be done using mice enriched by blood transfusions instead through gastrointestinal absorption. This is the major mechanism that thalassaemia major patients (and patients suffering from other types of anaemia) obtain excess iron and develop iron overload. This method of iron acquisition is very different than the one studied here, thus it might affect the organs in completely different way.

Finally, this work showed some signs that thalassaemic mice might have increased iron amounts in their brains. A more thorough work on this is needed, as brain iron might be correlated with neurodegenerative diseases like Alzheimer, Parkinson and Neurodegeneration with Brain Iron Accumulation (NBIA) [65,66]. If this is the case, as life expectancy of thalassaemic patients increases, these diseases might affect them in the future. Hence, it is necessary to address this possibility in advance in order to prevent or minimize unnecessary complications and health risks.

Patients:

A significant number of β-thalassaemia intermedia patients showed ferritin-like iron in their RBC samples, in contrast to the thalassaemia major patients. Unfortunately, from the given medical data, this could not be explained. Therefore, as a future work it is important to investigate the RBC ferritin of the β-thalassaemia intermedia patients in more detail, as it might be linked to their elevated liver iron concentrations. If a correlation can be proven, RBC ferritin can be used as a supplementary biomarker for assessing iron overload and thus, iron chelation therapy can become more effective and efficient, reducing the associated morbidity.

Published work from this PhD thesis

I. Charitou, G., Petousis, V., Tsertos, C., Parpottas, Y., Kleanthous, M., Phylactides, M. et al. (2018) First study on iron complexes in blood and organ samples from thalassaemic and normal laboratory mice using Mössbauer spectroscopy. European Biophysics Journal, 47, 131–8. https://doi.org/10.1007/s00249-017-1234-6

Abstract: Measurements of iron complexes and iron stores in the body are crucial for evaluation and management of chelation therapy targeted against iron accumulation or overload in blood and organs. In this work, blood and tissue samples from one normal and one thalassaemic laboratory mouse were studied using 57Fe Mössbauer spectroscopy at 78 K for the first time. In contrast to human patients, these laboratory mice did not receive any medical treatment, thus the iron components present in the samples are not altered from their natural state. The Mössbauer spectra of blood, liver and spleen samples of the thalassaemic mouse were found to differ in shape and iron content compared with corresponding spectra of the normal mouse. These results demonstrate a basis for further exploitation of the thalassaemic mouse model to study thalassaemia and its treatment in more detail using Mössbauer spectroscopy.

II. Charitou, G., Tsertos, C., Parpottas, Y., Kleanthous, M., Lederer, C. and Phylactides, M. (2019) ^{57}Fe enrichment in mice for beta-thalassaemia studies via Mossbauer spectroscopy of blood samples. https://arxiv.org/abs/1903.01245 **(Submitted)**

Abstract: In this work, *wild-type* and heterozygous beta-thalassaemic mice were enriched with ^{57}Fe through gastrointestinal absorption to characterize in more details the iron complexes appeared in the measured Mossbauer spectra. The ^{57}Fe enrichment method was validated and Mossbauer spectra were obtained at 80K from blood samples from *wild-type* and beta-thalassaemic mice at 1, 3, 6, and 9 months of age. As expected, the haemoglobin levels of the thalassaemic mice were lower than from normal mice indicating anaemia. Furthermore, significant amounts of ferritin-like iron were observed in the thalassaemic mice samples, which decreased with mouse age, reflecting the pattern of reticulocyte count reduction reported in the literature.

III & IV. Two more papers are prepared and will be submitted for publication soon. The first one covers the results from the ^{57}Fe enriched organs, and the second one covers the results obtained from the thalassaemia patients.

References

[1] Crichton, R.R. and Boelaert, J.R. (2001) Inorganic biochemistry of iron metabolism: from molecular mechanisms to clinical consequences. 2nd ed. Wiley, Chichester ; New York. (ISBN 978-0-471-49223-8)

[2] Abbaspour, N., Hurrell, R. and Kelishadi, R. (2014) Review on iron and its importance for human health. *Journal of Research in Medical Sciences*, 11.

[3] Zhang, D.-L., Ghosh, M.C. and Rouault, T.A. (2014) The physiological functions of iron regulatory proteins in iron homeostasis - an update. *Frontiers in Pharmacology*, **5**. https://doi.org/10.3389/fphar.2014.00124

[4] Eleftheriou, A. (2003) About thalassaemia. Thalassaemia International Federation Publications, Cyprus. (ISBN 978-9963-623-40-2)

[5] Ganz, T. (2013) Systemic Iron Homeostasis. *Physiological Reviews*, **93**, 1721–41. https://doi.org/10.1152/physrev.00008.2013

[6] Winter, W.E., Bazydlo, L.A.L. and Harris, N.S. (2014) The Molecular Biology of Human Iron Metabolism. *Laboratory Medicine*, **45**, 92–102. https://doi.org/10.1309/LMF28S2GIMXNWHMM

[7] Lopez, A., Cacoub, P., Macdougall, I.C. and Peyrin-Biroulet, L. (2016) Iron deficiency anaemia. *The Lancet*, **387**, 907–16. https://doi.org/10.1016/S0140-6736(15)60865-0

[8] Himmelfarb, J. (2007) Iron Regulation. *Journal of the American Society of Nephrology*, **18**, 379–81. https://doi.org/10.1681/ASN.2006101097

[9] McCord, J.M. (2004) Iron, Free Radicals, and Oxidative Injury. *The Journal of Nutrition*, **134**, 3171S-3172S. https://doi.org/10.1093/jn/134.11.3171S

[10] Gozzelino, R. and Arosio, P. (2016) Iron Homeostasis in Health and Disease. *International Journal of Molecular Sciences*, **17**, 130. https://doi.org/10.3390/ijms17010130

[11] Kohgo, Y., Ikuta, K., Ohtake, T., Torimoto, Y. and Kato, J. (2008) Body iron metabolism and pathophysiology of iron overload. *International Journal of Hematology*, **88**, 7–15. https://doi.org/10.1007/s12185-008-0120-5

[12] Ponka, P., Koury, M.J. and Sheftel, A.D. (2013) Erythropoiesis, Hemoglobin Synthesis, and Erythroid Mitochondrial Iron Homeostasis. *Handbook of Porphyrin Science*, World Scientific Publishing Company. p. 41–84. (ISBN 978-981-4407-78-6) https://doi.org/10.1142/9789814407755_0011

[13] Bunn, H.F. (2013) Erythropoietin. *Cold Spring Harbor Perspectives in Medicine*, **3**, a011619–a011619. https://doi.org/10.1101/cshperspect.a011619

[14] Hoffbrand, A.V., Higgs, D.R., Keeling, D. and Mehta, A.B., editors. (2016) Postgraduate haematology. Seventh edition. John Wiley and Sons, Inc, Chichester, West Sussex ; Hoboken, NJ. (ISBN 978-1-118-85432-7)

[15] Politis, C. (2013) Haemoglobinopathies: genetic and clinical aspects with an impact on blood transfusion. *ISBT Science Series*, **8**, 229–32. https://doi.org/10.1111/voxs.12055

[16] Schechter, A.N. (2008) Hemoglobin research and the origins of molecular medicine. *Blood*, **112**, 3927–38. https://doi.org/10.1182/blood-2008-04-078188

[17] Knovich, M.A., Storey, J.A., Coffman, L.G., Torti, S.V. and Torti, F.M. (2009) Ferritin for the clinician. *Blood Reviews*, **23**, 95–104. https://doi.org/10.1016/j.blre.2008.08.001

[18] Harrison, P.M. and Arosio, P. (1996) The ferritins: molecular properties, iron storage function and cellular regulation. *Biochimica et Biophysica Acta (BBA) - Bioenergetics*, **1275**, 161–203. https://doi.org/10.1016/0005-2728(96)00022-9

[19] Kalantar-Zadeh, K. (2006) The Fascinating but Deceptive Ferritin: To Measure It or Not to Measure It in Chronic Kidney Disease? *Clinical Journal of the American Society of Nephrology*, **1**, S9–18. https://doi.org/10.2215/CJN.01390406

[20] Cappellini, M., Cohen, A., Porter, J., Taher, A. and Viprakasit, V., editors. (2014) Guidelines for the management of transfusion dependent thalassaemia (TDT). Thalassaemia International Federation Publications, Nicosia, Cyprus. (ISBN 978-9963-717-06-4)

[21] Patel, M. and Ramavataram, D.V.S.S. (2012) Non Transferrin Bound Iron: Nature, Manifestations and Analytical Approaches for Estimation. *Indian Journal of Clinical Biochemistry*, **27**, 322–32. https://doi.org/10.1007/s12291-012-0250-7

[22] Galanello, R. and Origa, R. (2010) Beta-thalassemia. *Orphanet Journal of Rare Diseases*, **5**, 11. https://doi.org/10.1186/1750-1172-5-11

[23] Moon, P. (1951) Resonant Nuclear Scattering of Gamma-Rays: Theory and Preliminary Experiments. *Proceedings of the Physical Society*, **64**, 76–82. https://doi.org/10.1088/0370-1298/64/1/311

[24] Gütlich, P., Bill, E. and Trautwein, A. (2011) Mössbauer spectroscopy and transition metal chemistry: fundamentals and application. Springer, Berlin ; Heidelberg. (ISBN 978-3-540-88427-9)

[25] Mössbauer, R.L. (1959) . *Naturforsch*, **14a**, 211.

[26] Mössbauer, R.L. (1958) . *Naturwiss*, **45**, 538.

[27] Frauenfelder, H. (1962) Mössbauer effect.

[28] Vij, D.R., editor. (2006) Handbook of applied solid state spectroscopy. Springer, New York. (ISBN 978-0-387-32497-5)

[29] Fultz, B. (2012) Mössbauer Spectrometry. In: Kaufmann EN, editor. *Characterization of Materials*, John Wiley & Sons, Inc., Hoboken, NJ, USA. (ISBN 978-0-471-26696-9) https://doi.org/10.1002/0471266965.com069.pub2

[30] Chen, Y.-L. and Yang, D.-P. (2007) Mössbauer Effect in Lattice Dynamics http://doi.wiley.com/10.1002/9783527611423. Wiley-VCH Verlag GmbH & Co. KGaA, Weinheim, Germany. (ISBN 978-3-527-61142-3) https://doi.org/10.1002/9783527611423

[31] Bé, M.-M. (2004) Table of radionuclides. Vol. 1: A=1 to 150. BIPM, Sèvres. (ISBN 978-92-822-2206-5)

[32] ICEoxford. 4IceBath System - Operator's Handbook.

[33] Maddock, A.G. (1997) Mössbauer spectroscopy: principles and applications. Horwood, Chichester. (ISBN 978-1-898563-16-7)

[34] Douvalis, A.P., Polymeros, A. and Bakas, T. (2010) IMSG09: A ^{57}Fe-^{119}Sn Mössbauer spectra computer fitting program with novel interactive user interface. *Journal of Physics: Conference Series*, **217**, 012014. https://doi.org/10.1088/1742-6596/217/1/012014

[35] WissEl. WinNormos-for-Igor Software Package http://www.wissel-gmbh.de/index.php?option=com_content&task=view&id=55&Itemid=116.

[36] YANG, B., KIRBY, S., LEWISt, J., DETLOFF, P.J., MAEDA, N. and SMITHIES, O. (1995) A mouse model for 10-thalassemia. *Proc Natl Acad Sci USA*, 5.

[37] Gardenghi, S., Marongiu, M.F., Ramos, P., Guy, E., Breda, L., Chadburn, A. et al. (2007) Ineffective erythropoiesis in -thalassemia is characterized by increased iron absorption mediated by down-regulation of hepcidin and up-regulation of ferroportin. *Blood*, **109**, 5027–35. https://doi.org/10.1182/blood-2006-09-048868

[38] Holmes-Hampton, G.P., Chakrabarti, M., Cockrell, A.L., McCormick, S.P., Abbott, L.C., Lindahl, L.S. et al. (2012) Changing iron content of the mouse brain during development. *Metallomics*, **4**, 761. https://doi.org/10.1039/c2mt20086d

[39] Chakrabarti, M., Cockrell, A.L., Park, J., McCormick, S.P., Lindahl, L.S. and Lindahl, P.A. (2015) Speciation of iron in mouse liver during development, iron deficiency, IRP2 deletion and inflammatory hepatitis. *Metallomics*, **7**, 93–101. https://doi.org/10.1039/C4MT00215F

[40] Wofford, J.D., Chakrabarti, M. and Lindahl, P.A. (2017) Mössbauer Spectra of Mouse Hearts Reveal Age-dependent Changes in Mitochondrial and Ferritin Iron Levels. *Journal of Biological Chemistry*, **292**, 5546–54. https://doi.org/10.1074/jbc.M117.777201

[41] Gabbasov, R.R., Cherepanov, V.M., Chuev, M.A., Polikarpov, M.A., Nikitin, M.P., Deyev, S.M. et al. (2012) Study of Nature of Paramagnetic Doublet in Mössbauer Spectra of Mice Liver Using External Magnetic Field. *Solid State Phenomena*, **190**, 729–32. https://doi.org/10.4028/www.scientific.net/SSP.190.729

[42] Chuev, M., Cherepanov, V., Nikitin, M.P. and Polikarpov, M. (2012) Biodegradation of Nanoparticles in a Body from Mössbauer and Magnetization Measurements. *Solid State Phenomena*, **190**, 725–8. https://doi.org/10.4028/www.scientific.net/SSP.190.725

[43] Jackson Laboratory. (2007) Physiological Data Summary – C57BL/6J (000664) http://jackson.jax.org/rs/444-BUH-304/images/physiological_data_000664.pdf. The Jackson Laboratory.

[44] Oshtrakh, M.I. (1998) The Features of Mössbauer Spectra of Hemoglobin in Relation to the Quadrupole Splitting and Heme Iron Stereochemistry. *Zeitschrift Für Naturforschung A*, **53**. https://doi.org/10.1515/zna-1998-6-755

[45] Chua-anusorn, W., Webb, J., Macey, D.J. and Pierre, T.G.S. The effect of prolonged iron loading on the chemical form of iron oxide deposits in rat liver and spleen. *Biochimica et Biophysica Acta*, 10.

[46] Chua-anusorn, W., Pierre, T.G.St., Webb, J., Macey, D.J., Yansukon, P. and Pootrakul, P. (1994) Mössbauer spectroscopic study of the forms of iron in normal human liver and spleen tissue. *Hyperfine Interactions*, **91**, 905–10. https://doi.org/10.1007/bf02064626

[47] Bauminger, E.R., Cohen, S.G., Ofer, S. and Rachmilewitz, E.A. (1979) Quantitative studies of ferritinlike iron in erythrocytes of thalassemia, sickle-cell anemia, and hemoglobin Hammersmith with Mossbauer spectroscopy. *Proceedings of the National Academy of Sciences*, **76**, 939–43. https://doi.org/10.1073/pnas.76.2.939

[48] de Laeter, J.R., Böhlke, J.K., De Bièvre, P., Hidaka, H., Peiser, H.S., Rosman, K.J.R. et al. (2003) Atomic weights of the elements. Review 2000 (IUPAC Technical Report). *Pure and Applied Chemistry*, **75**, 683–800. https://doi.org/10.1351/pac200375060683

[49] National Research Council. (1995) Nutrient Requirements of Laboratory Animals,: Fourth Revised Edition, 1995. National Academies Press, Washington, D.C. (ISBN 978-0-309-05126-2) https://doi.org/10.17226/4758

[50] Hoy, G.R., Cook, D.C., Berger, R.L. and Friedman, F.K. (1986) Mössbauer spectroscopic studies of hemoglobin and its isolated subunits. *Biophysical Journal*, **49**, 1009–15. https://doi.org/10.1016/S0006-3495(86)83729-8

[51] Oshtrakh, M.I. and Semionkin, V.A. (1986) Mössbauer spectroscopy of haemoglobins: Study of the relationship of Fe^{2+} electronic and molecular structure of the active site. *FEBS Letters*, **208**, 331–6. https://doi.org/10.1016/0014-5793(86)81044-4

[52] Oshtrakh, M.I., Berkovsky, A.L., Kumar, A., Kundu, S., Vinogradov, A.V., Konstantinova, T.S. et al. (2010) 57Fe quadrupole splitting and isomer shift in various oxyhemoglobins: study using Mössbauer spectroscopy. *Hyperfine Interactions*, **197**, 301–7. https://doi.org/10.1007/s10751-010-0232-1

[53] Oshtrakh, M.I., Alenkina, I.V., Milder, O.B. and Semionkin, V.A. (2011) Mössbauer spectroscopy with a high velocity resolution in the study of iron-containing proteins and model compounds. *Spectrochimica Acta Part A: Molecular and Biomolecular Spectroscopy*, **79**, 777–83. https://doi.org/10.1016/j.saa.2010.08.052

[54] Kaufman, K.S., Papaefthymiou, G.C., Frankel, R.B. and Rosenthal, A. (1980) Nature of iron deposits on the cardiac walls in β-thalassemia by Mössbauer spectroscopy. *Biochimica et Biophysica Acta (BBA) - General Subjects*, **629**, 522–9. https://doi.org/10.1016/0304-4165(80)90157-9

[55] Jiang, K., Ma, W.Y., Ortalli, I., Pedrazzi, G., Zhang, X. and Izzi, G.C. (1994) Some comments on the effectiveness of the therapy for B-thalassemia. *Hyperfine Interactions*, **91**, 859–63. https://doi.org/10.1007/BF02064619

[56] Chua-anusorn, W., Webb, J., Macey, D.J., de la Motte Hall, P. and St. Pierre, T.G. (1999) The effect of prolonged iron loading on the chemical form of iron oxide deposits in rat liver and spleen. *Biochimica et Biophysica Acta (BBA) - Molecular Basis of Disease*, **1454**, 191–200. https://doi.org/10.1016/S0925-4439(99)00036-8

[57] Charitou, G., Petousis, V., Tsertos, C., Parpottas, Y., Kleanthous, M., Phylactides, M. et al. (2018) First study on iron complexes in blood and organ samples from thalassaemic and normal laboratory mice using Mössbauer spectroscopy. *European Biophysics Journal*, **47**, 131–8. https://doi.org/10.1007/s00249-017-1234-6

[58] Darshan, D., Vanoaica, L., Richman, L., Beermann, F. and Kühn, L.C. (2009) Conditional deletion of ferritin H in mice induces loss of iron storage and liver damage. *Hepatology*, **50**, 852–60. https://doi.org/10.1002/hep.23058

[59] Bou-Abdallah, F., Carney, E., Chasteen, N.D., Arosio, P., Viescas, A.J. and Papaefthymiou, G.C. (2007) A comparative Mössbauer study of the mineral cores of human H-chain ferritin employing dioxygen and hydrogen peroxide as iron oxidants. *Biophysical Chemistry*, **130**, 114–21. https://doi.org/10.1016/j.bpc.2007.08.003

[60] Hackett, S., Chua-anusorn, W., Pootrakul, P. and St Pierre, T.G. (2007) The magnetic susceptibilities of iron deposits in thalassaemic spleen tissue. *Biochimica et Biophysica Acta (BBA) - Molecular Basis of Disease*, **1772**, 330–7. https://doi.org/10.1016/j.bbadis.2006.12.007

[61] Bell, S.H., Weir, M.P., Dickson, D.P.E., Gibson, J.F., Sharp, G.A. and Peters, T.J. (1984) Mössbauer spectroscopic studies of human haemosiderin and ferritin. *Biochimica et Biophysica Acta (BBA) - Protein Structure and Molecular Enzymology*, **787**, 227–36. https://doi.org/10.1016/0167-4838(84)90313-3

[62] Semin, B.K., Novakova, A.A., Aleksandrov, A.Yu., Ivanov, I.I., Rubin, A.B. and Kuzmin, R.N. (1982) Mössbauer spectroscopy of iron metabolism and iron intracellular distribution in liver of rats. *Biochimica et Biophysica Acta (BBA) - General Subjects*, **715**, 52–6. https://doi.org/10.1016/0304-4165(82)90048-4

[63] Rimbert, J.N., Dumas, F., Kellershohn, C., Girot, R. and Brissot, P. (1985) Mössbauer spectroscopy study of iron overloaded livers. *Biochimie*, **67**, 663–8. https://doi.org/10.1016/S0300-9084(85)80209-1

[64] Cairo, G., Rappocciolo, E., Tacchini, L. and Schiaffonati, L. (1991) Expression of the genes for the ferritin H and L subunits in rat liver and heart. Evidence for tissue-specific regulations at pre- and post-translational levels. *Biochemical Journal*, **275**, 813–6. https://doi.org/10.1042/bj2750813

[65] Sadrzadeh, S.M.H. and Saffari, Y. (2004) Iron and Brain Disorders. *Pathology Patterns Reviews*, **121**, S64–70. https://doi.org/10.1309/EW0121LG9N3N1YL4

[66] Bartzokis, G., Tishler, T.A., Shin, I.-S., Lu, P.H. and Cummings, J.L. (2004) Brain Ferritin Iron as a Risk Factor for Age at Onset in Neurodegenerative Diseases. *Annals of the New York Academy of Sciences*, **1012**, 224–36. https://doi.org/10.1196/annals.1306.019

[67] Bauminger, E.R., Cohen, S.G., Ofer, S. and Rachmilewitz, E.A. (1979) Mössbauer studies of ferritin-like iron in red blood cells of thalassemia sickle-cell anemia and hemoglobin Hammersmith. *Le Journal de Physique Colloques*, **40**, C2-502-C2-504. https://doi.org/10.1051/jphyscol:19792176

[68] Xuanhui, G., Nanming, Z., Xiufang, Z., Naifei, G., Youwen, H. and Rongxin, W. (1988) Study on Mössbauer spectra of hemoglobin in thalassemia. *Hyperfine Interactions*, **42**, 897–900. https://doi.org/10.1007/BF02395534

[69] Marshall, D., Kales, N., Christiani, D.C. and Goldman, R.H. Are Reference Intervals for Carboxyhemoglobin Appropriate? A Survey of Boston Area Laboratories. 5.

[70] Origa, R., Galanello, R., Ganz, T., Giagu, N., Maccioni, L., Faa, G. et al. (2007) Liver iron concentrations and urinary hepcidin in -thalassemia. *Haematologica*, **92**, 583–8. https://doi.org/10.3324/haematol.10842

[71] Taher, A., El Rassi, F., Isma'eel, H., Koussa, S., Inati, A. and Cappellini, M.D. (2008) Correlation of liver iron concentration determined by R2 magnetic resonance imaging with serum ferritin in patients with thalassemia intermedia. *Haematologica*, **93**, 1584–6. https://doi.org/10.3324/haematol.13098

[72] Piperno, A., Taddei, M.T., Sampietro, M., Fargion, S., Arosio, P. and Fiorelli, G. (1984) Erythrocyte Ferritin in Thalassemia Syndromes. *Acta Haematologica*, **71**, 251–6. https://doi.org/10.1159/000206596

[73] Bennett, P. and Williamson, C., editors. (2010) Basic science in obstetrics and gynaecology: a textbook for MRCOG Part I. 4th ed. Churchill Livingstone, Edinburgh ; New York. (ISBN 978-0-443-10281-3)

[74] Konijn, A.M., Hershko, C. and Izak, G. (1979) Ferritin synthesis and Iron uptake in developing erythroid cells. *American Journal of Hematology*, **6**, 373–9. https://doi.org/10.1002/ajh.2830060409

[75] Kafina, M.D. and Paw, B.H. (2017) Intracellular iron and heme trafficking and metabolism in developing erythroblasts. *Metallomics*, **9**, 1193–203. https://doi.org/10.1039/C7MT00103G

[76] Bresgen, N. and Eckl, P. (2015) Oxidative Stress and the Homeodynamics of Iron Metabolism. *Biomolecules*, **5**, 808–47. https://doi.org/10.3390/biom5020808

Appendix I:

The output file of the WinNormos software which was used for the analysis of the Mössbauer spectra, normalizes the scale of the absorption (y) axis of the spectrum to the background counts $\bar{N}$ (average counts of the points at the extrema of the spectra where no absorption occurs, after spectra folding). Thus, the y- axis is given in units of relative transmission; the value at the extrema of the spectrum is 1 and the y-value of each point decreases, corresponding to the measured counts.

The statistical error of each point in not given by the software, and it was calculated by:

$$Error = Rel.Transmission \times \frac{1}{\sqrt{\bar{N}}} \quad \text{(I.1)}$$

Because the counts of each channel after the folding procedure is not given by the software, $\bar{N}$ was used for the error estimation. Due to the relatively small absorption, $\bar{N}$ represents well the value of each point, even at the resonances. $\bar{N}$ is calculated and given by the software.

To transform the y- axis in order to represent percentage absorption (%), the following formula was used:

$$Absorption(\%) = (1 - Rel.Transmission) \times 100 \quad \text{(I.2)}$$

and the error of each point after the transformation:

$$Error_{Absorption}(\%) = Rel.Transmission \times \frac{1}{\sqrt{N}} \times 100 \quad \text{(I.3)}$$

Appendix II:
Supplementary Mössbauer Spectra

(This page intentionally left blank)

MS spectra for chapter 4 (mice):

Blood spectra

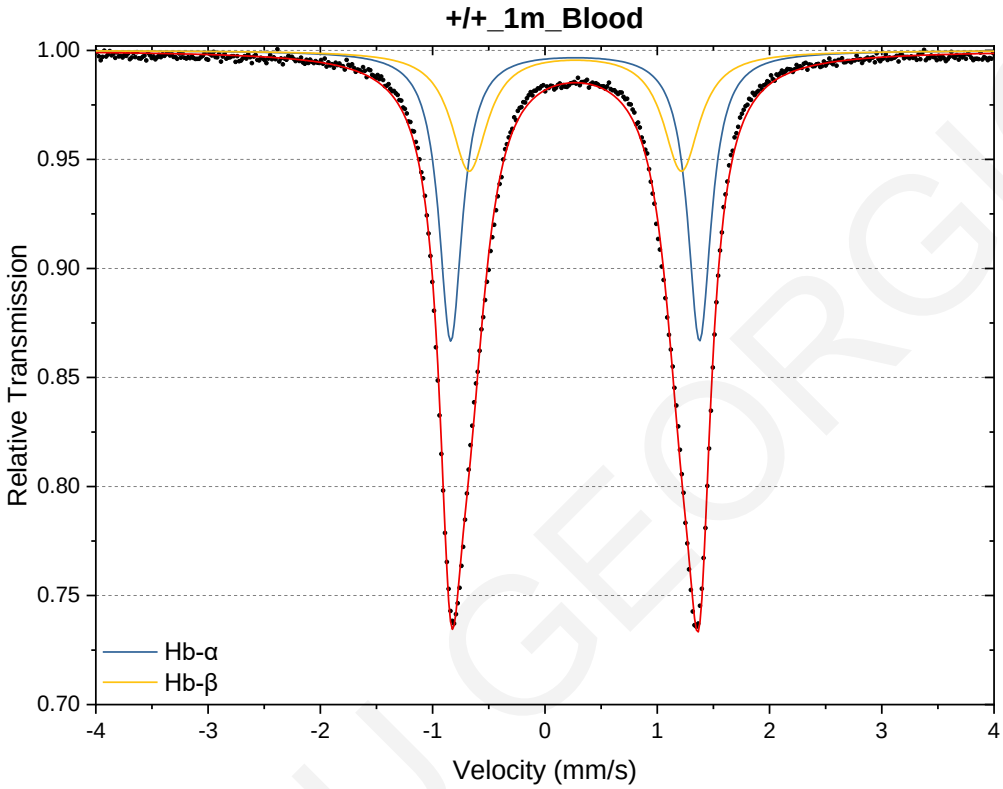

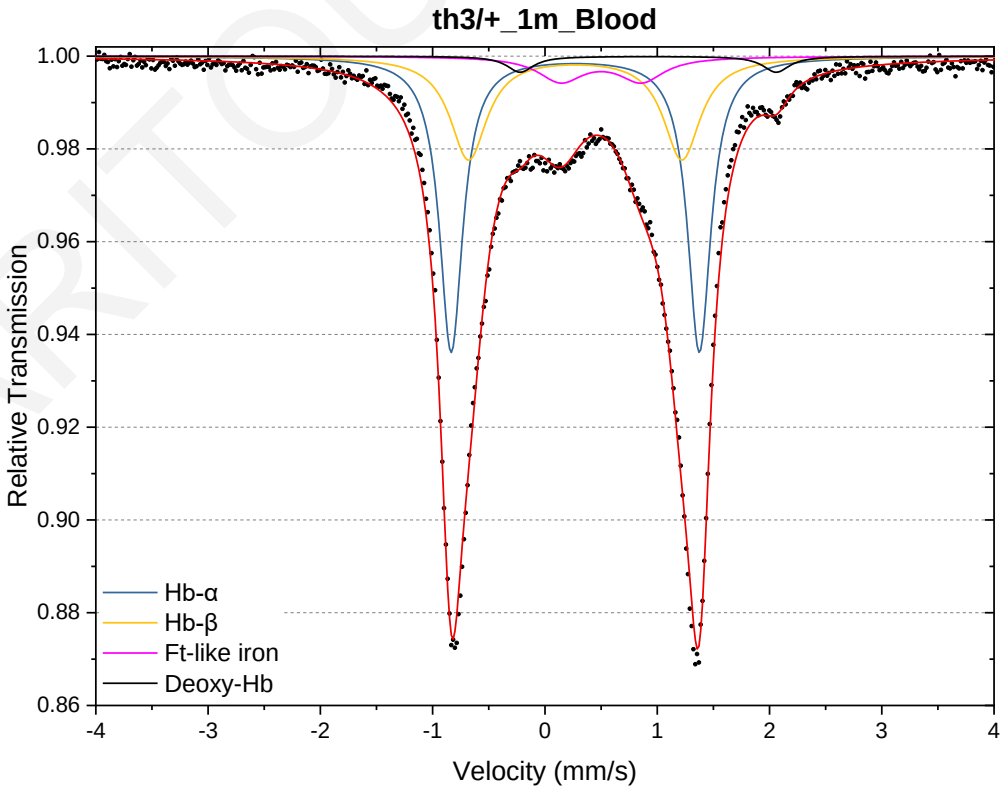

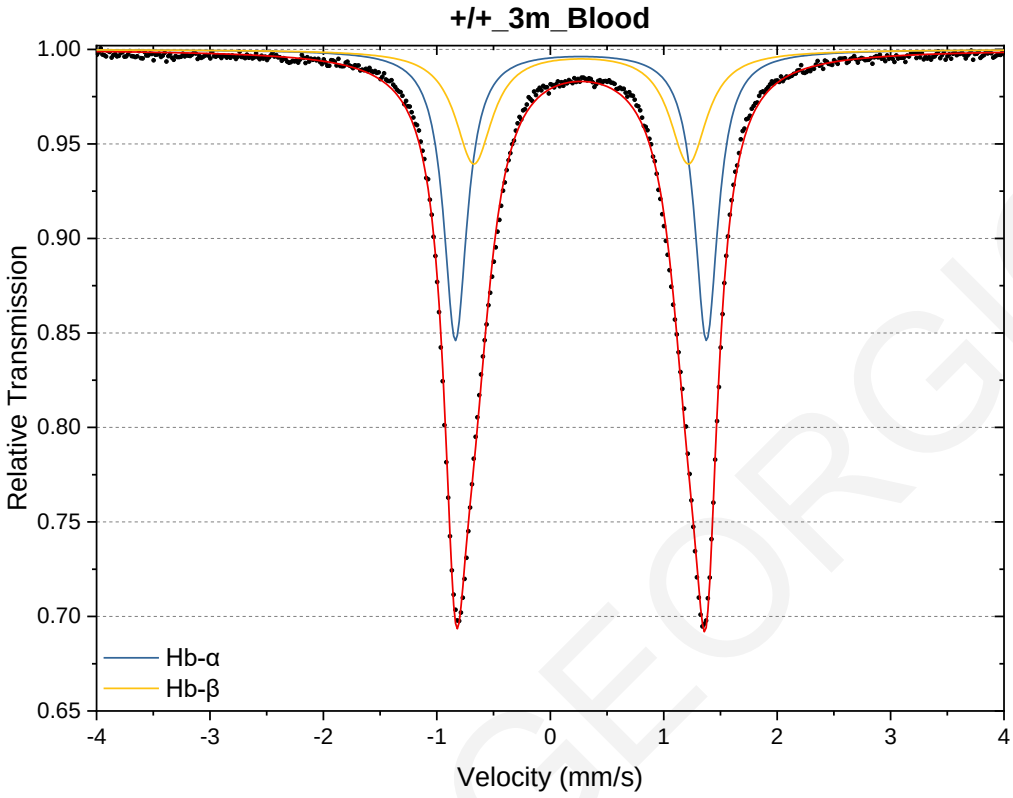

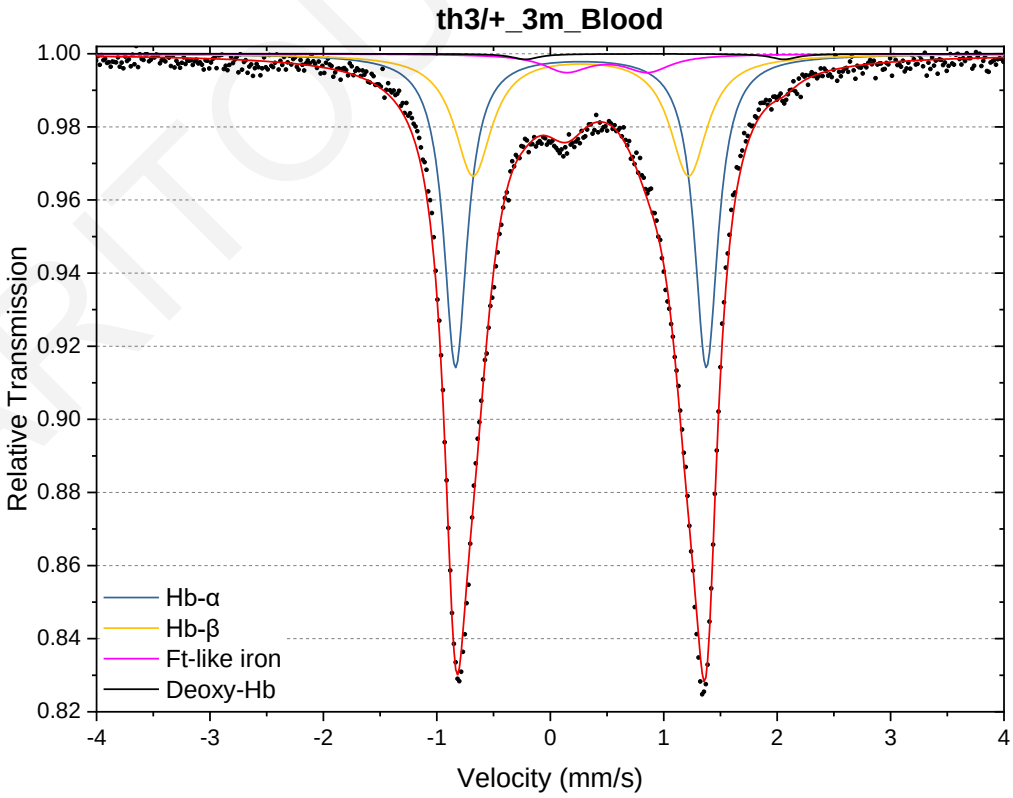

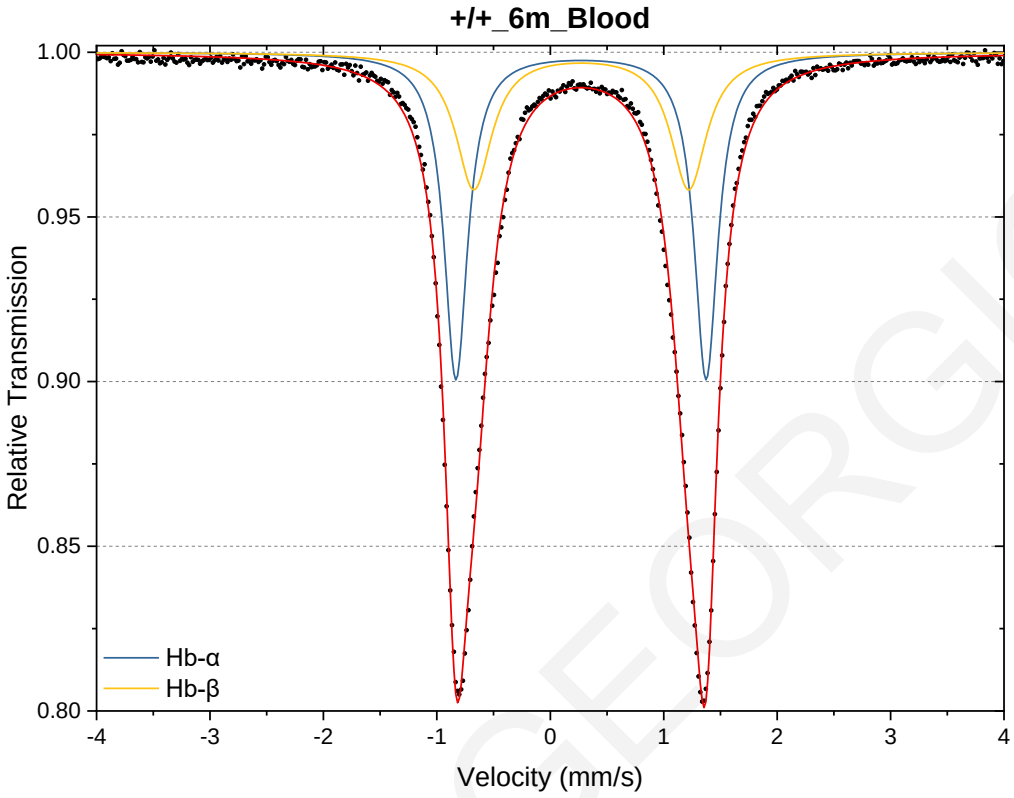

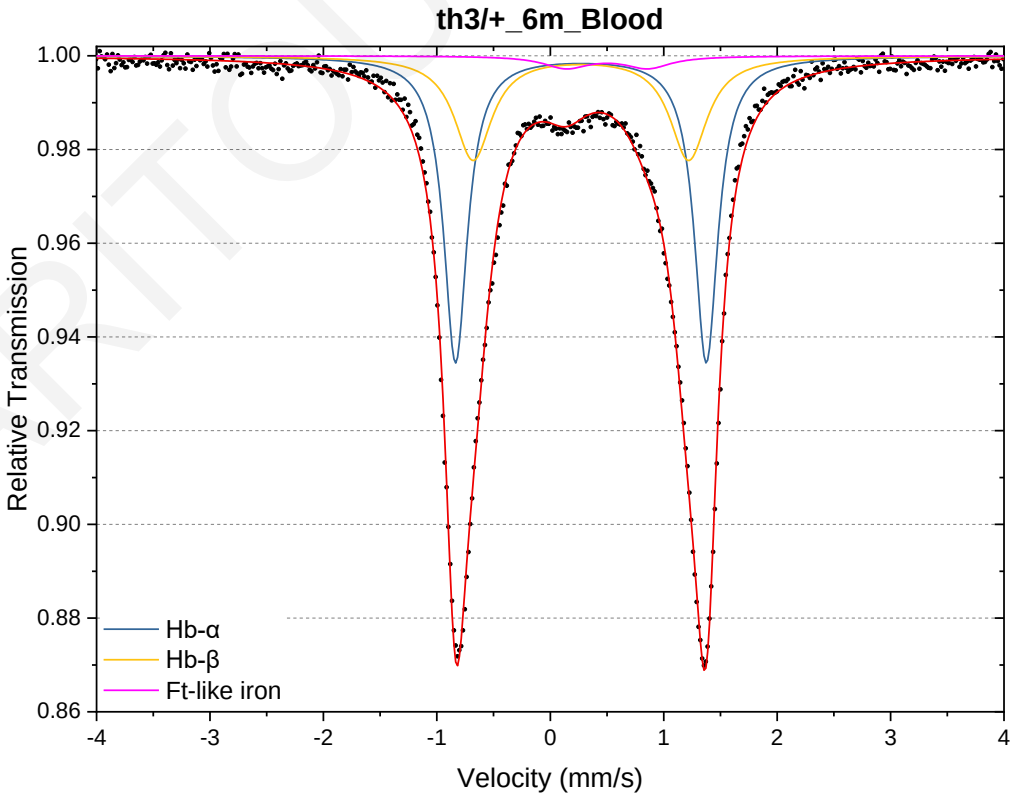

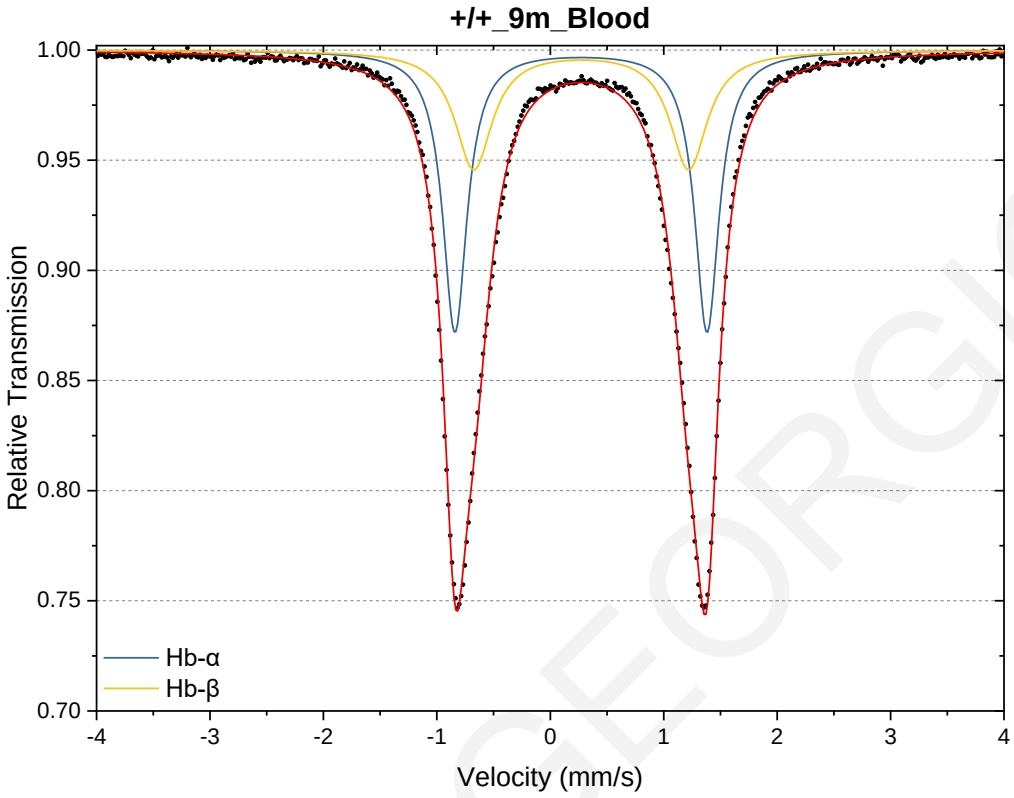

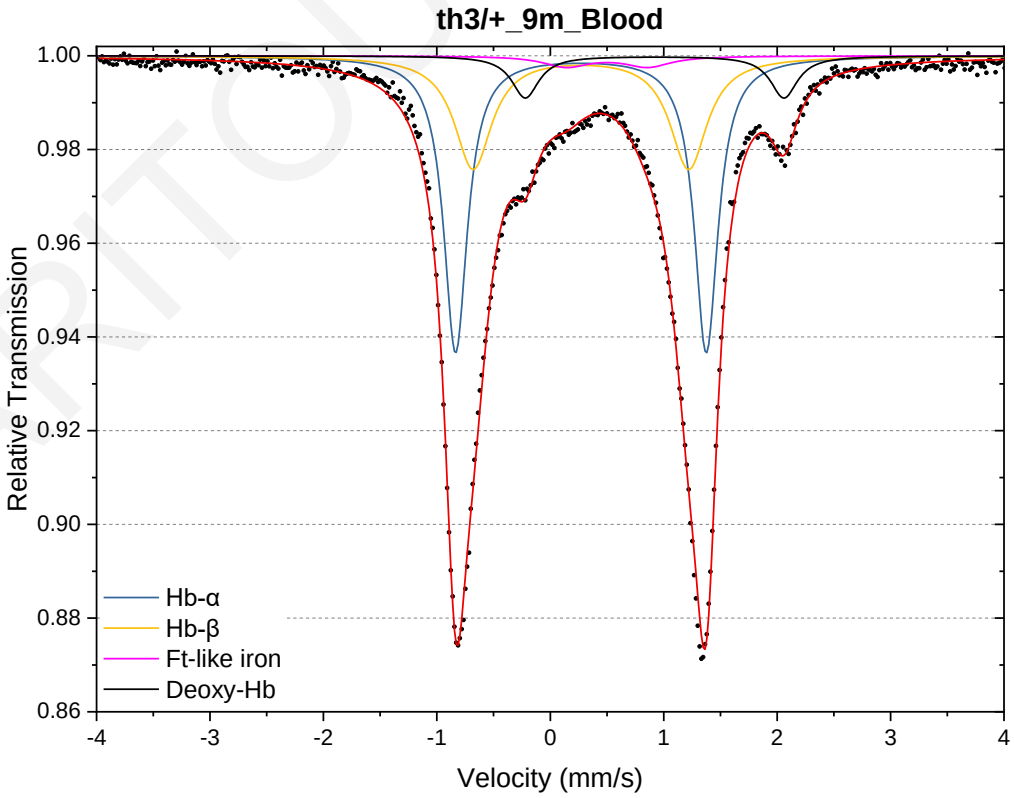

Heart spectra:

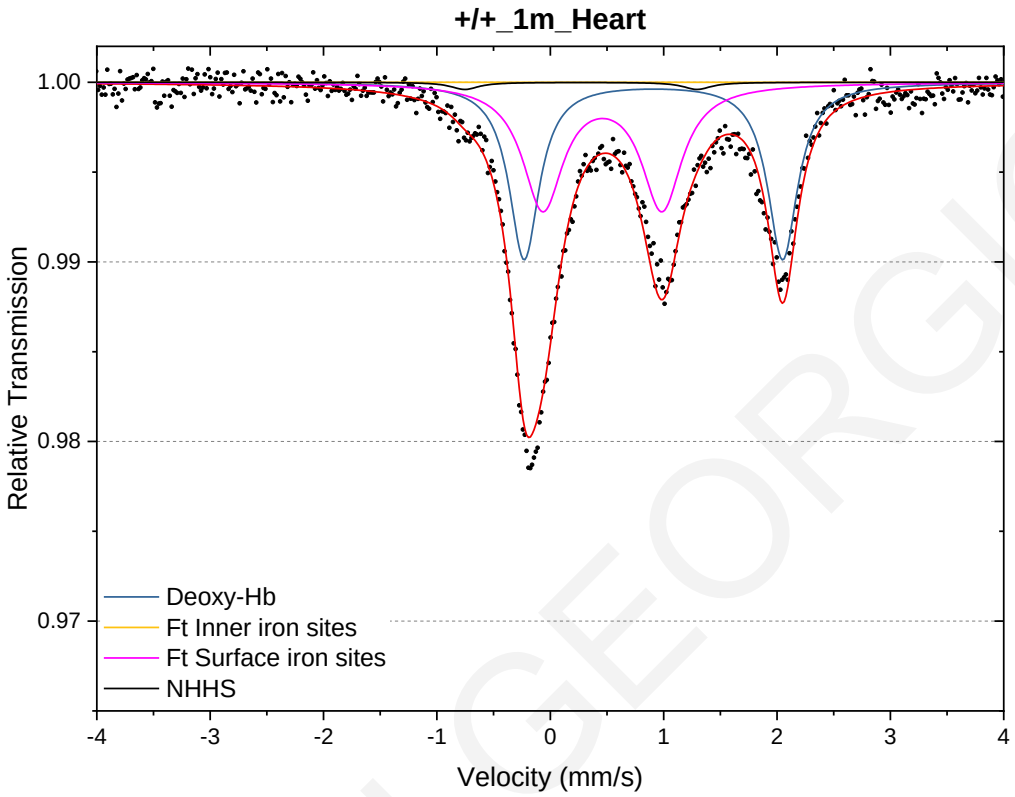

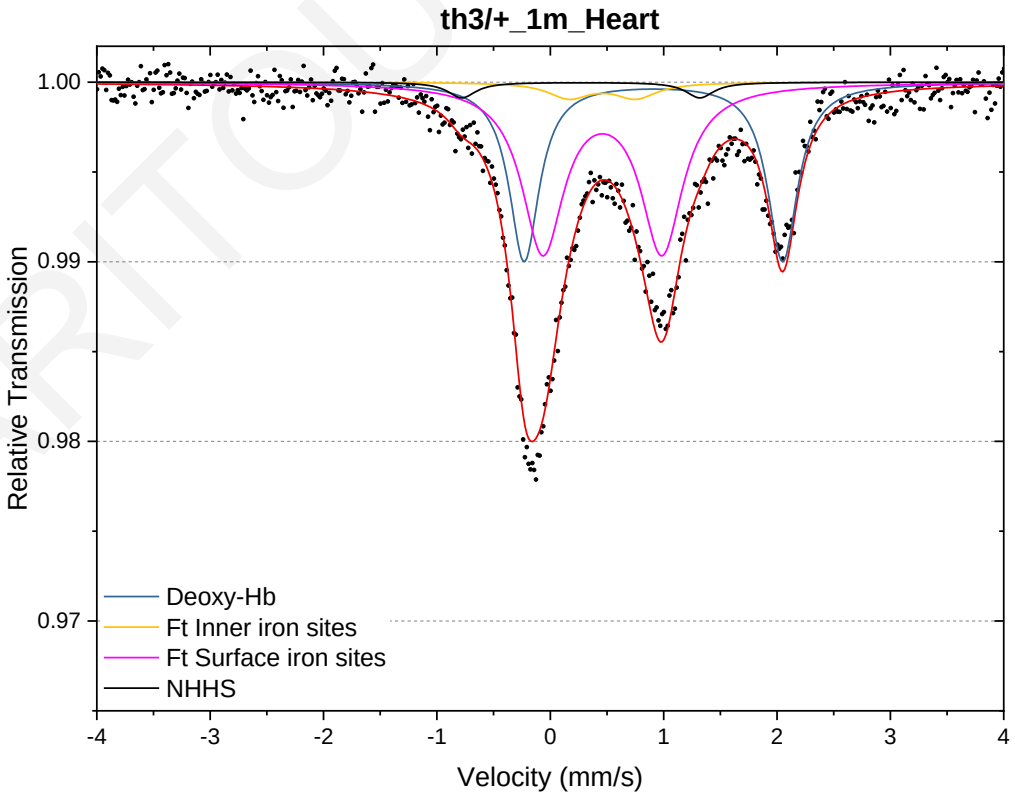

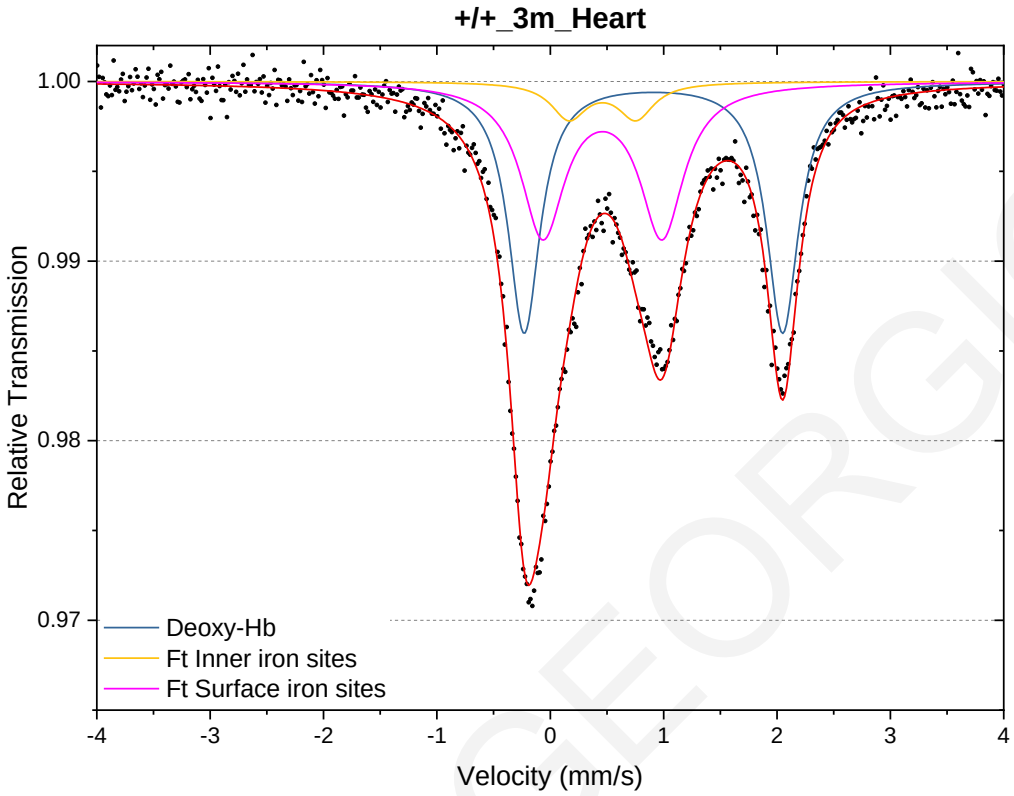

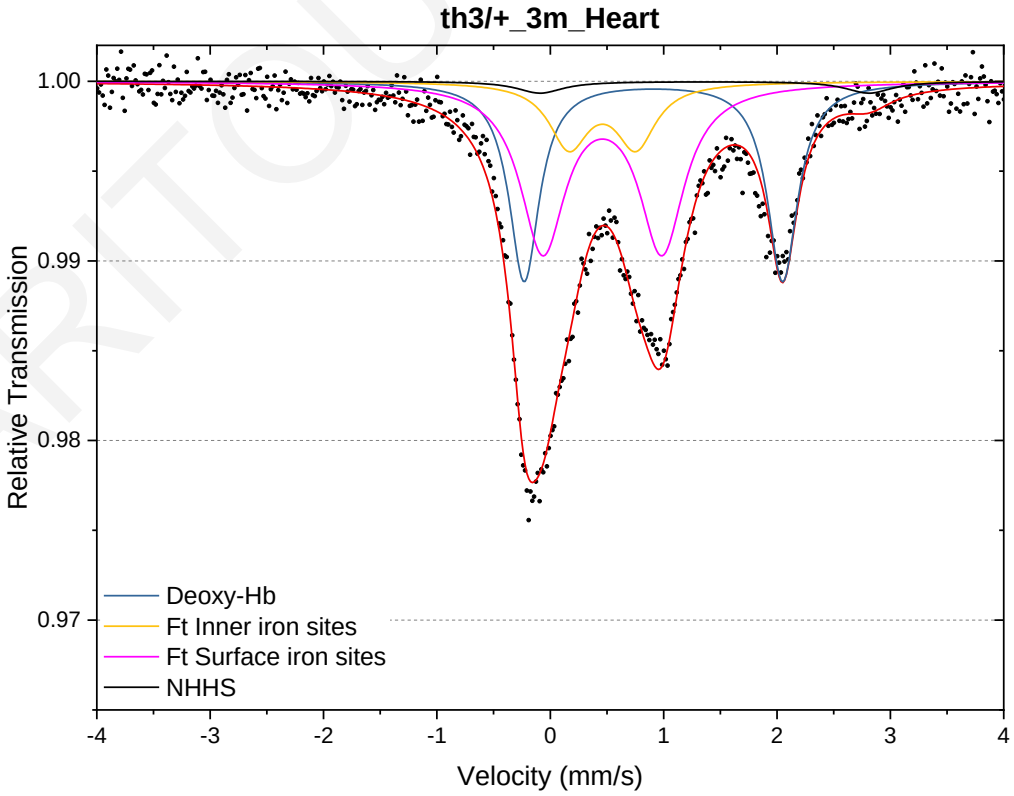

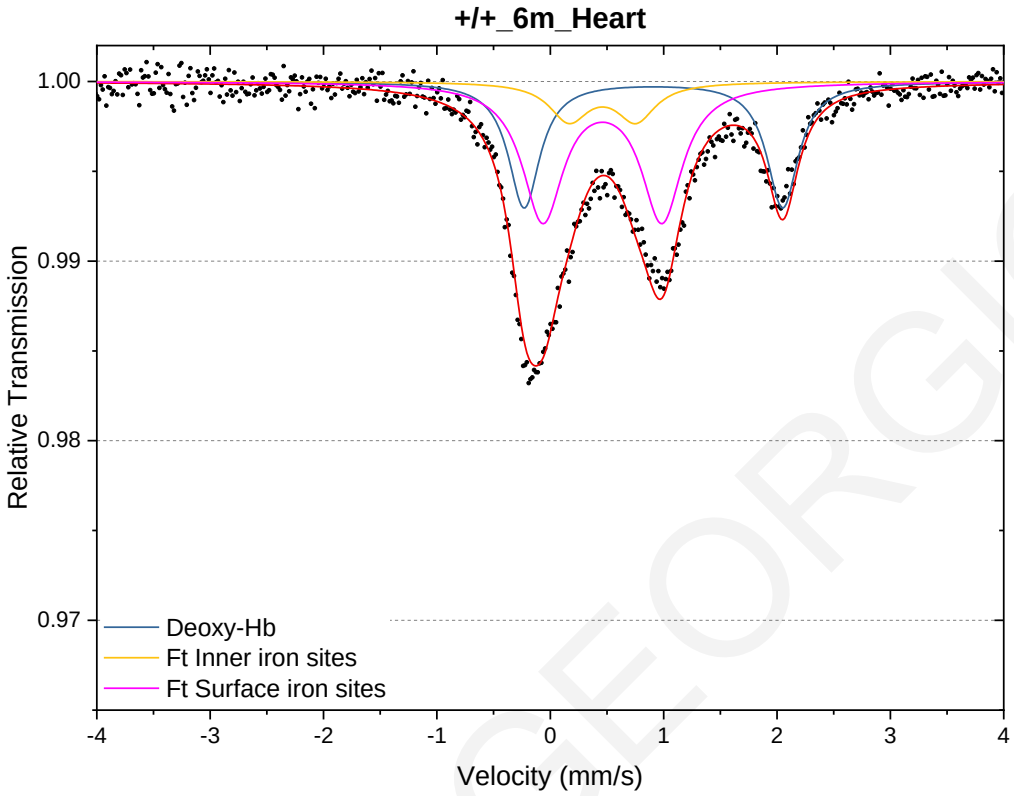

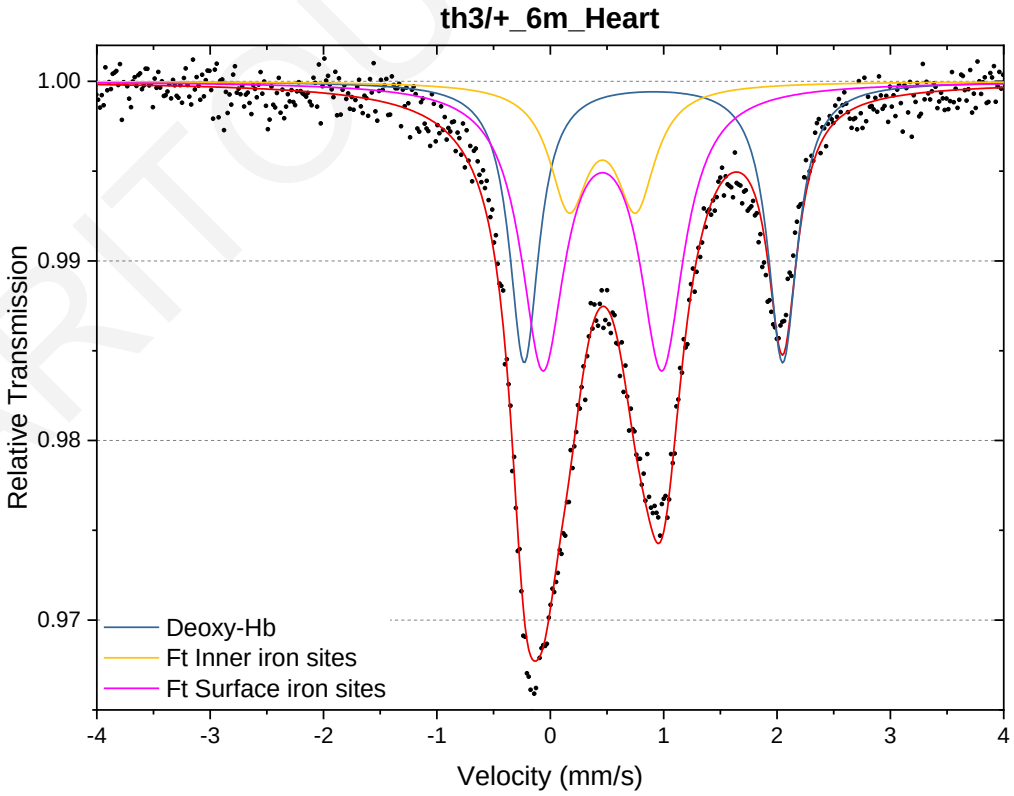

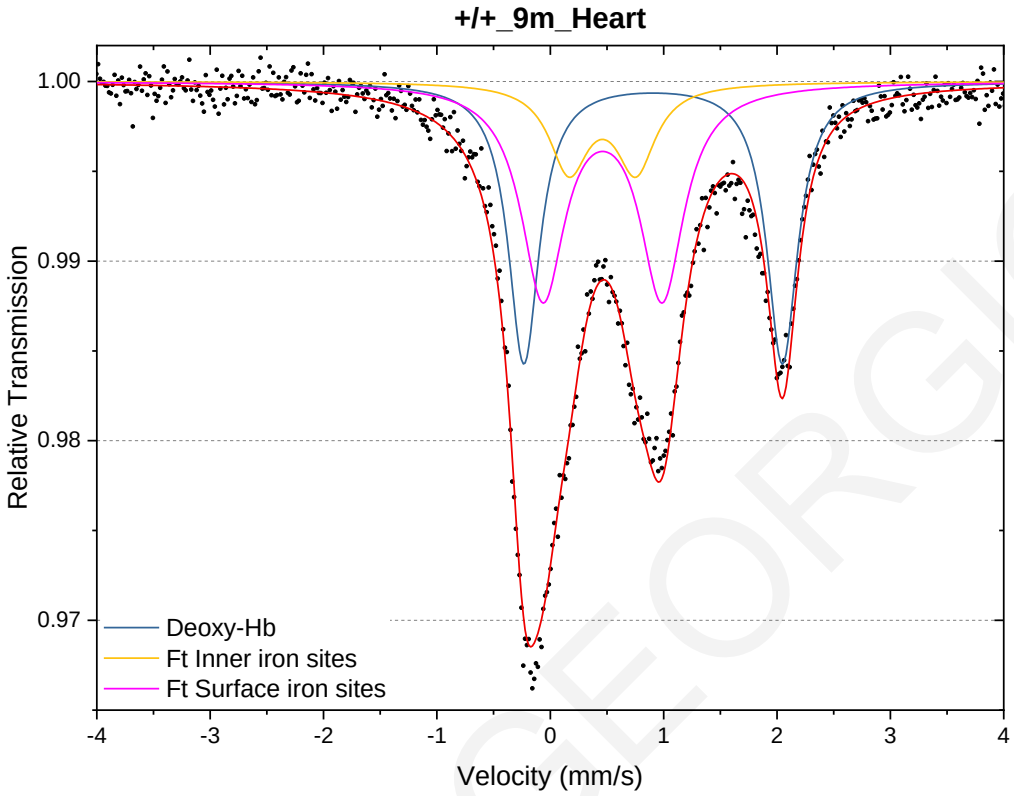

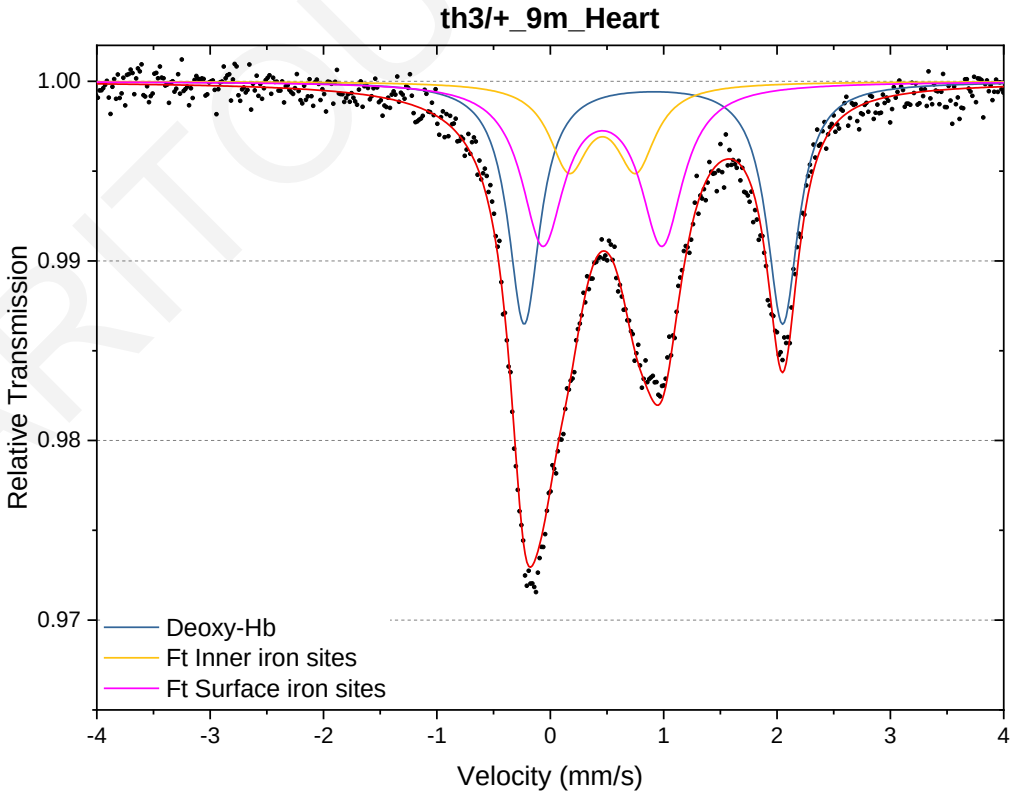

Kidney Spectra

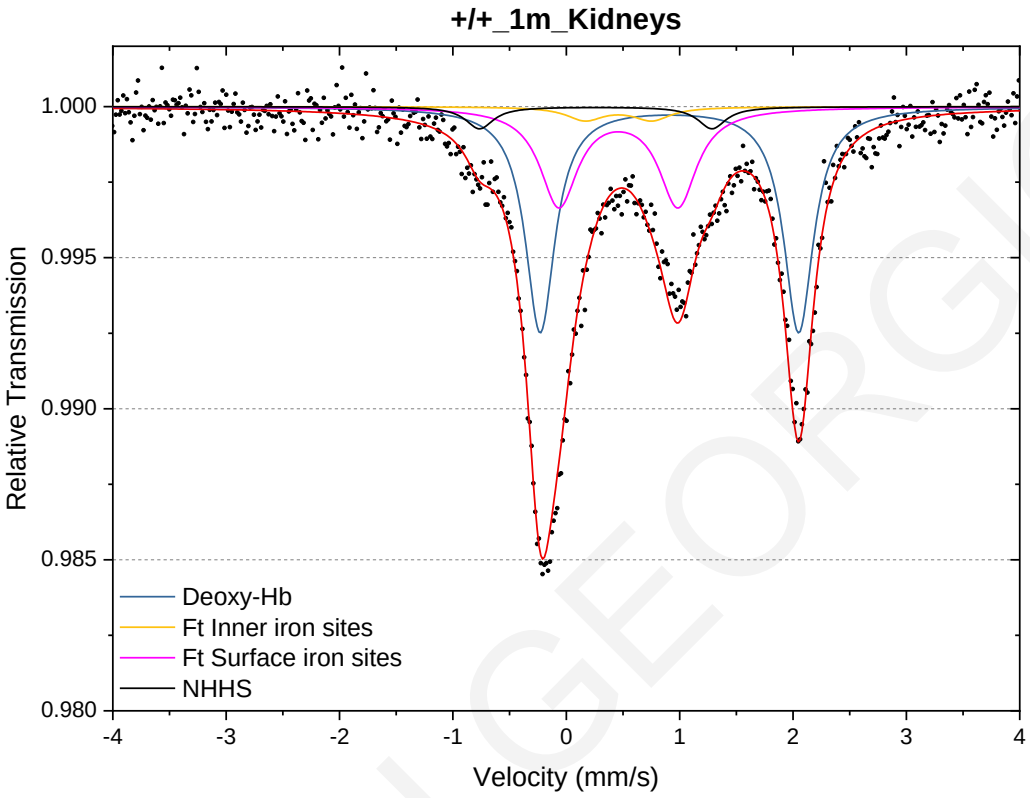

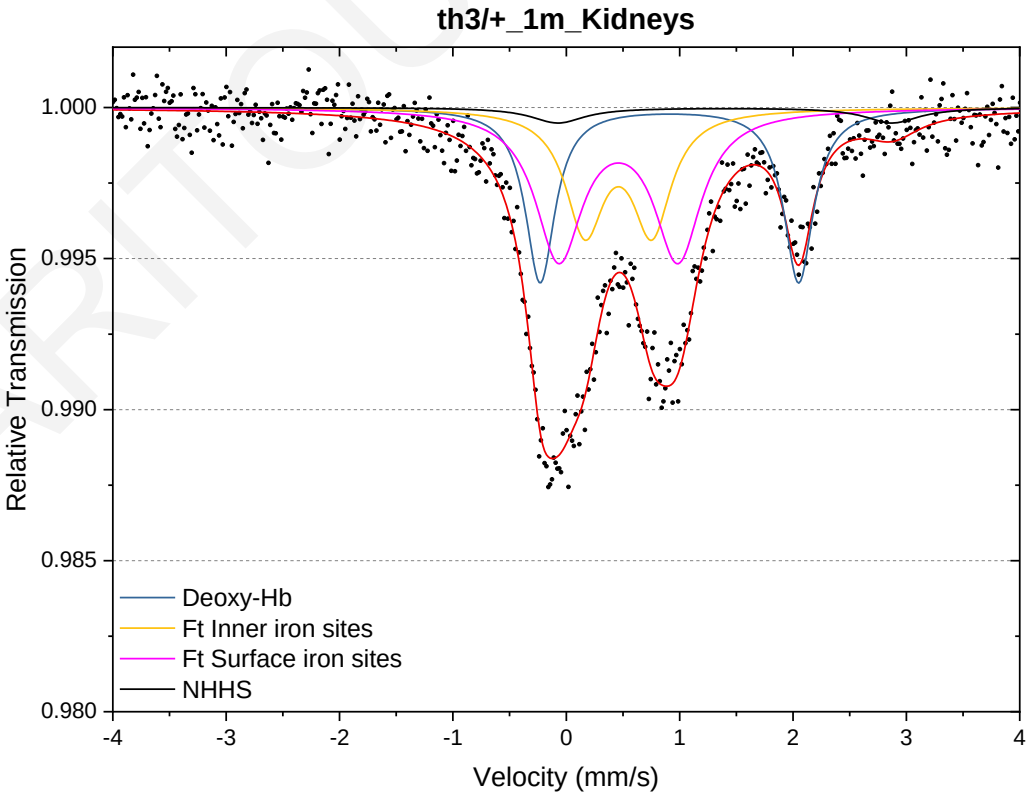

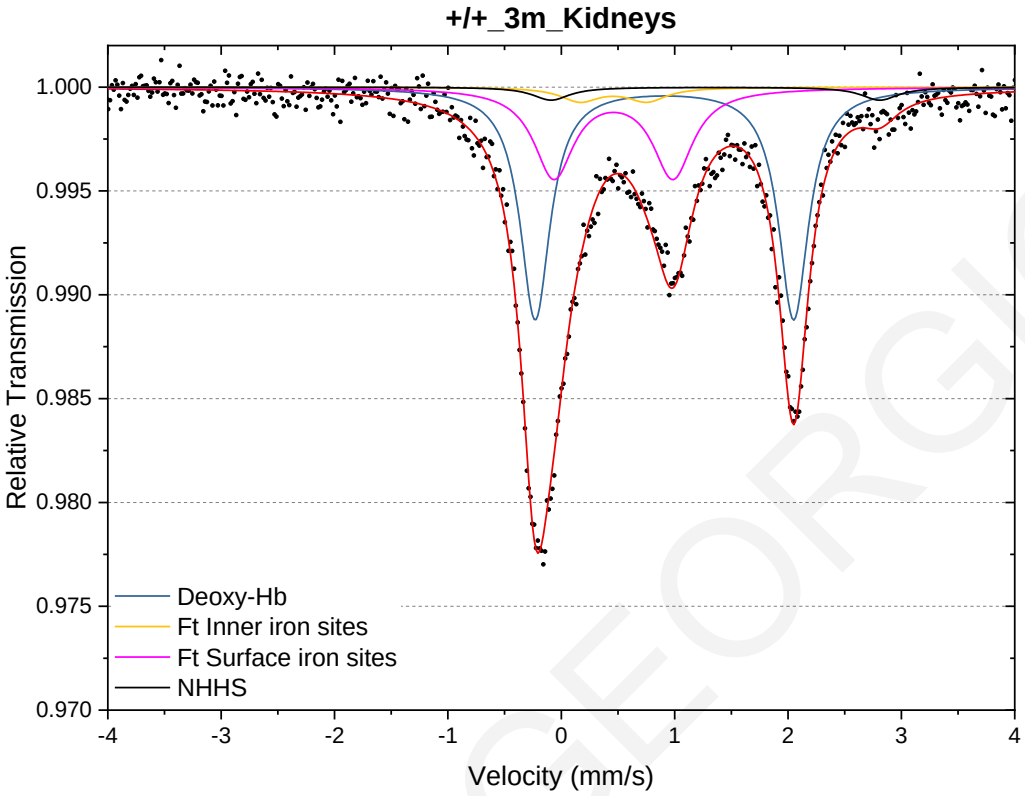

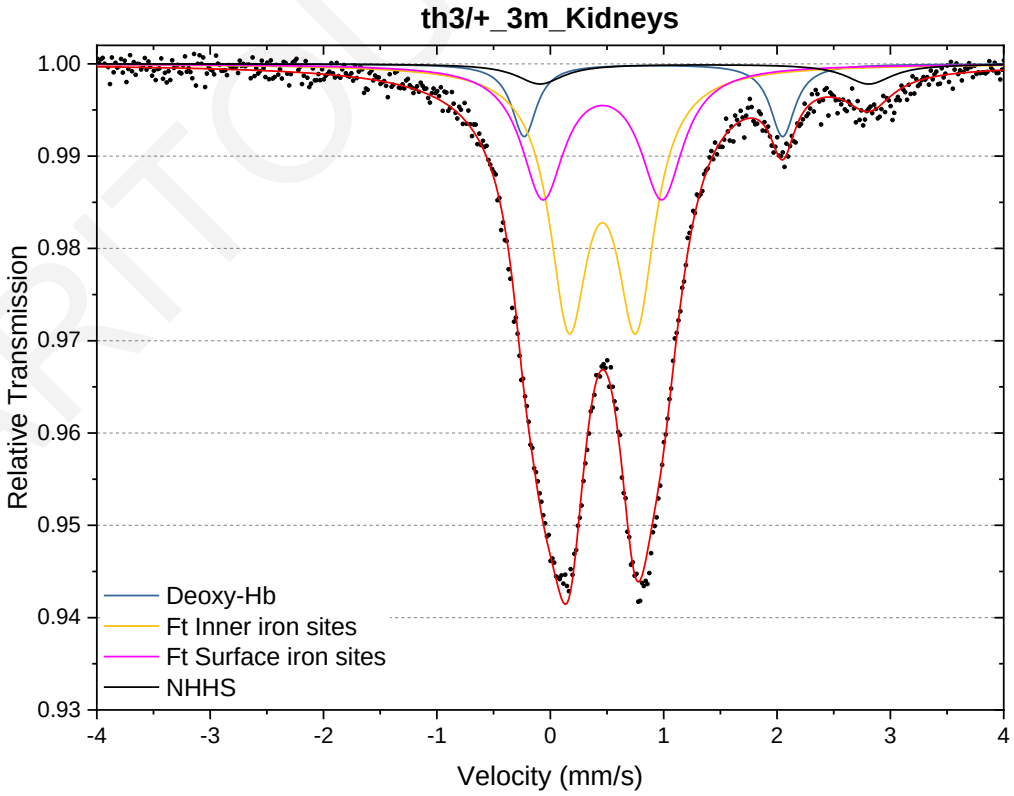

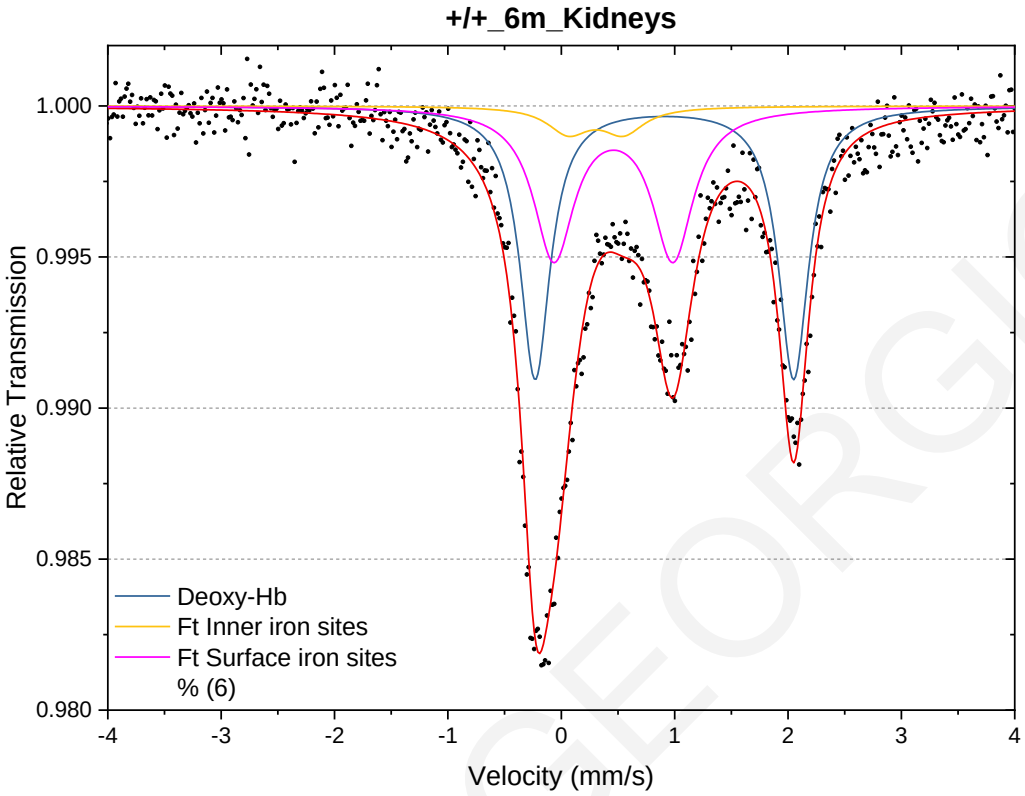

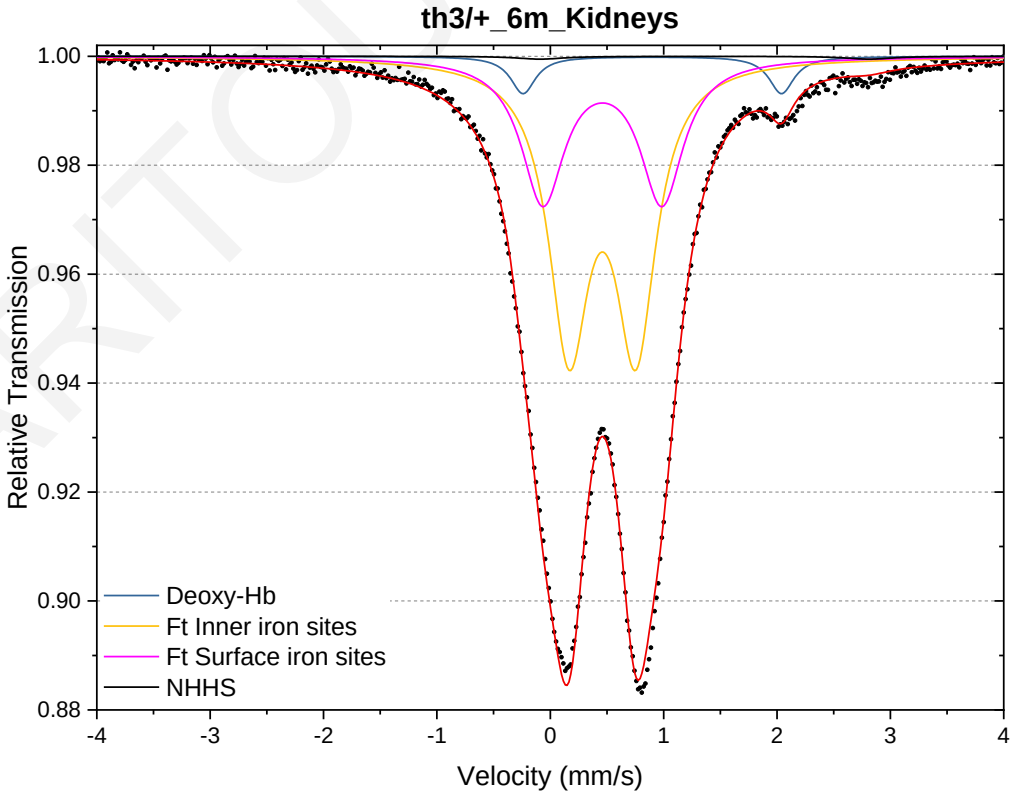

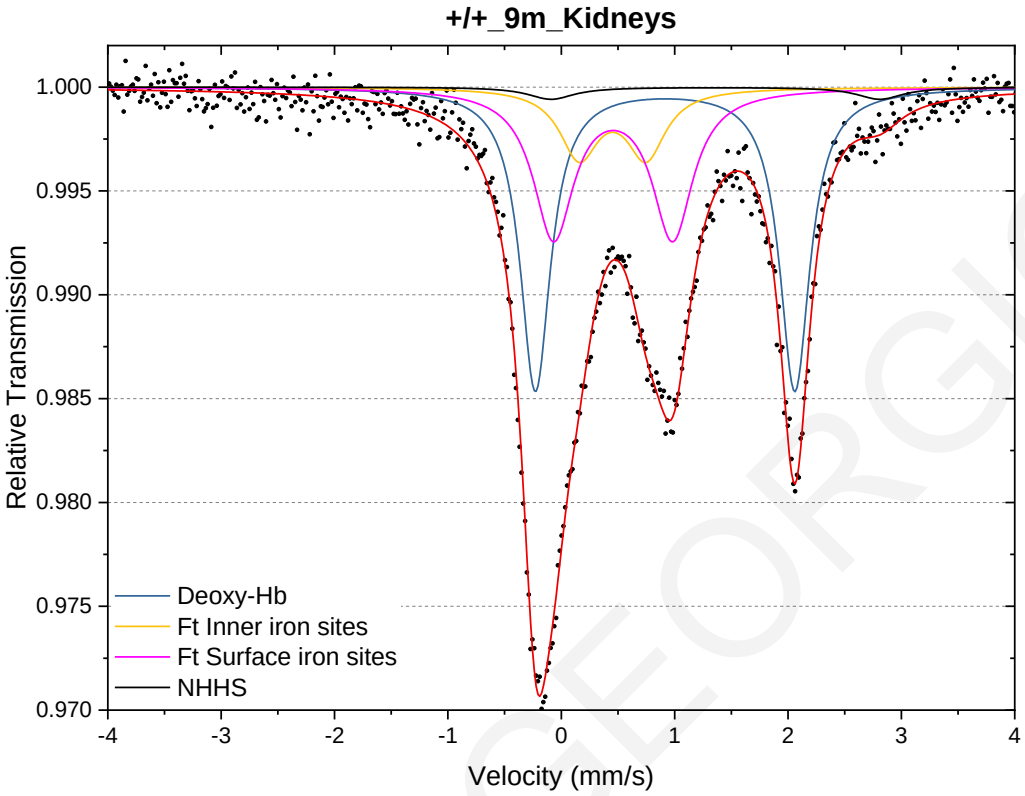

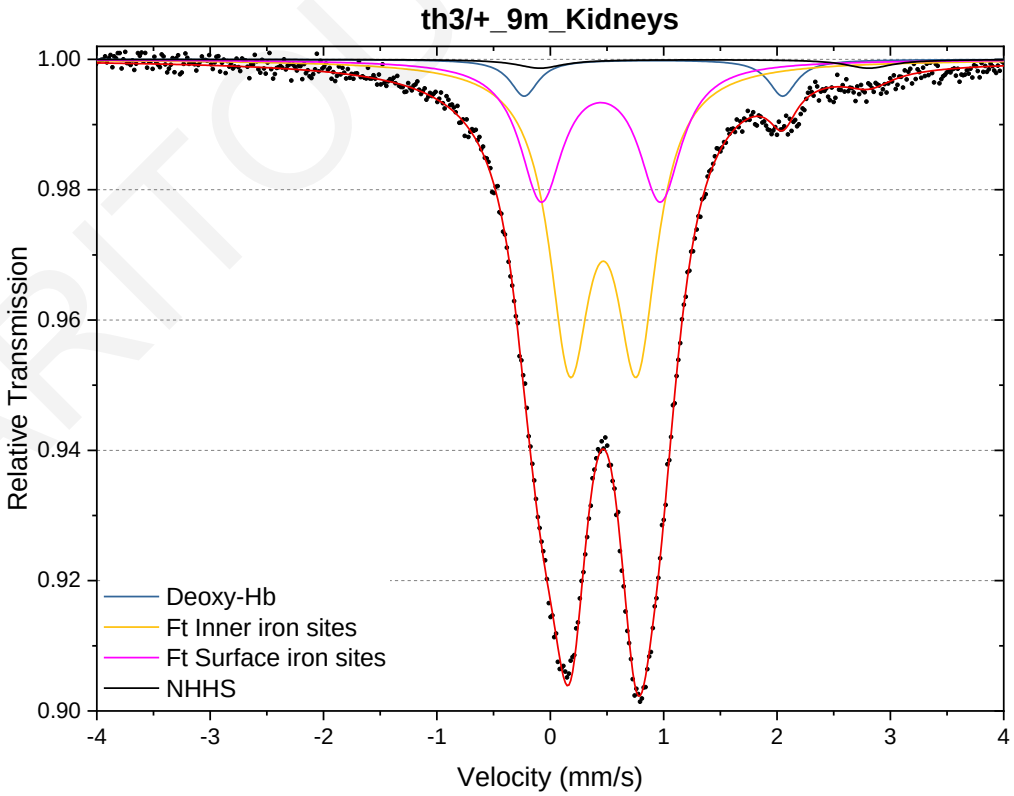

Brain Spectra

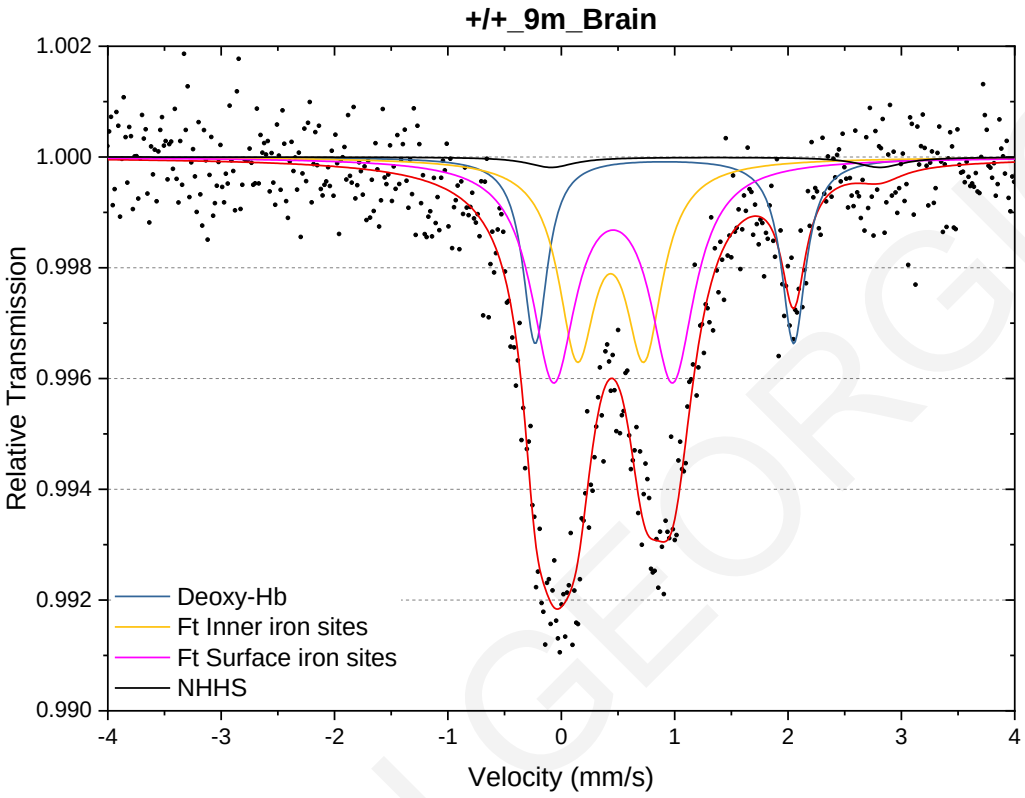

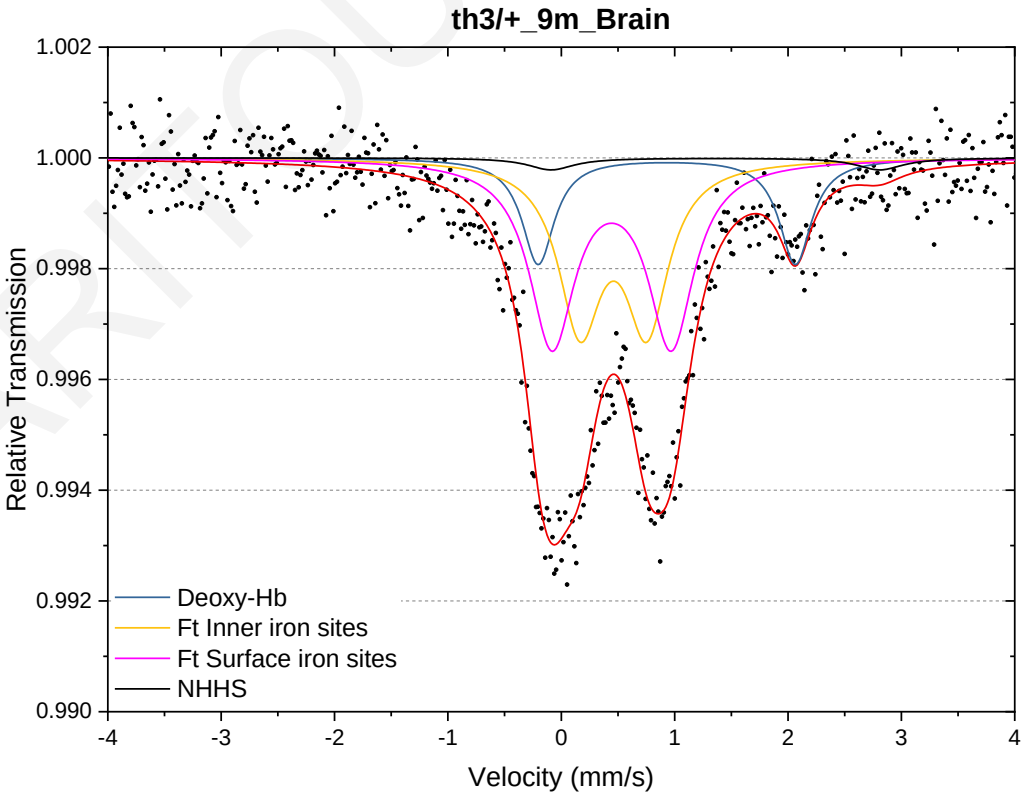

Liver Spectra

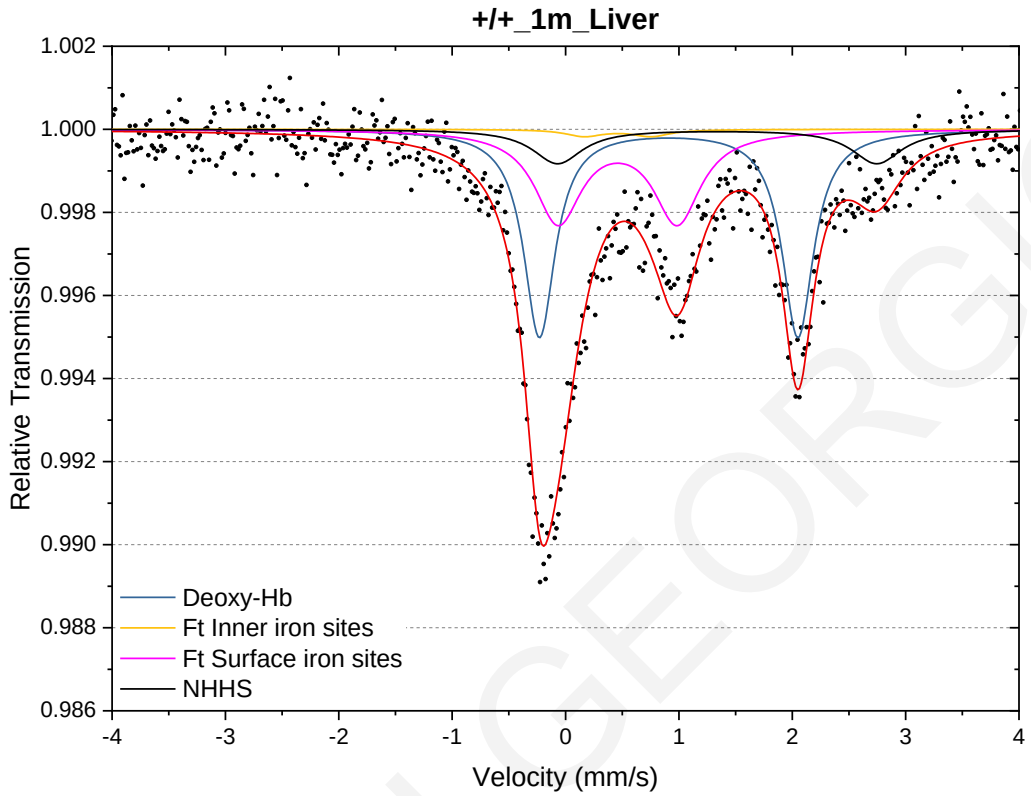

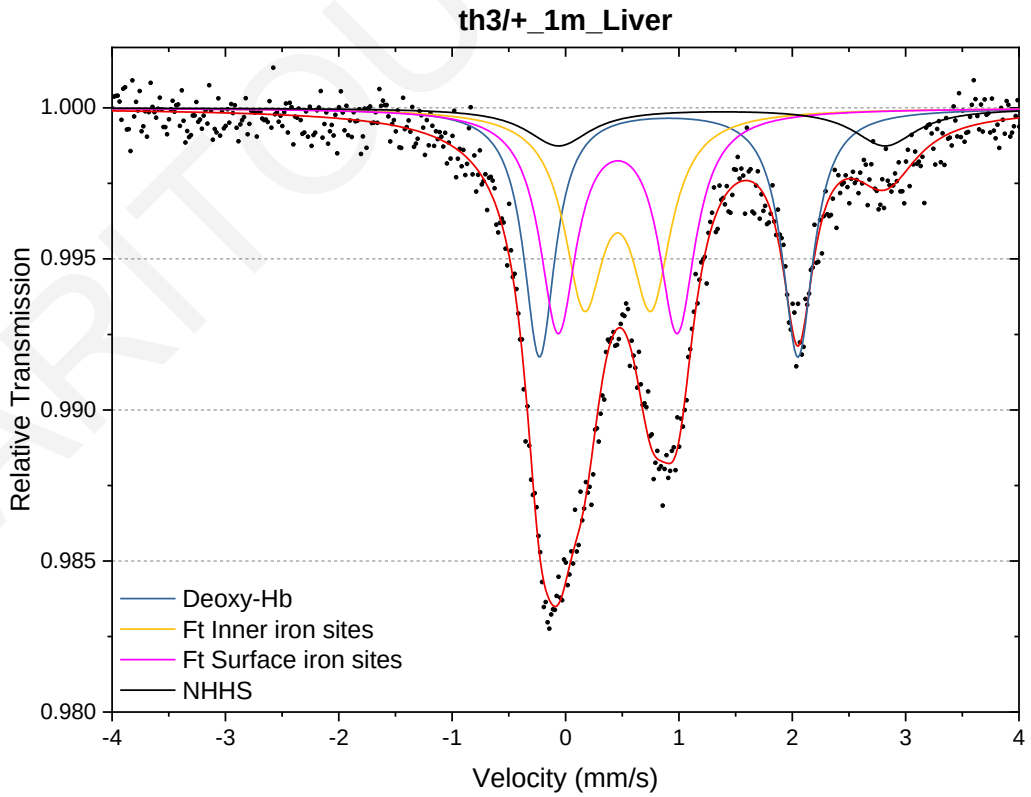

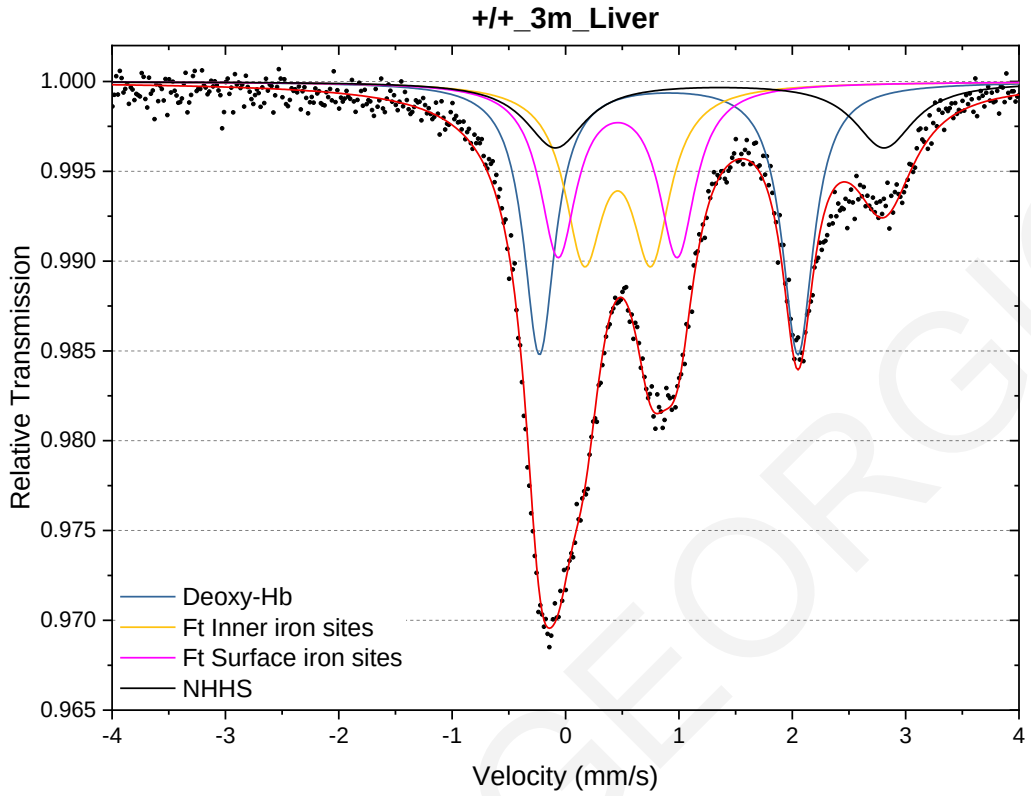

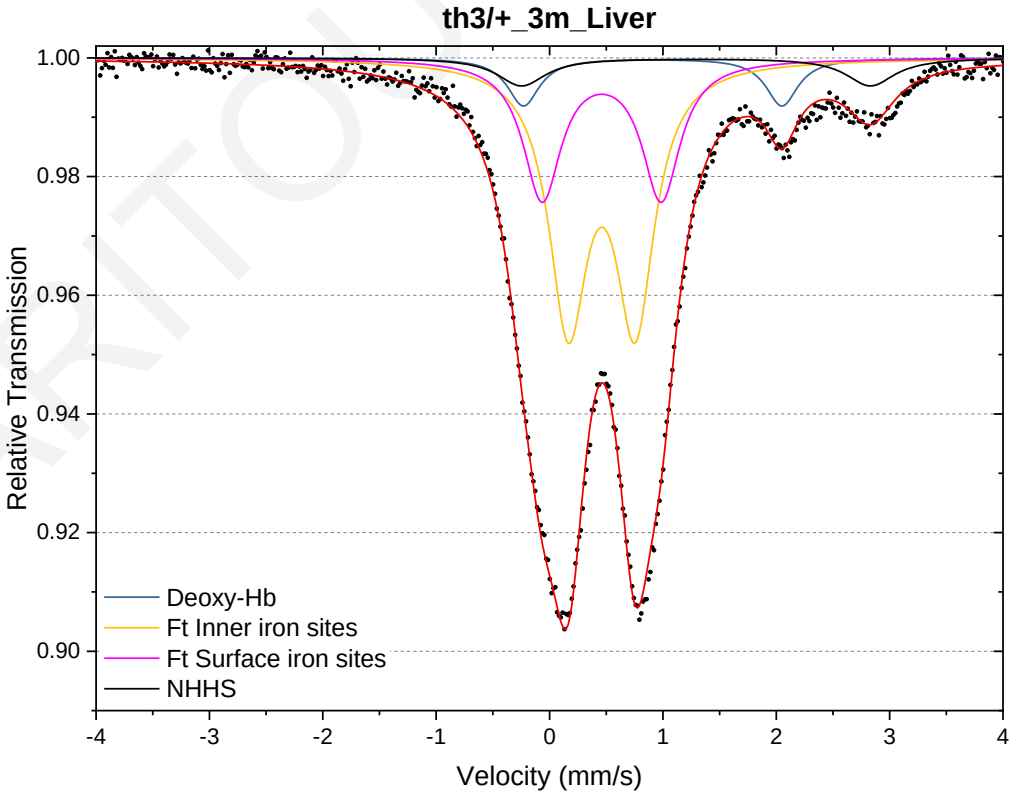

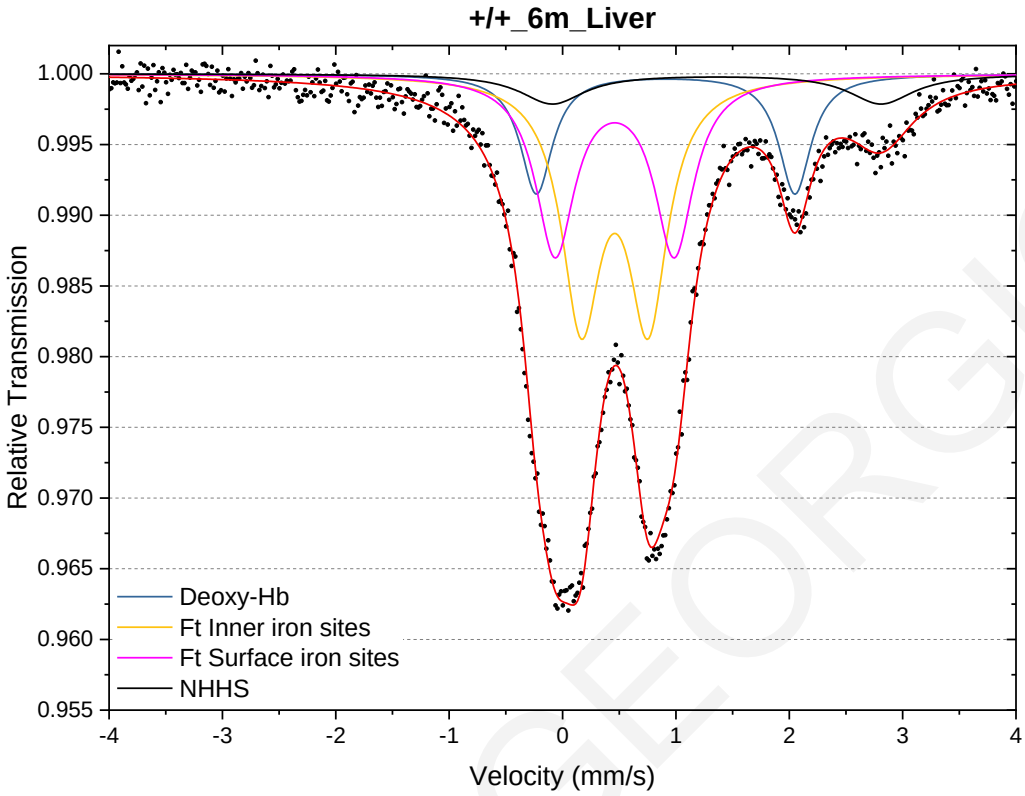

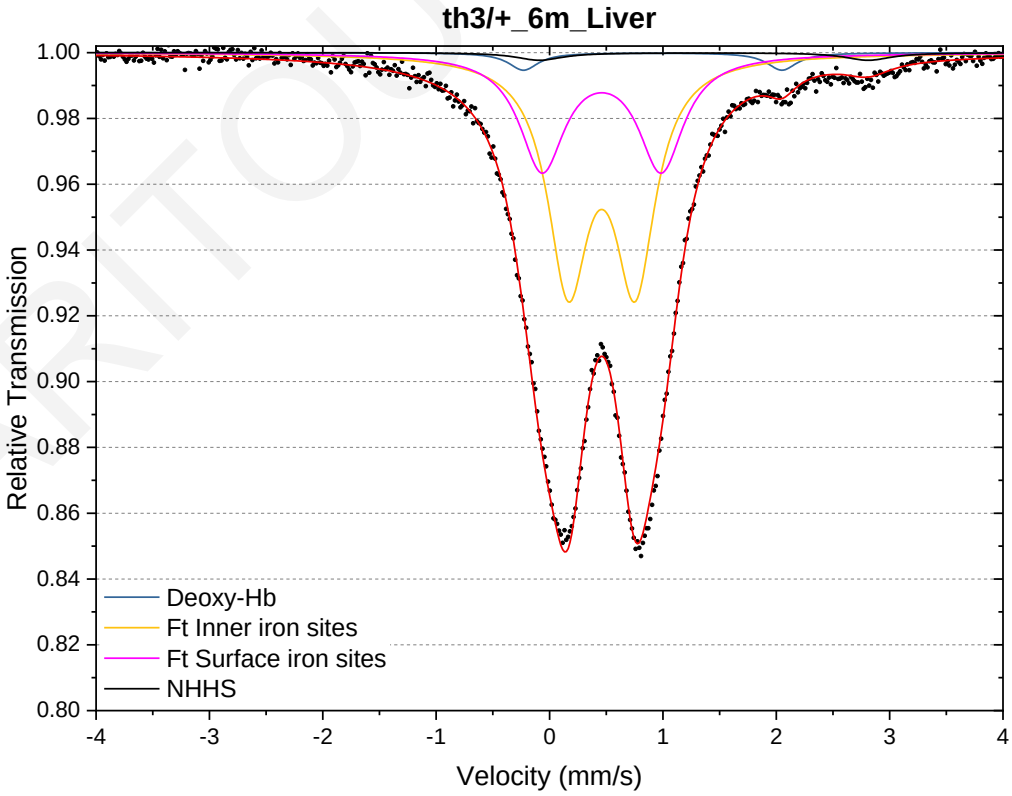

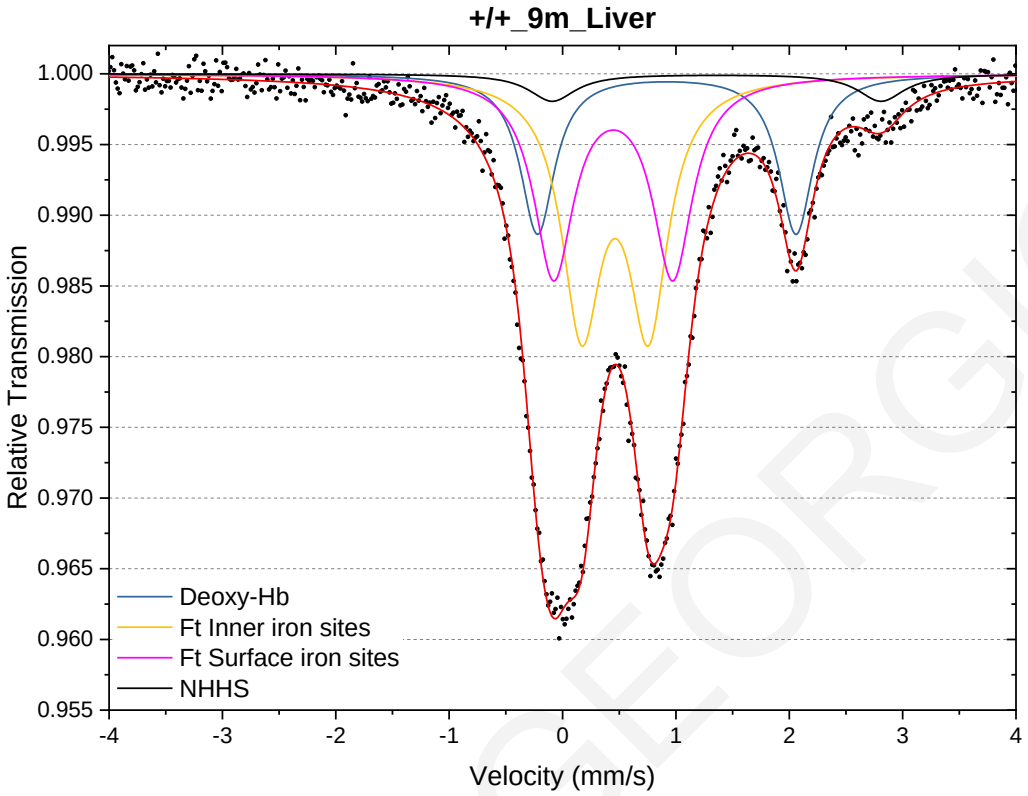

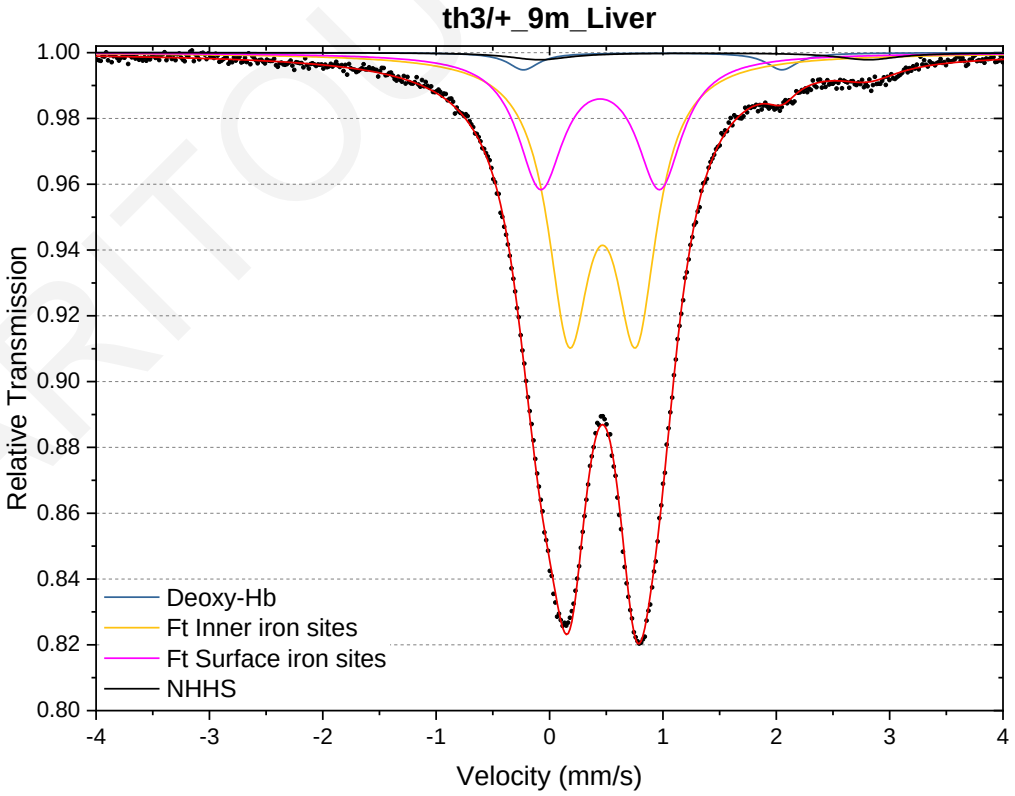

Spleen Spectra

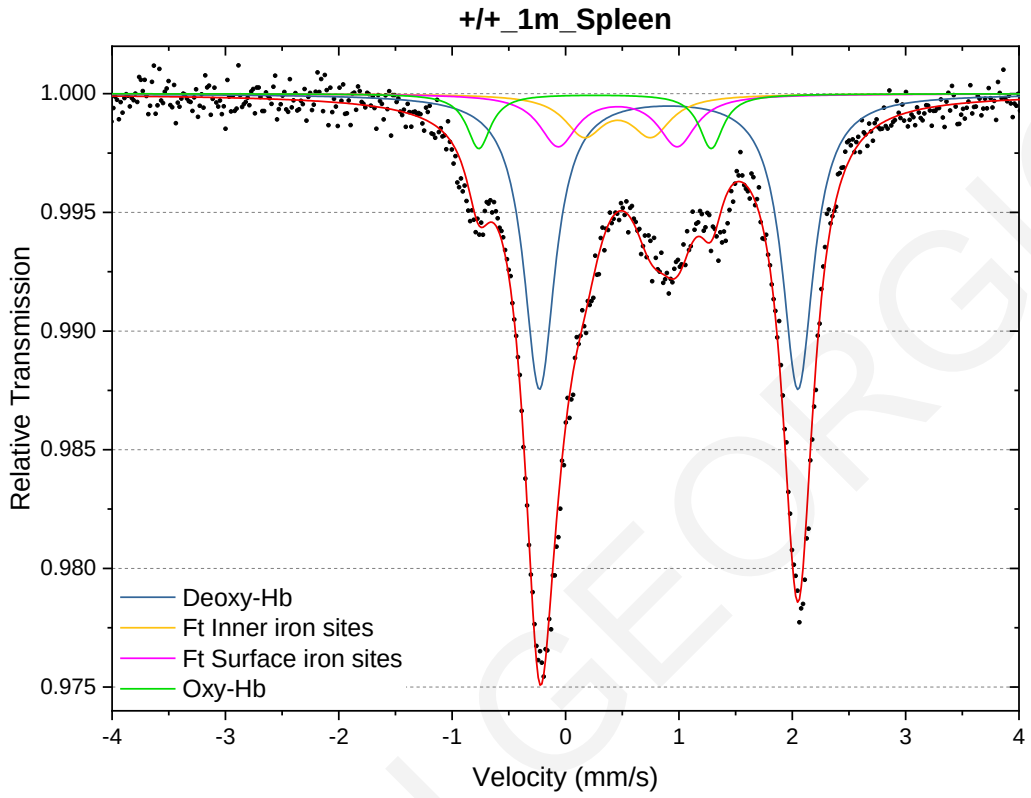

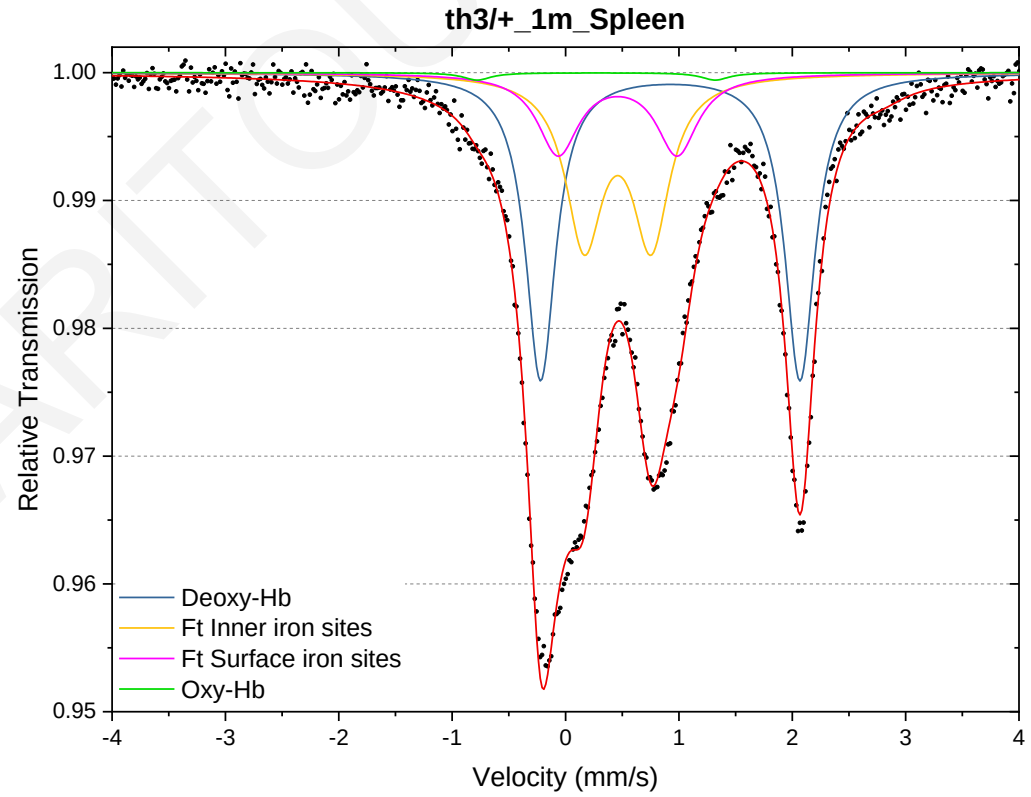

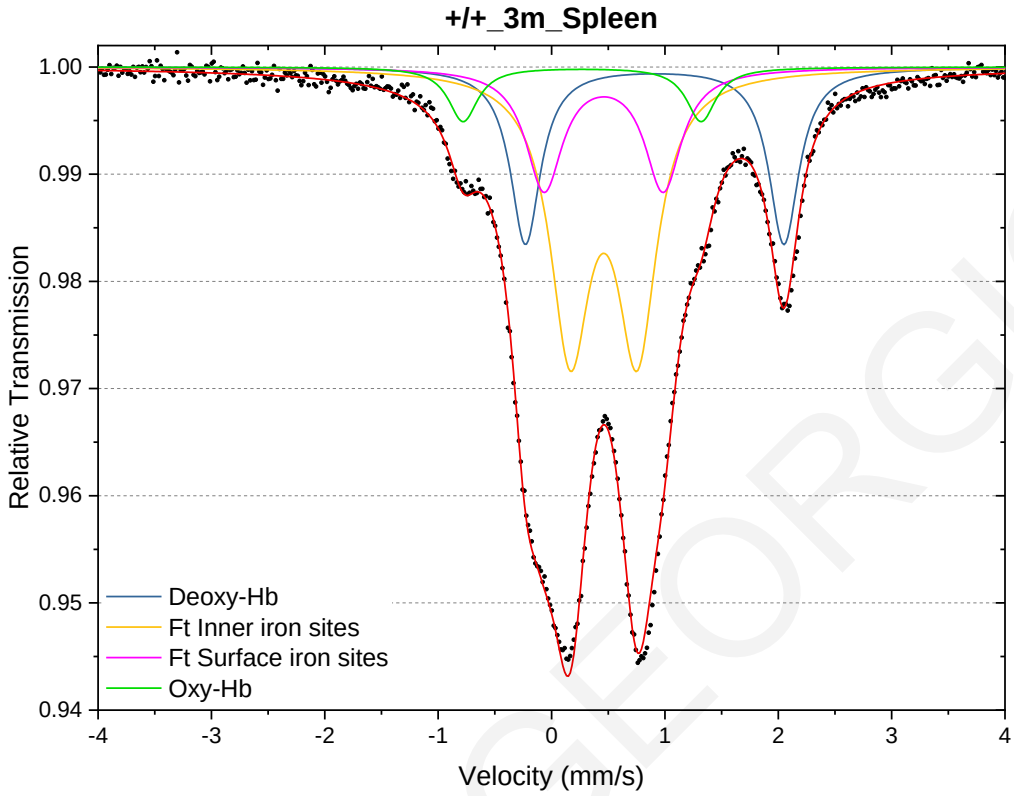

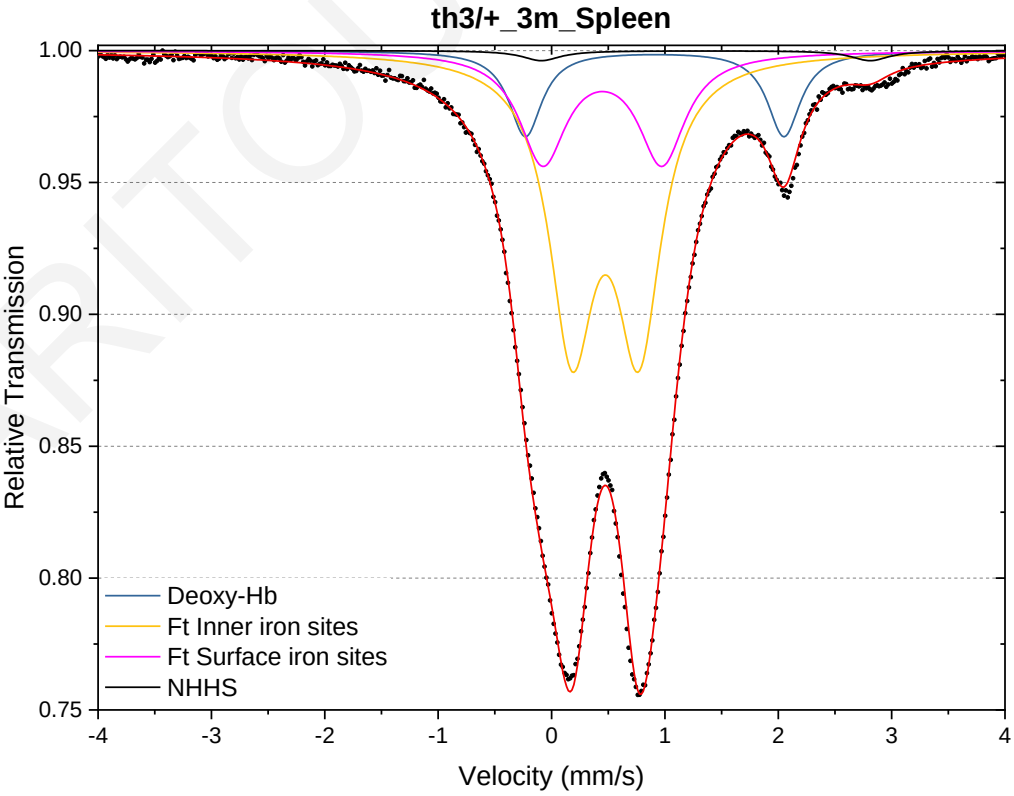

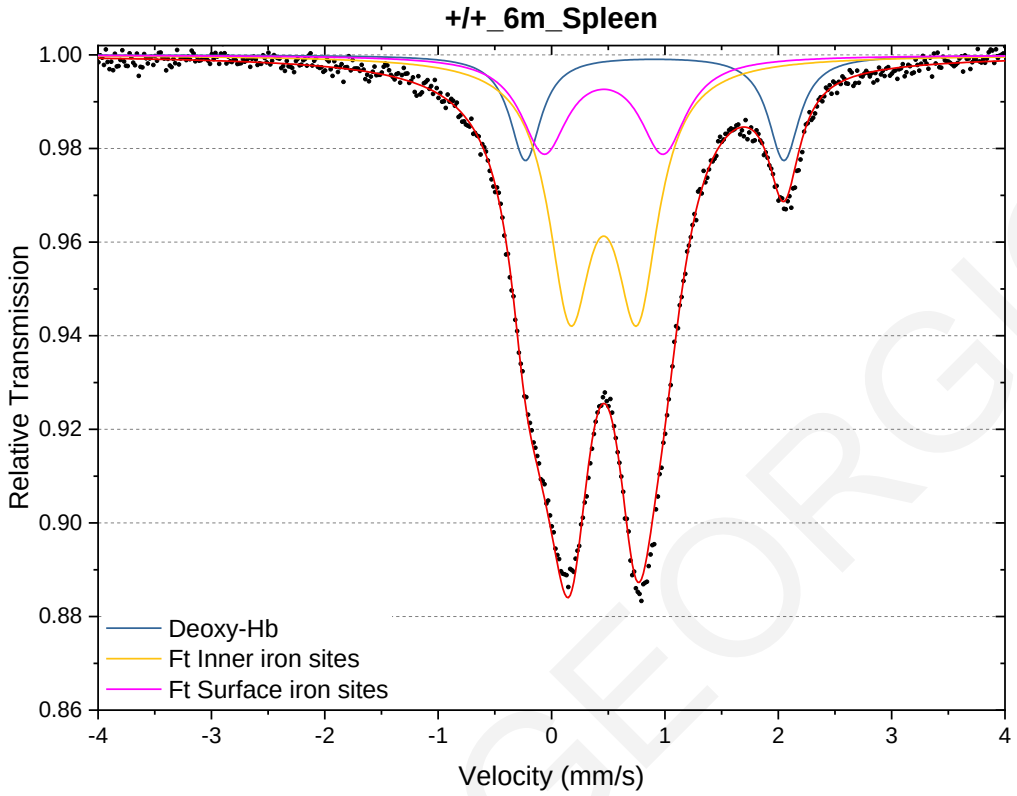

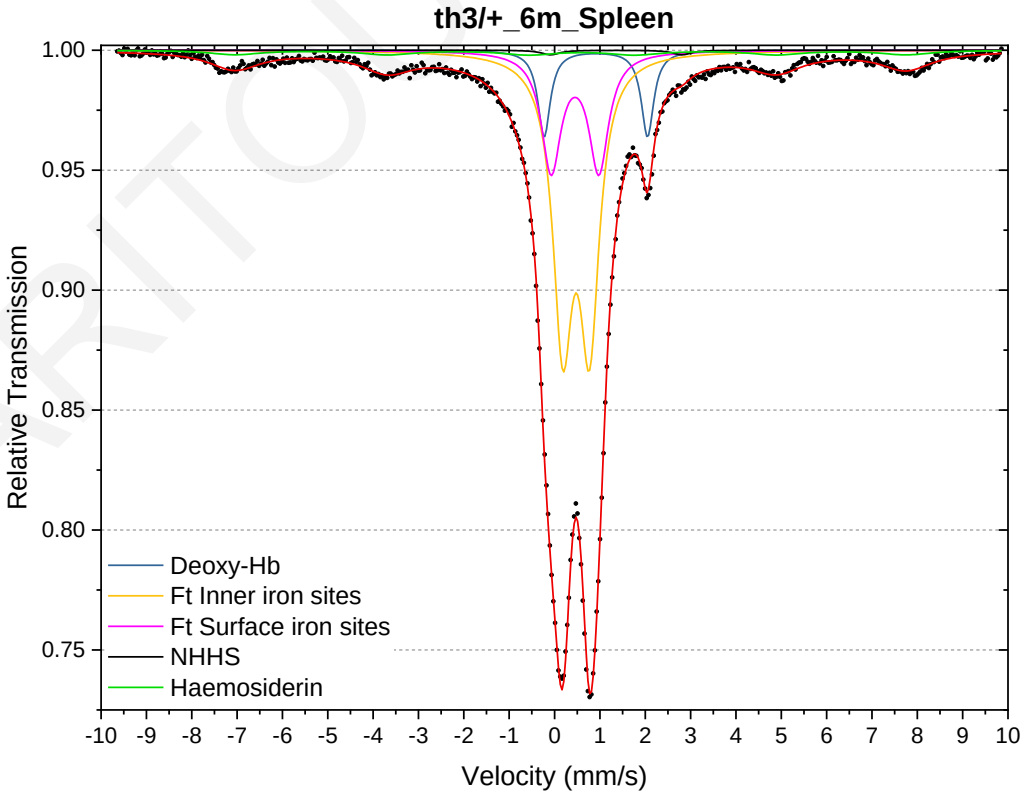

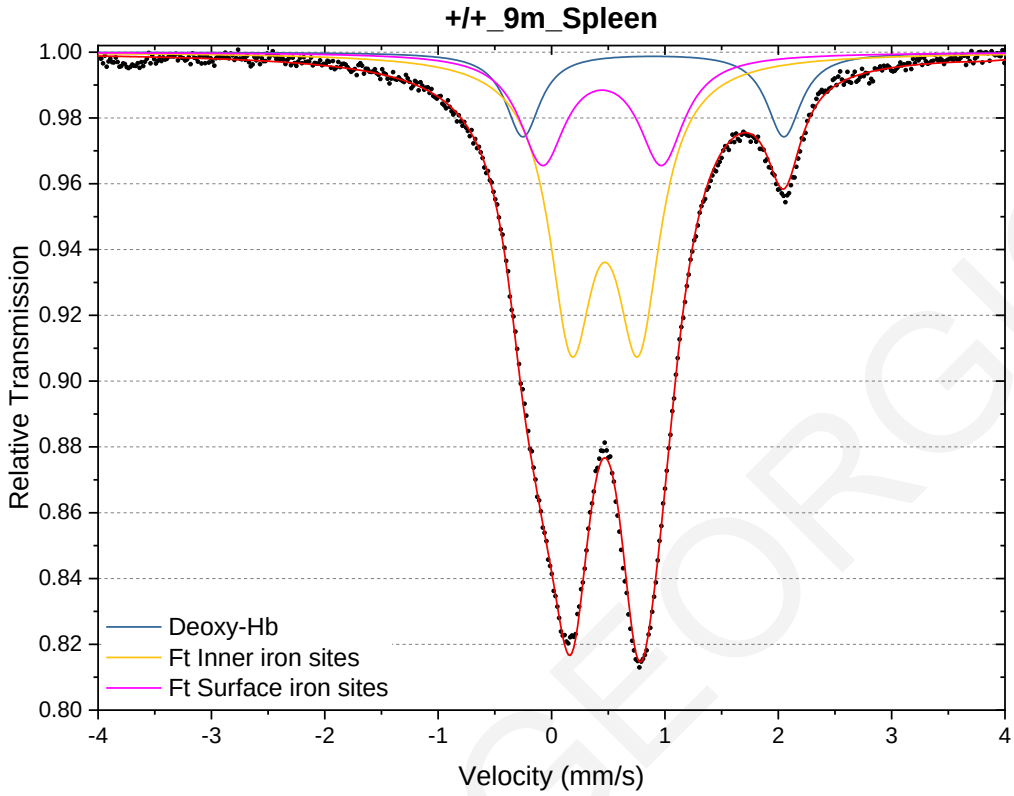

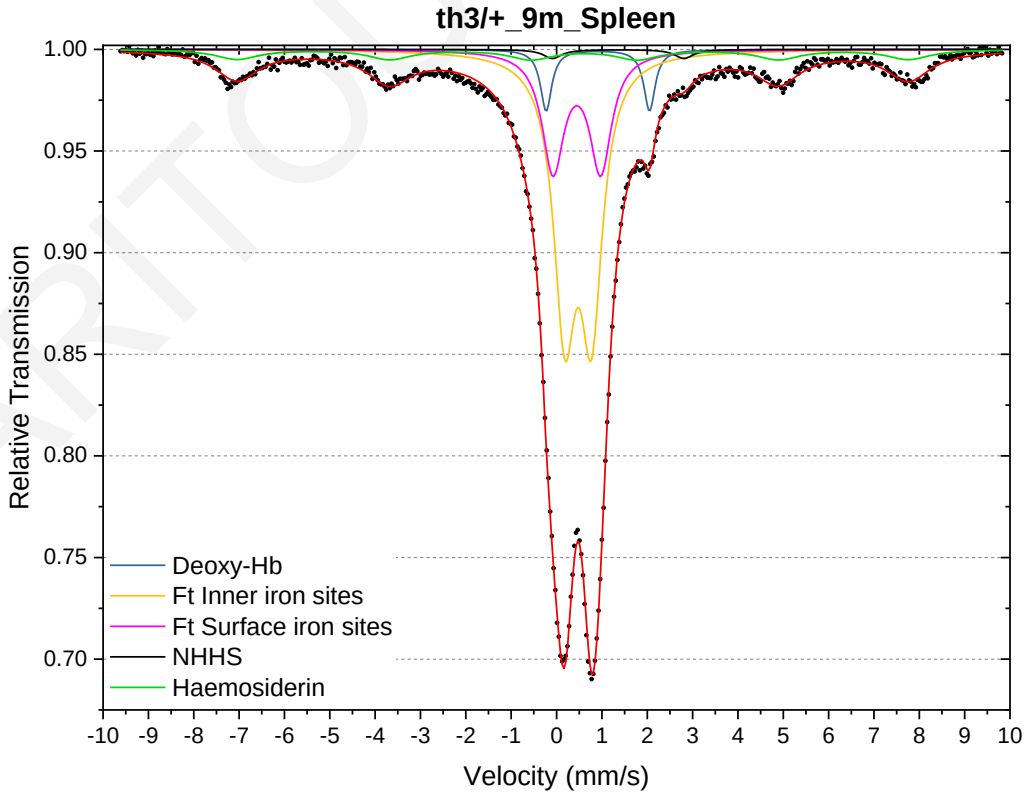

MS spectra for Chapter 5 (human volunteers):

Control samples

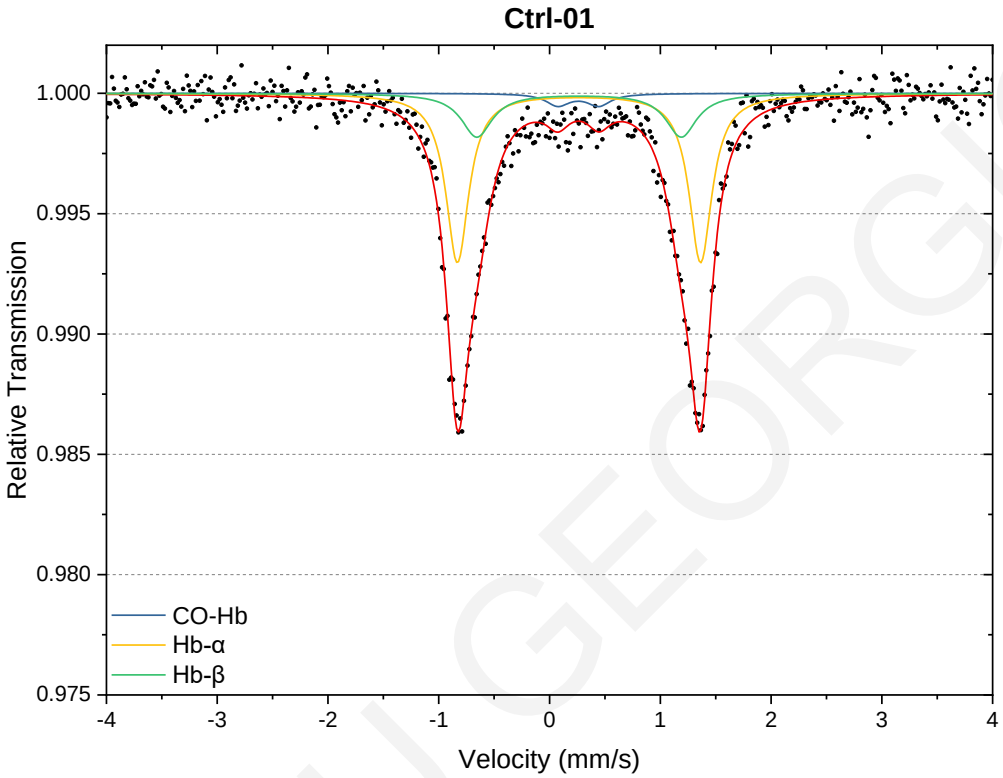

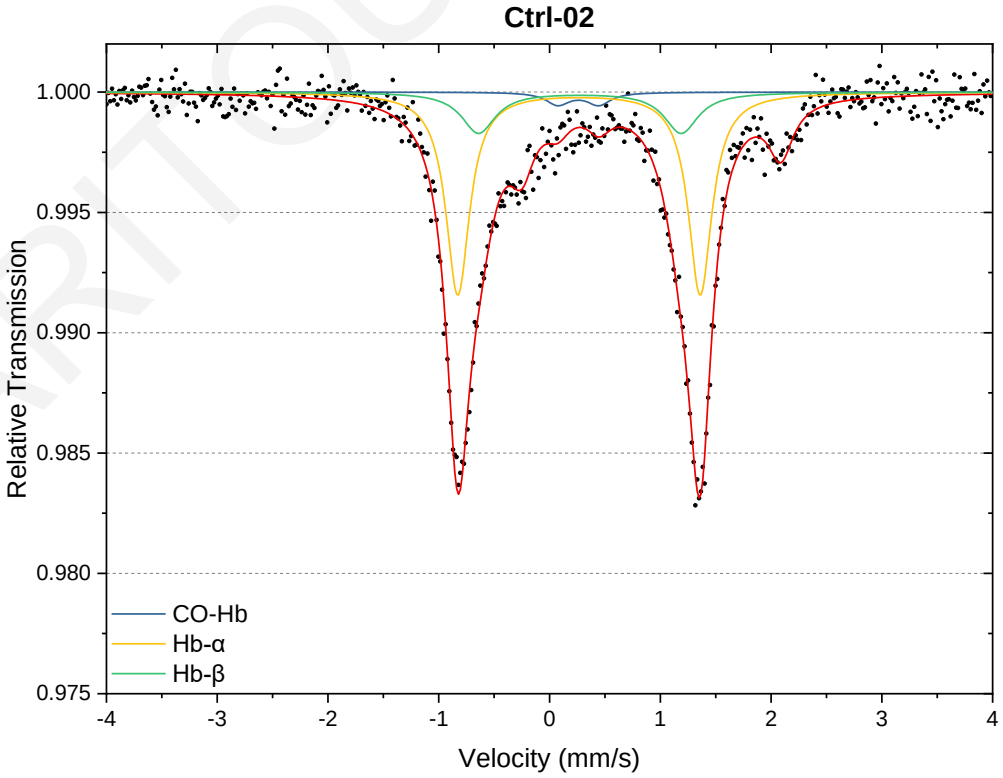

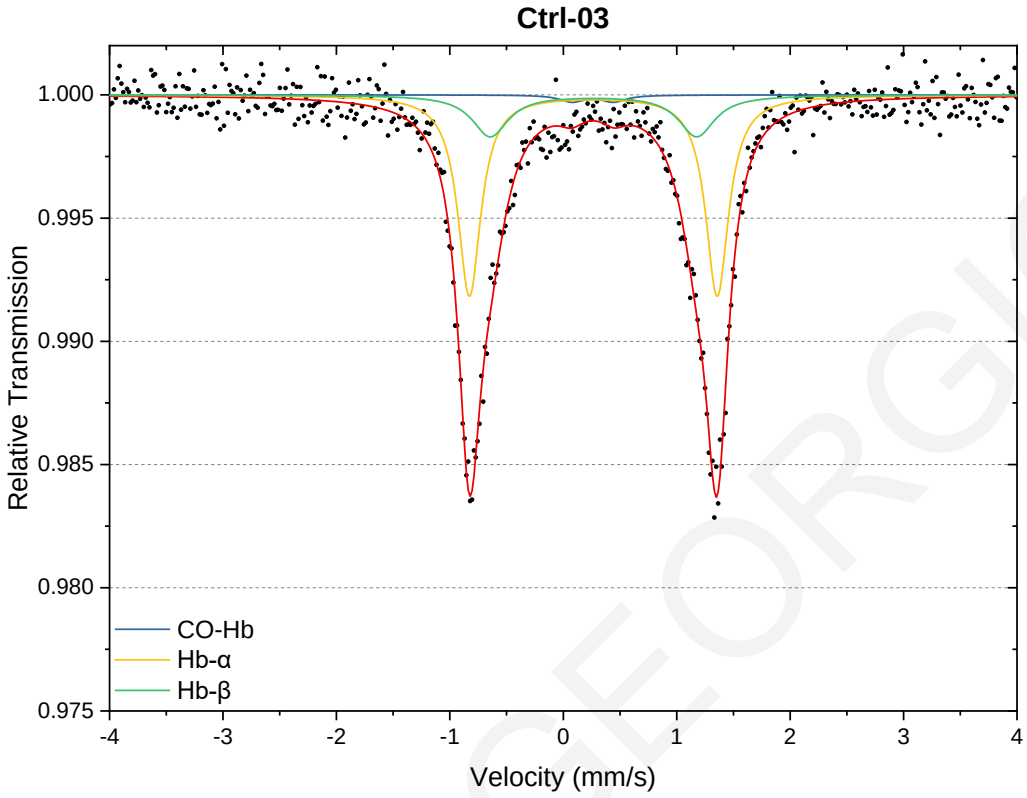

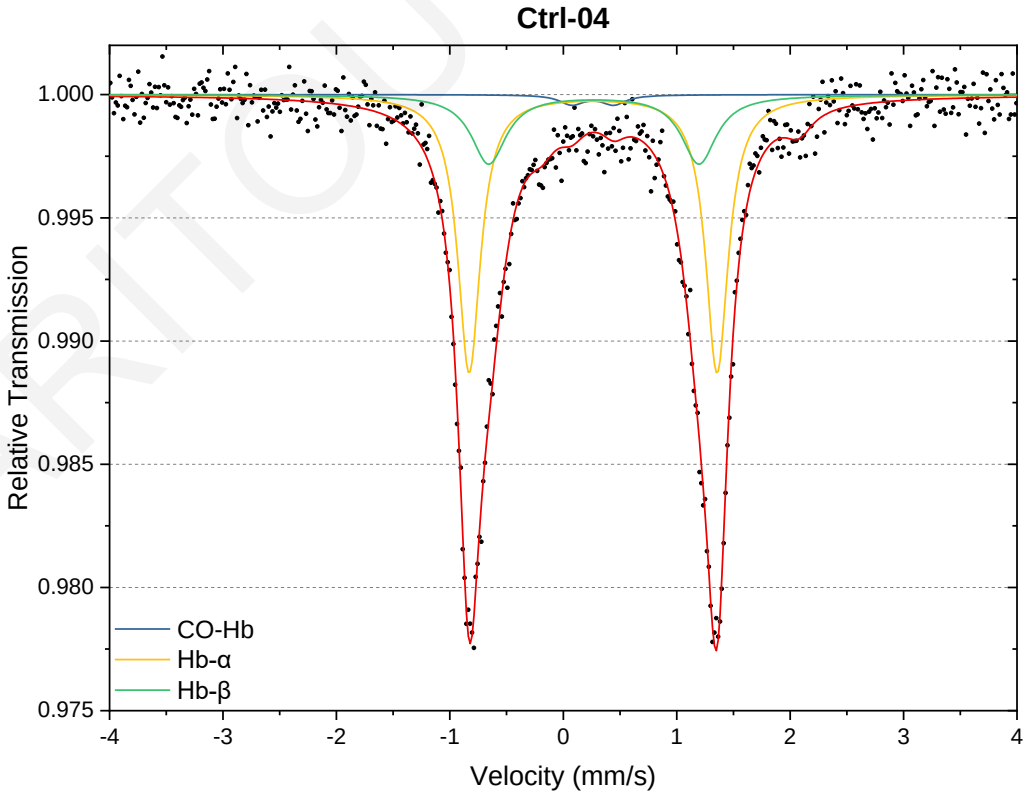

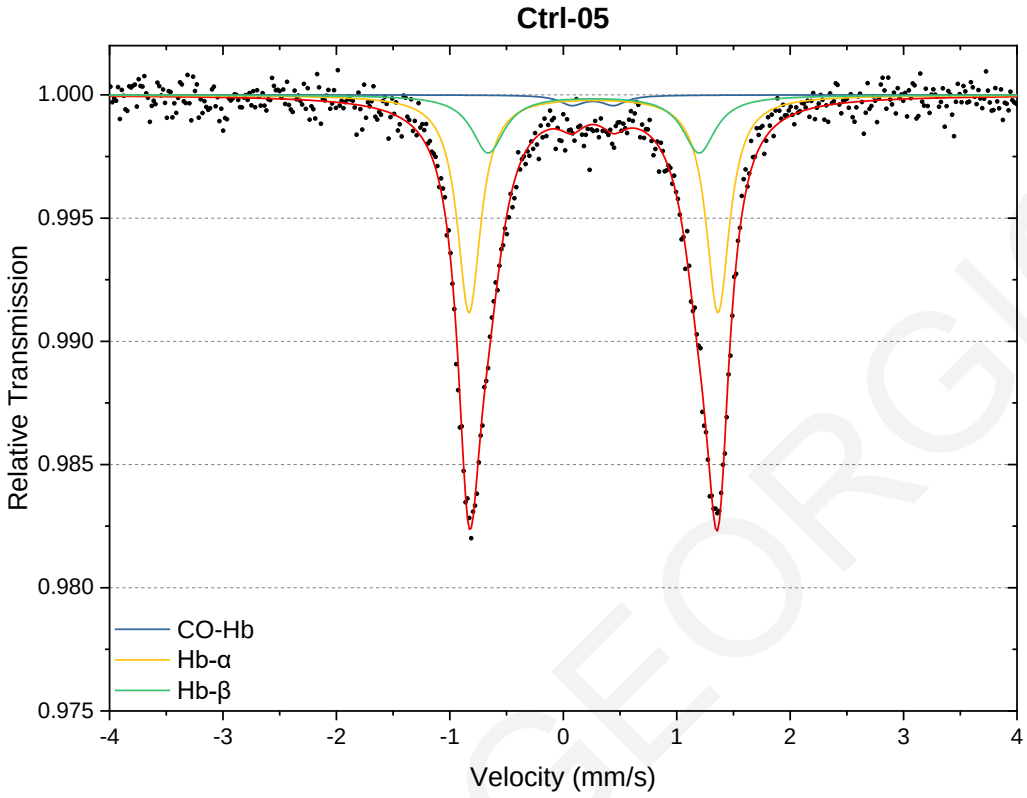

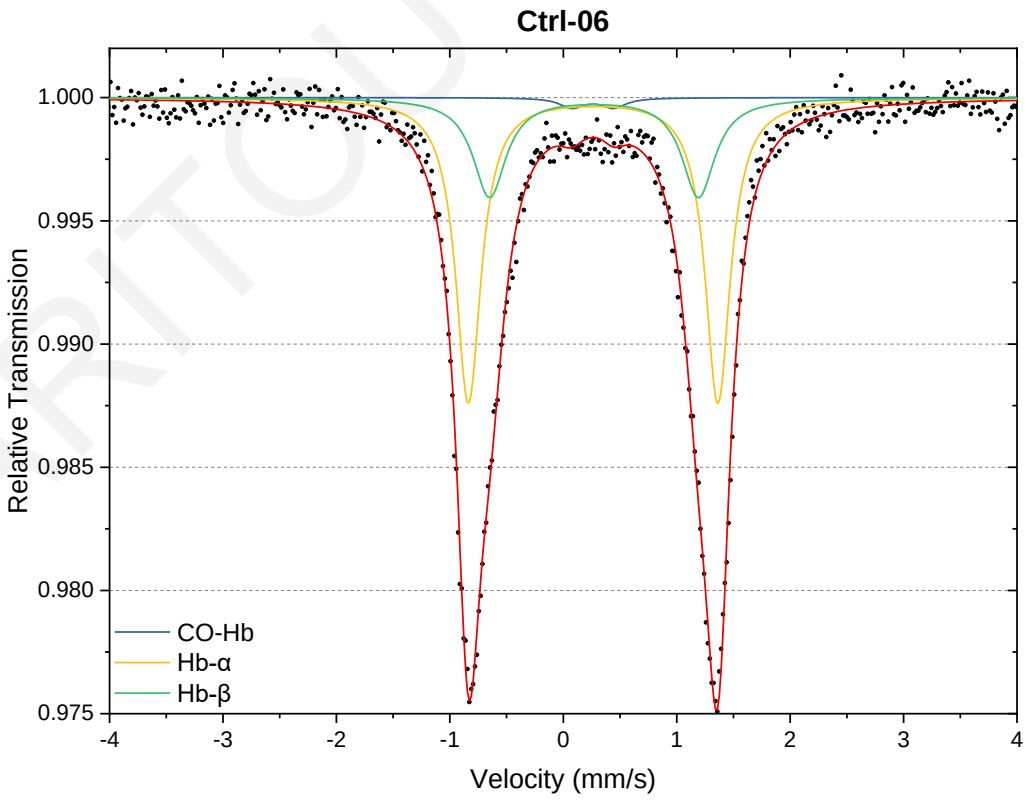

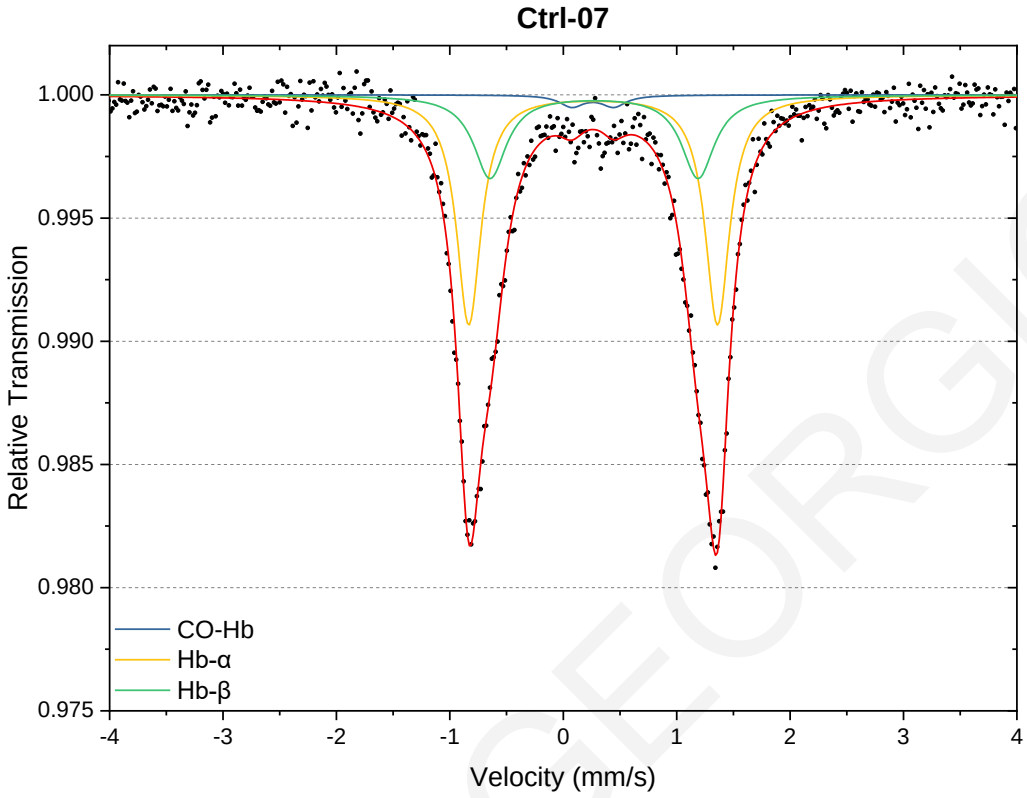

Thalassaemia Major Patients

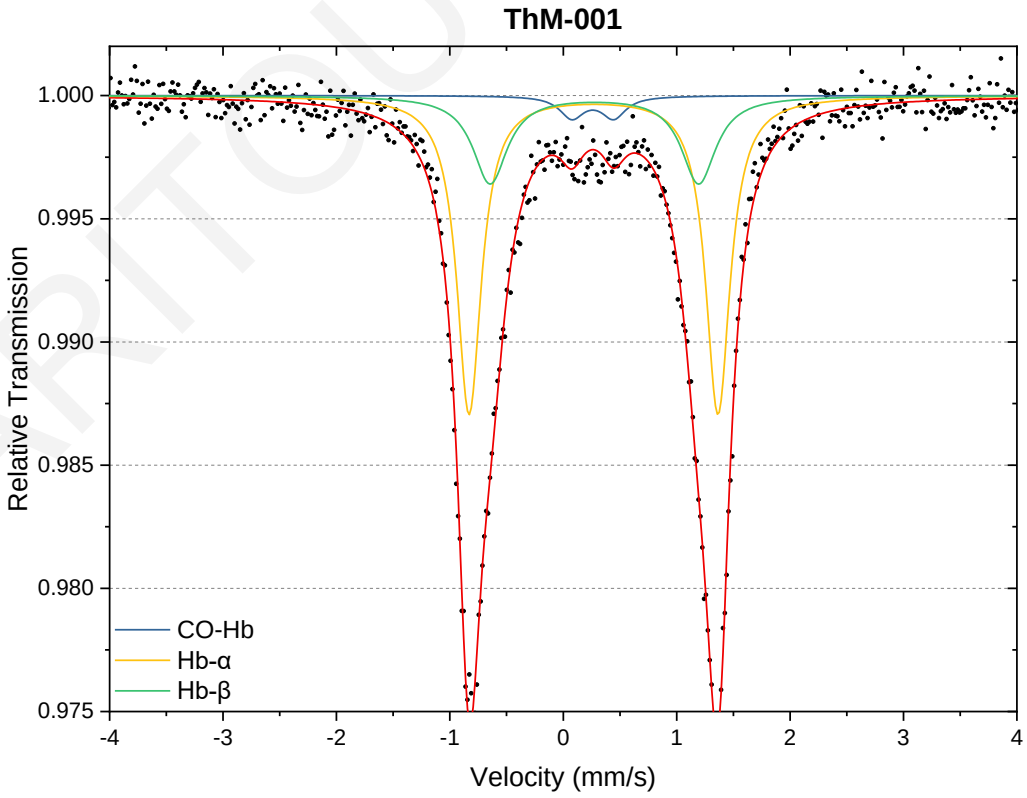

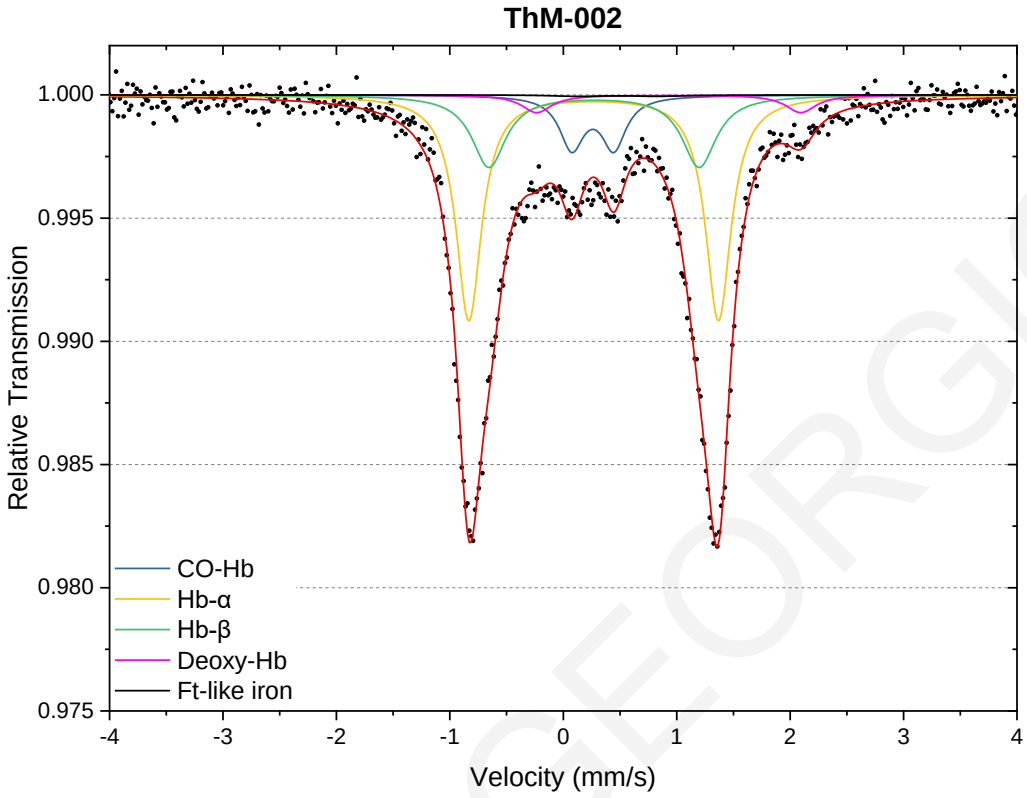

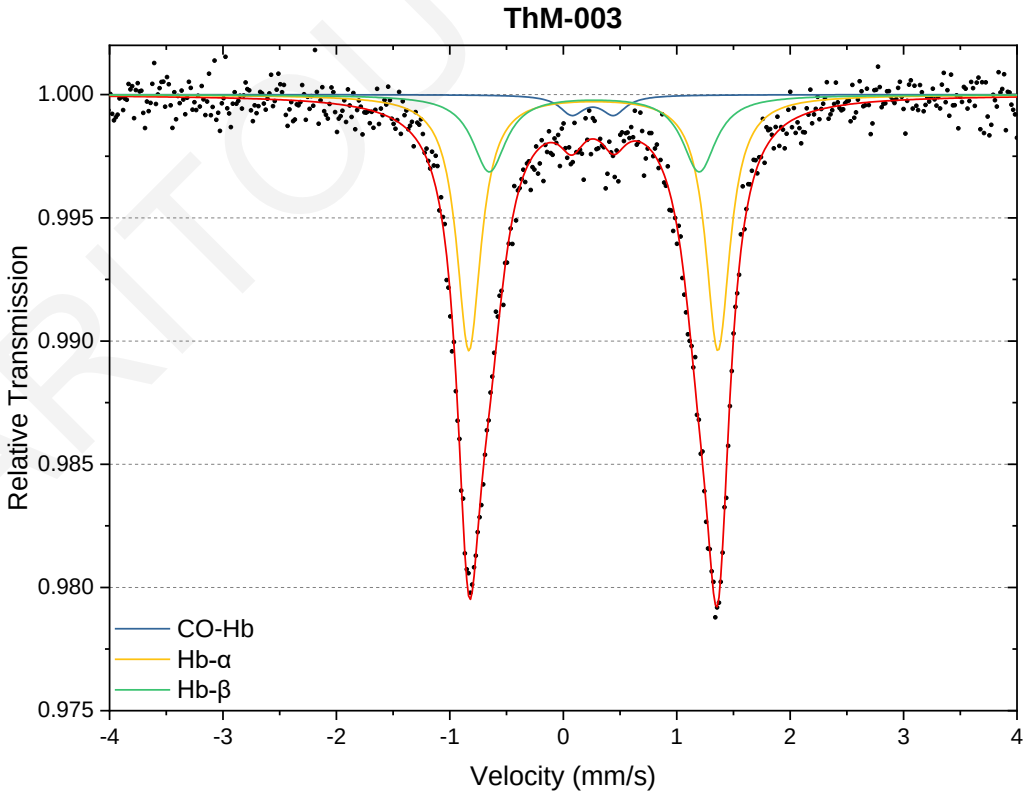

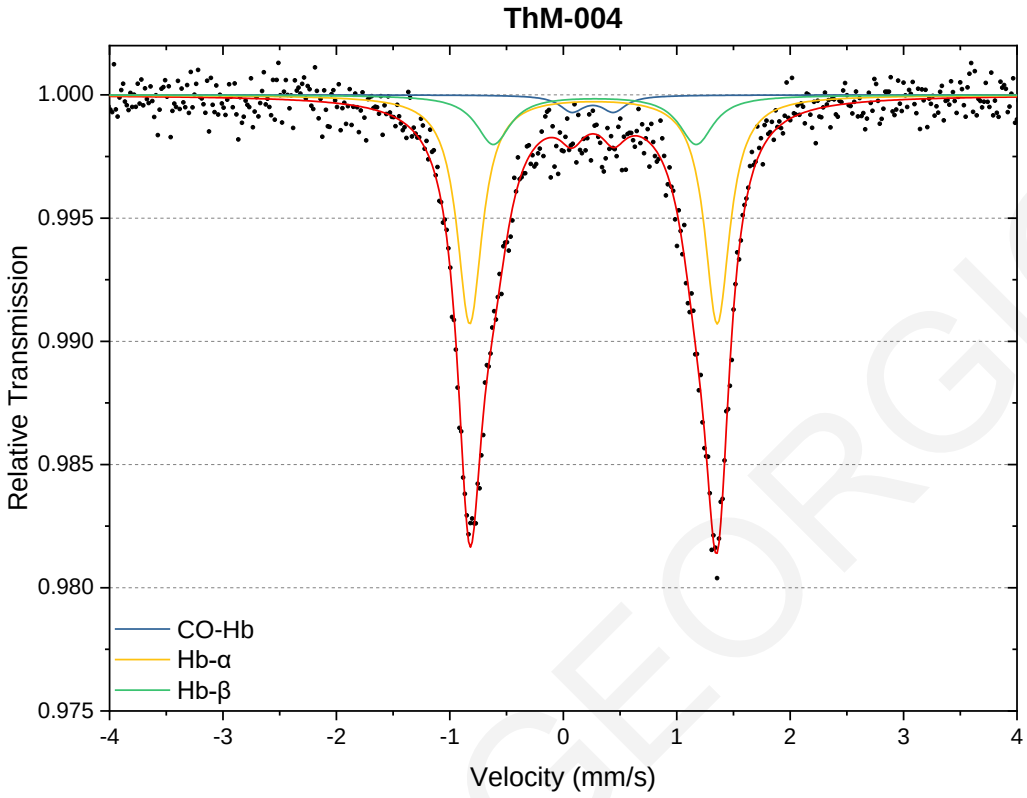

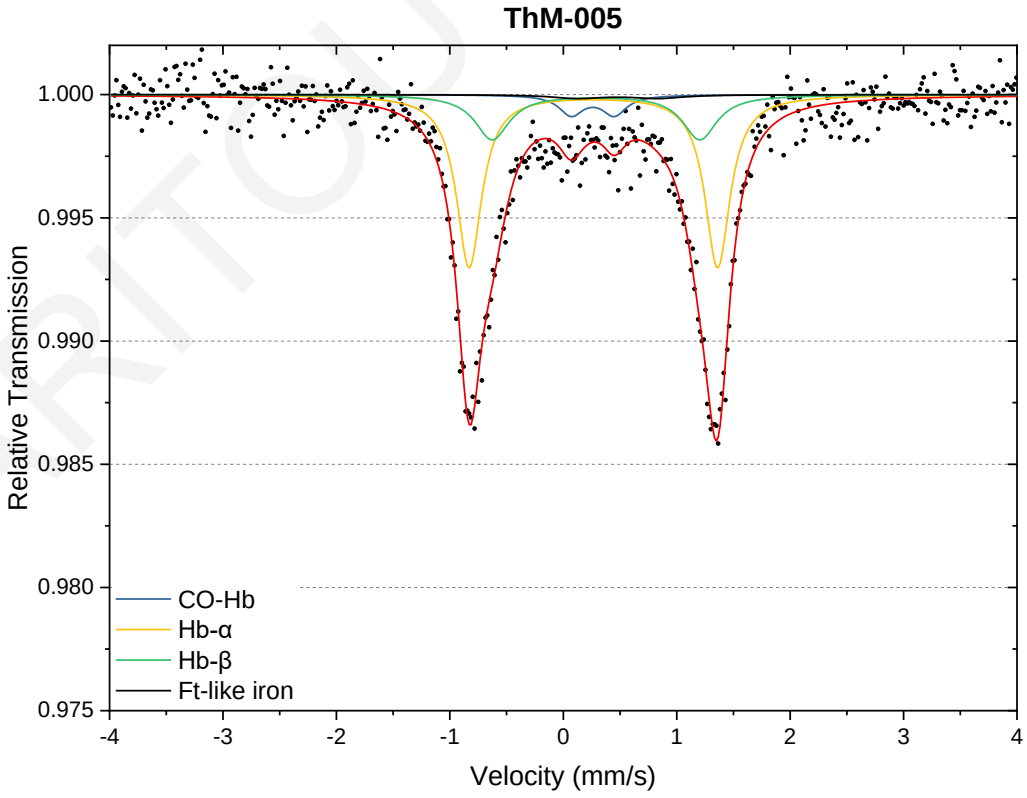

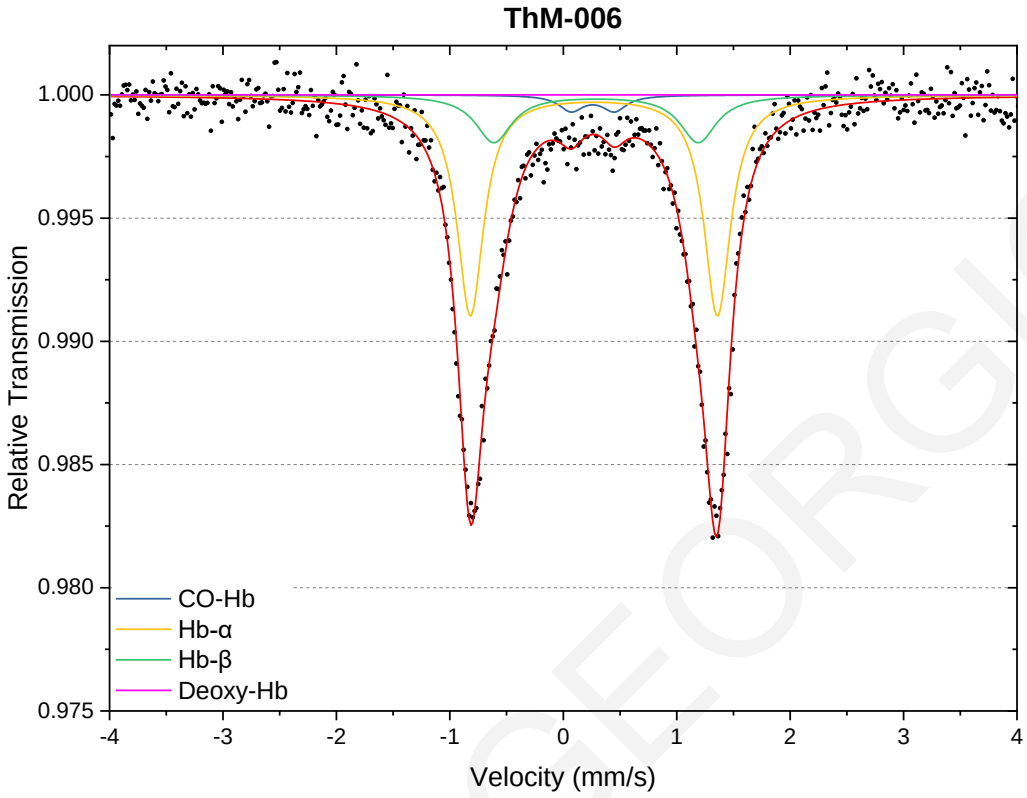

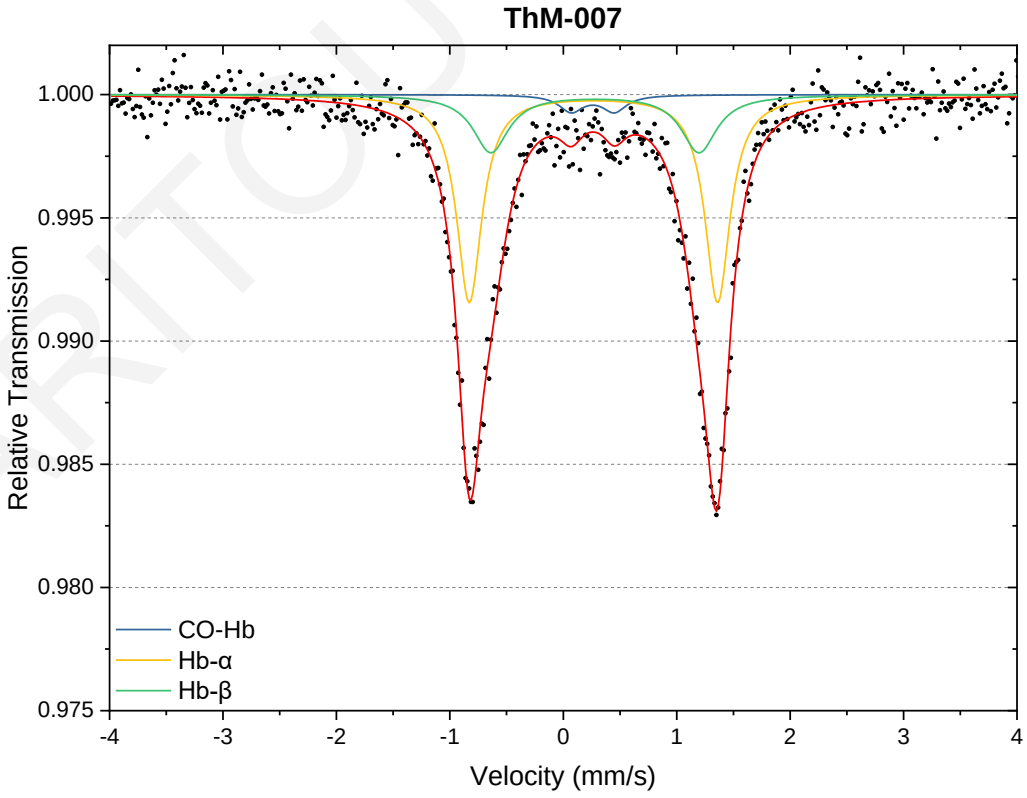

Thalassaemia Intermedia Patients

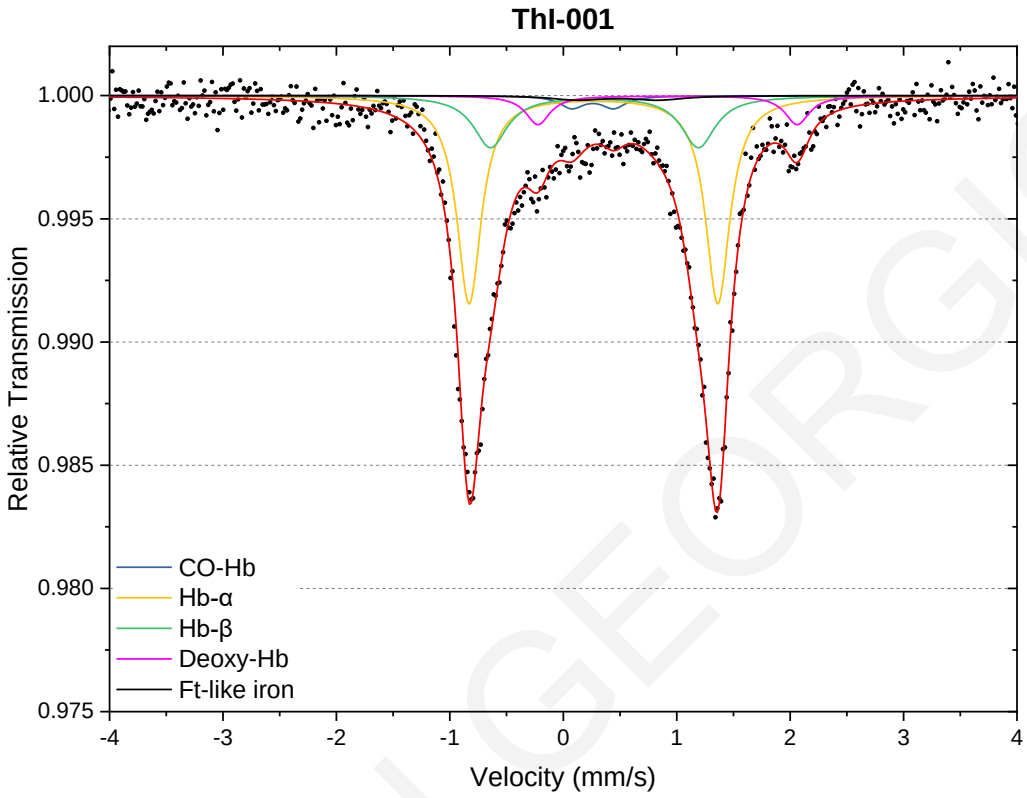

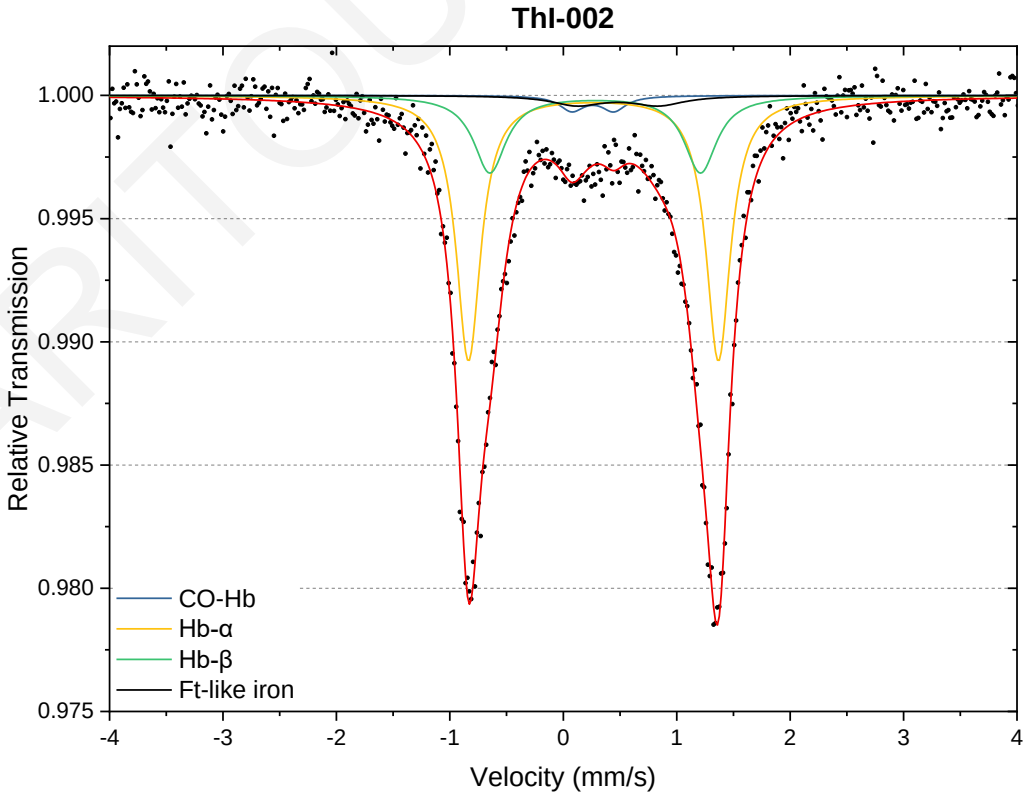

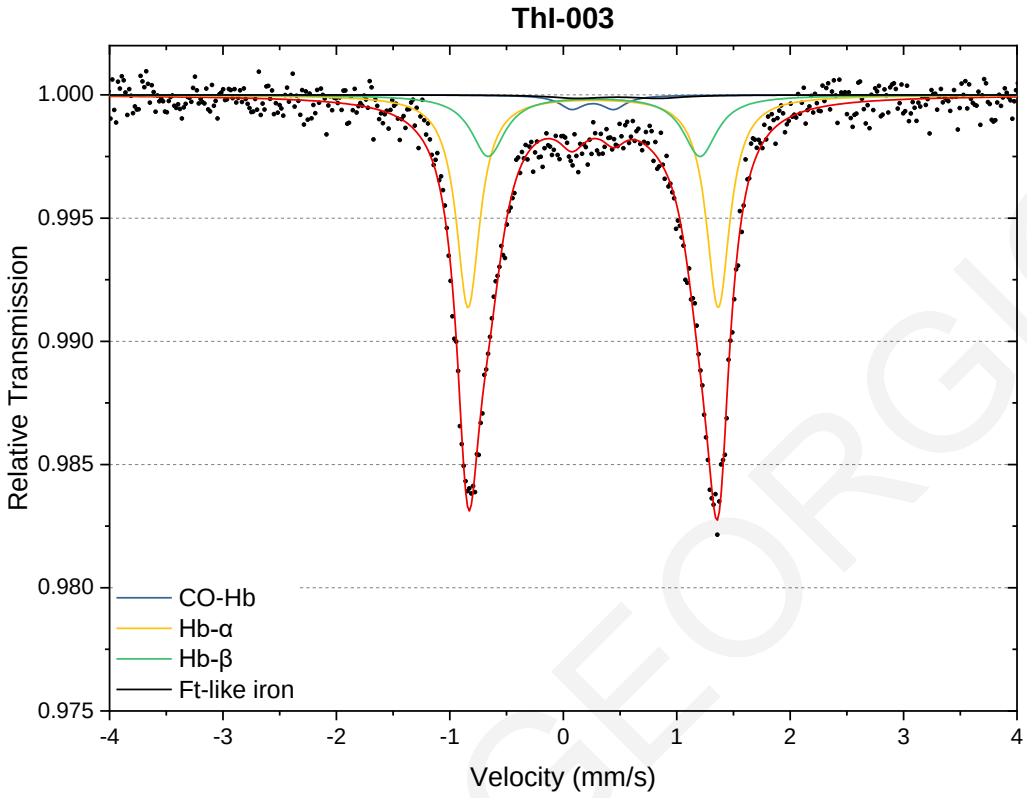

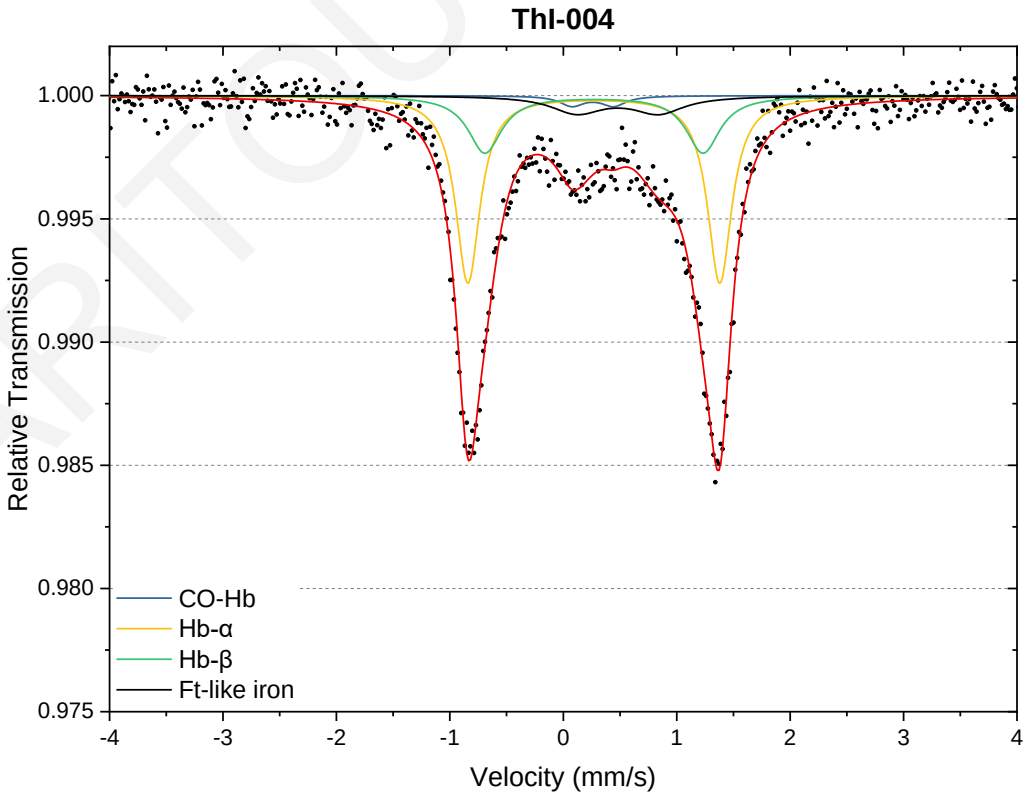

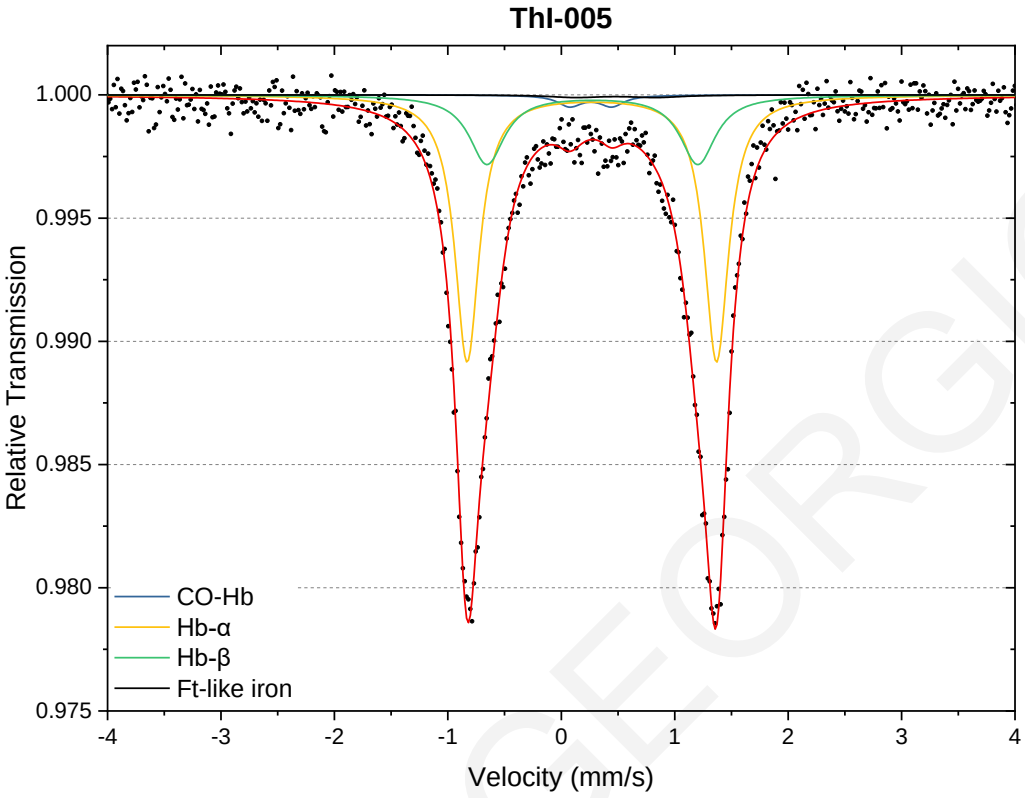

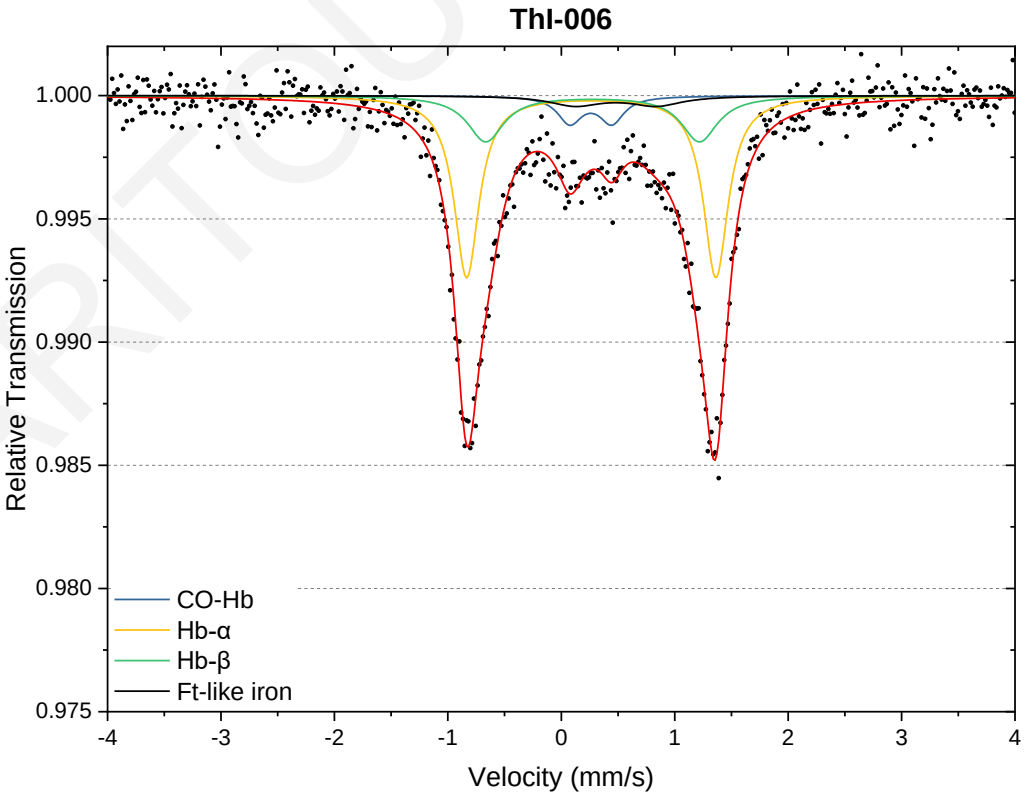

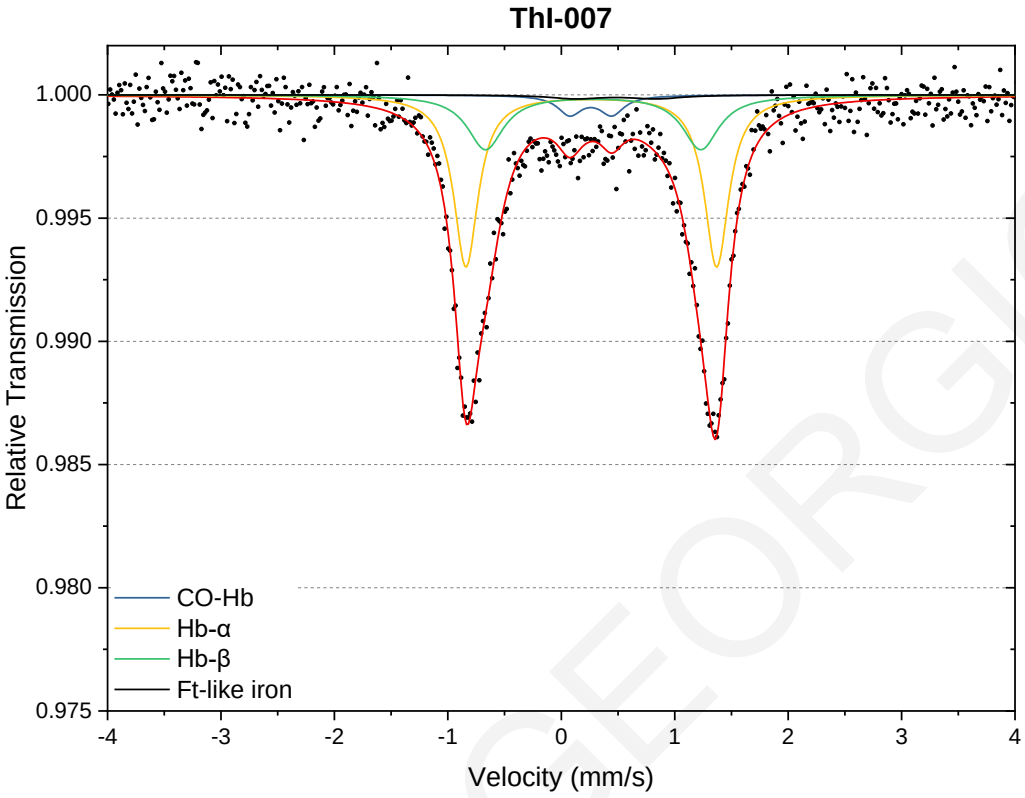

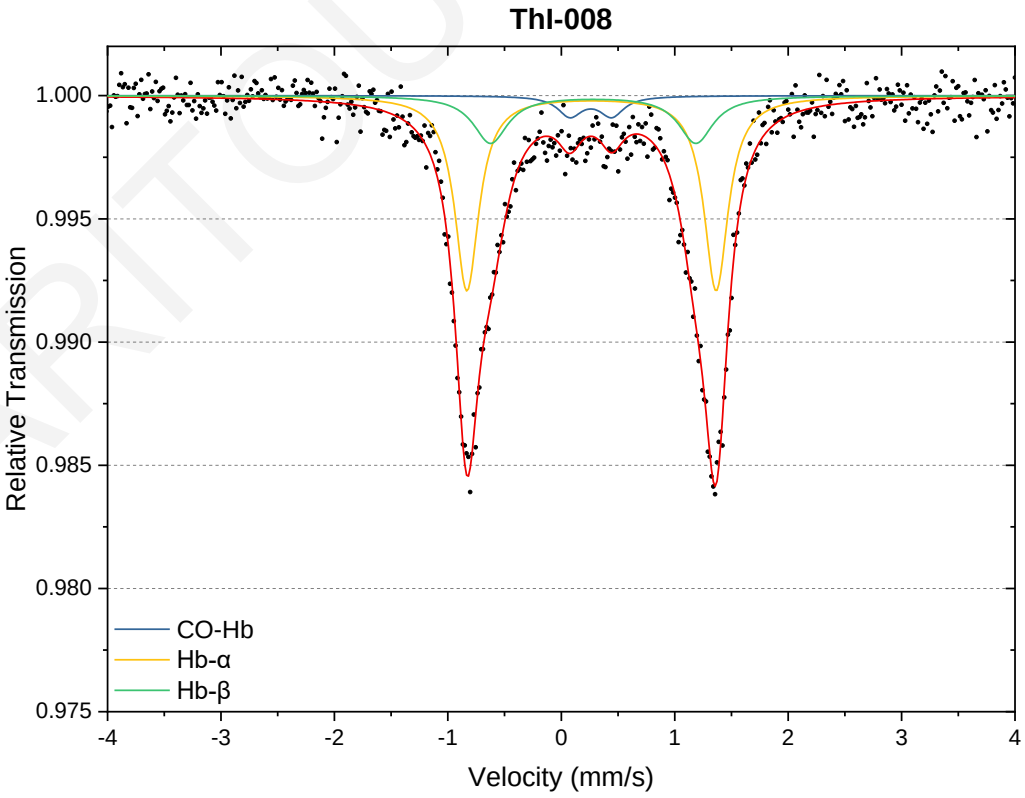

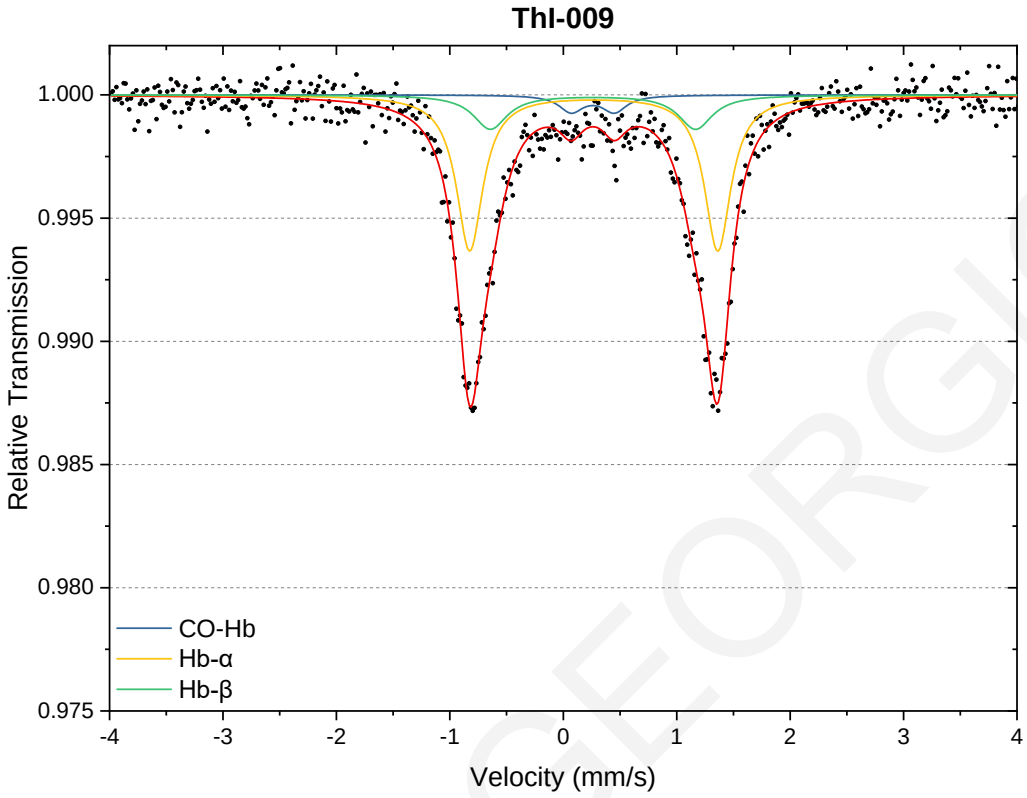

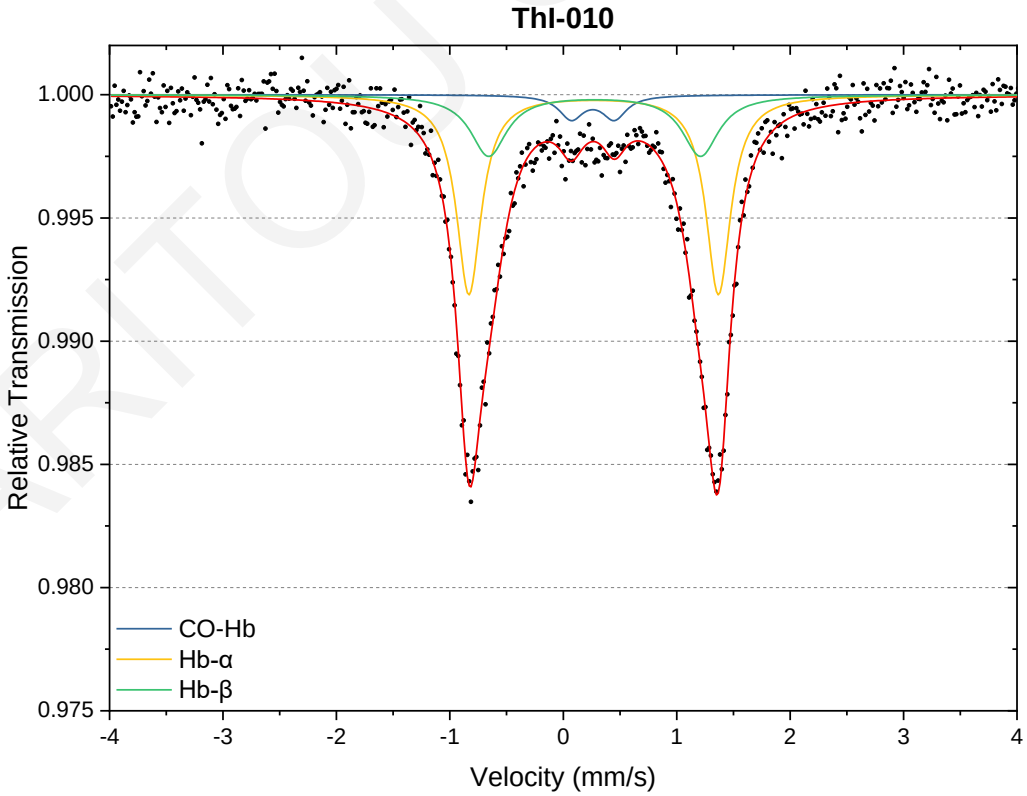

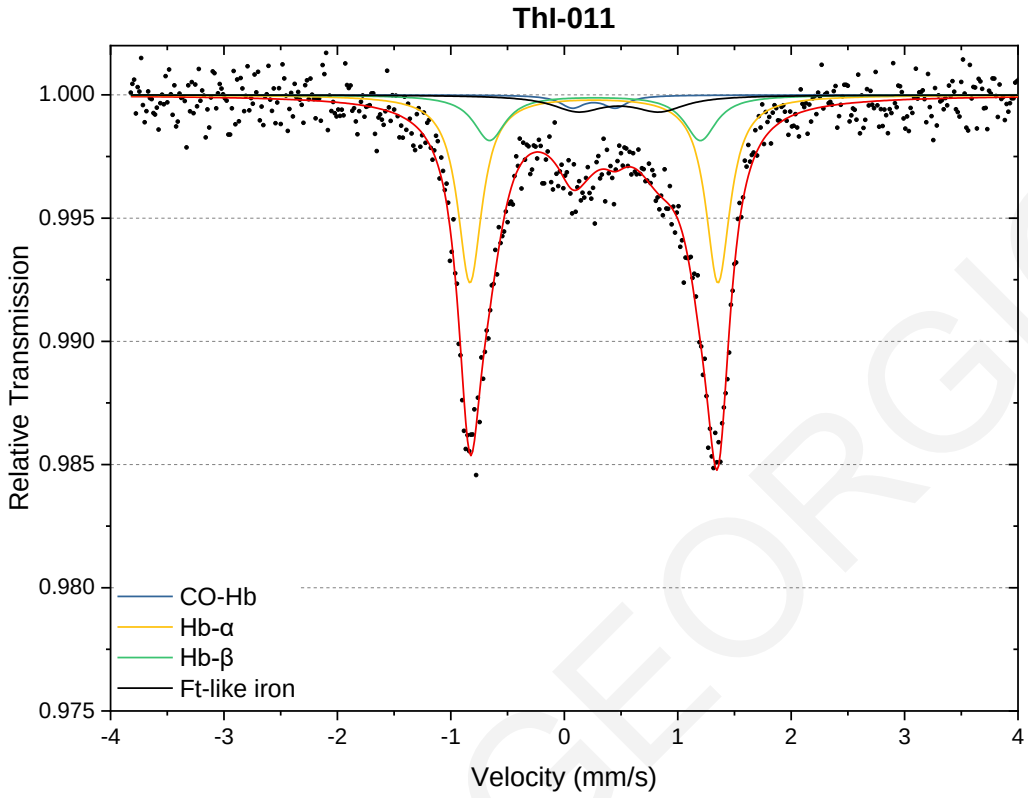

Appendix III:
Extracted Mössbauer Parameters

***Table 0.1**: Mössbauer parameters extracted from the spectra of mice **hearts**. The experimental error is <0.03mm/s. The error shown is the statistical error from the fit. Values without error where fixed.*

	Age	Component	Relative Percentage (%)	Doublet's Area	Γ (mm/s)	δ (mm/s)	ΔEq (mm/s)
+/+	1	Deoxy-Hb	43	0.0118±0.002	0.32±0.01	0.91	2.28
		Ft, Inner iron	0	0		0.46	0.59
		Ft, surface iron	55	0.0151±0.0002	0.43±0.01	0.46	1.05
		NHHS Fe(II)	0				
		Blood residues	2	0.0004±0.0001	0.3	0.27	2.1
+/+	3	Deoxy-Hb	43	0.0179±0.0002	0.34±0.01	0.91	2.28
		Ft, Inner iron	8	0.0032±0.0003	0.38±0.04	0.46	0.59
		Ft, surface iron	49	0.0205±0.0005	0.47±0.01	0.46	1.05
		NHHS Fe(II)	0				
+/+	6	Deoxy-Hb	30	0.0075±0.0002	0.34±0.01	0.91	2.28
		Ft, Inner iron	14	0.0035±0.0002	0.42	0.46	0.59
		Ft, surface iron	56	0.0134±0.0002	0.44	0.46	1.05
		NHHS Fe(II)	0				
+/+	9	Deoxy-Hb	33	0.0170±0.0002	0.33±0.01	0.91	2.28
		Ft, Inner iron	17	0.0084±0.0003	0.42	0.46	0.59
		Ft, surface iron	50	0.0254±0.0005	0.47±0.01	0.46	1.05
		NHHS Fe(II)	0				
th3/+	1	Deoxy-Hb	33	0.0098±0.0002	0.32±0.01	0.91	2.28
		Ft, Inner iron	6	0.0017±0.0002	0.45	0.46	0.59
		Ft, surface iron	60	0.0180±0.0002	0.45	0.46	1.05
		NHHS Fe(II)	0				
		Blood residues	3	0.0008±0.0001	0.3	0.27	2.1
th3/+	3	Deoxy-Hb	28	0.0102±0.0003	0.32±0.01	0.91	2.28
		Ft, Inner iron	15	0.0056±0.0004	0.42±0.03	0.46	0.59
		Ft, surface iron	52	0.0191±0.0005	0.48±0.01	0.46	1.05
		NHHS Fe(II)	4	0.0015±0.0002	0.5	1.36	2.9
th3/+	6	Deoxy-Hb	26	0.0136±0.0003	0.32±0.01	0.91	2.28
		Ft, Inner iron	19	0.0100±0.0005	0.42±0.02	0.46	0.59
		Ft, surface iron	56	0.0294±0.0006	0.47±0.01	0.46	1.05
		NHHS Fe(II)	0				
th3/+	9	Deoxy-Hb	37	0.0162±0.0002	0.34±0.01	0.91	2.28
		Ft, Inner iron	19	0.0084±0.0004	0.42±0.02	0.46	0.59
		Ft, surface iron	43	0.0188±0.0005	0.45±0.01	0.46	1.05
		NHHS Fe(II)	0				

Table 0.2: *Mössbauer parameters extracted from the spectra of mice **kidneys**. The experimental error is <0.03mm/s. The error shown is the statistical error from the fit. Values without error where fixed*

	Age	Component	Relative Percentage (%)	Doublet's Area	Γ (mm/s)	δ (mm/s)	ΔEq (mm/s)
+/+	1	Deoxy-Hb	53	0.0106±0.0002	0.32±0.01	0.91	2.28
		Ft, Inner iron	5	0.0010±0.0002	0.40	0.46	0.59
		Ft, surface iron	38	0.0075±0.0004	0.40±0.02	0.46	1.05
		NHHS Fe(II)	0				
		Blood residues	5	0.0009±0.0001	0.30	0.27	2.10
+/+	3	Deoxy-Hb	53	0.0157±0.0002	0.32±0.01	0.91	2.28
		Ft, Inner iron	6	0.0016±0.0002	0.42	0.46	0.59
		Ft, surface iron	37	0.0108±0.0003	0.43±0.01	0.46	1.05
		NHHS Fe(II)	5	0.0014±0.0001	0.40	1.36	2.90
+/+	6	Deoxy-Hb	45	0.0113±0.0002	0.32±0.01	0.91	2.28
		Ft, Inner iron	9	0.0021±0.0004	0.45±0.09	0.46	0.59
		Ft, surface iron	46	0.0116±0.0005	0.44±0.02	0.46	1.05
		NHHS Fe(II)	0				
+/+	9	Deoxy-Hb	42	0.0183±0.0002	0.32±0.01	0.92±0.01	2.28
		Ft, Inner iron	16	0.0069±0.0004	0.42±0.02	0.45±0.01	0.59
		Ft, surface iron	38	0.0163±0.0005	0.43±0.01	0.46±0.01	1.05
		NHHS Fe(II)	4	0.0018±0.0002	0.50	1.36	2.90±0.05
th3/+	1	Deoxy-Hb	22	0.0045±0.0002	0.32±0.02	0.91	2.28
		Ft, Inner iron	26	0.0053±0.0004	0.42±0.02	0.46	0.59
		Ft, surface iron	47	0.0097±0.0006	0.50±0.02	0.46	1.05
		NHHS Fe(II)	6	0.0013±0.0004	0.58±0.18	1.1±0.06	2.94±0.11
th3/+	3	Deoxy-Hb	7	0.0061±0.0003	0.26±0.01	0.91	2.28
		Ft, Inner iron	52	0.0491±0.0005	0.41±0.01	0.46	0.59
		Ft, surface iron	35	0.0328±0.0006	0.46±0.01	0.46	1.05
		NHHS Fe(II)	6	0.0060±0.0003	0.50	1.36	2.90
th3/+	6	Deoxy-Hb	3	0.0055±0.0002	0.27±0.01	0.91	2.28
		Ft, Inner iron	61	0.1074±0.0004	0.43±0.01	0.46	0.59
		Ft, surface iron	36	0.0632±0.0005	0.46±0.01	0.46	1.05
		NHHS Fe(II)	1	0.0015±0.0002	0.50	1.36	2.90±0.02
th3/+	9	Deoxy-Hb	4	0.0056±0.0002	0.30	0.91	2.28
		Ft, Inner iron	62	0.0931±0.0006	0.44±0.01	0.47±0.01	0.59
		Ft, surface iron	32	0.0486±0.0007	0.45±0.01	0.45±0.01	1.05
		NHHS Fe(II)	2	0.0037±0.0003	0.50	1.36	2.90

Table 0.3: *Mössbauer parameters extracted from the spectra of mice **brains**. The experimental error is <0.03mm/s. The error shown is the statistical error from the fit. Values without error where fixed*

	Age	Component	Relative Percentage (%)	Doublet's Area	Γ (mm/s)	δ (mm/s)	ΔEq (mm/s)
+/+	9	Deoxy-Hb	14	0.0019±0.0002	0.26±0.03	0.91	2.28
		Ft, Inner iron	32	0.0044±0.0004	0.40±0.03	0.44±0.01	0.59
		Ft, surface iron	52	0.0072±0.0005	0.47±0.03	0.46±0.01	1.05
		NHHS Fe(II)	3	0.0004±0.0002	0.5	1.36	2.90
th3/+	9	Deoxy-Hb	14	0.0017±0.0002	0.35±0.05	0.93±0.02	2.27±0.03
		Ft, Inner iron	37	0.0046±0.0004	0.46±0.03	0.46±0.01	0.59
		Ft, surface iron	47	0.0058±0.0004	0.49±0.04	0.11±0.01	1.05
		NHHS Fe(II)	3	0.0004±0.0002	0.5	1.36	2.90

Table 0.4: *Mössbauer parameters extracted from the spectra of mice **livers**. The experimental error is <0.03mm/s. The error shown is the statistical error from the fit. Values without error where fixed*

	Age	Component	Relative Percentage (%)	Doublet's Area	Γ (mm/s)	Δ (mm/s)	ΔEq (mm/s)
+/+	1	Deoxy-Hb	41	0.0061±0.0002	0.33±0.01	0.91	2.28
		Ft, Inner iron	2	0.0003±0.0003	0.40	0.46	0.59
		Ft, surface iron	40	0.006±0.0004	0.50±0.03	0.46	1.05
		NHHS Fe(II)	17	0.0026±0.0003	0.54±0.08	1.34±0.02	2.82±0.05
+/+	3	Deoxy-Hb	28	0.0148±0.0003	0.34±0.01	0.91	2.28
		Ft, Inner iron	25	0.0137±0.0003	0.41±0.01	0.46	0.59
		Ft, surface iron	23	0.0125±0.0004	0.39±0.01	0.46	1.05
		NHHS Fe(II)	24	0.0130±0.0004	0.64±0.02	1.36	2.90
+/+	6	Deoxy-Hb	14	0.0095±0.0003	0.34±0.01	0.91	2.28
		Ft, Inner iron	41	0.0280±0.0004	0.42±0.01	0.46	0.59
		Ft, surface iron	31	0.0210±0.0005	0.42±0.01	0.46	1.05
		NHHS Fe(II)	14	0.0097±0.0006	0.69±0.04	1.36	2.90
+/+	9	Deoxy-Hb	20	0.0137±0.0003	0.37±0.01	0.92±0.01	2.28
		Ft, Inner iron	40	0.0278±0.0005	0.42±0.01	0.46±0.01	0.59
		Ft, surface iron	34	0.0232±0.0006	0.43±0.01	0.45±0.01	1.05
		NHHS Fe(II)	6	0.0044±0.0002	0.50	1.36	2.90±0.03
th3/+	1	Deoxy-Hb	25	0.0072±0.0003	0.33±0.01	0.91	2.28
		Ft, Inner iron	30	0.0087±0.0004	0.43±0.02	0.46	0.59
		Ft, surface iron	30	0.0087±0.0005	0.39±0.02	0.46	1.05
		NHHS Fe(II)	16	0.0046±0.0005	0.68±0.08	1.38±0.02	2.88±0.05
th3/+	3	Deoxy-Hb	7	0.0111±0.0005	0.34±0.02	0.91	2.28
		Ft, Inner iron	55	0.0860±0.0006	0.41±0.01	0.46	0.59
		Ft, surface iron	29	0.0452±0.0008	0.41±0.01	0.46	1.05
		NHHS Fe(II)	9	0.0148±0.0007	0.52±0.03	1.29±0.01	3.08
th3/+	6	Deoxy-Hb	2	0.0059±0.0005	0.32±0.03	0.91	2.28
		Ft, Inner iron	58	0.1378±0.0009	0.43±0.01	0.46	0.59
		Ft, surface iron	37	0.0877±0.0011	0.48±0.01	0.46	1.05
		NHHS Fe(II)	3	0.0062±0.0004	0.50	1.36	2.90
th3/+	9	Deoxy-Hb	2	0.0060±0.0003	0.33	0.91	2.28
		Ft, Inner iron	6	0.1696±0.0006	0.45±0.01	0.47±0.01	0.59
		Ft, surface iron	35	0.0994±0.0008	0.49±0.01	0.45±0.01	1.05
		NHHS Fe(II)	3	0.0098±0.0007	0.66±0.04	1.36	2.90

Table 0.5: *Mössbauer parameters extracted from the spectra of mice* ***spleens****. The experimental error is <0.03mm/s. The error shown is the statistical error from the fit. Values without error where fixed*

Group	Age	Component	Relative Percentage (%)	Doublet's Area	Γ (mm/s)	δ (mm/s)	ΔEq (mm/s)	HMF (T)
+/+	1	Deoxy-Hb	64	0.0219±0.0002	0.33±0.01	0.91	2.28	-
		Ft, Inner iron sites	14	0.0047±0.0002	0.42±0.02	0.46	0.59	-
		Ft, surface iron sites	16	0.0055±0.0002	0.40	0.46	1.05	-
		NHHS Fe(II)	0					
		Blood residues	7	0.0024±0.0001	0.26	0.27	2.10	-
+/+	3	Deoxy-Hb	20	0.0200±0.0002	0.32±0.01	0.91	2.28	-
		Ft, Inner iron sites	54	0.0542±0.0003	0.42±0.01	0.46	0.59	-
		Ft, surface iron sites	21	0.0207±0.0005	0.39±0.01	0.46	1.05	-
		NHHS Fe(II)	0					
		Blood residues	6	0.0060±0.0002	0.32±0.01	0.27	2.10	-
+/+	6	Deoxy-Hb	14	0.0266±0.0004	0.33±0.01	0.91	2.28	-
		Ft, Inner iron sites	59	0.1154±0.0008	0.46±0.01	0.46	0.59	-
		Ft, surface iron sites	27	0.0528±0.0010	0.50±0.01	0.46	1.05	-
		NHHS Fe(II)	0					
+/+	9	Deoxy-Hb	12	0.0369±0.0004	0.37±0.01	0.90±0.01	2.30±0.01	-
		Ft, Inner iron sites	62	0.1934±0.0008	0.47±0.01	0.47±0.01	0.59	-
		Ft, surface iron sites	26	0.0816±0.0010	0.49±0.01	0.45±0.01	1.05	-
		NHHS Fe(II)	0					
th3/+	1	Deoxy-Hb	42	0.0332±0.0002	0.32	0.92	2.29	-
		Ft, Inner iron sites	35	0.0274±0.0003	0.40±0.01	0.46	0.59	-
		Ft, surface iron sites	21	0.0164±0.0003	0.44	0.46	1.05	-

		NHHS Fe(II)	0					
		Blood residues	1	0.0007±0.0002	0.30	0.27	2.10	-
		Haemosiderin	0					-
th3/+	3	Deoxy-Hb	10	0.0422±0.0004	0.35±0.01	0.91	2.28	-
		Ft, Inner iron sites	62	0.2564±0.0007	0.48±0.01	0.48±0.01	0.59	-
		Ft, surface iron sites	26	0.1094±0.0009	0.50±0.01	0.45±0.01	1.05	-
		NHHS Fe(II)	2	0.0067±0.0004	0.41±0.03	1.36	2.90	-
		Haemosiderin	0					-
th3/+	6	Deoxy-Hb	7	0.0366±0.0004	0.33	0.91	2.28	-
		Ft, Inner iron sites	53	0.2931±0.0007	0.52±0.01	0.48±0.01	0.59	-
		Ft, surface iron sites	23	0.1261±0.0008	0.52	0.45±0.01	1.05	-
		NHHS Fe(II)	1	0.0045±0.0006	0.50	1.36	2.90	-
		Haemosiderin	17	0.0957±0.0050	1.37±0.06	0.48±0.01	-0.25	45.91±0.11
th3/+	9	Deoxy-Hb	3	0.2201±0.0006	0.30	0.91	2.28	-
		Ft, Inner iron sites	51	0.3546±0.0010	0.59±0.01	0.48±0.01	0.59	-
		Ft, surface iron sites	23	0.1621±0.0011	0.59	0.45±0.01	1.05	-
		NHHS Fe(II)	1	0.0090±0.0007	0.50	1.36	2.90	-
		Haemosiderin	22	0.1546±0.0052	1.15±0.03	0.48±0.01	-0.25	45.91±0.06

Table 0.6: MS parameters of the spectra from the RBCs of healthy volunteers (Ctrl), β-thalassaemia intermedia (Thl), β-thalassaemia major (ThM) and H-disease (HbH). The experimental error is <0.03mm/s. The error shown is the statistical error from the fit. Values without error where fixed.

Sample	Component	Relative Percentage (%)	Γ (mm/s)	δ (mm/s)	ΔEq (mm/s)
Ctrl-001	Hb-α	64±3	0.25	0.27±0.01	2.20±0.01
	Hb-β	31±4	0.33±0.03	0.27±0.01	1.85±0.03
	CO-Hb	5±1	0.26	0.26	0.37
	Deoxy-Hb	0			
	Ft-like iron	0	0.55	0.48	0.72
Ctrl-003	Hb-α	61±2	0.26±0.01	0.27±0.01	2.18±0.01
	Hb-β	26±2	0.37±0.02	0.27±0.01	1.83
	CO-Hb	4±1	0.26	0.26	0.37
	Deoxy-Hb	10±1	0.27±0.03	0.92±0.01	2.34±0.02
	Ft-like iron	0			
Ctrl-006	Hb-α	65±2	0.25±0.01	0.26±0.01	2.18±0.01
	Hb-β	33±2	0.39±0.02	0.27±0.01	1.82
	CO-Hb	2±1	0.26	0.26	0.37
	Deoxy-Hb	0			
	Ft-like iron	0	0.55	0.48	0.72
Ctrl-009	Hb-α	59±6	0.24±0.01	0.26±0.01	2.19±0.01
	Hb-β	35±6	0.37±0.03	0.27±0.01	1.85±0.04
	CO-Hb	2±1	0.26	0.26	0.37
	Deoxy-Hb	4±1	0.3	0.94±0.04	2.26±0.09
	Ft-like iron	0			
Ctrl-010	Hb-α	64±2	0.25	0.27±0.01	2.19±0.01
	Hb-β	33±3	0.35±0.02	0.27±0.01	1.86±0.02
	CO-Hb	3	0.26	0.26	0.37
	Deoxy-Hb	0			
	Ft-like iron	0	0.55	0.48	0.72
Ctrl-011	Hb-α	63±3	0.27±0.01	0.26±0.01	2.20±0.01
	Hb-β	35±4	0.35±0.01	0.27±0.01	1.84±0.02
	CO-Hb	2±1	0.26	0.26	0.37
	Deoxy-Hb	0			
	Ft-like iron	0			
Ctrl-012	Hb-α	58±5	0.26±0.01	0.26±0.01	2.19±0.01
	Hb-β	39±5	0.35±0.02	0.27±0.01	1.83±0.02
	CO-Hb	3±1	0.26	0.26	0.37
	Deoxy-Hb	0			
	Ft-like iron	0	0.55	0.48	0.72
Thl-001	Hb-α	57±2	0.26	0.27±0.01	2.19±0.01
	Hb-β	27±3	0.36±0.03	0.27±0.01	1.83±0.02
	CO-Hb	3±1	0.26	0.26	0.37
	Deoxy-Hb	8±1	0.26	0.92±0.01	2.29±0.02
	Ft-like iron	5±2	0.55	0.48	0.72
Thl-002	Hb-α	58±2	0.26	0.27±0.01	2.2±0.01
	Hb-β	30±2	0.35±0.02	0.28±0.01	1.86±0.02
	CO-Hb	3±1	0.26	0.26	0.37

	Deoxy-Hb	0			
	Ft-like iron	9±1	0.55	0.48	0.72
ThI-003	Hb-α	58±7	0.25±0.01	0.26±0.01	2.20±0.01
	Hb-β	34±8	0.36±0.03	0.27±0.01	1.87±0.04
	CO-Hb	4±1	0.26	0.26	0.37
	Deoxy-Hb	0			
	Ft-like iron	4±2			
ThI-004	Hb-α	49±3	0.26	0.27±0.01	2.22±0.01
	Hb-β	29±4	0.36±0.03	0.27±0.01	1.92±0.03
	CO-Hb	2±1	0.26	0.26	0.37
	Deoxy-Hb	0			
	Ft-like iron	20±2	0.55	0.48	0.72
ThI-005	Hb-α	61±2	0.26	0.27±0.01	2.20±0.01
	Hb-β	33±3	0.38±0.02	0.27±0.01	1.86±0.02
	CO-Hb	3±1	0.26	0.26	0.37
	Deoxy-Hb	0			
	Ft-like iron	3±2			
ThI-006	Hb-α	52±13	0.26±0.03	0.26±0.01	2.20±0.02
	Hb-β	29±15	0.39±0.05	0.28±0.01	1.88±0.09
	CO-Hb	7±1	0.26	0.26	0.37
	Deoxy-Hb	0			
	Ft-like iron	12±2	0.55	0.48	0.72
ThI-007	Hb-α	52±4	0.26	0.26±0.01	2.21±0.01
	Hb-β	37±6	0.39±0.03	0.28±0.01	1.90±0.04
	CO-Hb	6±1	0.26	0.26	0.37
	Deoxy-Hb	0			
	Ft-like iron	5±2			
ThI-008	Hb-α	62±5	0.26±0.01	0.27±0.01	2.20±0.01
	Hb-β	31±6	0.37±0.03	0.28±0.01	1.81±0.04
	CO-Hb	7±1	0.26	0.26	0.37
	Deoxy-Hb	0			
	Ft-like iron	0	0.55	0.48	0.72
ThI-009	Hb-α	69±8	0.28±0.01	0.27±0.01	2.19±0.01
	Hb-β	25±9	0.36±0.06	0.26±0.01	1.81±0.07
	CO-Hb	6±1	0.26	0.26	0.37
	Deoxy-Hb	0			
	Ft-like iron	0	0.55	0.48	0.72
ThI-010	Hb-α	55±8	0.26±0.01	0.27±0.01	2.20±0.01
	Hb-β	37±9	0.39±0.04	0.28±0.01	1.87±0.05
	CO-Hb	6±1	0.26	0.26	0.37
	Deoxy-Hb	0			
	Ft-like iron	1±1	0.55	0.48	0.72
ThI-011	Hb-α	54±3	0.26	0.26±0.01	2.19±0.01
	Hb-β	23±1	0.34±0.04	0.27±0.01	1.87±0.04
	CO-Hb	3±1	0.26	0.26	0.37
	Deoxy-Hb	0			
	Ft-like iron	20±2	0.55	0.48	0.72

ThM-001	Hb-α	62±4	0.26±0.01	0.27±0.01	2.19±0.01
	Hb-β	34±5	0.37±0.02	0.27±0.01	1.84±0.03
	CO-Hb	4±1	0.26	0.26	0.37
	Deoxy-Hb	0			
	Ft-like iron	0	0.55	0.48	0.72
ThM-002	Hb-α	52±6	0.27±0.01	0.27±0.01	2.20±0.01
	Hb-β	30±7	0.36±0.03	0.27±0.01	1.85±0.04
	CO-Hb	11±1	0.26	0.26	0.37
	Deoxy-Hb	6±1	0.33±0.05	0.93±0.02	2.33±0.03
	Ft-like iron	1±1	0.55	0.48	0.72
ThM-003	Hb-α	61±2	0.26	0.27±0.01	2.20±0.01
	Hb-β	35±3	0.36±0.02	0.27±0.01	1.85±0.02
	CO-Hb	4±1	0.26	0.26	0.37
	Deoxy-Hb	0			
	Ft-like iron	0	0.55	0.48	0.72
ThM-004	Hb-α	68±6	0.27±0.01	0.27±0.01	2.18±0.01
	Hb-β	27±6	0.37±0.04	0.28±0.01	1.79±0.04
	CO-Hb	5±1	0.26	0.26	0.37
	Deoxy-Hb	0			
	Ft-like iron	0	0.55	0.48	0.72
ThM-005	Hb-α	59±3	0.27±0.01	0.27±0.01	2.19±0.01
	Hb-β	29±4	0.37±0.04	0.29±0.01	1.83
	CO-Hb	6±1	0.26	0.26	0.37
	Deoxy-Hb	0			
	Ft-like iron	5±3	0.55	0.48	0.72
ThM-006	Hb-α	68±6	0.28±0.01	0.27±0.01	2.18±0.01
	Hb-β	27±6	0.39±0.04	0.29±0.01	1.8±0.05
	CO-Hb	4±1	0.26	0.26	0.37
	Deoxy-Hb	0			
	Ft-like iron	0	0.55	0.48	0.72
ThM-007	Hb-α	62±8	0.27±0.02	0.27±0.01	2.19±0.01
	Hb-β	34±9	0.38±0.04	0.28±0.01	1.84±0.05
	CO-Hb	5±1	0.26	0.26	0.37
	Deoxy-Hb	0			
	Ft-like iron	0	0.55	0.48	0.72
HbH-001	Hb-α	54±14	0.26±0.03	0.27±0.01	2.20±0.02
	Hb-β	40±14	0.40±0.04	0.28±0.01	1.89±0.08
	CO-Hb	6±1	0.26	0.26	0.37
	Deoxy-Hb	0			
	Ft-like iron	0	0.55	0.48	0.72